RANDOM WALK NUMERICAL SIMULATION OF ELECTRON DYNAMICS IN SOLAR CELLS BASED ON DISORDERED MATERIALS

Ph.D. Thesis

José Pablo González Vázquez

Sevilla, 2012

RANDOM WALK NUMERICAL SIMULATION OF ELECTRON DYNAMICS IN SOLAR CELLS BASED ON DISORDERED MATERIALS

Memoria presentada por

José Pablo González Vázquez

para optar al título de Doctor con Mención Europea

Director

Juan Antonio Anta Montalvo

Profesor Titular de la Universidad Pablo de Olavide

DEPARTAMENTO DE SISTEMAS FÍSICOS, QUÍMICOS Y NATURALES
ÁREA DE QUÍMICA FÍSICA
UNIVERSIDAD PABLO DE OLAVIDE

Sevilla, 1 de Julio del 2012

Department of Physical, Chemical and Natural Systems

University Pablo de Olavide

Juan Antonio Anta Montalvo, profesor titular del Departamento de Sistemas Físicos, Químicos y Naturales de la Universidad Pablo de Olavide

CERTIFICA:

Que la presente memoria titulada "Random Walk Numerical Simulation of Electron Dynamics in Solar Cells Based on Disordered Materials" presentada por José Pablo González Vázquez para la obtención del título de Doctor, ha sido realizada bajo mi dirección en este departamento, dentro del programa de Ciencia y Tecnología de Coloides e Interfases y cumple los requisitos para poder optar a la Mención Europea.

Sevilla, Julio de 2012

Juan Antonio Anta Montalvo

RESUMEN

Esta tesis se centra en el estudio teórico de semiconductores desordenados utilizados en celdas solares de nueva generación. Se presentan y discuten resultados obtenidos mediante Simulación Numérica de Marcha Aleatoria (RWNS, del inglés Random Walk Numerical Simulation). Este método proporciona una eficiente herramienta con la cual estudiar, a partir de postulados básicos, mecanismos de transporte y recombinación de carga en sistemas donde el desorden (tanto energético como espacial) presenta un papel clave. Más aún, esto se ha conseguido en escalas de espacio y tiempo no abordables por métodos ab initio.

Principalmente, esta tesis tiene como objetivo discernir los mecanismos de transporte y recombinación que tienen lugar en una Celda Solar Sensibilizada con Colorante (DSC, del inglés Dye-sensitized Solar Cell). En primer lugar, en el Capítulo 4 se lleva a cabo un análisis del comportamiento del coeficiente de difusión electrónico en función del nivel de Fermi y de la temperatura suponiendo una probabilidad de transferencia electrónica entre estados localizados dada por la fórmula de Miller-Abrahams. Asimismo, se hace uso del concepto de energía de transporte para la interpretación de resultados. Por otro lado, en el Capítulo 5, se utiliza el modelo de Multiple-Trapping como marco para el cálculo de la vida media y la longitud de difusión electrónica en presencia de una probabilidad de recombinación independiente de la energía. En el Capítulo 6 se realiza un estudio más amplio del origen de la recombinación no lineal observada en una celda DSC. Así, se consigue explicar de manera satisfactoria este fenómeno mediante un proceso de transferencia de carga entre una distribución exponencial de estados localizados en el óxido y una distribución de estados aceptores en el electrolito gobernada por el modelo de Marcus-Gerisher.

El papel que desempeña la morfología del electrodo fotoactivo de una celda solar nanoestructurada es también analizado en el Capítulo 7. Así, se lleva a cabo un estudio completo de la dependencia de la eficiencia de recolección con el grado de orden inducido externamente en la dirección perpendicular al electrodo. De esta manera, se obtienen resultados para varios grados de iluminación y diversas probabilidades de recombinación, lo cual se utiliza luego para discutir en qué circunstancias es beneficioso trabajar con electrodos ordenados y en qué casos no.

Finalmente, el Capítulo 8 de la tesis presenta un modelo para heterouniones entre semiconductores desordenados. En primer lugar, se estudia el proceso de separación de carga en términos del Fotovoltaje Superficial (SPV), estudiando su dependencia con respecto al alineamiento de las bandas, la distribución de estados localizados y la densidad electrónica. Estos resultados se discuten luego en función de las evidencias experimentales encontradas en celdas inorgánicas ETA. Por otro lado, se incluye luego en los cálculos un término de generación continua de carga para estudiar el comportamiento en estado estacionario de una heterounión desordenada. Así, se hacen cálculos tanto del voltaje a circuito abierto como de la corriente de recombinación y estos resultados se analizan, bajo ciertas suposiciones, en relación al funcionamiento de una celda orgánica BHJ.

ABSTRACT

This thesis is focused on the use of computational tools for the study of disordered semiconductors with applications in new generation solar cells. Theoretical results as obtained by Random Walk Numerical Simulation (RWNS), a type of Monte Carlo calculation, are shown and discussed. It is proved that RWNS provides an efficient method to study from first principles microscopic mechanisms of charge transport and recombination where both spatial and energy disorder are taken into account. Importantly, this has been accomplished in the long time and spatial scales, non accessible to quantum-mechanical methods.

This thesis mainly focuses on discerning actual electron dynamics involved in Dye-Sensitized Solar Cells (DSC). On the one hand, a thorough study of the electron diffusion in the nanostructured oxide as a function of the Fermi level is carried out. For this purpose the two most widely accepted models of transport in disordered semiconductors are taken into account: Hopping and Multiple-Trapping. In Chapter 4, the electron diffusion coefficient is measured with respect to the Fermi level and the temperature from the Miller-Abrahams hopping rates in the context of the hopping model. In addition, the concept of the transport energy level is utilized and analysed to interpret the results. In Chapter 5, the multiple-trapping model is used as a framework in which both the electron diffusion length and lifetime are determined from RW calculations using a constant recombination rate. Finally, the origin of non-linear recombination mechanism in a DSC is further studied in Chapter 6 by checking the interplay between an exponential energy distribution of intra-band localized states in the nanostructured oxide and the Marcus-Gerischer model with regard to the energy distribution of acceptor states in the electrolyte.

The role of morphology of a photoactive electrode in the context of nanostructured solar cells applications is investigated in Chapter 7. Thus, a complete study of the dependence of the electron collecting efficiency on an externally induced order in one direction of a disordered electrode is carried out. Results of efficiencies with respect to various degrees of illumination and recombination rates are shown. This is utilized to discuss in which circumstances working with an ordered electrode is beneficial and in which others it is not.

Finally, a disordered semiconductor heterojunction model is developed in Chapter 8. First of all, charge separation is studied in terms of the Surface Photovoltage (SPV) and its dependence on different band-offsets, energy distributions of traps in each semiconductor and initial densities in the absorber are analysed. The results are interpreted in terms of experimental evidence collected in Extremely Thin Absorber Solar Cells (ETA). Secondly, a charge generation term is included in the calculations so that the steady-state behaviour of a disordered semiconductor heterojunction can be studied. This is then applied to the functioning of a Bulk Heterojunction (BHJ) Organic Solar Cell under certain assumptions and both the open-circuit voltage and the recombination current are determined and analysed.

Contributing work and publications

The work included in this thesis is mostly based on the following papers:

González-Vázquez J.P., Anta J. A., Bisquert J., *Random Walk Numerical Simulation for Hopping Transport at Finite Carrier Concentrations: Diffusion Coefficient and Transport Energy Concept*, Physical Chemistry Chemical Physics, **2009**, 44, 10359.

González-Vázquez J.P., Anta J.A., Bisquert J., *Determination of the Electron Diffusion Length in Dye-Sensitized Solar Cells by Random Walk Simulation: Compensation Effects and Voltage Dependence*, Journal of Physical Chemistry C, **2010**, 114, 18, 8552–8558.

González-Vázquez J.P., Morales-Flórez V., Anta J.A., *How Important is Working with an Ordered Electrode to Improve the Charge Collection Efficiency in Nanostructured Solar Cells?*, Journal of Physical Chemistry Letters, **2012**, 3, 3, 386–393.

González-Vázquez J.P., Oskam G., Anta J.A., *Origin of Non-linear Recombination in Dye-Sensitized Solar Cells*, **2012**, submitted to Journal of Physical Chemistry C.

González-Vázquez J.P., Dittrich T., Anta J.A., *Random Walk Numerical Simulation of Disordered Heterojunctions*, **2012**, in preparation.

The following papers are also related with the contents included and discussed in this thesis.

Kytin, V.G., González-Vázquez J.P., Anta J.A., Bisquert J. *Influence of Electron Solvation at the Surface of Nanostructured Semiconductors on the Electronic Density of States*, Selected Topics in Quantum Electronics, **2010**, 16, 1581-1586.

Bigeriego, G. González-Vázquez J.P., Anta J.A., *Influence of the Charge Generation Profile on the Collection Efficiency of Nanostructured Solar Cells: a Random Walk Numerical Simulation Study*, **2012**, accepted in Molecular Simulation.

Contents

CHAPTER 1

Photovoltaic Solar Cells

This Chapter provides an overview of photovoltaic solar energy. First of all, a brief summary of the origin and historical development of photovoltaic devices is presented. In this context, the three generations of solar cells are introduced and discussed. Afterwards, the basic functioning of a solar cell is detailed. The main aspects of a solar cell that determine the photovoltaic effect are discussed. Thus, the requirements for efficient processes of photon absorption, charge separation and charge collection are considered. The *p-n* junction is taken into account in this discussion as the classic charge-selective contact system. However, in a last section, we pay attention to other charge selective contact structures, based on the heterojunction of disordered semiconductors, which constitute the newest field of research on photovoltaics.

1. Photovoltaic Solar Cells

1.1. Solar energy

Nowadays, there is a recognized challenge to achieve a compromise between two different aspects of energy consumption. First of all, it is expected that the world energy demand will double by the year 2050[1] mainly due to the increase in global population. Therefore, a long-term energy supply is essential for political and economic stability. Secondly, global warming is a well-known environmental problem which countries need to address. Indeed, although in recent years more reserves of fossil energy have been found, and the exhaustion of energy reserves does not seem to be the main problem at the moment, the contamination of the atmosphere remains a major environmental problem.

An energy revolution involving the development of carbon-free sources would be highly desirable[2]. Among others, nuclear energy in the form of uranium isotope U235 and others does not seem to be a long-term alternative, due to undesirable effects of pollution from radioactive nuclear waste by-products. Fortunately, there are other ways of energy supply from natural processes. Renewable sources make use of an energy coming from naturally replenished resources. One of the most promising options is the conversion of sunlight directly into electric energy using photovoltaic devices. The idea of such a clean and direct process of energy conversion has motivated scientist to investigate in photovoltaic technology since the 19th century. However, solar cells are still unable to compete with fossil fuels or nuclear energy, mainly due to the high price of PV modules.

Photovoltaic devices are commonly separated in three generations, depending on the strategy followed to achieve competitive energy conversion. The first generation of solar cells is defined by the use of crystalline silicon as photovoltaic material. Currently, the photovoltaic technology marketplace is dominated by crystalline and polycrystalline silicon-based solar cells with achieved efficiencies of 25% and 20.4% respectively[3]. However, in contrast, the need of a large amount of material (the slice of *p*-type silicon must be a few hundred microns thick) as well as the high temperatures required during the process of fabrication result in high costs for the fabrication of silicon modules.

Other materials, concretely some *II–VI* and *III–V* compounds, like gallium arsenide (GaAs), have been used in photovoltaic devices as alternatives to crystalline silicon. A second generation of solar cells comprises the so-called *thin-film* solar cells. These solar cells are

based on semiconductors with higher absorption coefficients as compared to crystalline Si, thereby allowing for a light absorption in a layer of 1 μm in thickness or even less. Thin-film solar cells have cost advantages as they can be fabricated with fewer processing steps as well as with a simpler manufacturing technology. Currently, amorphous silicon (a-Si), cadmium telluride (CdTe), copper indium selenide (CIS) and copper indium gallium (di)selenide (CIGS) are the main materials for second generation solar cells production.

It is only recently that materials are developed mainly for their application in photovoltaics. In this sense, new types of photovoltaic solar cells based on new concepts (different from the traditional *p-n* junction used in previous solar cells) and materials (mostly disordered inorganic and organic materials) are currently under intense investigation and constitute the *Third Generation* of solar cells. Dye-sensitized solar cells (DSC), organic solar cells or extremely thin absorber solar cells (ETA) are some examples of this new generation of solar devices. They are very promising as low-cost photovoltaic solar cells but still in a phase of investigation as the actual mechanisms of charge separation, transport or recombination are not fully understood yet. This new generation solar cells are made of disordered semiconductors, which brings about important consequences in these mechanisms. The main objective of this thesis is to study these consequences from the theoretical point of view, taking into account the effect of the disorder in their functioning.

1.2. Fundamentals of solar cells

Solar cells are devices that convert directly solar energy into electric energy. The basic physical principle underlying the photovoltaic effect is the absorption of photons by an appropriate material and the generation of electron-hole pairs. Besides, solar cells have some kind of internal mechanism to locally separate the photogenerated charge carriers and to transport them independently to the corresponding contacts before they disappear by recombination.

Charge separation is a crucial process in every photovoltaic device. In standard devices (for example, in classical silicon-based solar cells) it is achieved by the use of an appropriate junction between two electronically different materials, generally a *p-* and an *n*-type semiconductor. Under dark conditions both materials are in equilibrium and their chemical potentials are equal. When the *p-n* junction is illuminated electrons pass across the interface and move towards the *n*-side whereas and that of holes toward the *p*-side. As a consequence, a photocurrent is produced due to the excess of carriers. At open-circuit conditions, the

separation of photogenerated charge carriers sets up a potential difference between the edges of the material which is known as the *open-circuit voltage*, V_{oc}. At the same time, if the two contacts are short-circuited the flow of photocarriers into the circuit constitutes a current density equal to the photocurrent (if the series resistance is zero) which is known as the *short-circuit current density J_{sc}*.

When a load is present, a potential difference is developed between the terminals of the cell generating a current which opposes to the photocurrent, reducing the *short-circuit current* value. This reverse current is called the *dark current* because it is in general equal to the current which flows across the solar cell under a forward bias in the dark[4]. In most of the cases, the behaviour of a solar cell in the dark resembles that of a rectifying diode and the current-voltage characteristics of the solar cell under illumination can be seen as the superposition of the dark current and the photocurrent (superposition principle). The *I–V* characteristic of a solar cell can be described by Eq. (1.1) (diode equation)

$$J = J_{sc} - J_0 \left[\exp\left(qV/mk_BT - 1 \right) \right] \tag{1.1}$$

where k_B is the Boltzmann constant, T is the absolute temperature, q is the elementary charge, J_0 is called the *saturation current*, V is the voltage at the terminals of the cell and m is the so-called *ideality factor*. Eq. (1.1) sets up in fact the same as the characteristic curve of a current
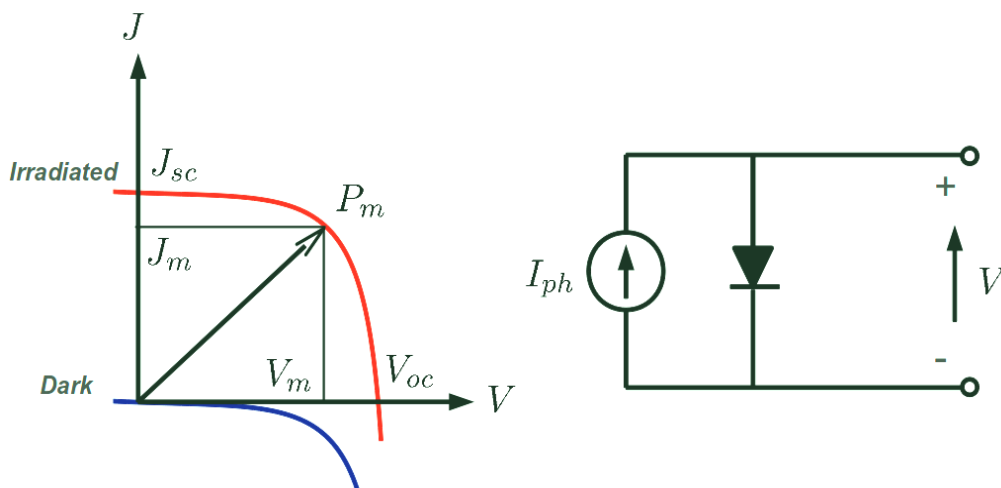
Fig. (1.1) I-V characteristics of a solar cell and equivalent circuit of an ideal solar cell. The sign convention for current and voltage in photovoltaics is such that the photocurrent is positive.

generator in parallel with a diode (see Fig. (1.1).

If the total current under illumination is zero (open-circuit condition), then solution of Eq. (1.1) gives

$$V_{oc} = \frac{mk_BT}{q} ln\left(\frac{J_{sc}}{J_0} + 1\right) \tag{1.2}$$

As the short-circuit photocurrent is proportional to illumination, the open-circuit voltage increases logarithmically with light intensity. The regime in which a solar cell operates coincides with the range of bias from zero to V_{oc}. Likewise, the maximum electric power density ($P=J \cdot V$) that a solar cell can generate occurs at an intermediate voltage V_m with a corresponding intermediate current density J_m. This situation corresponds to the so-called *maximum power point*. Finally, the *fill factor* (*FF*) can be defined according to Eq. (1.3)

$$FF = \frac{J_m V_m}{J_{sc} V_{oc}} \tag{1.3}$$

This parameter is useful for describing the square shape of the *I–V* curve and the ideality of the solar cell. The higher *FF* is the more it corresponds to an ideal behaviour of the solar cell ($m = 1$).

The *efficiency* of the cell (η) is defined by the power density supplied at the maximum power point divided by the incident light power density (I). According to this definition, an expression containing the main photovoltaic parameters can be obtained

$$\eta = \frac{J_{sc} V_{oc} FF}{I} \tag{1.4}$$

From Eq. (1.4), it is immediate that in order to improve the efficiency of a solar cell it is necessary to maximize the three photovoltaic parameters (J_{sc}, V_{oc}, *FF*). Following on from this, we move to a description of the most significant aspects of the performance of a solar cell and their implications for achieving high conversion efficiencies.

Absorption of the incident light

To excite an electron by the absorption of a photon it is needed that the photon energy equals or exceeds the band gap energy of the semiconductor E_g. The band gap energy thus defines the fundamental absorption edge of the material. In general, only photons with energies higher than E_g lead to band-to-band transitions, with the subsequent production of excitons and free charge carriers. However, in disordered materials, with a considerable density of intra-band localized states, other absorption processes are also possible, like band-to-localized-states, that can also lead to free electrons and holes.

The absorption coefficient $\alpha_{ab}(\lambda)$, defined as the probability of absorption of a photon with a wavelength λ, is a key parameter, characteristic of each material. The absorption coefficient is strongly dependent on whether the transition process involves a change at the momentum of the electron-hole or not, that is, whether the material has a direct or non-direct band gap. Thus, "direct" materials, like GaAs, show values of α_{ab} up to 10^4 cm^{-1}, while "indirect" materials, like Si, show smaller absorption coefficients, due to the fact that a
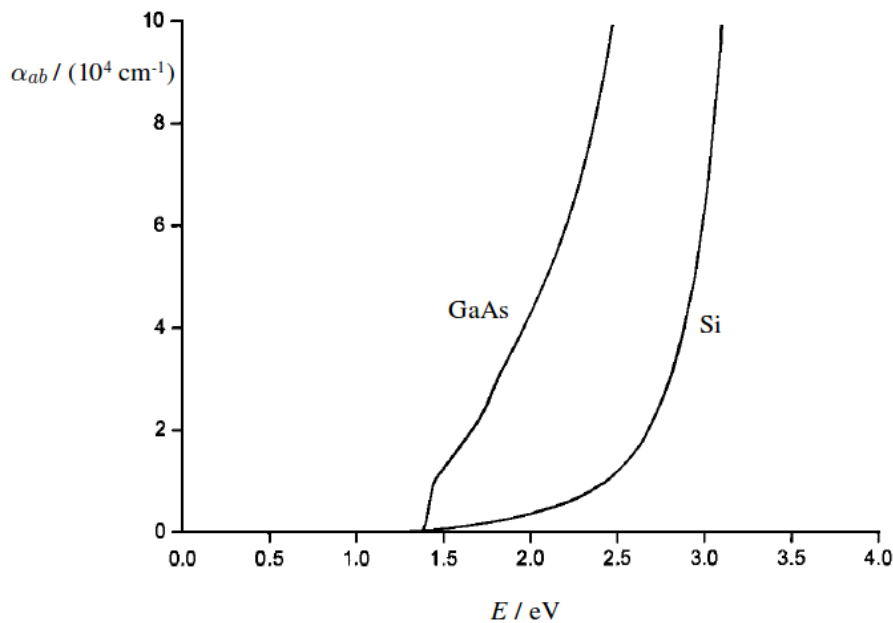
Fig. (1.2) Absorption coefficient α_{ab} of the "direct" semiconductor gallium arsenide and the "indirect" semiconductor Silicon. Adapted from figure 3.17. of reference 2.

phonon is required for each electron-hole creation event to satisfy the conservation of momentum. The penetration depth or *absorption length*, $L_{ab} = 1/\alpha_{ab}$, defined as the distance from the surface at which the illumination intensity is attenuated by a factor of e, is also a property of the material and likewise dependent on the type of transition. Thus, while solar cells made of direct materials do not have a thickness larger than a few μm, solar cells based on indirect materials must typically have a thickness of more than 100 μm.

In the absence of reflection, interferences or scattering processes, the light intensity $I(\lambda,x)$ at a point x of the solar cell is given by the *Lambert-Beer law*.

$$I(\lambda, x) = I_0(\lambda) \exp\left[-x/L_{ab}(\lambda)\right] \tag{1.5}$$

where $I_0(\lambda)$ is the light intensity at $x = 0$. However, the wave properties of light are also important as reflection can take place at the interfaces of the device as well as interference and scattering effects within the cell. In addition, processes of light *trapping* inside the material through a series of scattering processes can also occur, which reduces the optical thickness of the semiconductor[5].

Absorber materials can be organic or inorganic semiconductors. In third generation solar cells, light absorption is also accomplished by dye molecules or quantum dots. In all cases, absorbers with transition energies appropriate to maximize the different photovoltaic parameters (like the open-circuit voltage, the photocurrent and the solar spectrum) have to be used. In this respect, although the optimum energy is situated around 1.5 eV[4], band gaps between 1 eV and 2 eV are commonly utilized in order to achieve relatively high efficiency.

Transport and charge separation

In addition to good absorption properties, materials that can provide high charge carrier mobilities are necessary. This is one of the reasons for the use of semiconductors as photovoltaic materials. The absorption of photons is accomplished through the excitation of charges into states of higher energies. After that, this extra energy is lost by generation of phonons. In metals, due to the continuous band structure, the latter process is very fast and takes place on a time scale of 10^{-12} s. In semiconductors, however, thanks to the particular structure of two bands separated by a band gap, once electrons have reached the lower edge of the conduction band further energy dissipation requires the loss of E_g in a single step, which is much less probable that deexcitation through a continuous distribution of states. As a

consequence, electrons can remain in the conduction band much more time without suffering a recombination process[2].

In a semiconductor, photogenerated charge carriers can move as a consequence of two driving forces: an electric field and/or a concentration gradient. Thus, the electron and hole current density, J_n and J_p, can be calculated as the sum of both components.

$$J_n = -\mu_n nE - D_n \nabla n$$

(1.6)

$$J_p = -\mu_p pE + D_p \nabla p$$

where n (p), $\mu_{n\,(p)}$ and $D_{n\,(p)}$ are the photogenerated electron (hole) density, mobility and diffusion coefficient respectively and E is the electric field. The total current density is $J = J_n + J_p$.

It has already been mentioned that an essential aspect of the working principle of a photovoltaic device is the definition of an specific structure, generally asymmetric, in which illumination takes place in a situation where there is a preference for the electron to move in one direction while holes move in the opposite, thereby producing their separation. In this sense, although the classical structure is the *p-n* junction, there are many more possibilities that lead to a photovoltaic functioning. In connection with transport mechanisms, there are two ways of achieving charge separation: by a *built-in* electric field that *drifts* the carriers in different directions or by a *built-in* effective force field (for instance different electron and hole chemical potentials) that leads electrons and holes to diffuse in opposite directions.

Recombination losses

Electron and hole generation is a process that can be reverted by means of a recombination process in which electrons and holes are annihilated. There are several types of recombination mechanisms in a solar cell.

Radiative recombination is a mechanism in which an electron reacts with a hole and a photon is produced. It is the inverse process of direct absorption and cannot be avoided due to the *principle of detailed* balance[6]. This process increases its rate U_{rad} with the density of electrons and holes and has the following form[7]

$$U_{rad} = B(np - n_i^2) \qquad\qquad (1.7)$$

where B is a constant that depends on the semiconductor, n and p are the photogenerated electron and hole densities respectively and n_i is the intrinsic carrier density. In a pure semiconductor in thermal equilibrium the density of electrons in the conduction band, n_0, is equal to the intrinsic density. Moreover, as electrons are originated from the valence band, the density of holes in the valence band p_0 is also equal to n_i.

Non-radiative recombination includes carrier-loss processes in which phonons and/or other electrons and holes are involved. *Auger* recombination is the process in which the energy released by recombination is absorbed by a free carrier. This energy is subsequently dissipated by generating phonons in collision with the lattice. In the case in which the third carrier involved is an electron the rate has the form

$$U_{Aug} = C(n^2 p - n_0^2 p_0) \qquad\qquad (1.8)$$

where C is a proportionality constant that depends on the temperature. Auger recombination becomes more important when carrier densities are high (low band gap materials or doped
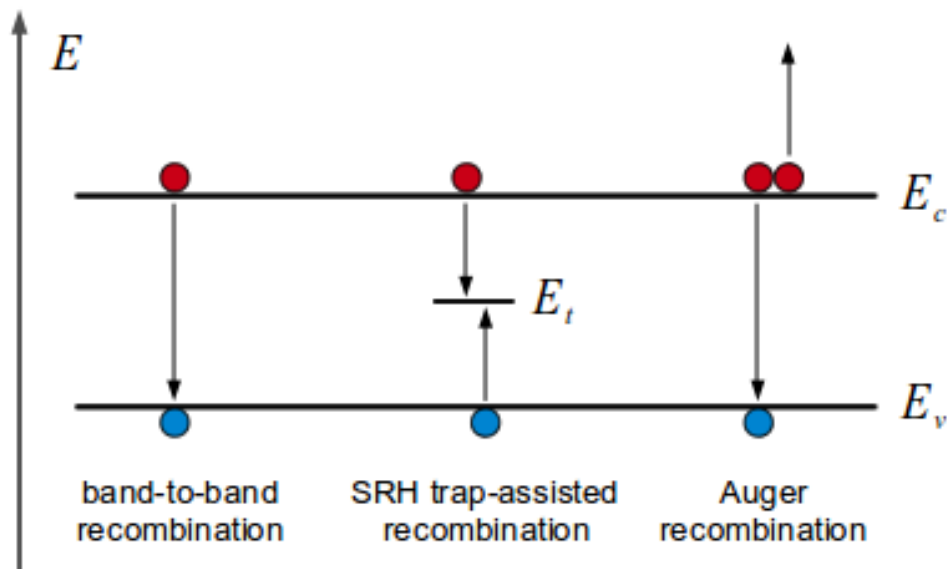
Fig. (1.3). Illustration of the main types of recombination presented in a solar cell.

materials), and it is another unavoidable process as it depends on the intrinsic properties of the material.

Non-radiative recombination via defects or impurities in the crystal is known as *Shockley-Read-Hall* mechanism. It is a process in which charge carriers give up their energy in a process of trapping and this energy is released as phonons or photons or both. From this time, if the trap captures a carrier of the opposite sign before the first carrier is detrapped a recombination event is then produced. The following expression gives the rate corresponding to recombination via a single trap with energy E_t.[8]

$$U_{SRH} = \frac{np - n_i^2}{\tau_{n,SRH}\left(p + p_t\right) + \tau_{p,SRH}\left(n + n_t\right)} \tag{1.9}$$

where $\tau_{n,SRH}$ and $\tau_{p,SRH}$ are defined as the lifetimes for the electron and hole trapping by the single state, and n_t and p_t are the electron and hole densities when the electron and hole Fermi levels are equal to the trap level. Fig. (1.3) shows an illustration of the different types of recombination mechanisms here described.

Recombination is often studied experimentally via the measurement of the carrier *lifetime*, a characteristic time constant that reflects the kinetics of the recombination of minority carriers. This magnitude is defined by the time for the system to recover equilibrium under a small perturbation of the steady state. It is defined in its more general form by[9,10].

$$\tau_n = \left(\frac{\delta U_{rec}}{\delta n}\right)_n^{-1} \tag{1.10}$$

where U_{rec} is the recombination rate and n is the total electron density (or the carrier density, in a more general situation). Determination of the lifetime as well as the diffusion length, the average distance that electrons travel between recombination events, are key for the characterization of a solar cell and the understanding of its recombination kinetics. As a part of this thesis, both quantities have been determined by computational tools and related to microscopic parameters describing an specific recombination mechanism.

In connection with the electric model described in Fig. (1.1) there is also a source of voltage losses from series and parallel resistances that prevent the fill factor from being
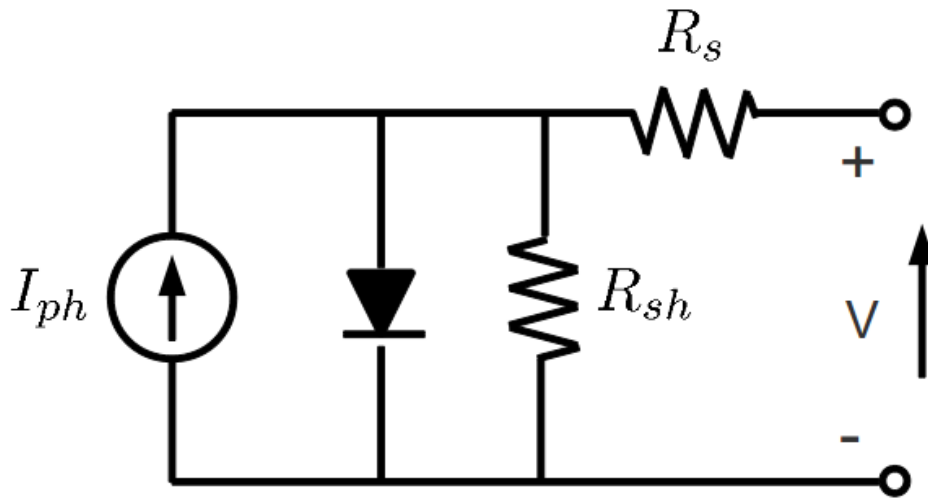
Fig. (1.4) Equivalent circuit of a real solar cell. Adapted from 4.

maximized[4]. On the one hand, series resistances, R_s, are commonly related to resistance of the contacts and interconnections. On the other hand, current leakages are often responsible for parallel or shunt resistances, R_{sh}. Both resistances must be considered in real solar cells, requiring the use of a modified electric model (equivalent circuit) as presented in Fig. (1.4).

In a real solar cell absorption, transport and recombination determine the conversion efficiency. In accordance with the *Shockley-Queisser limit*[6], which establishes a maximum theoretical efficiency of a single-junction solar cell in terms of the principle of detailed balance, the maximum efficiency of a single-junction solar cell operating at 1 sun is calculated to be 32.9 %. Similarly, the same solar cell operating under maximum concentration can theoretically reach an efficiency above 40%[11]. The aim of the third generation of solar cells is to design devices that can reach conversion efficiencies beyond the *Shockley–Queisser limit*. The new strategy consists of defining alternative concepts for charge separation that do not need the *p-n* junction of traditional photovoltaic structures. A brief description of three of these alternatives is presented in the coming section.

1.3. New generation solar cells

1.3.1. Dye-sensitized solar cells

One of the most promising solar cell technologies nowadays is the so-called *dye-sensitized solar cell* (DSC). This is based on the heterojunction between a nanostructured porous wide band gap semiconducting oxide (typically TiO_2) and a hole conducting electrolyte solution containing a redox couple (usually I_3^-/I^-) whereas light absorption is achieved by dye molecules adsorbed to the semiconductor[12,13]. The nanostructured film is deposited onto a transparent conductive oxide (TCO) electrode, through which the light incides[14] and is permeated by the electrolyte solution. The cell is completed by another glass plate coated with a platinum catalyst[15].

The reason to use a nanoporous film is the fact that it favours light harvesting as the roughness of the surface allows for a larger number of dye molecules to adsorb directly to the
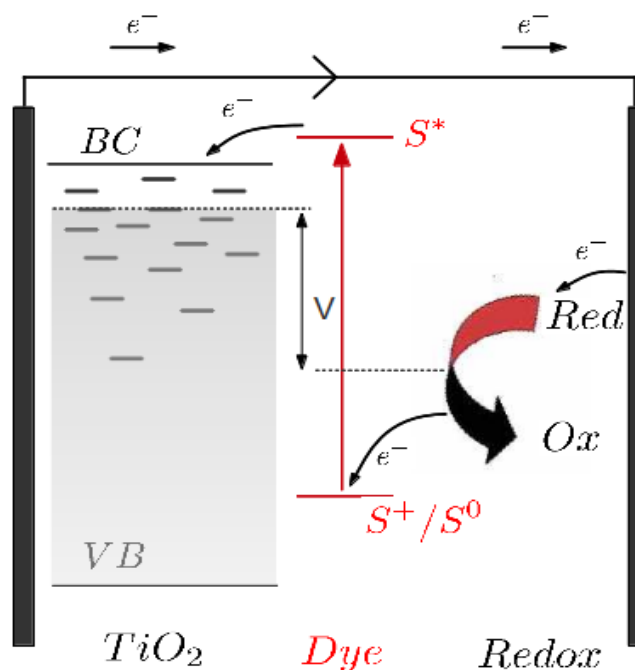
Fig. (1.5) Charge transfer processes at the oxide/dye/electrolyte interfaces of a Dye-sensitized solar cell. Adapted from figure 1.3. of reference 16.

surface while being simultaneously in direct contact to the redox electrolyte[17]. Besides, high charge injection efficiencies close to one are normally measured, due to injection rates orders of magnitude faster than dye-electron recombination rates in those cases where a favourable kinetic balance exists[18]. Another important feature of DSC is the long lifetimes and diffusion lengths that are obtained for separated species in these systems, which are of the order of microns, in spite of the proximity of positive and negative charge carriers.

Fig. (1.5) shows a scheme of charge transport and interfacial transfer processes in a typical DSC. Under light irradiation, excited electrons in the adsorbed dyes are injected into the conduction band of TiO_2 and the injected electrons diffuse in the TiO_2 to TiO_2/TCO interface, where electrons are extracted to the external circuit. Resulting dye cations are reduced by I^-. The I_3^- ions formed during the regeneration step diffuse to the glass plate coated with the platinum catalyst and the passage of electrons through the external circuit to the cathode completes the cycle[19].

Due to the complex morphology and heterogeneous character, the system is in general more complicated than other solar cells. Thus, despite the nature of transport and recombination is not well-known yet, it is seems that the nanostructured nature of the n-type TiO_2 is determinant to clear up the actual dependences of the main dynamic magnitudes. With respect to transport, electron trapping and detrapping from localized states within the band gap is expected to occur. On the other hand, electrons can suffer recombination by two different ways, either by reaction with the dye cations or with electron acceptors in the hole conductor (electrolyte) and neither of them are expected to be linear with electron density[20].

However, although the system is complex in general, some simplifications can be made for dye-sensitized systems[20]. For example, at least in the case of liquid junctions, the electrolyte is concentrated enough and the ions mobile enough within the porous structure that electric fields are not expected to exist within the electrolyte over more than a few nm. The small size of the nanocrystals and the doping density of TiO_2 add to the restriction that the porous film cannot sustain electric fields. This leads to the conclusion that transport should occur by *diffusion* only[21–23] (second term in Eq. (1.6)).

Furthermore, due to the fact that the density and mobility of charged species in the electrolyte is high, transport of ionic species is presumed to be facile for common solvents and only electron transport needs to be considered to explain transient phenomena. The electron diffusion coefficient D_n depends on the nanoparticulate film preparation method and the size
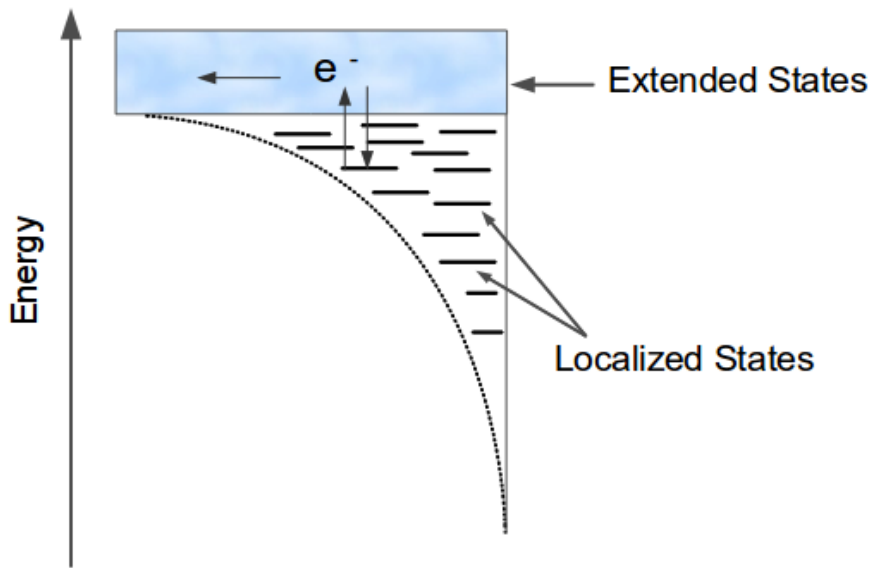
Fig. (1.6) Illustration of a energy distribution of intra-band gap localized states in a DSC. Adapted from reference 16.

of nanoparticles by means of percolation effects. In addition, it is known that there is a power-law dependence of D_n on the electron density. This behaviour is interpreted in terms of charge-filling effects in the presence of an exponential energy distribution of localized states within the band gap of the TiO$_2$ film[15,24,25] (see Fig. (1.6)).

The open-circuit voltage is most likely related with the difference between the Fermi level of semiconductor electrode and the redox potential of the electrolyte. This is given by the Nernst equation[26]

$$E_{redox} = E_0 + \frac{k_B T}{n_e q} \ln \frac{[ox]}{[red]} \tag{1.11}$$

where E_0 is the standard reduction potential of the *redox* couple and n_e is the number of transferred electrons. The maximum theoretical potential difference is limited by the energy level of the highest occupied molecular orbital (HOMO) and the lowest unoccupied molecular orbital (LUMO) of the sensitizer dyes. At the same time, the Fermi level of TiO$_2$ is related with the density of injected electrons and the density of charge traps in the band gap of TiO$_2$ (in situations of nonequilibrium the Fermi level should be replaced by the "quasi-Fermi level". However, for the sake of brevity, this distinction will be omitted in this thesis)

Assuming fill factors around 75%, the maximum conversion efficiency is expected to be around 14-15% at 1 sun for the standard solar spectrum. DSCs continue to attract attention as potential low-cost alternatives to traditional photovoltaic devices[27]. However, far from leading to important improvements in the efficiency, this interest does not result in real progress. The latest in the series of solar cell efficiency tables collated by Green et al. lists the record validated AM 1.5 DSC efficiency as (11.4 ± 0.3) % for approximately 1 cm² cell[3]. Recently, a new record of 12.3% has been reported using a modified porphyrin as dye and cobalt complexes as redox couples[28]. Nevertheless, the good behaviour of a DSC at low illumination levels and moderate temperatures, and the possibility of designing flexible and transparent devices, make this technology interesting for other applications in the photovoltaic market, for example, as building integrated photovoltaic (BIPV) systems.

1.3.2. Organic solar cells

Organic solar cells (OSC) are based on the use of conjugated polymers, including crystalline or polycrystalline films of conjugated molecules or amorphous films of small molecules. A key property of these cells is that they can be processed from solution at ambient temperature by application of spin coating or conventional printing techniques. These materials also have high absorption coefficients (of the order of 10^5 cm^{-1}) so polymer films can be very thin (100 nm). In addition, as in DSC solar cells, they allow for the possibility of manufacturing flexible devices[29–32].

Photon absorption is controlled by optical excitation of partly delocalised π–bands. Under illumination electrons are excited from the π– orbital to π^*–band, which corresponds to the optical excitation from the highest occupied molecular orbital (HOMO) to the lowest unoccupied molecular orbital (LUMO). Most of organic semiconductors have a band gap of 2 eV and therefore limitations in light harvesting. Due to the low dielectric constant of organic materials, the absorption of photons leads to the creation of *bound* electron-hole pairs – excitons – which diffuse within the material in which they are created[33]. Thus, excitons only become free electrons and holes provided that some type of dissociation phenomenon takes place supplying an input of energy between 0.1 and 1 eV. Normally, this last is accomplished by the existence of a band offset between the two polymers. If both electron affinity and ionisation potential are greater in one material (the electron acceptor, generally fullerene) than in the other (the electron donor) then the interfacial electric field can drive charge separation. An illustration of the charge separation process can be seen in Fig. (1.7).
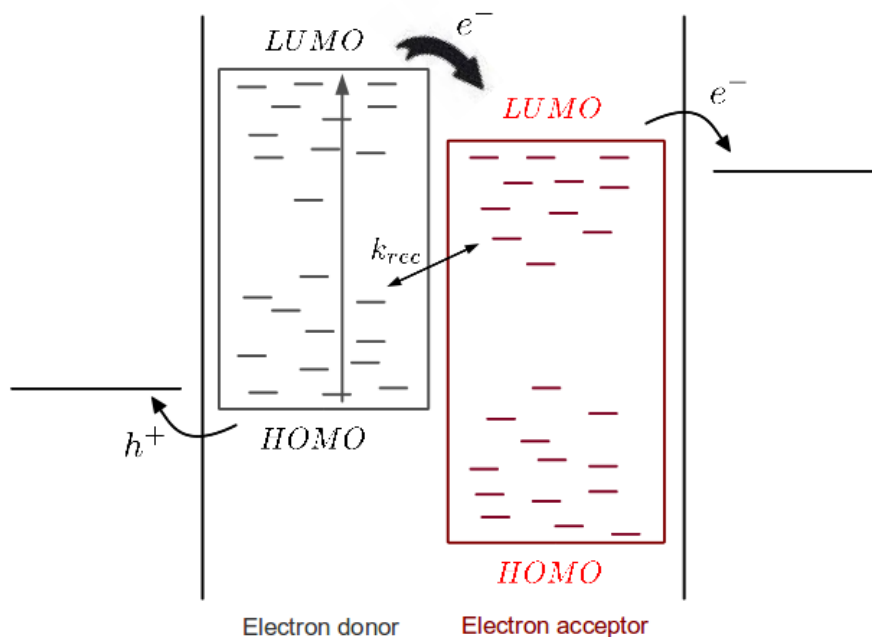
Fig. (1.7). Scheme of the energy band diagram of a donor-acceptor heterojunction. Adapted from figure 2 of reference 32.

Exciton generation occurs generally in the light absorbing donor. The separation process is then accomplished when the electron transfers to the LUMO of the acceptor while the hole remains on the donor. This photoinduced charge transfer takes place very rapidly within less than 100 femtoseconds so the charge separated state is quite stable[34]. Recent reports have pointed out that photon absorption may result in a primary excitation where electrons and holes are more delocalized than the relaxed exciton. Thus, diffusion of the unrelaxed electron-hole pair to the interface can occur before relaxation (i.e. exciton formation) is taking place. In this manner, the apparent contradiction between the mentioned ultrafast charge separation process and the limited distance than an exciton can actually diffuse in such short scale of time can be explained[35].

Once the charge carriers have been separated, they need to be conducted to their respective electrodes. This is achieved by the fact that the donor material sustains hole transport whereas the acceptor material serves as electron conductor. In addition, charge selective contacts are placed in both the anode and the cathode, hence favouring the separation of charges and the creation of a measurable photovoltage in the external circuit[36]. Charge transport seems to occur by hopping between localized states, rather than through a band[37,38]. Indeed, impurities are believed to act as deep traps that mainly act as recombination

sites within the film resulting in lower mobilities as well as stronger dependences on the temperature[39]. Another transport feature relies on the fact that each phase has to be continuously connected for the transport of the respective charge carrier to separate electrodes so percolation effects have to be taken into account in order to avoid recombination on isolated traps.

The processes of carrier generation and charge transport are intimately related. As a consequence of the low mobilities, photoexcitation will only lead to dissociation if the exciton is formed very close to the interface between the acceptor and the donor polymers. Therefore, both charge carrier generation and transport are highly dependent on the internal phase structure of the blend. This is an important limitation because only a portion of absorbed photons can effectively contribute to the photocurrent . A crucial development in organic photovoltaics came with the introduction of a dispersed heterojunction, where the electron acceptor and donor materials are intimately blended together forming a *bulk heterojunction* (BHJ) *solar cell*[40–42]. The idea is that if the domain size of each phase is on the nanometer scale then charge carrier generation will occur close to the interface, thereby leading to a more probable charge separation process. Note here the analogy with the DSC described above, where the structuring in the nanoscale also leads to good light harvesting and subsequent photogeneration of carriers.

The enhanced charge dissociation achieved within a BHJ involves the disadvantage of longer charge collection paths and of increased bimolecular recombination due to the higher interfacial area between the two phases. In fact, organic solar cell technology is still new and the field is clearly wide open. Theoretical studies are needed to enhance charge separation and transport processes[36]. Therefore, further investigation on a fundamental understanding of the interfacial mechanisms involved in this type solar cell is necessary. Organic bulk heterojunction achieve a AM 1.5 efficiency of (10.0 ± 0.3) % for approximately 1 cm^2 in area as reported by Green et al.[3], thus yet competing with DSCs. Furthermore, the "learning curve" has a much larger "slope" than that of the DSC, showing the great potential and rapid progress made by this technology.

1.3.3. Extremely thin absorber solar cells

Extremely thin absorber (ETA) solar cells are a type of solid-state device based on the use of an inorganic semiconductor, acting as the absorber, that is placed between two transparent nanostructured semiconductors. These solar cells are characterized by the high interpenetration between its components as well as the strong confinement of the thin layer between the semiconducting layers. As in DSC and BHJ solar cells, rough materials are required as extremely thin absorbers to enhance the surface by a factor of 100 in the best cases, thereby permitting the possibility of reducing the thickness in the same order of magnitude.

ETA solar cells and dye solar cells have in common that both consist of interpenetrating electron and hole conductors between which an absorber is sandwiched. The main difference here is the concept of a photovoltaic device composed entirely of inorganic materials, including the absorber. In this case, the fact of using extremely thin absorbers leads to lower purity requirements because carriers are likely to be generated in the proximity
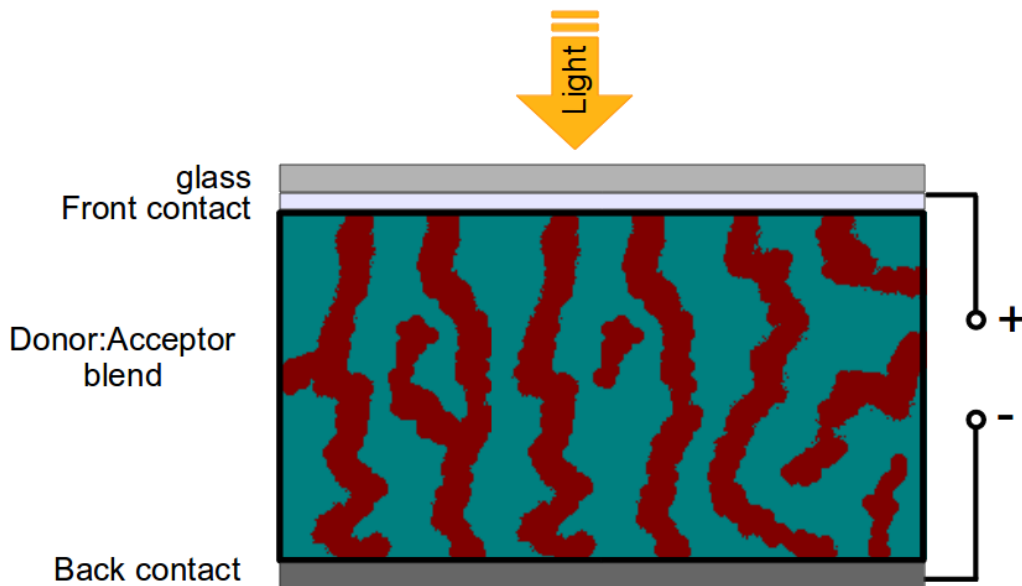
Fig. (1.8). Schematic diagram of ETA solar cell showing a superstrate arrangement on a conducting glass substrate. Adapted from figure 1 of reference 43.
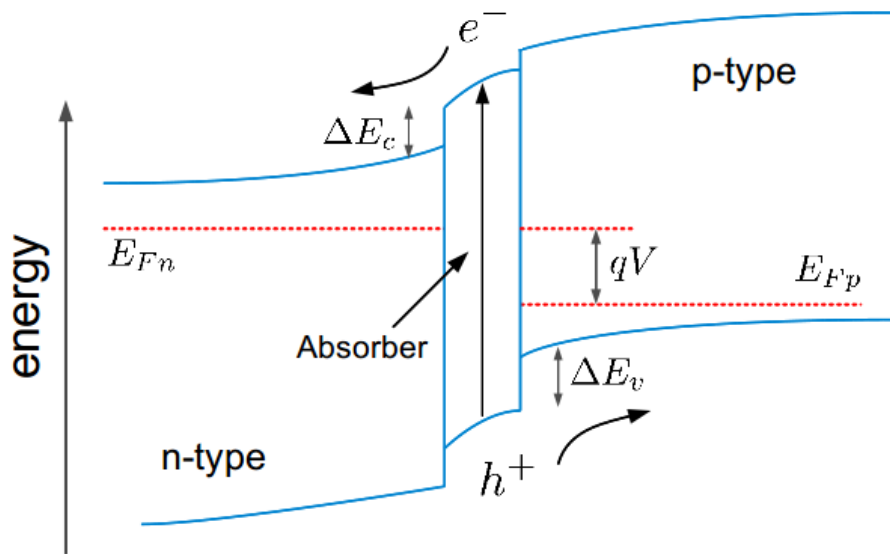
Fig. (1.9). Band alignment of a ETA solar cell. Adapted from figure 7 of reference 44.

of the interfaces so high diffusion lengths are not needed to reach the *n*- and *p*-type semiconductors. Thus, inexpensive inorganic materials can be used, most of them not yet widely investigated by photovoltaic scientists. In any case, materials have to be chosen in order to guarantee efficient charge separation.

An energy diagram of this type of solar cell is shown in Fig. (1.9). It can be seen that the band alignment of the three semiconductors is such that electrons tend to move only to the *n*-contact while hole transfer occurs only to the *p*-type layer. Thus, hole transfer to *n*-type semiconductor and electron transport into *p*-type layer are blocked due to the high band offset between bands in both cases. Cell assembling techniques have to be aimed at achieving that both absorber and *p*-type conductor are deposited throughout the nanostructured *n*-type semiconductor layer. Therefore, a method allowing for the controlled infiltration of the reactants into the pores of the electron conductor film is required. In general, annealing at high temperature is necessary[45]. Spray ion layer gas reaction[46,47], chemical bath deposition[48] or spray pyrolysis[49] are some of these methods.

There are several types of ETA solar cells currently being researched. The use of CuSCN as *p*-type conductor is widely extended and gives the highest conversion efficiencies until now. Concerning the *n*-type the two most utilized materials are nanoporous layers of TiO$_2$ or wet chemically prepared ZnO nanorod arrays. For each *n*-type materials, the working

principles of solar cells based on many different absorbers have been demonstrated. TiO_2 has been used in combination with $CuInS_2$, $In(OH)_xS_y/In_xPb_yS$, or In_2S_3 as the absorber reaching energy conversion efficiencies of up to 4%, 2.9% and 2.3% respectively[50]. Similarly, the $ZnO/In_2S_3/CuSCN$ solar cell is currently one of the most investigated ZnO-based ETA solar cell[51] and has achieved an efficiency of 4.2%[52]. In so-called two-component ETA solar cells the absorber also serves as p-type semiconductor. In this case the p-component is usually CdTe or $CuInS_2$ while the n-type is often TiO_2.

In summary, conversion efficiencies of the order of 2-5% have been obtained for different concepts of inorganic nanostructured solar cells. Recently, the development of ETA hybrid solar cells with conducting polymers replacing the inorganic hole conductor has resulted in improved efficiencies, demonstrating the potential of the original concept of ETA solar cells. Thus, conversion efficiencies of 5.1% and 6.2% have been obtained for P3HT[53] and PCPDTBT[54] respectively. This research field is actually very new and there does not exist a well-established theoretical background yet. To encourage development of this solar cells, a better fundamental knowledge of the nanostructured interface that is responsible for the charge separation process is required. In this sense, time-resolved surface photovoltage (SPV) measurements constitute a useful experimental method to study charge separation in nanostructured semiconductors[55–57]. This thesis dedicates Chapter 8 to a detailed study of different kinds of heterojunctions, including simulations of SPV measurements.

References to Chapter 1

(1)   Nezhad, H. World energy scenarios to 2050: issues and options, **2009**.

(2)   Wurfel, P. *Physics of solar cells. From principles to new concepts*; Wiley, **2005**.

(3)   Green, M. A.; Emery, K.; Hishikawa, Y.; Warta, W.; Dunlop, E. D. *Progress in Photovoltaics: Research and Applications* **2011**, *20*, 12–20.

(4)   Nelson, J. *The Physics of Solar Cells*; Imperial College Press: London, **2003**.

(5)   Mihi, A.; Calvo, M. E.; Anta, J. A.; Miguez, H. *Journal of Physical Chemistry C-Letters* **2008**.

(6)   Shockley, W.; Queisser, H. J. *Journal of Applied Physics* **1961**, *32*, 510.

(7)   Fonash, S. *Solar cell device physics*; Elsevier B.V., **2010**.

(8)   SHOCKLEY, W.; READ, W. *PHYSICAL REVIEW* **1952**, *87*, 835–842.

(9)   Bisquert, J.; Fabregat-Santiago, F.; Mora-Seró, I.; Garcia-Belmonte, G.; Giménez, S. *The Journal of Physical Chemistry C* **2009**, *113*, 17278–17290.

(10)   Hsiao, P.-T.; Teng, H.-S. *Journal of the Taiwan Institute of Chemical Engineers* **2010**, *41*, 676–681.

(11)   Brown, A. S.; Green, M. A. *Physica E: Low-dimensional Systems and Nanostructures* **2002**, *14*, 96–100.

(12)   Wang, Q.; Ito, S.; Gratzel, M.; Fabregat-Santiago, F.; Mora-Sero, I.; Bisquert, J.; Bessho, T.; Imai, H. *Journal of Physical Chemistry B* **2006**, *110*, 25210–25221.

(13)   Lunt, R. R.; Osedach, T. P.; Brown, P. R.; Rowehl, J. A.; Bulović, V. *Advanced Materials* **2011**, *23*, 5712–5727.

(14)   Bisquert, J.; Cahen, D.; Hodes, G.; Ruhle, S.; Zaban, A. *Journal of Physical Chemistry B* **2004**, *108*, 8106–8118.

(15)   Peter, L. M. *Journal of Physical Chemistry C* **2007**, *111*, 6601–6612.

(11)   Guillen, E. Photoelectrochemical Characterization Of Dye Solar Cells Based On Nanostructured Zinc Oxide Substrates, Ph.D Thesis, Pablo de Olavide: Sevilla, **2011**.

(17)   O'Regan, B.; Gratzel, M. *Nature* **1991**, *353*, 737–740.

(18)   The 2010 Millennium Technology Grand Prize: Dye-Sensitized Solar Cells - ACS Nano

(19)   Characterization of Electron Trapping in Dye-Sensitized Solar Cells by Near-IR Transmittance Measurements - The Journal of Physical Chemistry C

(20)   Nelson, J. In *Semiconductor electrodes and photoelectrochemistry*; Wiley, **2002**.

(21)   Hagfeldt, A.; Lindquist, S.-E.; Grätzel, M. *Solar Energy Materials and Solar Cells* **1994**, *32*, 245–257.

(22)   Lagemaat, J. van de; Benkstein, K. D.; Frank, A. J. *Journal of Physical Chemistry B* **2001**, *105*, 12433–12436.

(23)   Gentilini, D.; Gagliardi, A.; Auf der Maur, M.; Vesce, L.; D'Ercole, D.; Brown, T. M.; Reale, A.; Di Carlo, A. *J. Phys. Chem. C* **2011**, *116*, 1151–1157.

(24)   Anta, J. A.; Nelson, J.; Quirke, N. *Physical Review B* **2002**, *65*.

(25)   Anta, J. A.; Mora-Sero, I.; Dittrich, T.; Bisquert, J. *Physical Chemistry Chemical Physics* **2008**, *10*, 4478–4485.

(26)   Crow, D. R. *Principles and Applications of Electrochemistry*; Stanley Thornes, **1994**.

(27)   Bisquert, J. *ChemPhysChem* **2011**, *12*, 1633–1636.

(28)   Yella, A.; Lee, H.-W.; Tsao, H. N.; Yi, C.; Chandiran, A. K.; Nazeeruddin, M. K.; Diau, E. W.-G.; Yeh, C.-Y.; Zakeeruddin, S. M.; Grätzel, M. *Science* **2011**, *334*, 629–634.

(29)   Hoppea, H, S., N.S. *Journal of Materials Research* **2004**, *19*, 1924–1945.

(30)   *Nanostructured Materials for Solar Energy Conversion*; Soga, T., Ed.; Elsevier B.V., **2006**.

(31)   Brabec, C. J.; Sariciftci, N. S.; Hummelen, J. C. *Advanced Functional Materials* **2001**,

11, 15–26.

(32)   Nelson, J. *Current Opinion in Solid State and Materials Science* **2002**, *6*, 87–95.

(33)   Gregg, B. .; Hanna, M. C. *Journal of Applied Physics* **2003**, *93*, 3605.

(34)   Brabec, C. J.; Zerza, G.; Cerullo, G.; Silvestri, S. D.; Luzzati, S.; Hummelen, J. C.; Sariciftci, S. *Chem. Phys. Lett.* **2001**, *340*, 232.

(35)   Cowan, S. R.; Banerji, N.; Leong, W. L.; Heeger, A. J. *Advanced Functional Materials* **2012**, *22*, 1116–1128.

(36)   Bisquert, J.; Garcia-Belmonte, G. *The Journal of Physical Chemistry Letters* **2011**, *2*, 1950–1964.

(37)   Arkhipov, V. I.; Heremans, P.; Emelianova, E. V.; Adriaenssens, G. J.; Bassler, H. *Journal of Physics-Condensed Matter* **2002**, *14*, 9899–9911.

(38)   Arkhipov, V. .; Emelianova, E. .; Adriaenssens, G. .; Bässler, H. *Journal of Non-Crystalline Solids* **2002**, *299-302*, 1047–1051.

(39)   Forrest, S. R. *Nature* **2004**, *428*, 911–918.

(40)   Yu, G.; Heeger, A. J. *Journal of Applied Physics* **1995**, *78*, 4510.

(41)   Yu, G.; Hummelen, J. C.; Wudl, F.; Heeger, A. J. *Science* **1995**, *270*, 1789.

(42)   Halls, J. J. M.; Walsh, C. A.; Greenham, N. C.; Marseglia, E. A.; Friend, R. H.; Moratti, S. C.; Holmes, A. B. *Nature* **1995**, *376*, 498–500.

(43)   Ernst, K.; Belaidi, A.; Konenkamp, R. *SEMICONDUCTOR SCIENCE AND TECHNOLOGY* **2003**, *18*, 475–479.

(44)   Emin, S.; Singh, S. P.; Han, L.; Satoh, N.; Islam, A. *Solar Energy* **2011**, *85*, 1264–1282.

(45)   Dittrich, T.; Kieven, D.; Belaidi, A.; Rusu, M.; Tornow, J.; Schwarzburg, K.; Lux-Steiner, M. C. *Journal of Applied Physics* **2009**, *105*, 034509.

(46)   Belaidi, A.; Dittrich, T.; Kieven, D.; Tornow, J.; Schwarzburg, K.; Kunst, M.; Allsop, N.; Lux-Steiner, M.-C.; Gavrilov, S. *Solar Energy Materials and Solar Cells* **2009**, *93*, 1033–1036.

(47)   Herzog, C.; Belaidi, A.; Ogacho, A.; Dittrich, T. *Energy & Enviromental Science* **2009**, *2*, 962–964.

(48)   Itzhaik, Y.; Niitsoo, O.; Page, M.; Hodes, G. *The Journal of Physical Chemistry C* **2009**, *113*, 4254–4256.

(49)   Nezu, S.; Larramona, G.; Choné, C.; Jacob, A.; Delatouche, B.; Péré,, D.; Moisan, C. *The Journal of Physical Chemistry C* **2010**, *114*, 6854–6859.

(50)   Dittrich, T.; Belaidi, A.; Ennaoui, A. *Solar Energy Materials and Solar Cells* **2011**, *95*, 1527–1536.

(51)   Belaidi, A.; Dittrich, T.; Kieven, D.; Tornow, J.; Schwarzburg, K.; Lux-Steiner, M. *physica status solidi (RRL) – Rapid Research Letters* **2008**, *2*, 172–174.

(52)   Krunks, M.; Kärber, E.; Katerski, A.; Otto, K.; Oja Acik, I.; Dedova, T.; Mere, A. *Solar*

Energy Materials and Solar Cells **2010**, *94*, 1191–1195.

(53)   Chang, J. A.; Rhee, J. H.; Im, S. H.; Lee, Y. H.; Kim, H.; Seok, S. I.; Nazeeruddin, M. K.; Gratzel, M. *Nano Letters* **2010**, *10*, 2609–2612.

(54)   Im, S. H.; Lim, C.-S.; Chang, J. A.; Lee, Y. H.; Maiti, N.; Kim, H.-J.; Nazeeruddin, M. K.; Grätzel, M.; Seok, S. I. *Nano Lett.* **2011**, *11*, 4789–4793.

(55)   Dittrich, T.; Bönisch, S.; Zabel, P.; Dube, S. *Review of Scientific Instruments* **2008**, *79*, 113903.

(56)   Qian, X.; Qin, D.; Song, Q.; Bai, Y.; Li, T.; Tang, X.; Wang, E.; Dong, S. *Thin Solid Films* **2001**, *385*, 152–161.

(57)   Dittrich, T.; Mora-Sero, I.; Garcia-Belmonte, G.; Bisquert, J. *Physical Review B* **2006**, *73*.

CHAPTER 2

Disordered Semiconductors

A general description of the main features of disordered semiconductors is presented in this Chapter. The existence of a quasi-continuous distribution of intra-band localized states in these materials is highlighted as the main difference with respect to crystalline semiconductors. We then relate their particular characteristics with dynamics properties. On the one hand, dispersive transport is presented and discussed in detail. The two main charge transport models, hopping and multiple-trapping, are also described. Moreover, an study of the main aspects of the electron diffusion process in disordered semiconductors is presented. On the other hand, on account of recombination, a trap-assisted mechanism is pointed out as the main annihilation process. Specifically, we describe the most relevant aspects of the recombination process in a DSC. Finally, the electron diffusion length concept, a key magnitude to determine transport and recombination mechanisms in disordered semiconductors, is introduced.

2. Disordered Semiconductors

2.1. Properties of disordered semiconductors

For approximately 30 last years many efforts have been conducted to use disordered semiconductors for multiple applications such as thin film transistors, electrophotografic printers and copiers, photovoltaic solar cells and many other optoelectronic devices. Disordered materials are defined by the absence of long-range order in the arrangement of atoms and translation symmetry[1], what results in a number of unique effects that makes it possible to fabricate low cost devices based on new concepts. Polycrystalline or amorphous systems, chalcogenide glasses, organic materials or nanostructured semiconductors are some examples of this definition.

However, characterization of disordered materials are often given in comparison with crystalline properties and this circumstance makes rather confusing to know for sure whether a certain material is disordered or not. In the one hand, real crystals does not have an infinite long-range order because of surface defects or doping effects. On the other hand, despite not having a translation symmetry, disordered semiconductors do have certain short-range order (nearest neighbours) as well as medium-range order of atomic arrangement. Hence, sometimes it is not straightforward to characterize an specific sample as a crystalline or disordered material because the length of ordering corresponding to a crystal can be subject to interpretation.

The electronic spectral structure determines all the classical properties of crystalline semiconductors. It is well-known that solid state classic theory establishes that there is a conduction and a valence band, separated by a band gap. In non-crystalline semiconductors, where there is no periodic lattice, disorder varies the energy spectrum of the system although it maintains the features of a band spectrum. Hence, regions of high density of states (the allowed bands of the crystal) still exist and are separated by regions with much lower density of states (the energy gaps of the crystalline semiconductor). The former states are usually called *extended states* because, due to the high density, electrons are allowed to move through them under the influence of concentration gradient or electrical field.

A crucial aspect of disordered semiconductors electronic spectrum is the existence of a great number of localized states, that is, as defined by P. Anderson[2], a state where an electron
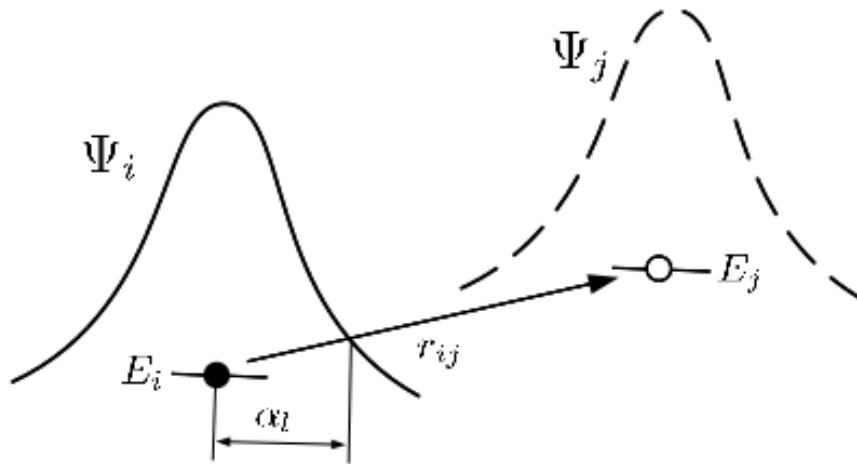
Fig. (2.1). Exponential decay of wave function in localization states. Adapted from figure 2.2 of reference 3.

with energy $E + \Delta E$, located in volume large enough to satisfy the uncertainty principle, does not diffuse from this volume. These states are produced from extended states in the presence of a high number of defects or bounds. Localization involves that the wave function decays exponentially from some point vector $\vec{r}_i$

$$\Psi(r) \sim exp(-|\vec{r} - \vec{r}_i|/\alpha_l) \tag{2.1}$$

where α_l is the localization radius. For a sufficiently strong disorder, even all states can happen to be localized (as for instance in a condensed phase of small molecules). Nevertheless, in most of disordered semiconductors, localized and extended states coexist in the system at different energies. Hence, it is defined an specific energy E_c called the *mobility edge* that separates electron extended states from those localized. Likewise, a mobility edge for holes E_v can be introduced. The region between E_c and E_v, where all of the states are localized, is called the *mobility gap* in analogy with the band gap of a crystalline semiconductor. The major difference with respect to crystalline materials, where intra-band gap localized states can also be found, is that whereas in crystals they exist as discrete energy levels, in disordered media they occur as a quasi-continuous energy density of localized states (DOLS).
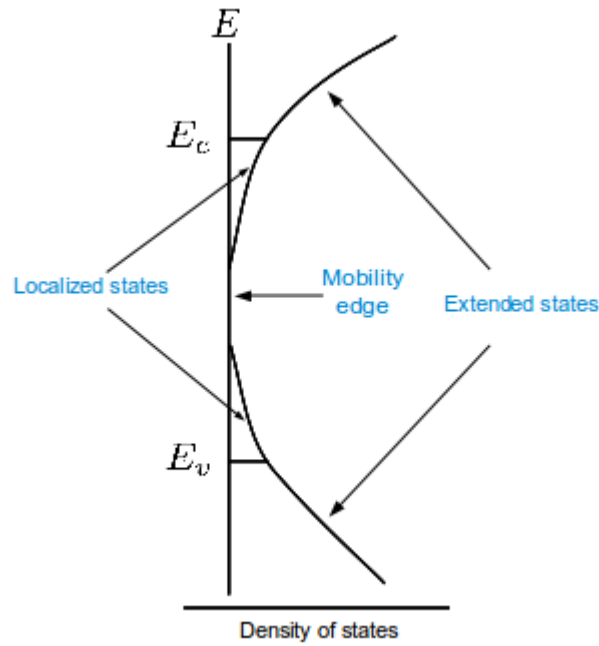
Fig. (2.2). Schematic representation of the energy spectrum of a disordered semiconductor.

The particular form of the DOLS is not well known for most disordered materials. However, the experimental evidence leads to believe that in most inorganic non-crystalline materials, such as amorphous, polycrystalline or nanostructured semiconductors the localized states for electrons are distributed according to an exponential DOLS[3]

$$g(E) = \frac{N_l}{k_B T_0} \exp\left[-\frac{(E_c - E)}{k_B T_0}\right] \qquad (2.2)$$

where N_l is the total concentration of localized states in the band tail and $k_B T_0$ determines the mean energy of the distribution, which is believed to vary approximately between 0.025 and 0.1 eV, corresponding to characteristic temperatures, T_0, between 300 and 1100 K.

Analogously, there is wide agreement in considering that for organic materials the density of localized states follows a Gaussian distribution of site energies in accordance with the Gaussian dipole model[5,6]

$$g(E, E_1) = \frac{N_l}{\sqrt{2\pi}\sigma_1} \exp\left[-(E - E_1)^2 / 2\sigma_1{}^2\right] \qquad (2.3)$$
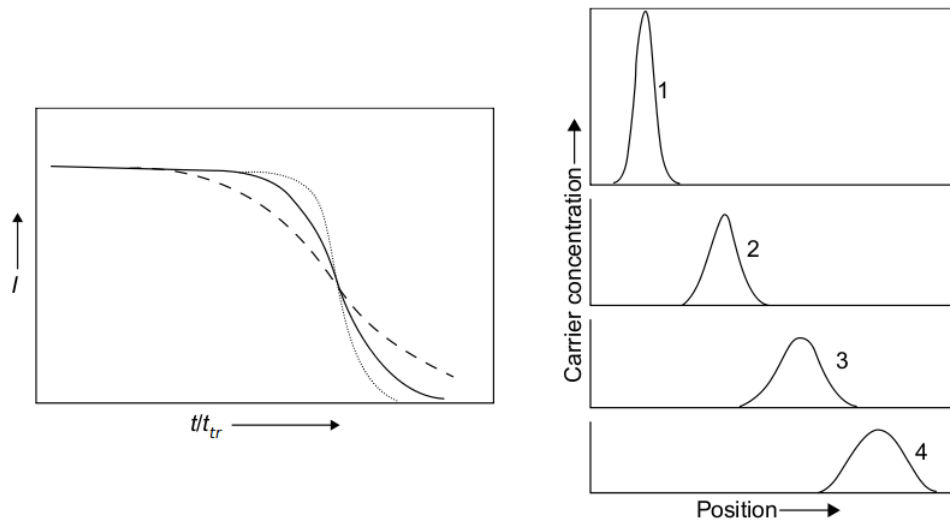
Fig. (2.3). Time dependence of photocurrent density $I(t)$ (left panel) and time evolution of the distribution of carriers (right panel) for the case of normal dispersive transport. Adapted from reference 4.

where E_1 is the centre of the distribution and σ_1 is the width.

The existence of an exponential distribution of localized states in the mobility gap of disordered inorganic materials is supported by the experimental observation of anomalous dispersive characteristics as obtained from transient photodecay techniques, such as time-of-flight experiments[3]. This technique allows to study the time dependence of the photocurrent density $I(t)$ following carrier excitation by means of a short pulse of illumination and then extract the dispersion of transit times for charge carriers. Conventional dispersion of the form of the left panel of Fig (2.3) is related to carriers that move exclusively in extended states. This dispersive characteristics, associated with random variations in the transit time of individual charge carriers, result from a Gaussian profile of a discrete packet of carriers that progressively becomes broader (Fig (2.3) right panel). Hence, this transport regime is often called *Gaussian transport*.

The behaviour exhibited in non-crystalline solids differs considerably. In this case, as it can be seen in the left panel of Fig. (2.4), the photocurrent appears to decrease continuously with increasing time over the whole time range of the measurement. In addition, the spread of arrival times of individual carriers at the electrode, reflected in the behaviour at times greater than t_{tr} is much greater than expected from conventional theory. Even at times greater than t_{tr} the magnitude of the current is such that it suggests that a significant number of carriers
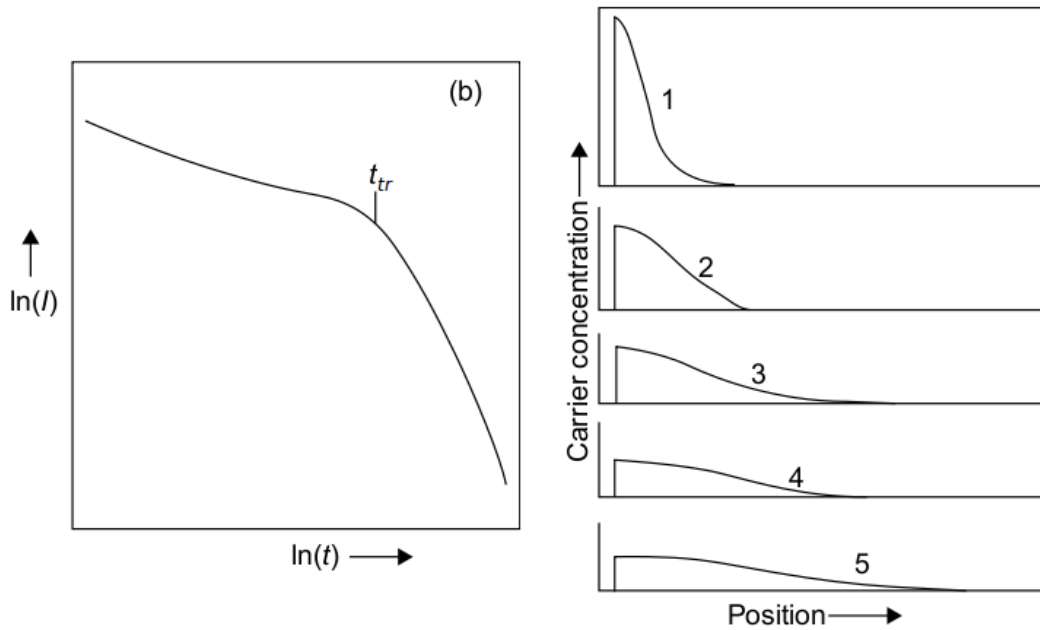
Fig. (2.4). Time dependence of photocurrent density $I(t)$ (left panel) on a double-logarithmic scale and time evolution of the distribution of carriers (right panel) for the case of anomalous dispersive transport. Adapted from reference 4.

remain within the system. Representation of the curve on a double-logarithmic scale (Fig. (2.4), left panel) involves two approximately linear regimes where it is possible to determine a time related to the change in the slopes (t_{tr}). Thus, one can describe both regimes of $I(t)$ in the form

$$I_1(t) \propto t^{-(1-\alpha_1)} \qquad (0 < t < t_{tr})$$

$$(2.4)$$

$$I_2(t) \propto t^{-(1+\alpha_2)} \qquad (t > t_{tr})$$

where α_1 and α_2 are smaller that unity and often identical.

In the right panel of Fig. (2.4) it is shown that the broadening is much more pronounced, and a significant number of carriers remain localized close to the top electrode even when other members of the distribution have approached or reached the extraction electrode. The observed dispersion of transit times was first explained by Scher and Montroll[7]. They suggested that the continuous random walk of a charge carrier could arise in a regime in which carriers would move only between localized states and, thus, would undergo successive

trapping events during their random walk. Afterwards, Pollak[8] showed that the broad dispersion of transient times could only be explained if there was in turn a broad energy dispersion of traps.

2.2. Charge transport in disordered semiconductors

In accordance with the energy bands model described in the previous section charge carrier transport in non-crystalline semiconductors can be possible either via extended states, via localized states states or a combination of both. The motion of charge carriers through one or other type of states depends on the temperature of the system. On the one hand, at sufficiently high temperatures (as compared with the characteristic temperature of the DOLS, T_0), a large number of electrons are found in extended states and hence, they dominate charge transport. In this case charge transport is similar to that of crystalline semiconductors. On the other hand, at lower temperatures, the concentration of electrons in extended states decreases exponentially so its contribution to transport decreases. Instead of this, tunnelling transitions of electrons between localized states with the assistance of phonons become significative. This regime is called *hopping transport* and it is known to occur in many applications of interest at working conditions.

2.2.1. Hopping transport

Charge conduction via tunnelling transitions between traps is produced at a range of temperatures where carriers are excited to intra-band gap localized states. At this point, a charge carrier jump from a localized state i to a lower in energy localized state j depends on the spatial separation r_{ij} between sites i and j as

$$\nu_{ij} \downarrow = \nu_0 \exp\left[-\left(\frac{2r_{ij}}{\alpha_l} \right) \right] \tag{2.5}$$

where we assume the localization radius, α_l, to be equal for sites i and j. The prefactor ν_0 is usually called the *attempt-to-jump frequency*. It is simply assumed to be of the order of the phonon frequency $\sim 10^{13}$ s^{-1}, although larger values of ν_0 are often necessary to adjust experimental data. Hence, this factor is frequently considered as a fitting parameter.

According to the hopping model when an electron performs a transition upward in energy from a localized state i to a localized state j higher in energy, the transition rate depends on the energy difference between the states. This difference has to be compensated, for example, by absorption of a phonon with the adequate energy.

$$\nu_{ij} \uparrow = \nu_0 \exp\left[-\left(\frac{2r_{ij}}{\alpha_l}\right)\right] \exp\left[-\left(\frac{E_j - E_i}{k_B T}\right)\right] \tag{2.6}$$

Both formulas (2.5) and (2.6) can be condensed in one:

$$\nu_{ij} \uparrow = \nu_0 \exp\left[-\left(\frac{2r_{ij}}{\alpha_l}\right)\right] \exp\left[-\left(\frac{E_j - E_i + |E_j - E_i|}{2k_B T}\right)\right] \tag{2.7}$$

This is the well-known *Miller-Abraham formula*[9] and was written for the case in which electron occupies site i whereas site j is empty. If the system is in thermal equilibrium, the occupation probabilities of sites with different energies are determined by the Fermi-Dirac statistics[3]. With the help of Eq. (2.7) the problem of the theoretical description of hopping conduction can be easily formulated and applied to a considerable amount of materials and devices, like new generation solar cells. The key issue is commonly to calculate the conductivity or the diffusion coefficient produced by transition events described by Eq. (2.7) for a given distribution of localized states.

Two limiting cases can be distinguished in hopping systems: nearest-neighbour hopping and variable-range hopping.

1. *Nearest-neighbour hopping* is produced when the states are strongly localized and the inequality $N_l\alpha_l{}^3 >> 1$ is fulfilled. In such case, hopping can be produced between nearest-neighbours provided that the temperature of the system is high enough. This type of transport takes place in many real systems. When nearest neighbour hopping is the dominant mechanism, transport is mainly determined by the spatial terms in Eq. (2.7). Therefore charge transport is extremely influenced by the average number of neighbouring sites and percolation effects has to be taken into account in order to determine transport properties.

2. *Variable-range hopping* is produced at low temperatures with respect to the characteristic temperature of the DOLS. In such case, nearest-neighbour hopping decreases and jumps
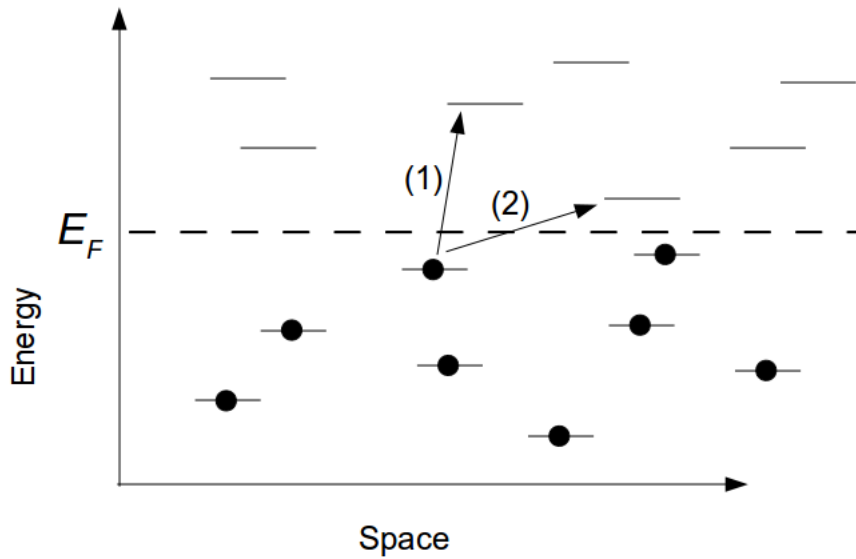
Fig. (2.5). Types of hopping transport between localized states. Transitions (1) and (2) correspond to nearest-neighbour hopping and variable-range hopping regimes respectively. Adapted from Figure (2.4) of reference 3.

between two sites with smaller energy differences become more probable. The most efficient transitions for transport in this regime are given between states with energies in the vicinity of the Fermi level, since only in this energy range filled and available states with close energies are found. The conductivity temperature dependence for this limiting case, given by Mott[10], is characterized by a $T^{-1/4}$ behaviour.

The transport energy concept

We will focus now on the exponential DOLS (Eq. (2.2)). In this case the concept of the *transport energy* is commonly useful. This is defined as a particular energy level below the mobility edge that maximizes the probability of upward transitions independently of its initial energy. Under some assumptions, it is useful to discriminate those localized states that effectively contribute to the transport from those that not.

The important role of the transport energy in an exponential DOLS was first pointed out by Grünewald and Thomas[11]. They came to the conclusion that the vicinity of some particular energy level dominates the hopping transport of electrons in the DOLS. In parallel, Monroe[12] showed that an electron, starting a relaxation process from the mobility edge, after
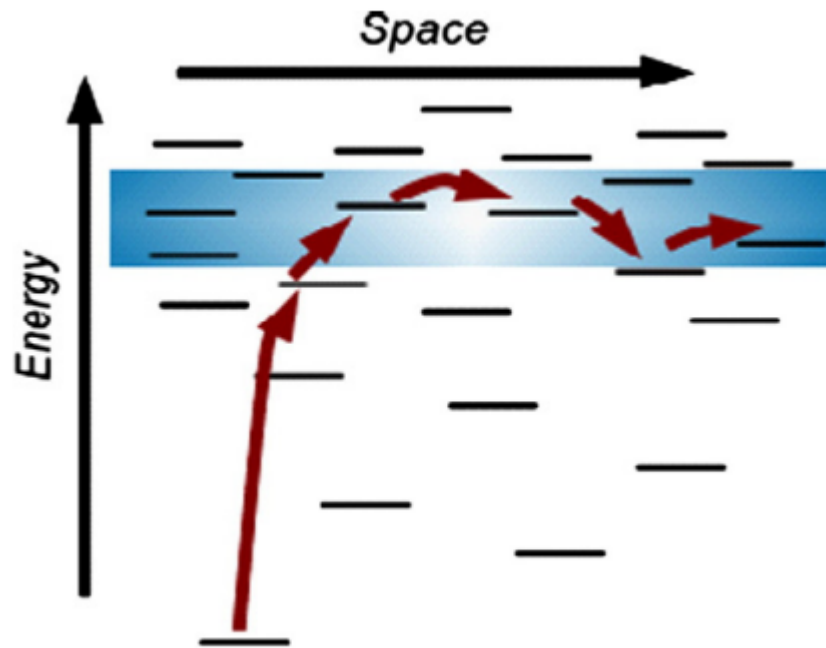
Fig. (2.6). Illustration of hopping conduction in the framework of an exponential DOLS. A hopping process via the transport energy (shown in blue) is produced.

making a series of hops downward in energy, changed its behaviour at some particular energy E_{tr}, which he called the *transport energy* and that was finally recognized to be the same energy level than that discovered by Grünewald and Thomas for equilibrium hopping transport.

The classic way of computing the transport energy can be obtained by considering the expression for upward hops in the presence of an exponential DOLS and then finding the energy difference δ which provides the fastest typical hopping rate for an electron placed initially at energy E_i. According to Eq. (2.6) the typical rate of an upward hop of a carrier with energy E_i can be expressed as

$$\nu_{ij} \uparrow (E_i, \delta) = \nu_0 \exp\left[-\left(\frac{2r(E_j)}{\alpha_l}\right)\right] \exp\left[-\left(\frac{\delta}{k_B T}\right)\right] \tag{2.8}$$

where $\delta = E_j - E_i$ and $r(E)$ is the average distance of traps for energies below E:

$$r(E) = \left[\frac{4\pi}{3} \int_{-\infty}^{E} dx g(x) \right]^{-1/3} \qquad (2.9)$$

So, the energy difference δ that provides the fastest typical hopping rate for an electron placed initially at energy E_i can be determined by the condition $\frac{d\nu_{ij}\uparrow(E_i,\delta)}{d\delta} = 0$. Using Eqs. (2.2) and (2.8) the maximum hopping rate is obtained as follows[13].

$$\delta = 3k_B T_0 ln \frac{3k_B T_0 (4\pi/3)^{1/3} N_l^{1/3} \alpha_l}{2k_B T} - E_i \qquad (2.10)$$

We see from Eq. (2.10) that the fastest hop occurs to a state with energy in the vicinity of the transport energy, independently of the initial E_i. The first term in the right-hand side of Eq. (2.10) determines the classical value of the transport energy E_{tr}

$$E_{tr} = 3k_B T_0 ln \frac{3k_B T_0 (4\pi/3)^{1/3} N_l^{1/3} \alpha_l}{2k_B T} \qquad (2.11)$$

An alternative derivation of the transport energy is due to Arkhipov and coworkers.[14,15] This procedure, which has been put into question by Baranoskii, is based on computing averages of the hopping frequencies expressed in Eq. (2.6) times the density of localized states over the whole energy spectrum. For energies well below the band tail, the averaging of Arkhipov proves to be independent of the starting site, and this leads to the definition of a transport energy that determines the behaviour of the mobility.

The concept of *effective* transport energy, in the definition of Arkhipov's theories, will be specially relevant in this thesis. The necessity of introducing this concept is easily understood if we consider that after an energetically upward jump into a hopping site, which belongs to the transport level, a carrier will make several downward jumps to different states from the starting one. However, as the target site is still a localized state it has only a few hopping neighbours accessible for the next jump. Therefore, the starting site can inevitably be one of those states, and it is quite possible that, after an upward jump, a carrier could return to the initially occupied deeper site contributing to neither transport nor energy relaxation. Therefore, Arkhipov and coworkers[14,15] argued that one must distinguish between the energy level onto which occur the most probable jumps from deeper traps (Baranovskii's thesis) and

the *effective* transport level, which is the one that will most probably draw the carrier away from the initially occupied state, avoiding backward jumps. We will show in Chapter 4 that this effective transport energy is the one that governs the behaviour of the mobility and the diffusion coefficient

2.2.2 Multiple-trapping model

When it is assumed that tunnelling transitions of carriers between localized states are less probable than transitions between localized and extended states then the carrier transport and energy relaxation can be easily described in the framework of the so-called *multiple-trapping model*. In this model, it is assumed that localized states do not contribute to the transport and carriers can move only via extended states above E_c. The role of localized states is then to slow down charge carriers by a succession of trapping-detrapping events.

One can express the release rate of an electron placed in a localized state with energy E as
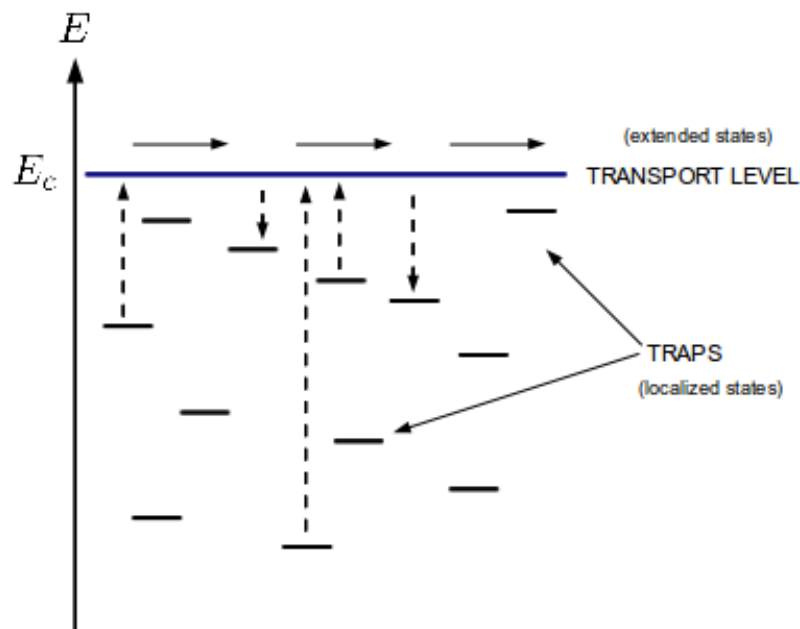
Fig. (2.7). Multiple-trapping mechanism of transport. Charges move through extended states but conduction is slowed down by successive trapping/detrapping events.

$$\nu(E) = \nu_0 \exp\left[(E_c - E)/k_B T\right] \qquad (2.12)$$

This model is widely used for interpretation of many transport properties in disordered semiconductors. In the context of the study of nanostructured materials used in novel devices, the question of whether multiple trapping approach can be applied is still opened[16,17]. One reason is that the particular morphology of this type of materials may prevent for the existence of extended states and therefore favour carrier jumps via localized states, according to hopping model. Anyway, it appears as a good approach in the sense that can explain, without the need of a more complex model, the characteristic *dispersive charge transport* that many disordered semiconductors exhibit and that appear in nanostructured solar cells, as we discussed above.

2.2.3. Electron diffusion coefficient in disordered media

In this section we describe the properties of the electron diffusion coefficient for activated transport in disordered materials. Experimental observations have demonstrated that values of the chemical diffusion coefficient in non-crystalline and nanocrystalline semiconductors lie several orders of magnitude below bulk (single crystal) values[18,19]. On the other hand, it is found that diffusion is strongly dependent on the electron density, with larger values found when the electron concentration is increased, either by illumination or by application of an external voltage[20–23]. This non-linear behaviour is caused by the fact that Fermi level moves in the band-gap as carriers density is increased so the cost of releasing a carrier to the transport level (either extended states or transport energy level) is significantly modified according to the occupation of the localized levels. This is the so-called *trap-filling effect*: as more electrons are added to the system, deep traps become filled and force electrons to move through shallower traps thereby enhancing charge transport.

In crystalline semiconductors, where electron transport only takes place in the conduction band, experimental information on the bulk diffusion is often derived by Fick's law, that relates the current density J_c to the gradient of the electron concentration.

$$J_c = -D_c \nabla n_c \qquad (2.13)$$

where n_c is the conduction band electron density and D_c is the conduction band electron
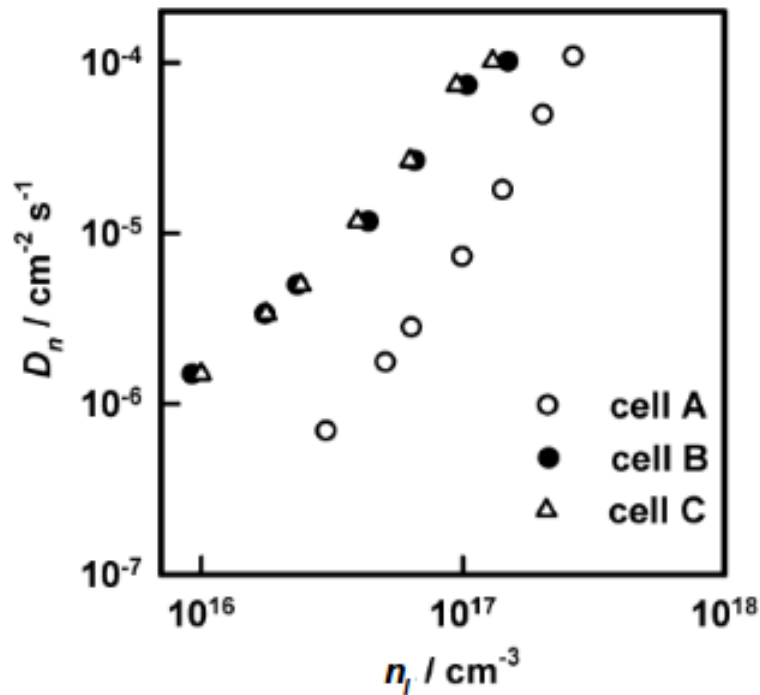
Fig. (2.8). Electron diffusion coefficient with respect localized electron density. Adapted from Fig. 6 of reference 25.

diffusion coefficient in the bulk (note that if there is drift component, this should be added to compute the total current density, as explained in Chapter 1, Eq. (1.6)). In contrast, in disordered semiconductors, where either hopping or multiple-trapping transport dominate diffusion, Eq. (2.13) is not valid, what makes more difficult to determine transport properties. Nevertheless, an analytical expression for the chemical diffusion coefficient of electrons in the presence of a distribution of localized states can be derived on the framework of the *multiple-trapping* model. Firstly, we state the equations of conservation for electron density in both extended and localized states assuming that are unmobile in localized states.

$$\frac{\partial n_c}{\partial t} = -\nabla J_c - r_c + r_r$$

$$\frac{\partial n_l}{\partial t} = r_c - r_r$$

(2.14)

where r_c and r_r are the rates of capture and release of traps respectively.

If we assume that free and trapped electrons maintain always a thermal quasi-

equilibrium even though the system is externally perturbed by, for example, a change in the illumination intensity, it is then possible to apply a model due to Bisquert and Vikhrenko[24]. In this formulation, the diffusion coefficient can be expressed as a function of the Fermi level, E_F. The model state a *quasi-static condition* by which free and trapped electrons maintain always an internal equilibrium. They have a common value of the Fermi level as long as a these particular evolution of the system is fulfilled

$$\frac{\partial n_l(t)}{\partial t} = \frac{\partial n_l}{\partial n_c} \frac{\partial n_c(t)}{\partial t} \tag{2.15}$$

where $\partial n_l / \partial n_c$ is a time-independent factor usually called *trapping factor* (δ_l). With these considerations, a complex problem of diffusion in the presence of trapping effects can be reduced to an effective Fick's law diffusion of electrons in the conduction band. Indeed, if we take into account Eqs. (2.14) and (2.15) we obtain the following expression

$$\frac{\partial n_c}{\partial t} \left(1 + \frac{\partial n_l}{\partial n_c} \right) = -\nabla J_c \tag{2.16}$$

So, we can reformulate Eq. (2.13) using an effective current density J_n

$$J_n = -D_n \nabla n_c \tag{2.17}$$

where the chemical diffusion coefficient D_n is defined as[24,26]

$$D_n = \left(1 + \frac{\partial n_l}{\partial n_c} \right)^{-1} D_c \tag{2.18}$$

If the approximation $\partial n_l / \partial n_c >> 1$ is fulfilled (what is accomplished in most of the cases in which there exist trapping effects in the dynamics) we obtain

$$D_n = \left(\frac{\partial n_c}{\partial n_l} \right) D_c \tag{2.19}$$

In a recent work[27] this equation has been used to construct a continuity equation for electrons in a DSC.

In this thesis it is important to make a distinction between the chemical diffusion coefficient, D_n, and the *jump diffusion coefficient D_j*. The former has already been defined as the diffusion of carriers as response to a change of the chemical potential in the disordered network. It is a *collective* quantity that depends on the overall carrier density (in fact it is commonly called the *collective diffusion coefficient* in Physical Chemistry textbooks). On the other hand, D_j is an individual property of the carrier, although it might be affected by interactions with other carriers. It is analogous to the self-diffusion coefficient normally utilized in Physical Chemistry. The jump diffusion coefficient is determined by the random walk of charge carriers by calculating the mean-squared displacement

$$< r^2(t) >= \frac{1}{N} \sum_{i=1}^{N} \left([x_i(t) - x_i(0)]^2 + [y_i(t) - y_i(0)]^2 + [z_i(t) - z_i(0)]^2\right) \qquad (2.20)$$

where x, y and z represent the absolute coordinates of the carriers and N is the total number of carriers. The relationship between these magnitudes is linear in *normal diffusion* processes. In these cases, the mean-squared displacement behaves as a linear function of time and the jump diffusion coefficient can be expressed as follows

$$D_J = \frac{1}{6t} < r^2(t) > \qquad (2.21)$$

In some cases, nevertheless, there is at first a given time during which the mean-squared displacement is not a linear function of time. When this occurs, the process is called *anomalous diffusion*[28] and Eq. (2.21) should be modified by introducing a power exponent which is usually smaller than unity.

The jump diffusion coefficient is the magnitude that actually can be computed by simulation and therefore it is essential for the results presented in this work. D_j is often expressed also as[29–31]

$$D_j =< \nu >< r^2 > \qquad (2.22)$$

in terms of a mean effective jump frequency $< \nu >$, and the square of effective jump length $< r^2 >$. This equation also takes a numerical prefactor of order 1 depending on the dimensionality. The relationship between chemical and jump diffusion coefficients is given by

the following expression[30,32]

$$D_n = \chi_n D_j \tag{2.23}$$

where χ_n is called the thermodynamic factor and it is found to be equal to[26]

$$\chi_n = \frac{n}{k_B T} \left(\frac{\partial n}{\partial E_F} \right)^{-1} \tag{2.24}$$

Actually, the definition of χ_n is often given in terms of the chemical potential, μ, so Eq. (2.24) is only valid if we assume that the conduction band position is not modified by a displacement of the Fermi level and therefore $\partial \mu = \partial E_F$. Note that in Eq. (2.24), n is the total electron density ($n_c + n_l$) and can be determined by integration

$$n = \int_{-\infty}^{\infty} g(E) f(E - E_F) dE \tag{2.25}$$

where $f(E - E_F)$ is the occupation probability and is given by the Fermi-Dirac distribution

$$f(E - E_F) == \frac{1}{1 + \exp\left[\frac{E - E_F}{k_B T} \right]} \tag{2.26}$$

Diffusion coefficient in exponential DOLS

In the following an analytical expression for the chemical diffusion coefficient will be derived considering a system with an exponential DOLS given by Eq. (2.2). We will proceed by calculating the trapping factor $\delta_l = \partial n_l / \partial n_c$ in Eq. (2.19). First of all, from Eqs. (2.25) and (2.26) we can compute the total electron density with respect to the Fermi level for this particular distribution

$$n = \int_{-\infty}^{\infty} g(E) f(E - E_F) dE = \int_{-\infty}^{E_F} g(E) dE = \int_{-\infty}^{E_F} \frac{N_l}{k_B T_0} \exp\left[\frac{E_F - E_c}{k_B T_0} \right] =$$

$$= N_l \exp\left[\frac{E_F - E_c}{k_B T_0}\right]$$

where we have used the zero-temperature limit of the Fermi-Dirac distribution. This equation shows that the total density is an exponentially increasing function of the Fermi level. Now, we can state that in the context of the multiple-trapping model, $n_l >> n_c$, and therefore $n \simeq n_l$. Hence we can use an expression for the density of localized states as a function of the Fermi level

$$n_l = N_l \exp\left[\frac{E_F - E_c}{k_B T_0}\right] = N_l \exp\left[\frac{\alpha\left(E_F - E_c\right)}{k_B T}\right] \tag{2.27}$$

where we have used $\alpha = T/T_0$ for the second equality. On the other hand we can assume that the density of free electrons can be well described by Boltzmann statistics provided that $E_c - E_F >> k_B T$ (Fermi level well below the transport level)

$$n_c = N_c \exp\left[\frac{\left(E_F - E_c\right)}{k_B T}\right] \tag{2.28}$$

where N_c is the effective density of states of electrons in the conduction band.

We are interested in determining the trapping factor as a function of both the Fermi level and the density. For the latter, we continue by calculating the localized electron density derivative from Eq. (2.27).

$$\frac{\partial n_l}{\partial E_F} = \frac{N_l}{k_B T_0} \exp\left[\frac{E_F - E_c}{k_B T_0}\right] \tag{2.29}$$

We obtain the DOLS at the Fermi level (see Eq. (2.2)). Similarly, from Eq. (2.28), the conduction band electron density derivative with respect to the Fermi level takes the form

$$\frac{\partial n_c}{\partial E_F} = \frac{N_c}{k_B T} \exp\left[\frac{E_F - E_c}{k_B T}\right] \tag{2.30}$$

And then, from Eqs. (2.29) and (2.30)

$$\frac{\partial n_c}{\partial n_l} = \frac{N_c T_0}{N_l T} \exp\left[(E_F - E_c)\left(\frac{1}{k_B T} - \frac{1}{k_B T_0}\right)\right] \tag{2.31}$$

The inverse of last equation can be derived directly if we take into account the two expressions for the free and localized electron density. Thus, from Eqs. (2.27) and (2.28)

$$n_l = \frac{N_l}{N_c^\alpha} n_c^\alpha \tag{2.32}$$

and then, one obtains by differentiatting Eq. (2.32)

$$\frac{\partial n_l}{\partial n_c} = \frac{\alpha N_l}{N_c^\alpha} n_c^{\alpha-1} \tag{2.33}$$

With these considerations, alternative analytical expressions for the chemical diffusion coefficient D_n, as a function of the Fermi level and the electron density can be finally obtained. On the one hand, taking into account Eqs. (2.19) and (2.31), we obtain a first expression in terms of the Fermi level, which takes the form[33]

$$D_n = \frac{N_c T_0}{N_l T} \exp\left[(E_F - E_c)\left(\frac{1}{k_B T} - \frac{1}{k_B T_0}\right)\right] D_c \tag{2.34}$$

On the other hand, considering again that $n \simeq n_l$, the following expression for D_n can be inferred from Eqs. (2.19) and (2.33)

$$D_n = \frac{N_c}{\alpha N_l^{\frac{1}{\alpha}}} n^{\frac{1-\alpha}{\alpha}} D_c \tag{2.35}$$

This is an important relation, as the total density is an experimentally accessible quantity. Anyway, from this equation, one can also obtain an expression for D_n as a function of the density of electrons in the extended states n_c. We just must take into account Eqs. (2.32) and (2.35) and use again that $n \simeq n_l$

$$D_n = \frac{N_c^\alpha}{\alpha N_l} n_c^{1-\alpha} D_c \tag{2.36}$$

Now, It is convenient to obtain an analytical expression for the jump diffusion coefficient D_j, as it is the quantity that we will be determined numerically by simulation. For that purpose, we have to determine first the form of the thermodynamic factor for an exponential distribution. Thus, considering again that $n \simeq n_l$, we can conclude from Eqs. (2.24) and (2.29) that χ_n is constant for an exponential DOLS and takes the form

$$\chi_n = \frac{T_0}{T} \tag{2.37}$$

Hence, according to Eqs (2.23), the jump diffusion coefficient D_j as a function of the Fermi is[21]

$$D_j = \frac{N_c}{N_l} \exp\left[(E_F - E_c)\left(\frac{1}{k_B T} - \frac{1}{k_B T_0} \right) \right] D_c \tag{2.38}$$

The concepts introduced for the multiple trapping model can be easily extended to any approach, like hopping transport. As we discussed before, the theory of diffusion often allows to separate the kinetic or jump diffusion coefficient in two factors, according to Eq. (2.22). With the help of the transport energy concept, Eq. (2.22) provides a useful approach to obtain analytical expressions for hopping transport as a function of Fermi level. Thus, introducing the classical value for the transport energy and taking into account Eqs (2.2) and (2.22) the jump diffusion coefficient as a function of the Fermi level can be calculated using[32,34]

$$D_j{}^H = \frac{9T_0^2}{4T^2}(1 - \frac{T}{T_0}) \exp\left[-3\frac{T_0}{T} - (E_{tr} - E_F)\left(\frac{1}{k_B T} - \frac{1}{k_B T_0} \right) \right] \alpha_l{}^2 \nu_0 \tag{2.39}$$

We see that this theoretical expression predicts an exponential behaviour with respect to the Fermi energy, in analogy with the multiple-trapping result as long as the transport energy can be considered constant. In the context of a DSC, the Fermi level dependence of the diffusion coefficient predicted by both Eq. (2.38) and (2.39) is observed experimentally. Therefore, further investigation is needed to establish which is the actual transport mechanism involved in these devices. In Chapter 4 this issue will be analysed in detail.

2.3. Recombination in disordered semiconductors

Recombination via intra-band localized states is the most common charge loss mechanism in disordered semiconductors. We presented in Chapter 1 the rate corresponding to SRH recombination in the presence of a single localized state (see Eq. (1.9)). The description of a recombination model when a quasi-continuous distribution of traps is involved is however a more complex problem. In this regard, it is useful to make a distinction between different traps according to whether a trap can adopt or not the role of a *recombination centre*. Thus, a trap will be act as a recombination centre when the rate for the capture of a carrier with the opposite polarity is comparable or larger than the release rate by thermal activation (*multiple-trapping or hopping model*). The so-called *demarcation levels*, defined by those energies at which both rates are equal, have been widely used for modelling of recombination mechanisms in disordered semiconductors[4,35]. Since release rates decrease as traps move further away from the mobility edges, electrons and holes situated between their respective demarcation levels, $E_{d,n}$ and $E_{d,p}$, would have a higher probability of recombination than that of release from their traps. As a consequence, there is a gap, between $E_{d,n}$ and $E_{d,p}$, where traps effectively act as recombination centres and recombination takes place with a larger rate.

These concepts, defined in general for trap-assisted recombination, actually depend on the properties of the particular system considered. Therefore, specific recombination models have to be formulated. A widely used recombination model for disordered semiconductors is a distance-dependent radiative recombination mechanism via localized states. This model is connected with the previous description and assumes that the creation of an electron-hole pair is immediately followed by a trapping of both charges by localized states placed in the mobility gap. Hence, if both charges are located between demarcation levels they can undergo recombination from these states with a transition rate given by the following expression[3]

$$\nu_r(R) = \tau_{r0}^{-1} \exp\left(-\frac{2R_{np}}{\alpha_l}\right) \tag{2.40}$$

where the prefactor is of the order of the typical dipole radiative rate $\sim 10^8 \ s^{-1}$ and R_{np} is the electron-hole pair separation. Note the analogy of Eq. (2.40) with the hopping model of Eq. (2.5).

Another classification of localized states can be made in terms of their different type of

involvement in transport and recombination events. In the one hand, we can define *shallow states* as those traps characterized by very small ionization energies (in the order of phonon energies). On the other hand, we call *deep states* those having much higher ionization energies where capture of carriers usually involve multiphonon transitions. At room temperatures, from a statistic point of view, whereas electrons and holes trapped in shallow traps are reemitted with high probabilities into delocalized states, charges located in deep traps are not released easily so spend much more time immobile. Moreover, shallow states are often empty traps located close to the mobility edges while deep traps are located below the Fermi levels (above in the case of holes). As we will see in Chapter 6, both types of traps can act as recombination centres in some disordered heterogeneous systems.

2.3.1. Recombination in dye-sensitized solar cells

It is widely reported in a DSC that τ_n decreases as illumination intensity or forward bias is increased[36]. This behaviour has been related to a progressive filling of traps in the nanostructured semiconductor as the light intensity is augmented. In this sense, an expression for the effective electron lifetime was proposed in relation with the free electron lifetime τ_c, that is, the lifetime in the absence of traps[37].

$$\tau_n = \tau_c \left(1 + \frac{\partial n_l}{\partial n_c} \right) \tag{2.41}$$

Eq. (2.41) is derived within a model that assumes the rate of recombination depends linearly on the free electron density[37]. In addition, it is assumed that capture and release rates are much faster than response times in typical experiments[24] (quasi-static approximation). In the case in which $\partial n_l / \partial n_c >> 1$, Eq. (2.41) adopts the form

$$\tau_n = \tau_c \left(\frac{\partial n_l}{\partial n_c} \right) \tag{2.42}$$

Thus, as the trapping factor $\delta_l = \partial n_l / \partial n_c$ is positive and larger than unity, we can observe that the resulting electron lifetime τ_n becomes larger that τ_c, what is intuitive in the sense that trapping effects reduce the probability of recombination in extended states.
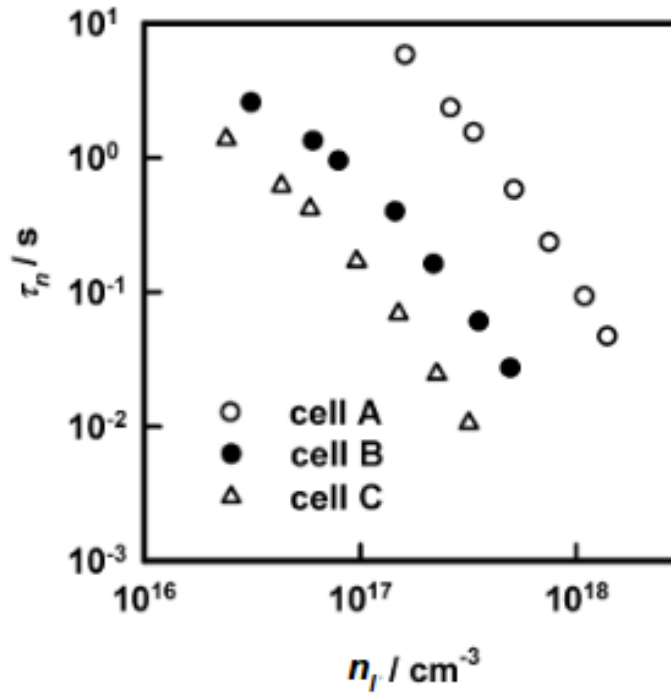
Fig. (2.9). Electron lifetime as a function of localized electron density. Adapted from Fig. 6 of reference 25

Assuming now that the DOLS in the TiO$_2$ has an exponential function as described in Eq. (2.2) the following expression can easily be derived from Eq (2.33)[24].

$$\tau_n = \frac{\alpha N_l}{N_c^\alpha} n_c^{\alpha-1} \tau_c \qquad (2.43)$$

Hence, one obtains a power law with respect to the free electron density. As for the electron diffusion coefficient, the electron lifetime can be expressed in terms of the total density. Indeed, taking into account Eq. (2.32) (and bearing in mind again that $n \simeq n_l$) the following relation is easily derived.

$$\tau_n = \frac{\alpha N_l^{\frac{1}{\alpha}}}{N_c} n^{\frac{\alpha-1}{\alpha}} \tau_c \qquad (2.44)$$

Again, a power law with respect the total density is derived, as normally found in the experiments[37].

An equivalent circuit corresponding to the main processes of a DSC is often utilized[38]. In this context, the concept of *recombination resistance R_{rec}* is usually introduced

$$R_{rec} = \frac{1}{qLA}\left(\frac{\partial U_{rec}}{\partial E_F}\right)^{-1} \tag{2.45}$$

where U_{rec} is the recombination rate, L is the thickness of the film and A is the cell surface area. If we assume that recombination rate is linear with respect to the free electron density, that is, $U_{rec} = k_r n_c$, then the recombination resistance adopts the following form

$$R_{rec} = R_0 \exp\left[-\frac{(E_F - E_{redox})}{k_B T}\right] \tag{2.46}$$

where E_{redox} is the *redox* potential of the acceptor species in solution and R_0 is the recombination resistance of a DSC in absence of illumination ($E_F = E_{redox}$). Note that to derive Eq. (2.46) we have used the following relation between the free electron concentration and the photovoltage, $V = q\,(E_F - E_{redox})$

$$n_c = n_0 \exp\left[\frac{(E_F - E_{redox})}{k_B T}\right] \tag{2.47}$$

being n_0 the electron density in the dark (see Eq. (2.28).

Eq. (2.46) describes the same effect than that of the electron lifetime, this is, the recombination resistance decreases as electron density increases, what augments the recombination rate. However, although the same dependences are observed in measurements of a DSC, recombination resistance curves with respect to the voltage usually show slopes different from the thermal voltage $k_B T/q$:

$$R_{rec} = R_0 \exp\left[-\frac{\beta\,(E_F - E_{redox})}{k_B T}\right] \tag{2.48}$$

where β is a dimensionless parameter. Values of β obtained from impedance measurements in a typical DSC are in the order of 0.5–0.7[39,40], meaning that the recombination rate is not simply proportional to the conduction band electron density but expressed as

$$U_n = k_r n_c^{\beta} \tag{2.49}$$

where k_r is a kinetic constant with units of $cm^{-3(1-\beta)} \, s^{-1}$. This non-linear behaviour of the recombination rate with respect to the conduction band electron density has been related to the fact that, as well as recombination through extended states, other channels of recombination are present in parallel in a DSC, for example direct charge transfer of electrons from a distribution of localized states close to the interface. Specifically, it has been proposed a charge transfer mechanism[39,41] from an *exponential* distribution of surface states in the oxide $g_s(E)$, given by Eq. (2.2). The model also assumes that the probability of electron transfer at the energy level E in the oxide to the distribution of acceptor species in the electrolyte is governed by the *Marcus-Gerischer* model[42] and takes the form[43]

$$\nu_{rec}(E) = k_0 \frac{2ck_BT}{\sqrt{4\pi\lambda k_BT}} \exp\left[-\frac{(E - E_{redox} - \lambda)^2}{4\lambda k_BT}\right] \tag{2.50}$$

where k_0 is a time constant for tunnelling, which is dependent on the distance of the acceptor to the surface and c the concentration of oxidized species in the electrolyte. The parameter λ represents the outer sphere *reorganization energy*, that is the activation energy for the process of transferring the solvation shell structure from equilibrium condition of the oxidized species to the most probable structure of the reduced species (or viceversa). This parameter is equal for both reduced and oxidized species so that

$$E_{redox} = E_{ox} - \lambda = E_{red} + \lambda \tag{2.51}$$

where E_{ox} and E_{red} are the most probable energies for the unoccupied and occupied states in solution, respectively (see Fig. (2.10)). An expression for the outer sphere reorganization of a redox-active ion at a semiconducting electrode can be calculated by the expression[44,45]

$$\lambda = \frac{e^2}{8\pi\epsilon_0}\left[\frac{1}{r}\left(\frac{1}{n_s^2} - \frac{1}{\epsilon_s}\right) - \frac{1}{2R}\left(\frac{n_{el}^2 - n_s^2}{n_{el}^2 + n_s^2}\frac{1}{n_s^2} - \frac{n_{el}^2 - \epsilon_s^2}{n_{el}^2 + \epsilon_s^2}\frac{1}{\epsilon_s^2}\right)\right] \tag{2.52}$$

where ϵ_0 is the vacuum permittivity, r is the radius of molecules, R the distance between the electrolyte and the electrode, n_s and ϵ_s are the refractive index and the static dielectric constant of the solvent, respectively and n_{el} and ϵ_{el} the dielectric constants of the electrode material (n_{el} = 2.5 and ϵ_{el} = 86 for anatase TiO$_2$).
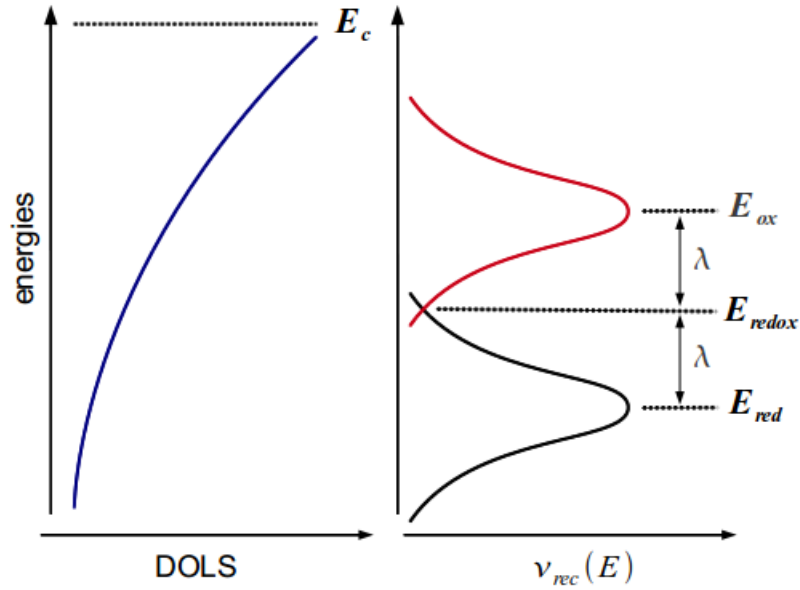
Fig. (2.10). Diagram illustrating the exponential distribution of donor states in the oxide and the Marcus-Gerischer transfer probability to the electrolyte.

Thus, in terms of this new charge transfer mechanism, the recombination rate can be calculated as[45]

$$U_{rec} = \int_{E_{redox}}^{E_c} g_s(E)f(E - E_F)\nu_{rec}(E)dE \tag{2.53}$$

The corresponding expression of the recombination resistance from Eq. (2.53) is then[41,43].

$$R_{rec}(E_F) = R_0' \exp\left[\frac{(E_F - E_{redox} - \lambda)^2}{4\lambda k_B T} - \frac{E_F - E_c}{k_B T_0}\right] \tag{2.54}$$

where R'_0 is a constant. After a mathematical treatment and under the approximations $E_F << \lambda$ and $E_F << \lambda(1 + 2\alpha)$ one obtains

$$R_{rec}(E_F) = R_0'' \exp\left[-\beta \frac{(E_F - E_{redox})}{k_B T}\right] \tag{2.55}$$

with

$$\beta = \frac{1}{2} + \alpha \tag{2.56}$$

so we obtain the same dependence of the recombination resistance than that given by Eq. (2.48). In this model, the recombination resistance decreases exponentially as a consequence of an increase of both density of donor states (Eq. (2.2)) and charge transfer probability ν_{rec} due to an increasing voltage. It is important to remark that eventually ν_{rec} may decrease at higher voltage, provided that Marcus inverted region is reached. In this situation Eq. (2.55) is not longer valid and we should use Eq. (2.54). In Chapter 6 we will use RWNS to describe recombination kinetics in a more general situation without approximations.

2.3.2. Diffusion length concept

Diffusion length was firstly introduced by Amaldi and Fermi in 1936 in the context of neutron diffusion in paraffin samples as the distance that "a neutron will diffuse before it gets captured by a proton"[46]. The diffusion length appears in the solution of the 1-D diffusion equation with a single recombination term governed by a certain lifetime τ_n. The solution of this equation is exponential, with the diffusion length occurring in the exponent: $\exp(-x/L_n)$. L_n is also the first moment of the probability distribution function, which shows that this parameter corresponds to the average value of the distance traveled by the particles before they disappear by recombination.

In the context of electron transport, L_n is a crucial parameter for any system in which diffusion is the main transport mechanism. For instance, it is widely utilized in DSCs. The diffusion length is commonly determined by independent measurements of the electron diffusion coefficient D_n and the electron lifetime τ_n, according to[47]

$$L_n = \sqrt{D_n \tau_n} \tag{2.57}$$

It is well-known that, in contrast to both electron diffusion coefficient and lifetime,

whose values cover a wide range of order of magnitudes with an increasing density, diffusion length values are usually maintained in the same order of magnitude. In the context of previous models, we can see from Eqs. (2.19) and (2.42) that there is a compensation effect when the diffusion length is calculated. Thus, electron diffusion length of Eq. (2.57) adopts the following form

$$L_n = \sqrt{D_c \tau_c} \qquad (2.58)$$

which is constant with electron density. Similarly, for the case of an exponential distribution of states, applying Eqs. (2.36) and (2.43) a constant diffusion length is again obtained due to the fact that the same factor lies in carrier equilibration for both chemical diffusion coefficient (D_n) and lifetime (τ_n)[24]. A more intuitive explanation of this compensation behaviour is based on the assumption that recombination is transport-limited[48–50] so that the recombination constant (the inverse of the lifetime) should be proportional to the diffusion coefficient. This implies that the product contained in Eq. (2.58) should remain constant upon variations of the Fermi level since diffusion and recombination have exactly the same Fermi level dependence. In other words, if the system diffuses more quickly it also recombines more quickly, so that the diffusion length remains constant.

However, increasing diffusion lengths with respect to the Fermi level have been reported in recent experiments in DSCs[43,51]. To solve this problem a reinterpretation of Eq. (2.41) has been made in terms of the *effective free electron* lifetime, τ_f [39,52]

$$\tau_n = \tau_f \left(1 + \frac{\partial n_l}{\partial n_c} \right) \qquad (2.59)$$

where τ_f is calculated taking into account the non-linear recombination rate given by Eq. (2.49)[39,52]

$$\tau_f = \frac{n_0^{1-\beta}}{\beta k_r} \exp \left[\frac{1-\beta}{k_B T} \left(E_F - E_{redox} \right) \right] \qquad (2.60)$$

Hence, Eqs. (2.59) and (2.60) lead to a Fermi level dependence of the electron lifetime τ_n given by[39]

$$\tau_n \sim \exp\left[(\alpha - \beta)\,\frac{qV_F}{k_BT}\right] \tag{2.61}$$

which predicts an increase of τ_n with respect to the free electron density but with an slope different than that given by Eq. (2.43).

With these new expressions it can be seen that factors in Eqs. (2.34) and Eq. (2.61) do not compensate so Eq. (2.57) leads to a non-constant diffusion length with respect to the Fermi level, given by[39]

$$L_n \sim \exp\left[\left(\frac{1-\beta}{2}\right)\left(\frac{E_F - E_{redox}}{k_BT}\right)\right] \tag{2.62}$$

In a recent paper it has been pointed out that the diffusion length, defined as the average value of the distance travelled by electrons until a recombination event occurs, is equivalent to the diffusion length obtained via Eq. (2.57) using a D_n and a τ_n obtained by small perturbation methods[52].

References to Chapter 2

(1)   Popov, A. *Disordered Semiconductors: Physics and Applications*; Pan Stanford Publishing Pte. Ltd., **2011**.

(2)   Anderson, P. W. *Phys. Rev.* **1958**, *109*, 1492–1505.

(3)   *Charge Transport in Disordered Solids with Applications to Electronics*; Baranovskii, S. D., Ed.; Wiley: Weinheim, **2006**.

(4)   Mikla, V. V.; Mikla, V. I. *Trap Level Spectroscopy in Amorphous Semiconductors*; **2010**.

(5)   Bassler, H. *Physica Status Solidi B-Basic Research* **1993**, *175*, 15–56.

(6)   Tessler, N.; Preezant, Y.; Rappaport, N.; Roichman, Y. *Advanced Materials* **2009**, *21*, 2741–2761.

(7)   Scher, H.; Montroll, E. W. *Physical Review B* **1975**, *12*, 2455–2477.

(8)   Pollak, M. *Philosophical Magazine B-Physics of Condensed Matter Statistical Mechanics Electronic Optical and Magnetic Properties* **1977**, *36*, 1157.

(9)   Miller, A.; Abrahams, E. *Physical Review* **1960**, *120*, 745–755.

(10)   Mott, N. F.; Davis, E. A. *Electronic processes in non-crystalline materials.*; Clarendon Press.; Oxford, **1979**.

(11)   Grünewald, M.; Thomas, P. *Physica Status Solidi (b)* **1979**, *94*, 125–133.

(12)   Monroe, D. *Physical Review Letters* **1985**, *54*, 146–149.

(13)   Baranovskii, S. D.; Thomas, P.; Adriaenssens, G. J. *Journal of Non-Crystalline Solids* **1995**, *190*, 283–287.

(14)   Arkhipov, V. I.; Emelianova, E. V.; Adriaenssens, G. J. *Physical Review B* **2001**, *6412*.

(15)   Arkhipov, V. I.; Heremans, P.; Emelianova, E. V.; Adriaenssens, G. J.; Bassler, H. *Journal of Physics-Condensed Matter* **2002**, *14*, 9899–9911.

(16)   Kopidakis, N.; Benkstein, K. D.; Lagemaat, J. van de; Frank, A. J.; Yuan, Q.; Schiff, E. A. *Physical Review B* **2006**, *73*.

(17)   Hagfeldt, A.; Boschloo, G.; Sun, L.; Kloo, L.; Pettersson, H. *Chemical Reviews* **2010**, *110*, 6595–6663.

(18)   Tiwana, P.; Docampo, P.; Johnston, M. B.; Snaith, H. J.; Herz, L. M. *ACS Nano* **2011**, *5*, 5158–5166.

(19)   Peter, L. M.; Dunn, H. K. *The Journal of Physical Chemistry C* **2009**, *113*, 4726–4731.

(20)   Vanmaekelbergh, D.; de Jongh, P. E. *Phys. Rev. B* **2000**, *61*, 4699–4704.

(21)   Anta, J. A.; Mora-Sero, I.; Dittrich, T.; Bisquert, J. *Physical Chemistry Chemical Physics* **2008**, *10*, 4478–4485.

(22)   Nelson, J.; Chandler, R. E. *Coordination Chemistry Reviews* **2004**, *248*, 1181–1194.

(23)   Cao, F.; Oskam, G.; Meyer, G. J.; Searson, P. C. *Journal of Physical Chemistry* **1996**, *100*, 17021–17027.

(24)   Bisquert, J.; Vikhrenko, V. S. *Journal of Physical Chemistry B* **2004**, *108*, 2313–2322.

(25)   Wang, H.; Peter, L. M. *The Journal of Physical Chemistry C* **2009**, *113*, 18125–18133.

(26)   Bisquert, J. *Journal of Physical Chemistry B* **2004**, *108*, 2323–2332.

(27)   Anta, J. A.; Idígoras, J.; Guillén, E.; Villanueva-Cab, J.; Mandujano-Ramirez, H. J.; Oskam, G.; Pelleja, L.; Palomares, E. J. *Physical Chemistry Chemical Physics* **2012,** DOI: 10.1039/c2cp40719a.

(28)   Metzler, R.; Barkai, E.; Klafter, J. *Physical Review Letters* **1999**, *82*, 3563–3567.

(29)   Reed, D. A.; Ehrlich, G. *Surface Science* **1981**, *102*, 588–609.

(30)   Gomer, R. *Rep. Prog. Phys.* **1990**, *53*, 917–1002.

(31)   Myshlyavtsev, A. V.; Stepanov, A. A.; Uebing, C.; Zhdanov, V. P. *Phys. Rev. B* **1995**, *52*, 5977–5984.

(32)   Bisquert, J. *Physical Chemistry Chemical Physics* **2008**, *10*, 1–20.

(33)   Bisquert, J. *Physical Chemistry Chemical Physics* **2008**, *10*, 49–72.

(34)   Bisquert, J. *Journal of Physical Chemistry C* **2007**, *111*, 17163–17168.

(35)   Bisquert, J.; Zaban, A.; Salvador, P. *Journal of Physical Chemistry B* **2002**, *106*, 8774–8782.

(36)   Peter, L. M. *Journal of Physical Chemistry C* **2007**, *111*, 6601–6612.

(37)   Zaban, A.; Greenshtein, M.; Bisquert, J. *Chemphyschem* **2003**, *4*, 859–864.

(38)   Fabregat-Santiago, F.; Bisquert, J.; Cevey, L.; Chen, P.; Wang, M.; Zakeeruddin, S. M.; Grätzel, M. *Journal of the American Chemical Society* **2009**, *131*, 558–562.

(39)   Bisquert, J.; Fabregat-Santiago, F.; Mora-Seró, I.; Garcia-Belmonte, G.; Giménez, S. *The Journal of Physical Chemistry C* **2009**, *113*, 17278–17290.

(40)   Guillén, E.; Peter, L. M.; Anta, J. A. *J. Phys. Chem. C* **2011**, *115*, 22622–22632.

(41)   *Dye-sensitized solar cells*; Kalyanasundaram, K., Ed.; EFPL Press, **2010**.

(42)   Marcus, R. A. *The Journal of Chemical Physics* **1965**, *43*, 679–701.

(43)   Wang, Q.; Ito, S.; Gratzel, M.; Fabregat-Santiago, F.; Mora-Sero, I.; Bisquert, J.; Bessho, T.; Imai, H. *Journal of Physical Chemistry B* **2006**, *110*, 25210–25221.

(44)   Kuciauskas, D.; Freund, M. S.; Gray, H. B.; Winkler, J. R.; Lewis, N. S. *The Journal of Physical Chemistry B* **2001**, *105*, 392–403.

(45)   Ondersma, J. W.; Hamann, T. W. *Journal of the American Chemical Society* **2011**, *133*, 8264–8271.

(46)   Amaldi, E.; Fermi, E. *Physical Review* **1936**, *50*, 899.

(47)   Harrick, N. J. *Journal of Applied Physics* **1956**, *27*, 1439.

(48)   Nelson, J.; Haque, S. A.; Klug, D. R.; Durrant, J. R. *Physical Review B* **2001**, *63*, 6320.

(49)   Kopidakis, N.; Benkstein, K. D.; Lagemaat, J. van de; Frank, A. J. *Journal of Physical Chemistry B* **2003**, *107*, 11307–11315.

(50)   Anta, J. A.; Casanueva, F.; Oskam, G. *Journal of Physical Chemistry B* **2006**, *110*, 5372–5378.

(51)   Jennings, J. R.; Li, F.; Wang, Q. *The Journal of Physical Chemistry C* **2010**, *114*, 14665–14674.

(52)   Bisquert, J.; Mora-Seró, I. *The Journal of Physical Chemistry Letters* **2010**, *1*, 450–456.

CHAPTER 3

Random Walk Numerical Simulation

The Random Walk Numerical Simulation (RWNS) method is presented in this Chapter. We firstly review the most relevant studies that have been carried out by means of the RW method. Later on, we describe in detail the basic functioning of the RW algorithm. The advantages of using RWNS to study disordered semiconductors with a broad dispersion of energies are discussed. We provide details of the most important properties of the simulation method and relate then to the dynamic models discussed in Chapter 2. The specific boundary conditions utilized in the calculations are also described. Finally, we describe the main properties that can be obtained from the calculations. Thus, extraction of energy level populations as well as dynamics properties, like the diffusion coefficient, the lifetime and the diffusion length are outlined.

3. Random Walk Numerical Simulation

3.1. Simulation and modelling

The use of electronic computing machines as a valuable method of research is well established. Its benefits are to gain insight in the internal mechanisms, which are not available to measurements, and therefore to enable interpretation of them. In addition, simulation and modelling provide information for improvements in device applications suggesting proper strategies. The recent rapid progress of performance of computers has allowed an inexpensive way to research in this direction. Among other techniques, the Monte Carlo method, based on the massive generation of random numbers, has been extensively applied in Condensed-Matter Physics and Theoretical Chemistry.[1] The Monte Carlo method provides a way to replace the solution to a particularly difficult analytical or numerical problem by proposing a suitable algorithm based in random numbers. This algorithm is then fed to a computer so that the difficult numerical work is done by the machine and valuable physical information can be obtained as a results of a thorough analysis.

Current research on new architectures for low-cost photovoltaic devices based on disordered materials and the boom in nanotechnology provides new exciting fields in which to apply computer simulation methods. An useful route to study the carrier transport in these photovoltaic systems is to use *random walk numerical simulation* (RWNS), a type of Monte Carlo simulation. It is useful for those cases in which one is interested in geometrical details of disordered semiconductors, for example, in the influence of a particular morphology on transport and recombination magnitudes. Likewise, it is specially suitable to study characteristics of materials from first principles in amorphous or nanostructured semiconductors. The main reason consist on the fact that RWNS allows, without huge computational demands, for a flexible description of randomly localized states with a broad dispersion in energies, what is crucial for the understanding of the transport and recombination in these devices, in the long time and spatial scales.

The use of RW methods to study charge transport in disordered materials goes back to the early eighties, mainly due to the works of Movaghar, Bässler, Baranovskii and coworkers[2–5] who used this simulation technique to test the validity of analytical results to describe hopping and trapping processes. The famous 1993 work of Bässler[2] illustrates the utility of the RW method to describe conduction in organic semiconductors. The applications to modelling of nanostructured TiO_2 solar cells were pioneered in 1999 by Nelson[6], who adapted the

Continuous Time Random Walk (CTRW) theory of Scher and Montroll to design a RW simulation algorithm that sampled efficiently the trap energy distribution characteristic of nanocrystalline titanium dioxide. Later on, RW calculations have been efficiently used to study electron mobilities[7], diffusion coefficients[8–10] and recombination properties[11–13] in dye-sensitized solar cells. It has also been applied to obtain surface photovoltage transients[14,15].

3.2. Main features of the random walk numerical algorithm

The RW simulation method[6,10,16,17] is a stochastic calculation in which particles are moved at random in a 3-dimensional network of traps arranged on a lattice not necessarily ordered. In the most simple version traps or sites are randomly distributed in space with the same average distance, although, as we will see, more complex configurations can be implemented[18]. RW methods allow for an analysis of different spatial disorder or morphologies, as well as different degrees of energy disorder in the studied material.

Energy disorder in a RW simulation is considered by making the traps to conform to an arbitrary distribution of energies. For example, it is possible the implementation of the two typical densities that are encountered in most of inorganic and organic disordered materials, i.e., Eqs. (2.2) and (2.3). In this thesis we will focus on the exponential distribution because, besides we deal mostly with inorganic materials, where exponential functions are generally assumed[19,20], it has been argued than a band tail can be also considered for organic solar cells when the Fermi level is well below the mobility edge (i.e. low carrier densities)[21,22]. This has also been demonstrated in nanocrystalline TiO_2 by Anta et al.[7] These authors used gaussian distributions to model the distribution or energies and found that, at realistic electron densities, only the tail of the distribution determined the behaviour of the conductivity. Hence, each trap i will be associated to a particular value of energy E_i according to Eq. (2.2). Moreover, the procedure for the assignment of energies to a particular trap is at random within this distribution so that no energy correlations between neighboured traps are considered.

The random walk method works by giving to each trap a *release time* according to a certain expression that depends on the model we use to describe the transport process. This way, RW simulation makes it possible to implement a specific mechanism of transport (the model) and check, *from first principles*, how the dynamic properties (diffusion coefficient, electron populations, recombination rates and so on) depend on the microscopic structure of the material, that is, the particular distribution of localized states and the morphological

features. In the context of solar cells applications[10,14,17], two alternatives are relevant and can be used for the computation of the release times, following models previously described in Chapter 2: *hopping and multiple-trapping*. In both cases, the transport implies that detrapping is thermally activated with the trap energy being the activation barrier.

If we use the multiple-trapping model[23–25] the release time to the transport level t_i is given by

$$t_i = -ln(R)t_0 \exp\left[(E_c - E_i)/k_B T\right] \tag{3.1}$$

where R is a random number uniformly distributed between 0 and 1 and t_0 $(=1/\nu_0)$ is the attempt-to-jump time. In this equation, E_c is a reference value of the energy that represents the transport level (i.e., the mobility edge).

Alternatively, if we use the hopping model[26–28], the release time, t_{ij}, for hopping between two sites i and j, is calculated via[29]

$$t_{ij} = -ln(R)t_0 \exp\left[\frac{2r_{ij}}{\alpha_l} + \frac{E_j - E_i + |E_j - E_i|}{2k_B T}\right] \tag{3.2}$$

where r_{ij} is the distance between the sites, α_l is the localization radius and E_i and E_j are the energies of the target and starting sites, respectively. In both models, the use of a random number R implies that different release times from a certain trap are possible. The factor factor $\ln(R)$ guarantees that the distribution of detrapping times for a single trap energy E_i conforms to a *Poisson* distribution (which is the characteristic distribution for first order relaxation kinetics governed by a single lifetime).

Actually, the release times that arise from Eqs. (3.1) and (3.2) correspond to the inverse of the frequencies or rates presented in Chapter 2 and used by some authors[2,30]. Thus, calculations in the time domain should lead to the same results.

Basic algorithm of a RW simulation based on times

A RW simulation based on times is organized as follows:

1. The simulation starts at time $t_0 = \nu_0^{-1}$ by distributing randomly the carriers in the traps.

2. Carriers are given release times according to Eqs. (3.1) or (3.2) for the energies and positions of the sites they visit. Waiting times are then defined as the difference between the release time of the carrier and the time already spent by the carrier in a particular site.

3. For each simulation step the carrier with the shortest waiting time (t_{min}) is allowed to move.

4. The waiting times for the rest of the carriers are reduced by t_{min}. On the other hand, it is computed a new release time for the carrier that has just moved, i.e., this carrier adopts the release time corresponding to the trap it jumped to.

5. The process is repeated by means of subsequent movements of the carrier with the shortest waiting time, so that the simulation advances by time steps of length t_{min}. This time increment is a variable quantity that depends on the current configuration of the system and the sites occupied at each particular moment.
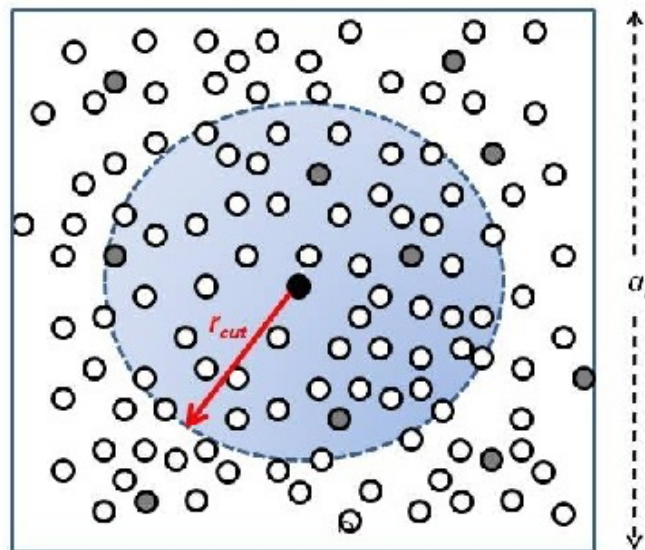
Fig. (3.1) Illustration of the random walk method employed in this work. Traps (open circles) are distributed on a simulation box of size a_L. Some of these traps are occupied by charge carriers (grey circles). For a certain carrier (black circle), hopping times to neighboured traps are computed but restricted to those traps within the cut-off radius r_{cut} that are not occupied.

Point 5 above shows that a RW numerical simulation is an adaptive time-step simulation procedure. The broad dispersion in energies of the sites in nanocomposites, as we can see in Eq. (2.2), leads to a variation in waiting times of various orders of magnitude, so an adaptive time-step is very convenient to describe transport adequately. For example, if at a given time the shortest waiting time correspond to a trap of a low energy E, then, the simulation advances a long time (corresponding to the release time of a very deep trap) only in one step, reducing the execution time of the simulation. This feature of the RW method is very important, because it makes it possible to study phenomena that occur in a very long time scale, not accessible to atomistic or "ab initio" methods[31].

Along the simulation, each carrier must have, as well as a waiting time, a most probable jump specified by the label of the trap it is aimed to jump to. This neighboured trap must accomplish some conditions:

• It must be located inside an sphere of a cut-off radius, r_{cut}. Therefore, given a trap i, a neighbouring trap j is not considered if the distance between the traps r_{ij}, is larger than r_{cut}.
• RW simulation is carried out with the restriction that no more than one carrier is allowed per site. Therefore, a move is forbidden if the trap is already occupied.
• If a given trap is already a target site for another carrier, then it is not considered either.

In the case of the multiple-trapping model, the release time does not depend on the target site (see Eq. (3.1)). Hence, the trap that finally acts as a target site is chosen randomly among all the available traps. On the contrary, in the hopping model, the release time does depend on the target site, (see Eq. (3.2)) and the trap that provides the shortest release time is chosen to act as target site among the rest of the traps for a particular carrier. Note that this process must be executed before the RW algorithm is started. On the other hand, convergence should be ensured by choosing a cut-off radius which is long enough (but not too long, to avoid excessive computational times).

Periodic boundary conditions along the three directions of space are applied by default in most of the simulations carried out in this thesis. Hence, a carrier crossing a simulation box boundary is automatically reinjected through the opposite side of the box. Proceeding this way, a stationary state (signalled by a constant carrier flux or a constant diffusion coefficient) is rapidly achieved. To implement the periodic boundary conditions it is necessary to keep records in the simulation of the absolute coordinates of the carriers, in order to compute properties (like the mean square displacement), which depend on them.
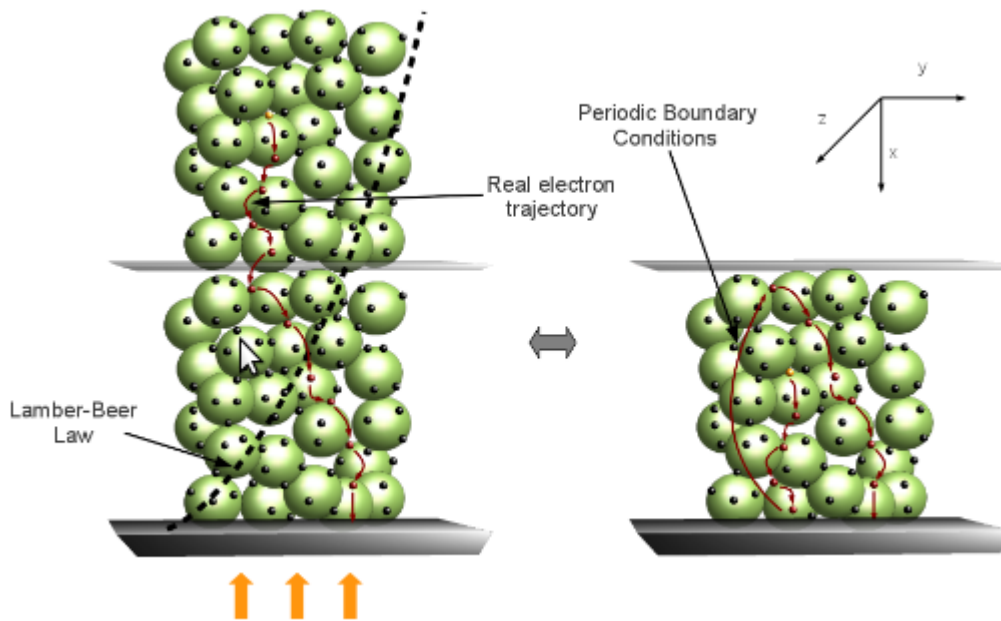
Fig. (3.2) Hopping transport in a packing of nanospheres. The simulation box is periodically replicated in the three directions of space to simulate the hopping transport (right), but real coordinates are considered to describe injection and collection (left). The dashed line stands for the carrier generation profile, which resembles a Lambert-Beer law for light coming on the x-direction. Black dots represent the traps on the surface of the nanospheres

However, in Chapter 7 an study of the charge collection efficiency on a surface is carried out, and this requires to consider charge generation in accordance to optical absorption lengths of the order of microns. However, the use of a simulation box of the order of microns is not computationally feasible for the trap densities characteristic of the materials studied here. To surmount this problem we have devised a numerical procedure where the actual distance of the carrier with respect to the collecting substrate is continuously stored during the simulation. In practise, we carry out a typical simulation of an infinite system (with periodic boundary conditions). However, in addition, the actual x-position of the carrier is also taken into account. This is considered in two steps of the algorithm: (1) when carriers are injected in the sample along x-direction according to the Lambert-Beer law (see Fig. (3.2)), and (2) when carriers are collected at $x = 0$. Therefore, the fictitious coordinates arising from the application of the periodic boundary conditions are only considered in Eqs. (3.2) and (2.2), but injection and collection are modeled according to a real coordinate. This way a macroscopic film with a size of microns can be adequately simulated with a manageable number of nanospheres and traps.

3.3. Extraction of Properties From RW Simulations

Energy Level Populations

It is known that, under equilibrium conditions, the electron concentration n is determined by the density of states $g(E)$ and the Fermi-Dirac distribution $f(E–E_F)$, dependent on the position of the Fermi energy E_F (or on a quasi-Fermi energy in the case of stationary excitation of electrons). This relation is given by Eqs. (2.25) and (2.26). RWNS calculations can be carried out for different electron densities in order to extract dynamic properties as a function of Fermi level. Thus, by running a long enough RWNS calculation it is possible to construct a histogram $N(E)$ of the number of carriers that occupy levels of energy between E and $E+dE$. From these histograms the corresponding occupancy probabilities can be extracted. Since we implement the distribution of states $g(E)$, we can compute the probability of a trap of energy between E and $E+dE$ to be occupied by means of $N(E)/\mathrm{g}(E)$. The result is that, as a consequence of the restriction that no more than one carrier is allowed per trap, this probability tends to adopt the Fermi-Dirac shape[7,10] with a well-defined Fermi level (see Fig. (3.3)) as the system approaches the stationary regime. It is important to notice that, in contrast to previous studies[32–34] the Fermi–Dirac function is not imposed a priori, but it arises naturally from the calculation instead.

Diffusion Coefficient

In accordance to the RW algorithm, carriers diffuse through the lattice of trap sites. Thus, the jump diffusion coefficient D_j can be computed from the mean-squared displacement $< r^2(t) >$ by Eq. (2.20). The mean square displacement is observed to be linear at longer times (normal diffusion). This allows extracting the diffusion coefficient from the slope of the curve in the time plot according to the following expression

$$D_j = \frac{1}{6t} \left\langle \left(\frac{1}{N} \sum_{i=1}^{N} \Delta r_i \right)^2 \right\rangle \qquad (3.3)$$

where N is the total number of carriers. Very high numerical demands are often required when simulating systems with a considerable number of carriers and trap states. In those cases, to compute jump diffusion coefficients (or other transport and recombination
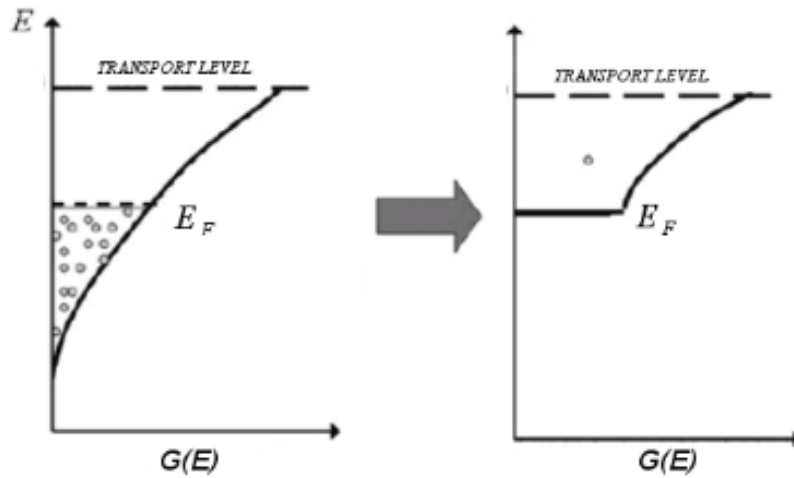
Fig. (3.3) Illustration of the trap energy distributions used in the multi-electron and single-electron RWNS calculations.

properties) with a reasonable computational time, the following approximation is implemented: the exponential distribution in Eq. (2.2) is truncated for energies below the Fermi level, hence assuming that deeper traps are always occupied. This is the so-called *one-electron approximation* that makes it possible to simulate transport at a given position of the Fermi level with the movement of a single carrier[10]. This idea is illustrated in Fig. (3.3).

Monte Carlo simulation has shown that the *tracer diffusion coefficient*, D^*, which gives the random walks of a single particle

$$D^* = \lim_{t \to \infty} \frac{1}{6Nt} \left\langle \sum_{i=1}^{N} (\Delta r_i)^2 \right\rangle \tag{3.4}$$

is practically equal to the jump diffusion coefficient defined by Eq. (3.3) in a broad range of densities and temperatures[35]. RWNS results for the diffusion coefficient versus Fermi level obtained from both types of calculations are essentially the same, which shows that collective diffusion is equivalent to the random walk of a single carrier[10]. This result shows that the kind of systems studied here behave ideally, and that carrier-carrier interaction can be neglected.

Lifetime and Diffusion Length

In most of the work accomplished in this thesis, we have implemented recombination of carriers in a RW simulation. Following classic[13,17,36] and recent literature[37,38] we assume that recombination in a DSC is determined by trapped-carriers. We make a further assumption giving a *recombining character* to both shallow and deep traps, as described in Chapter 2. Thereby, all the traps in the distribution are allowed to act as recombination centre. Hence, when a carrier reaches one of these traps, there is a probability, dependent on the specific recombination mechanism used for each system, to undergo recombination and be removed from the sample.

Taking into account this situation, we compute both the average time and the average distance that a carrier is moving until it becomes effectively recombined. In order to simulate
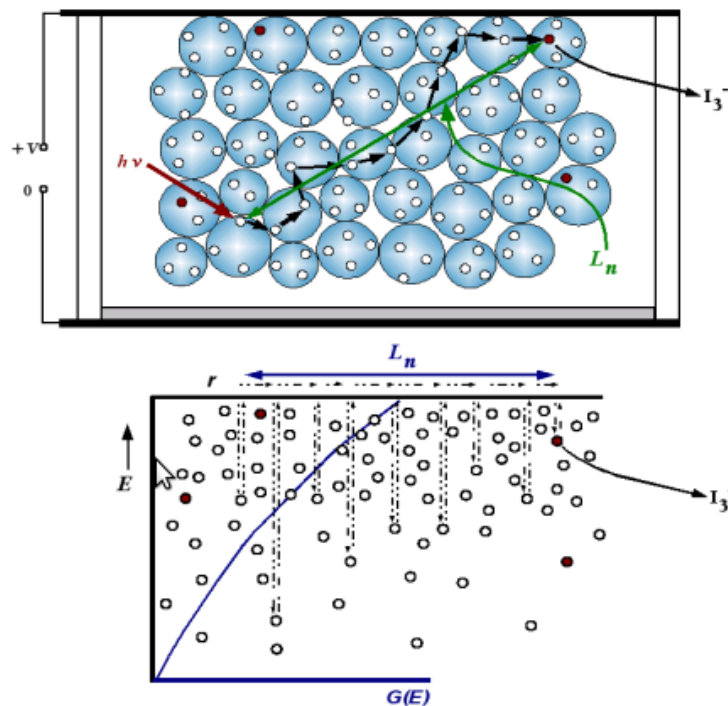
Fig. (3.4) Illustration of the random walk numerical procedure utilized in this thesis to compute the diffusion length L_n. A three-dimensional network of traps is distributed randomly and homogeneously in space. The energies of the sites are taken from an exponential distribution. A recombining character is given to an arbitrary amount of traps (solid circles) so that, when an electron reaches one of these traps, it may undergo recombination and be removed from the sample.

a solar cell at open-circuit conditions and under illumination a constant carrier density is maintained in the sample. This is achieved by imposing that when a carrier has just recombined another one is immediately injected into the system in another site at random. For this *fresh* carrier both time and distance are reset so that average time and distance between recombination events can be computed, stored and represented versus total simulation time. Finally, these magnitudes are renormalized by the total number of carriers and the total number of recombination events so that the result is effectively an average distance and time for one single carrier.

One can argue that these magnitudes are not computed as collective quantities defined from kinetic equations based on densities. Nevertheless, we will show in Chapter 5 that, despite computing individual diffusion length and lifetime from simulation averages, these magnitudes effectively correspond to those defined according to Eqs. (2.57) and (2.59) respectively.

The implementation of all the properties and procedures described in this Chapter have been programmed using Fortran 90. (For more details see Appendix C).

References to Chapter 3

(1)   Frenkel, D.; Smit, B. *Academic Press* **2002**.

(2)   Bassler, H. *Physica Status Solidi B-Basic Research* **1993**, *175*, 15–56.

(3)   Movaghar, B.; Grunewald, M.; Ries, B.; Bassler, H.; Wurtz, D. *Physical Review B* **1986**, *33*, 5545–5554.

(4)   Silver, M.; Schoenherr, G.; Baessler, H. *Physical Review Letters* **1982**, *48*, 352–355.

(5)   Baranovskii, S. D.; Efros, A. L.; Gelmont, B. L.; Shklovskii, B. I. *Journal of Physics C-Solid State Physics* **1979**, *12*, 1023–1034.

(6)   Nelson, J. *Physical Review B* **1999**, *59*, 15374–15380.

(7)   Anta, J. A.; Nelson, J.; Quirke, N. *Physical Review B* **2002**, *65*.

(8)   Kopidakis, N.; Benkstein, K. D.; Lagemaat, J. van de; Frank, A. J.; Yuan, Q.; Schiff, E. A. *Physical Review B* **2006**, *73*.

(9)   Benkstein, K. D.; Kopidakis, N.; Lagemaat, J. van de; Frank, A. J. *Journal of Physical Chemistry B* **2003**, *107*, 7759–7767.

(10)   Anta, J. A.; Mora-Sero, I.; Dittrich, T.; Bisquert, J. *Physical Chemistry Chemical Physics* **2008**, *10*, 4478–4485.

(11)   Petrozza, A.; Groves, C.; Snaith, H. J. *Journal of the American Chemical Society* **2008**,

130, 12912–12920.

(12)   Nelson, J.; Haque, S. A.; Klug, D. R.; Durrant, J. R. *Physical Review B* **2001**, *63*, 6320.

(13)   Kopidakis, N.; Benkstein, K. D.; Lagemaat, J. van de; Frank, A. J. *Journal of Physical Chemistry B* **2003**, *107*, 11307–11315.

(14)   Anta, J. A.; Mora-Sero, I.; Dittrich, T.; Bisquert, J. *Journal of Physical Chemistry C* **2007**, *111*, 13997–14000.

(15)   Mora-Sero, I.; Anta, J. A.; Dittrich, T.; Garcia-Belmonte, G.; Bisquert, J. *Journal of Photochemistry and Photobiology a-Chemistry* **2006**, *182*, 280–287.

(16)   Anta, J. A. *Energy and Enviromental Science* **2009**.

(17)   Nelson, J.; Chandler, R. E. *Coordination Chemistry Reviews* **2004**, *248*, 1181–1194.

(18)   Anta, J. A.; Morales-Florez, V. *Journal of Physical Chemistry C* **2008**, *112*, 10287–10293.

(19)   Bisquert, J.; Fabregat-Santiago, F.; Mora-Sero, I.; Garcia-Belmonte, G.; Barea, E. M.; Palomares, E. *Inorganica Chimica Acta* **2008**, *361*, 684–698.

(20)   Monroe, D. *Physical Review Letters* **1985**, *54*, 146–149.

(21)   Kirchartz, T.; Pieters, B.; Kirkpatrick, J.; Rau, U.; Nelson, J. *Physical Review B* **2011**, *83*.

(22)   MacKenzie, R. C. I.; Kirchartz, T.; Dibb, G. F. A.; Nelson, J. *The Journal of Physical Chemistry C* **2011**, *115*, 9806–9813.

(23)   Tiedje, T.; Rose, A. *Solid State Communications* **1981**, *37*, 49–52.

(24)   Bisquert, J. *Physical Review Letters* **2003**, *91*.

(25)   Vanmaekelbergh, D.; de Jongh, P. E. *Phys. Rev. B* **2000**, *61*, 4699–4704.

(26)   Hartenstein, B.; Bässler, H. *Journal of Non-Crystalline Solids* **1995**, *190*, 112–116.

(27)   Gonzalez-Vazquez, J. P.; Anta, J. A.; Bisquert, J. *Physical Chemistry Chemical Physics* **2009**, *11*, 10359.

(28)   Bisquert, J. *Journal of Physical Chemistry C* **2007**, *111*, 17163–17168.

(29)   Miller, A.; Abrahams, E. *Physical Review* **1960**, *120*, 745–755.

(30)   Novikov, S. V.; Dunlap, D. H.; Kenkre, V. M.; Parris, P. E.; Vannikov, A. V. *Physical Review Letters* **1998**, *81*, 4472–4475.

(31)   Calvo-Muñoz, E. M.; Selvan, M. E.; Xiong, R.; Ojha, M.; Keffer, D. J.; Nicholson, D. M.; Egami, T. *Phys. Rev. E* **2011**, *83*, 011120.

(32)   Arkhipov, V. I.; Heremans, P.; Emelianova, E. V.; Adriaenssens, G. J.; Bassler, H. *Applied Physics Letters* **2003**, *82*, 3245–3247.

(33)   Li, L.; Meller, G.; Kosina, H. *Applied Physics Letters* **2008**, *92*.

(34)   Bisquert, J. *Physical Chemistry Chemical Physics* **2008**, *10*, 1–20.

(35)   Uebing, C.; Gomer, R. *Journal of Chemical Physics* **1994**, *100*, 7759.

(36)   Peter, L. M. *Journal of Physical Chemistry C* **2007**, *111*, 6601–6612.

(37)   Villanueva-Cab, J.; Wang, H.; Oskam, G.; Peter, L. M. *The Journal of Physical Chemistry Letters* **2010**, *1*, 748–751.

(38)   Jennings, J. R.; Wang, Q. *The Journal of Physical Chemistry C* **2010**, *114*, 1715–1724.

CHAPTER 4

Random Walk Numerical Simulation for Hopping Transport at Finite Carrier Concentrations

The RWNS method is used to compute diffusion coefficients for hopping transport in a fully disordered medium at finite carrier concentrations. We use Miller–Abrahams jumping rates and an exponential distribution of energies to compute the hopping times in the random walk simulation. The computed diffusion coefficient shows an exponential dependence with respect to Fermi-level and Arrhenius behaviour with respect to temperature. This result indicates that there is a well-defined transport level implicit to the system dynamics. To establish the origin of this transport level we construct histograms to monitor the energies of the most visited sites. In addition, we construct "corrected" histograms where backward moves are removed. Since these moves do not contribute to transport, these histograms provide a better estimation of the effective transport level energy. The analysis of this concept in connection with the Fermi-level dependence of the diffusion coefficient and the regime of interest for the functioning of dye-sensitised solar cells is discussed.

4. Random Walk Numerical Simulation for Hopping Transport at Finite Carrier Concentrations

4.1. Introduction and methodology

As discussed in Chapter 2, the theoretical description of electron transport in disordered materials is a challenging issue with implications in the fields of dye-sensitised solar cells (DSC)[1], plastic solar cells[2], organic light emitting diodes[3] and organic electronics[4]. In these materials, the transport rates are determined by two kinds of microscopic disorder: energetic disorder characterized by a broad distribution of localized states[5] and spatial disorder, related to the morphological features of the material[6,7]. The correct description of the influence of these two kinds of disorder and their microscopic parameters on the transport features of the material is crucial to the design of better performing devices.

Two main approaches have been used to study electron transport in these materials: the multiple-trapping model and the hopping model. Both mechanisms have already been described in Chapter 2, where it was pointed out that, in order to obtain analytical expressions for the electron diffusion coefficient, it is necessary to make averages over spatial and energy disorder. This analysis is especially cumbersome in the context of the *hopping model* since both energetic and spatial disorder must be taken into account. However, this problem can be simplified if the distribution of energies for the localized states is very steep. In this case it has been shown that a particular level, known as *transport energy*, determines the dominant hopping events for carriers sitting in very deep states[8–13]. The existence of an effective transport level reduces the hopping transport to multiple trapping, with the transport energy playing the role of a mobility edge. This concept has been utilized to derive Eq. (2.39), a theoretical expression for the diffusion coefficient of electrons moving via a hopping mechanism in an exponential distribution of localized states[8]. Nevertheless, the transport energy has been shown to be affected by the fact that the system is not ideal, that is, correlations between carriers may play an important role. These correlations can be due to exclusion effects, which makes the transport energy depend on Fermi level position[9,14], or due to energetic correlations between charges and dipoles[15,16].

Hopping transport in disordered semiconductors has been amply studied over the last decades in relation to inorganic semiconductors such as amorphous silicon and also to organic conductors[17]. The interest in electronic transport in the presence of an exponential distribution

of states has increased with the application of nanostructured wide bandgap semiconductors in DSCs[18,19]. Indeed, it has been shown that for systems using relatively thick TiO$_2$ porous nanocrystalline layers, electron transport may impose limitations to charge extraction[20]. Hence, since DSC operate at large electron densities, it is crucial to determine the transport mechanism in these systems as a function of charge density and, especially at high Fermi levels, beyond the analytical approximations adopted previously, that use commonly multiple trapping arguments[8,21].

In this chapter we apply the random walk numerical simulation (RWNS) method[22–27] to obtain the jump diffusion coefficient in a hopping system with an exponential distribution of localized states and at finite carrier concentration. In addition, we use our calculations to cast light on the foundations of the transport energy approximation in this case. To do that, we implement the hopping mechanism via the Miller–Abrahams jumping rates[28], given by Eq. (2.7). The RWNS calculations yield the jump diffusion coefficient as a function of Fermi level and temperature[22]. We have carried out our simulations on a network of randomly distributed sites. Placing the sites on an ordered spatial arrangement has been shown to affect the results for the carrier mobility[29]. Thus, to work with a fully disordered system permits us to eliminate the effect of introducing an artificial spatial order on the simulation results.

We have used the simulations to construct histograms of the most visited energies so that the probability for the electrons to jump to target sites of specific energy can be calculated. The form of this histogram for jumps upward in energy will allow us to identify the existence of a well-defined maximum and how it depends on carrier concentration and Fermi level. As noted by Arkhipov et al.[11], the transport energy can differ noticeably from the energy of the most probable jump due to the influence of neighboured sites close in energy. These sites make carriers hop back and forth many times so that those moves do not contribute to transport and hence to the computation of the diffusion coefficient. The RWNS method makes it possible to remove those jumps from the calculation so that a better approximation to the "effective transport energy" can be obtained for the studied cases.

Calculations were carried out with 1–100 carriers and the size of the simulation box ranged between 10 and 65 nm. A density of traps of $N_l = 10^{27}$ m^{-3} was used in all cases. This corresponds to an average distance between traps of 1 nm. It must be stressed that, as traps are distributed randomly, hops can be executed for distances either longer or shorter than this averaged distance. Hereafter, the simulations are described by a label N/a_L where N is the number of carriers and a_L the size of the simulation box in nm's.
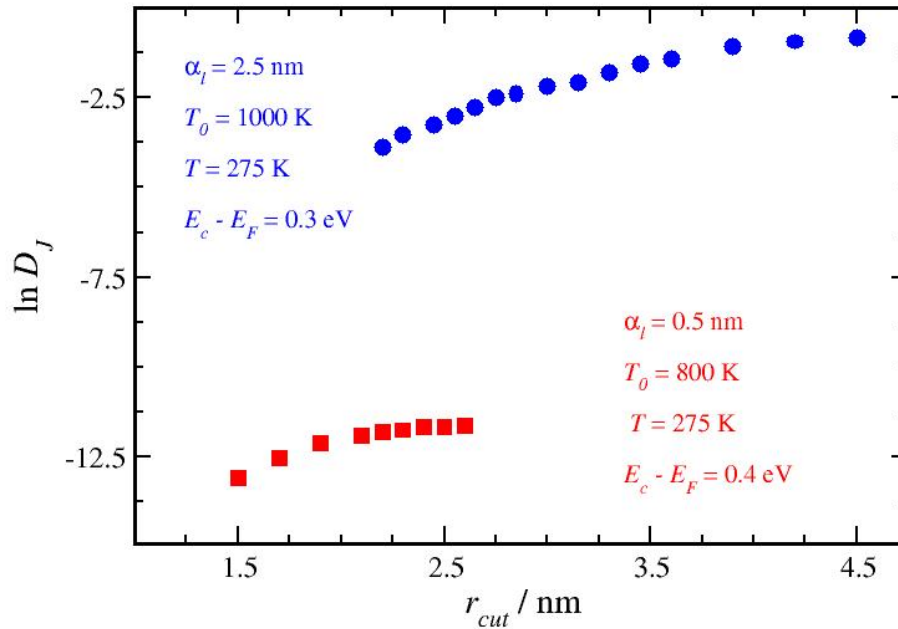
Fig. (4.1). Jump diffusion coefficient as a function of cut-off radius from RWNS calculations with Miller-Abrahams hopping rates.

As mentioned in Chapter 3, to save computing time a certain cut-off radius r_{cut} is introduced. Neighbours located beyond this distance are not considered as target sites. Since the hopping times in Eq. (3.2) do depend on distance between traps, the cut-off distance should be large enough to ensure that the results are not significantly affected. In Fig. (4.1) the diffusion coefficient as a function of r_{cut} is plotted for two values of the localization radius. As it could be expected, a larger localization radius requires a larger cut-off radius to ensure convergence. Hence, for $\alpha_l = 0.5$ nm and 2.5 nm a cut-off radius of 2.5 nm and 4.5 nm were found to be sufficient, respectively. These are the parameters used henceforth.

With the idea in mind that hopping transport can be rationalized using the concept of transport energy, we have monitored the energies of the target sites for jumps upward in energy in the RWNS calculations. The method followed here consists in computing an histogram of the energies of the target sites only when the energy of these traps is higher than the starting sites of electrons. Hence, in each step of simulation, if the target trap fulfils this condition, its energy is stored in the histogram. For reasons than will be discussed later, another kind of histogram of energies is implemented in the simulation. Now, in each step of

simulation, the energy of the target site is stored only when its energy is higher than the starting site and when in the previous step of simulation this site was not the starting one. In this manner, we ignore *backward jumps* for the computation of the histogram of upward jumps energies.

4.2. Results and discussion

Energy of the most probable jump and transport energy concept

For an exponential distribution of localized levels, the classical result[10,30] is that the fastest upward jump occurs in the vicinity of the so-called transport energy[10]

$$E_{tr} = E_c - \Delta E_{tr} \tag{4.1}$$

where ΔE_{tr} is given by Eq. (2.11) independently of the energy of the starting site. This expression is obtained by maximizing the upward hopping rate for an average hopping distance. Alternatively the transport energy can be obtained by averaging the hopping rate below a certain energy value as reported by Arkhipov[11,31]. This latter procedure has been put into question[32] due to the difficulty of considering the effect on transport of all relevant hops. In any case, the existence of a transport energy implies that the hopping model should behave in a similar way to the multiple trapping model, where there is a transport level by definition.

In connection with the transport energy approximation, we have monitored the energies of the target sites for jumps upward in energy in the RWNS calculations. These values were used to construct a histogram of energies. Results can be found in Fig. (4.2) for two densities corresponding to labels $100/12^3$ and $100/15^3$ ($\alpha_l = 0.5$ nm, $T_0 = 800$ K and $T = 275$ K). The results reveal that most carrier moves take place in the vicinity of a certain energy that always lies (as expected) above the Fermi energy for each particular case.

In this chapter we make a critical analysis of the following assumption: the maximum of the energy histogram, E_{max}, can be assimilated to the value of the transport energy. We must note that the former is just a simulation result whereas the latter is a theoretical concept obtained under certain approximations whose origin we want to test using numerical simulation. Monte Carlo simulation has been used by Cleve et al.[33] and Novikov and Malliaras with similar purposes[15]. However, Cleve et al.[33] investigate an empty system with no
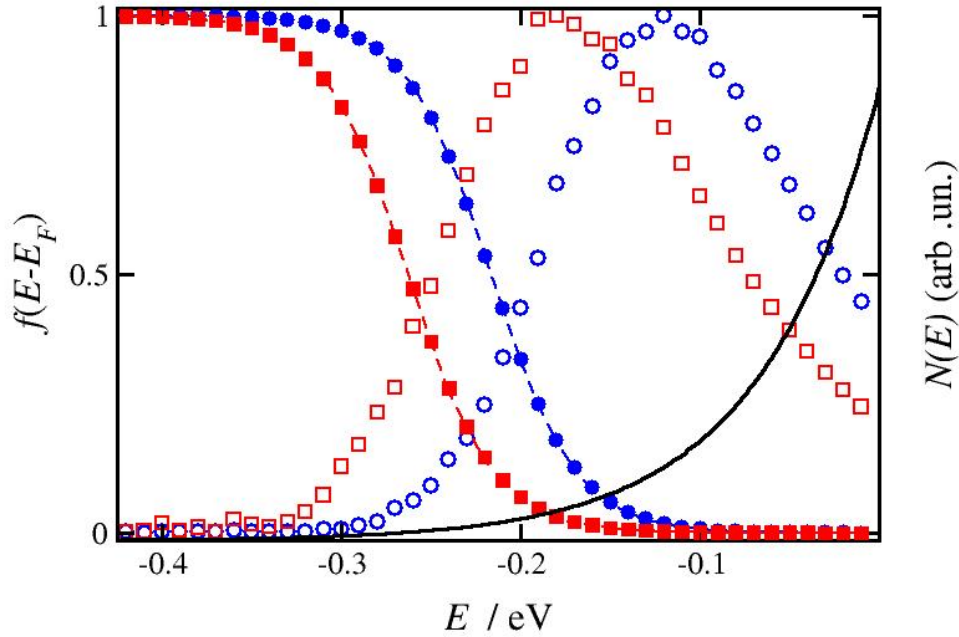
Fig. (4.2). Occupation probabilities ($f(E–E_F)$, full symbols) and histograms of the energies of target sites ($N(E)$, open symbols) in RWNS calculations for jumps upward in energy. The latter have been normalized with respect to the maxima. Parameter values are $\alpha_l = 0.5$ nm , $T_0 = 800$ K, $T = 275$ K and densities corresponding to labels $100/12^3$ (circles) and $100/15^3$ (squares). The following values are obtained from the simulations for both densities: E_F = -0.22 eV (E_{max} = -0.12 eV) and E_F = -0.26 eV (E_{max} = -0.18 eV) respectively. The solid line stands for an exponential trap distribution of $T_0 = 800$ K.

influence of the concentration of carriers. On the other hand, the work in Ref. 15 investigates a Gaussian distribution that applies in organic conductors.

The most relevant feature of the present calculations is that E_{max} is found to move upwards in the energy scale when the Fermi level is raised. A similar effect has been described for the transport energy with a Gaussian distribution of states[14]. The variation of E_{max} with density and Fermi level is shown in Fig. (4.3) for two characteristic temperatures ($T_0 = 600$ K and $T_0 = 800$ K). The calculations have been extended to the regime of very low densities, with Fermi levels between 0.17 and 0.61 eV and densities up to $7 \cdot 10^{16}$ cm^{-3}. It must be noted that at low densities the statistics of the simulation is very poor, which increases the uncertainty of E_{max}. This is extracted when the population distribution if found to relax to a
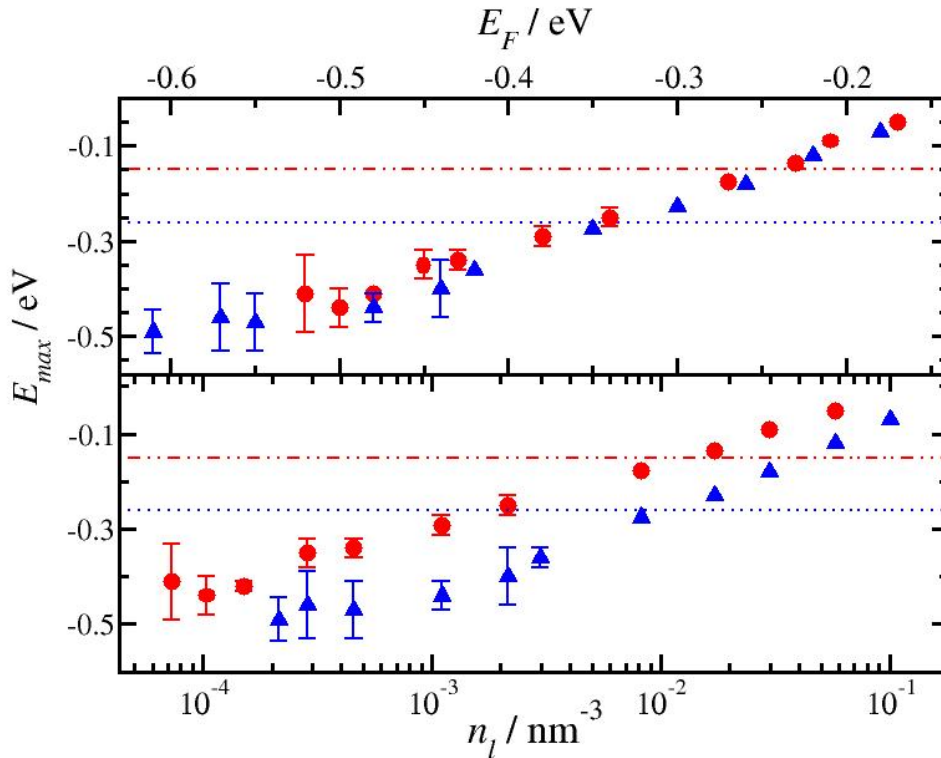
Fig. (4.3). Energy of the most probable jump versus Fermi level (upper panel) and carrier density (lower panel) as obtained from RWNS calculations with Miller-Abrahams hopping rates with $\alpha_l = 0.5$ nm. Results shown correspond to $T_0 = 600$ K (circles) and $T_0 = 800$ K (triangles). The dashed and dotted lines represent the classical values as obtained from Eq. (2.11).

Fermi–Dirac distribution with a well-defined Fermi level.

The poor statistics in the low density limit are related to the occurrence of spurious peaks in the energy histograms. These are due to carriers jumping many times back and forth between sites that happen to be close in distance and in energy and tend to disappear when the simulation is very long. As a matter of fact the RWNS predictions at low densities do not converge to the classical value of Eq. (2.11) as it could be expected. The reasons for this disagreement, in connection with the concept of effective transport energy of Arkhipov et al.[11] will be discussed below.

In any case, if we assume that E_{max} can be assimilated to the transport energy, the same behaviour is found by Arkhipov and coworkers[9] and Li and coworkers.[14] The carrier density dependence of E_{max} is a result of the progressive filling of the localized states, that

prevent carriers from hopping to neighboured sites for which the Miller–Abrahams formula yields high probability. The carriers are then forced to jump to levels of higher energies, hence producing a larger value of the transport energy. At very low concentrations this filling effect is negligible and E_{max} remains constant. Nevertheless, the real connection between E_{max} and the transport energy is subtle and requires further analysis, as discussed below.

Fermi level dependence of the diffusion coefficient

As explained before, the jump diffusion coefficient for carriers can be computed from the RWNS calculations as a function of Fermi level. Results in reduced units for two test cases ($\alpha_l = 0.5$ nm, $T_0 = 800$ K, $T = 275$ K and $\alpha_l = 2.0$ nm, $T_0 = 800$ K, $T = 275$ K) are presented in Fig. (4.4). The simulation data show that the logarithm of diffusion coefficient scales almost linearly with Fermi level. Diffusion coefficients are found to be higher for large localization
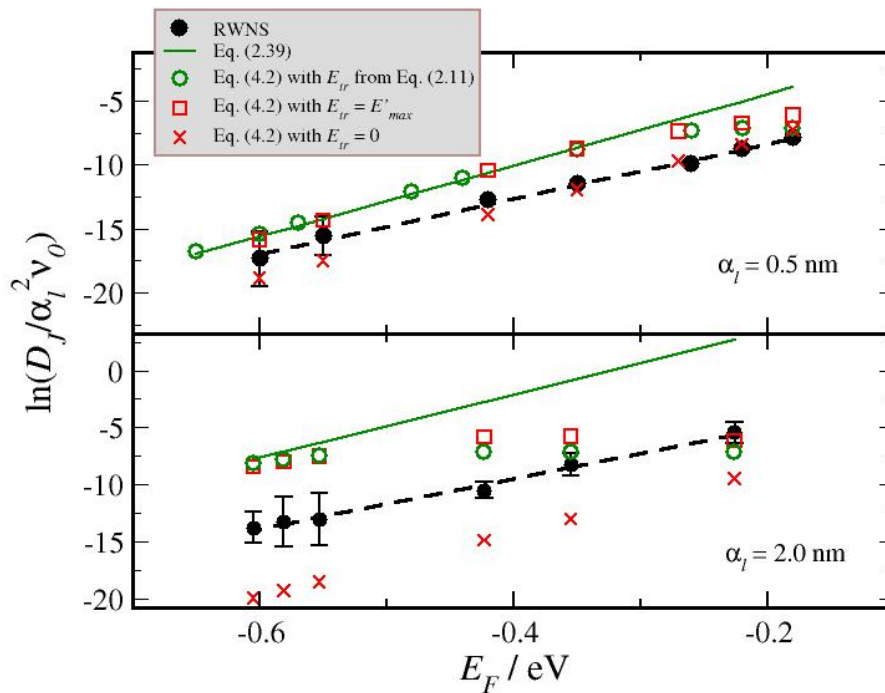
Fig. (4.4). Jump diffusion coefficient vs. Fermi level as obtained from RWNS calculations with Miller-Abrahams hopping rates (full circles) and several theoretical predictions (see text for details): Eq. (2.39) (solid line), Eq. (4.2) with E_{tr} taken from the classical value of Eq. (2.11) (open circles), Eq. (4.2) with $E_{tr} = E'_{max}$ (squares), Eq. (4.2) with $E_{tr} = 0$ (times). The dashed line is a linear fit of the simulation data. Results shown correspond to $T = 275$ K and $T_0 = 800$ and localization radius of $\alpha_l = 2$ nm and 0.5 nm.

radius. This is explained by the fact that delocalization favours jumps to traps further apart and produces shorter average hopping times.

The exponential dependence of the diffusion coefficient with respect to the position of the Fermi level is analogous to the typical prediction of the multiple trapping model. This result suggests that there should exist a well-defined transport level that controls the transport of carriers under equilibrium conditions. However, the results presented in the previous subsection reveal that the energy of the most probable jump does move to higher energies when the trap distribution becomes progressively filled. This appears to be contradictory to the fact that there is a fixed transport energy. In the next subsection this issue is discussed and clarified.

Diffusion coefficient and transport energy

In Chapter 2 it was established that the jump diffusion coefficient D_j can be separated in two factors according to Eq. (2.22) where $<r^2>$ is an average hopping distance and $<\nu>$ is an average hopping frequency[34–36]. In hopping transport, there is not a well defined separation between hopping at different distances and hopping at different energy levels. However, the rationale for the transport energy approximation is that the relevant jumps occur to a well defined level, and in this case Eq. (2.22) may provide a useful approach to obtain analytical expressions for hopping transport as a function of Fermi level. The numerical simulations performed in this work constitute an excellent tool to check the validity of such approximations. Therefore, following the work from previous authors[8,9], we compute the jump diffusion coefficient using Eq. (2.22). According to the transport energy concept both quantities can be calculated from

$$< r(E_{tr}) > = \left[\frac{4\pi}{3} \int_{-\infty}^{E_{tr}} g(E)dE \right]^{-1/3}$$

$$(4.2)$$

$$< \nu > = \frac{\int_{-\infty}^{E_{tr}} \nu(E, E_{tr}) g(E) f(E - E_F) dE}{\int_{-\infty}^{E_{tr}} g(E) f(E - E_F) dE}$$

where $< \nu(E, E_{tr}) >$ is the frequency for an upward hop from the energy E to the transport energy E_{tr} (Eq. (2.7)) at a fixed distance $r = < r >$.

By applying the zero-temperature limit of the Fermi–Dirac distribution in $<\nu>$ of Eq. (4.2) and introducing the classical value of Eq. (2.11) for the transport energy, Bisquert found the expression given in Eq. (2.39) for the diffusion coefficient[8]. This theoretical expression predicts an exponential behavior with respect to the Fermi energy, in analogy with the multiple-trapping result and in accordance with the simulation (see Fig. (4.4)). However, the theoretical slope (27.71 eV^{-1} for $T_0 = 800$ K and $\alpha_l = 0.5$ nm) is slightly larger than the simulation result.

In spite of this encouraging result, the exponential behavior of the diffusion coefficient is not consistent with the upward shift of the average hopping energies when the Fermi level is increased. As it can be observed in Fig. (4.2) and (4.3), the maximum of the energy histogram E_{max} lies always above and approximately at a constant distance with respect to the Fermi level. If we would assume that E_{max} can be assimilated to the transport energy, this behaviour would lead to a constant diffusion coefficient according to Eq. (2.39).

Effective transport energy

To disentangle from the paradox posed in the previous subsection, the concept of effective transport energy of Arkhipov and coworkers[11] is especially useful. These authors make a distinction between the energy that controls transport at equilibrium conditions and the energy of the most probable jumps. That these two are different has been already observed in Monte Carlo simulations for hopping systems in a Gaussian density of states[30].

As mentioned above, RWNS calculations at low densities produce energy histograms with spurious peaks in the low energy region. These peaks arise from carriers jumping back and forth between neighbouring sites. The consequence in the numerical simulation is that these "oscillatory" moves do not contribute to the diffusion of the carriers and therefore should be excluded in the estimation of the transport energy. Bearing this is mind, we have extended the computation of the histograms of hopping energies to the situation in which backward jumps are ignored. To achieve that, the coordinates of the starting site are stored for every move so that when the carrier returns to its original position, the target energy is not used to compute the energy histogram, since these jumps do not produce a net spatial displacement of electrons.

Results for both types of energy histograms are presented in Fig. (4.5) for calculations with a single carrier in an empty exponential trap distribution and for a finite density corresponding to label 10/15[3]. The most visible feature is that the spurious peaks tend to
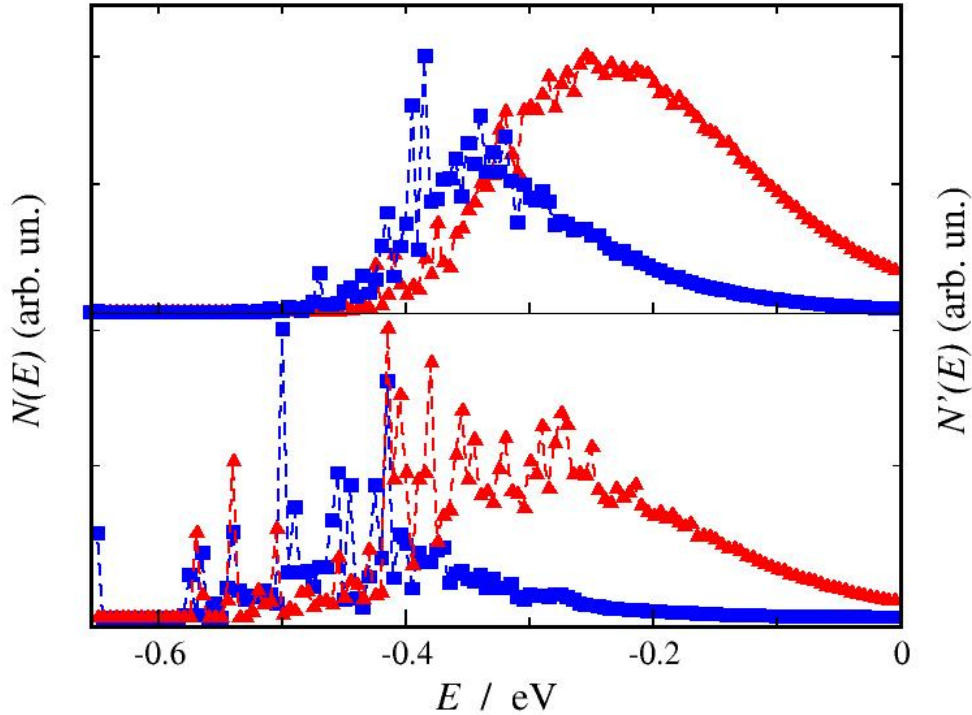
Fig. (4.5). Histograms of the energies of the target sites $N(E)$, (squares) and the same without considering backward jumps between pair of sites $N'(E)$ (triangles, see text for details). Results for simulations at a finite carrier density $(10/15^3)$ (upper panel) and for a single carrier (lower panel) are shown. The parameters used were $T = 275$ K, $T_0 = 800$ K and $\alpha_l = 0.5$ nm.

disappear when backward jumps are ignored. However, sharp peaks are not completely removed. This is due to the fact that oscillatory moves between pairs of sites are not the only moves that do not contribute to transport. Carriers can get "trapped" between small groups of sites and follow circular trajectories before escaping, especially at lower energies. Nevertheless to remove these "second-order" moves is much more difficult in the numerical computation and goes beyond the scope of the present work. The occurrence of spurious peaks is magnified in the present calculations by the fact that we perform our simulations on a random network of traps. As mentioned above, this leads to the possibility of traps that happen to be very close to each other. This problem does not appear in the simulations of Bässler and coworkers[30,33,37], which are executed on a cubic lattice. Simulations on-lattice reduce the numerical demands and produces results more in accordance to the assumptions of the theory (see first expression in Eq. (4.2) for instance) but at the cost of losing the subtleties of the positional disorder implicit to these kind of systems[29].
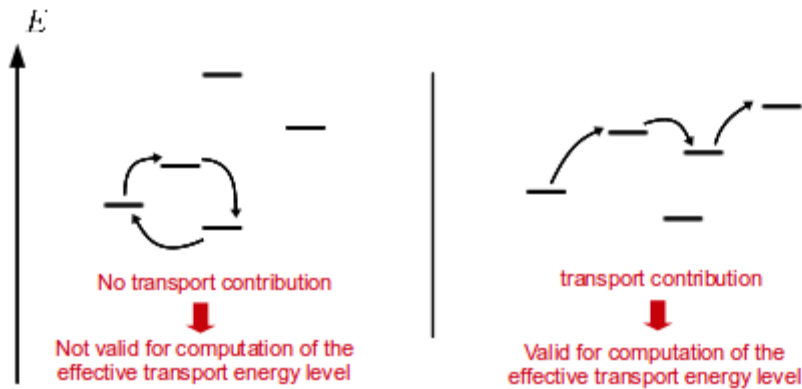
Fig. (4.6). Illustration of two different types of jumps. Upwards jumps of the left picture do not establish a real contribution to the diffusion coefficient so should not be stored in the energy histogram. In contrast, upward jumps of the right picture contribute to transport so the energy of the target sites should be stored in the energy histogram.

A second feature of the corrected histograms is that the maximum, that we call $E^{'}_{max}$, lies at higher energies than in the original histogram. That the effective transport energy lies above the energy of the most probable jump is the main conclusion of the work of Arkhipov et al.[11] and it is confirmed in the present calculations. The simulations of Hartenstein and Bässler[30] and Cleve et al.[33] also predict energies for the most probable jump below the classical value of Eq. (2.11). On the contrary, the computation of the histogram without backward jumps for a single carrier leads to a maximum much closer to the theoretical value of -0.26 eV predicted by Eq. (2.11) (see Fig. (4.5)). It must be born in mind that Eq. (2.11) is obtained under the assumption that all hops occur at a constant average distance whereas in the simulation traps can be occasionally very close to each other and this induces the appearance of the oscillatory moves mentioned above.

The energy of the maximum of the corrected histograms, $E^{'}_{max}$, allows us to propose a better estimate for the transport energy that is implicit to the diffusion coefficient dependence on the Fermi level. Results for this are collected in Fig. (4.7) together with the values of the most probable jump as computed in Fig. (4.3). Here it is observed that $E^{'}_{max}$, lies always above E_{max} and that it converges to the classical value of Eq. (2.11) at low densities.
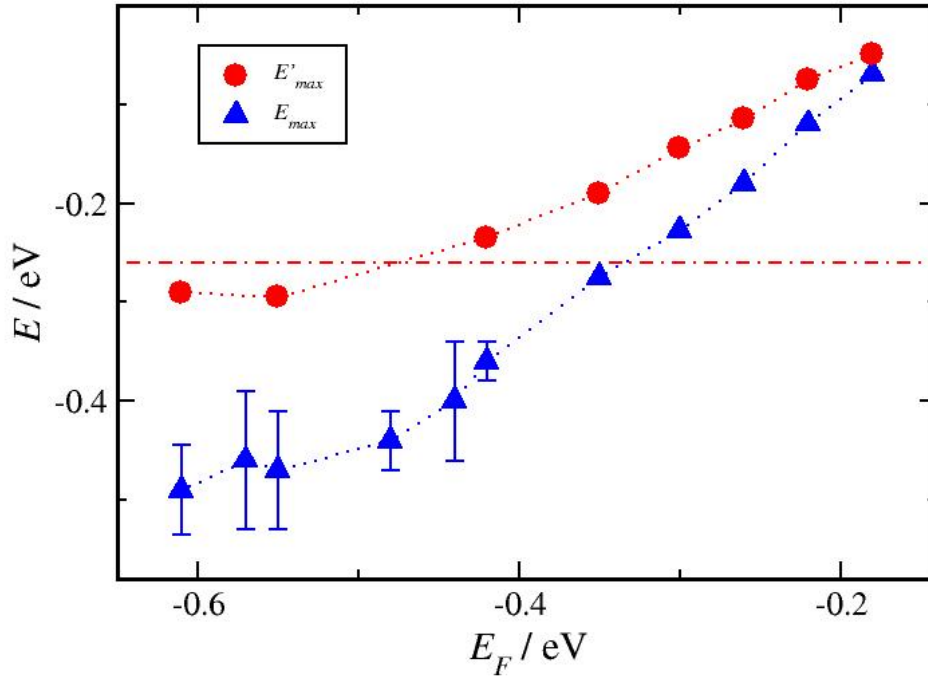
Figure (4.7). Energy of the most probable jump (triangles), E_{max}, and estimation of the effective transport energy, $E\,'_{max}$, (circles) as a function of Fermi level. The first are extracted from the maxima of the energy histograms whereas the latter are extracted from the maxima of the "corrected" histograms with backward jumps between pair of sites removed. The horizontal line represents the classical value predicted by Eq. (2.11). The parameters used were $T = 275$ K, $T_0 = 800$ K and $\alpha_l = 0.5$ nm.

Simulated diffusion coefficient versus theoretical predictions

The concepts introduced in the previous subsections allow us to use the $E\,'_{max}$ values from the simulated histograms to produce theoretical values of the diffusion coefficient according to Eqs. (2.22) and (4.2). The results, together with the simulated data and the predictions of the approximate formulas (2.11) and (2.39) can be found in Fig. (4.4).

We observe that Eq. (2.22) and (4.2) with the transport energy assimilated to $E\,'_{max}$ reproduce Bisquert's formula at low Fermi levels. This is not surprising if we take into account that the simulation reproduces the classical value of Eq. (2.11) in this regime as explained above. The agreement between the theories and the simulation is also good in the

low Fermi level region for the localized case. However, as we move towards large carrier densities the theoretical values separate from Bisquert's formula although they tend to remain close to the simulated data. This effect is basically a consequence that Eq. (2.39) is derived under the assumption that the Fermi level is well below the transport level. By introducing the proper Fermi–Dirac function in Eq. (4.2) the match with respect to the simulation is improved. This effect is more visible in the delocalized case ($\alpha_l = 2$ nm) for which the classical transport energy is -0.55 eV, than in the localized case ($\alpha_l = 0.5$ nm) for which the classical value equals -0.26 eV.

Due to this saturation effect, we find that Eqs. (2.22) and (4.2) in combination with the transport energy values obtained from the simulated histograms do predict a linear dependence at low values of the Fermi level only. Nevertheless the simulation predicts an almost linear dependence at all regimes. To understand this we have to take into account that at high occupations a substantial amount of the upward hopping moves go to levels close to the conduction band level (see Fig. (4.2)). This introduces a distortion in the average implicit to Eq. (2.39) because no hops above $E = 0$ are allowed. To ascertain the magnitude of this distortion we have performed calculations with Eqs. (2.22)-(4.2) assuming that the transport level coincides with the conduction band level, i.e., $E_{tr} = 0$. This calculation renders a linear dependence in the full density range. The agreement with the simulation data is good at high Fermi levels (where upwards hopping moves are controlled by the upper limit of $E = 0$ but poor at low Fermi levels, where transport is controlled by jumps to the transport energy level.

The results shown in Fig. (4.4) indicate that the real transport energy should lie between the classical value of Eq. (2.11) and the conduction band level $E = 0$. The values of E'_{max} obtained from our corrected histograms are close but not the same as E_{tr}. To obtain this we should distinguish moves that contribute effectively to transport from those that do not. This calculation would require to remove also the "second-order" moves discussed previously.

Temperature dependence of the diffusion coefficient

RWNS calculations were performed to obtain the effect of ambient temperature on the diffusion coefficient. *Arrhenius* plots for these calculations are shown in Figs. (4.8) and (4.9) in the temperature range 260 – 340 K. Nearly linear plots are obtained, with an activation energy that is larger for deeper Fermi levels, as it could be expected. The Arrhenius behavior is characteristic of the multiple-trapping transport[22,38.] This is an indication, as discussed above, that at a fixed Fermi level, there is a well-defined transport energy that makes transport
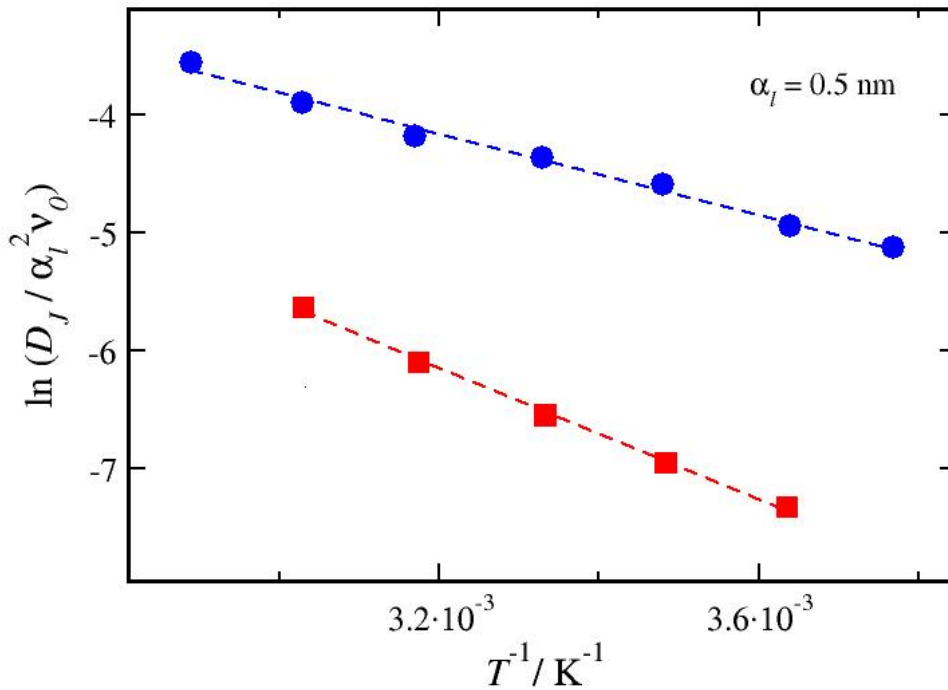
Fig. (4.8). Jump diffusion coefficient vs. inverse of ambient temperature as obtained from one-particle RWNS calculations with Miller-Abrahams hopping rates at $T_0 = 800$ K and $\alpha_l = 0.5$ nm. Results shown correspond to $E_f = -0.3$ eV (circles) and $E_f = -0.4$ eV (squares). The activation energies derived from both set of data are 0.15 and 0.24 eV respectively.

to occur effectively via thermal activation to a transport level. A similar result has been obtained by Vissenberg and Matters using percolation theory[39].

It must be noted that the theoretical framework contained in previous expressions is shown to predict a quasi Arrhenius behaviour as well. This is due to the fact that the temperature dependences of the prefactors and the transport energy are much weaker than the energetic exponential factor. Furthermore, the transport energy is either a constant (at low occupations) or it moves towards higher values (at high occupations). In both cases an Arrhenius behaviour with respect to temperature is expected.

The Arrhenius behavior is maintained if the characteristic temperature of the distribution is lower. Another important feature is that the activation energy is smaller for the delocalized case. This indicates that carrier percolation becomes facilitated when the range of the mean jump is larger, so that sites of similar energies are available for carriers.
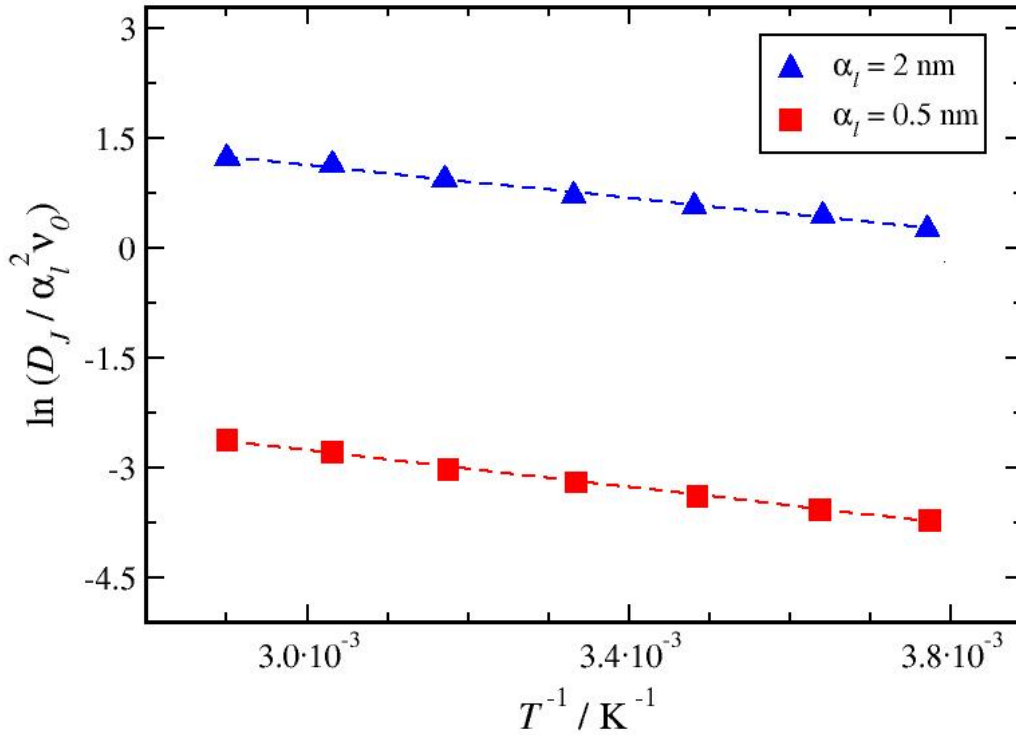
Fig. (4.9). Same as Fig. (4.8) but for $T_0 = 600$ K and multi-particle calculations for $\alpha_l = 0.5$ nm (squares) and $\alpha_l = 2.0$ nm (triangles). The activation energies derived from both set of data are 0.10 and 0.11 eV respectively.

4.3. Conclusions to Chapter 4

It is interesting to make a connection with the relevant regime in DSC and related devices. It is known that at 1 sun illumination the electron density inside the semiconductor oxide is approximately equal to 10^{17} cm^{-3} = 10^4 nm^{-3} (1 electron per nanoparticle[40]). For a characteristic temperature of $T_0 = 600–800$ K and a trap density of 10^{21} cm^{-3}, which are realistic values[27,41] for nanocrystalline TiO$_2$, this density corresponds to Fermi energies below 0.60 eV. As it can be observed in Figs. (4.3) and (4.7), this value corresponds to the regime for which the effective transport energy converges with the classical value given by Eq. (2.11). Hence the predicted behaviour for the diffusion coefficient is close to that yielded by the approximate formula (2.39) and thus indistinguishable from that predicted by the multiple-trapping model.

Furthermore, Arrhenius behavior with typical activation energies of 0.10–0.15 eV are

commonly found in the experiments[38] for nanocrystalline TiO_2. Best agreement with the simulation data is found for $T_0 = 800$ K and $\alpha_l = 0.5$ nm. Again the fact that there exists a well-defined transport level in the regimen relevant for the functioning of DSC under operating conditions produces Arrhenius like behaviour like the multiple-trapping model.

In summary, the random walk numerical simulation (RWNS) method has been used to compute diffusion coefficients for hopping transport in a fully disordered medium at finite carrier concentrations. The computed diffusion coefficient shows an exponential dependence with respect to Fermi-level and Arrhenius behavior with respect to temperature, what indicates that there is a well-defined transport level implicit to the system dynamics. To establish the origin of this transport level histograms to monitor the energies of the most visited sites have been constructed. In addition, we have constructed "corrected" histograms where backward moves are removed. The result is that since these moves do not contribute to transport, the latter histograms provide a better estimation of the *effective transport level* energy.

However, the difficulty of predicting the real transport energy from the simulation suggests that the best method to estimate its value could be from the results of the diffusion coefficient itself. Hence, the effective transport level would be defined as the value that reproduces the "experimental" D_j via Eq. (2.39). This value will always lie between the classical value of the transport energy (Eq. (2.11)) and $E = 0$.

References to chapter 4

(1)   O'Regan, B.; Gratzel, M. *Nature* **1991**, *353*, 737–740.

(2)   Brabec, C. J.; Sariciftci, N. S.; Hummelen, J. C. *Advanced Functional Materials* **2001**, *11*, 15–26.

(3)   Burroughes, J. H.; Bradley, D. D. C.; Brown, A. R.; Marks, R. N.; Mackay, K.; Friend, R. H.; Burns, P. L.; Holmes, A. B. *Nature* **1990**, *347*, 539–541.

(4)   Forrest, S. R. *Nature* **2004**, *428*, 911–918.

(5)   Bisquert, J. *Physical Chemistry Chemical Physics* **2008**, *10*, 1–20.

(6)   Benkstein, K. D.; Kopidakis, N.; Lagemaat, J. van de; Frank, A. J. *Journal of Physical Chemistry B* **2003**, *107*, 7759–7767.

(7)   Anta, J. A.; Morales-Florez, V. *Journal of Physical Chemistry C* **2008**, *112*, 10287–10293.

(8)   Bisquert, J. *Journal of Physical Chemistry C* **2007**, *111*, 17163–17168.

(9)   Arkhipov, V. I.; Heremans, P.; Emelianova, E. V.; Adriaenssens, G. J.; Bassler, H. *Applied Physics Letters* **2003**, *82*, 3245–3247.

(10)   Baranovskii, S. D.; Thomas, P.; Adriaenssens, G. J. *Journal of Non-Crystalline Solids* **1995**, *190*, 283–287.

(11)   Arkhipov, V. I.; Emelianova, E. V.; Adriaenssens, G. J. *Physical Review B* **2001**, *6412*.

(12)   Grünewald, M.; Thomas, P. *Physica Status Solidi (b)* **1979**, *94*, 125–133.

(13)   Shapiro, F. R.; Adler, D. *Journal of Non-Crystalline Solids* **1985**, *74*, 189–194.

(14)   Li, L.; Meller, G.; Kosina, H. *Applied Physics Letters* **2008**, *92*.

(15)   Novikov, S. V.; Malliaras, G. G. *Physica Status Solidi B-Basic Solid State Physics* **2006**, *243*, 387–390.

(16)   Novikov, S. V.; Dunlap, D. H.; Kenkre, V. M.; Parris, P. E.; Vannikov, A. V. *Physical Review Letters* **1998**, *81*, 4472–4475.

(17)   Tessler, N.; Preezant, Y.; Rappaport, N.; Roichman, Y. *Advanced Materials* **2009**, *21*, 2741–2761.

(18)   Gratzel, M. *Nature* **2001**, *414*, 338–344.

(19)   Bisquert, J. *Physical Chemistry Chemical Physics* **2008**, *10*, 49–72.

(20)   Hamann, T. W., J., R. A. *Energy & Enviromental Science*. 2008, pp. 66–78.

(21)   Bisquert, J. *Journal of Physical Chemistry B* **2004**, *108*, 2323–2332.

(22)   Anta, J. A.; Mora-Sero, I.; Dittrich, T.; Bisquert, J. *Physical Chemistry Chemical Physics* **2008**, *10*, 4478–4485.

(23)   Nelson, J. *Physical Review B* **1999**, *59*, 15374–15380.

(24)   Anta, J. A.; Nelson, J.; Quirke, N. *Physical Review B* **2002**, *65*.

(25)   Nelson, J. *Physical Review B* **2003**, *67*.

(26)   Anta, J. A. *Energy and Enviromental Science* **2009**.

(27)   Anta, J. A.; Mora-Sero, I.; Dittrich, T.; Bisquert, J. *Journal of Physical Chemistry C* **2007**, *111*, 13997–14000.

(28)   Miller, A.; Abrahams, E. *Physical Review* **1960**, *120*, 745–755.

(29)   Parris, P. E. *The Journal of Chemical Physics* **1998**, *108*, 218–226.

(30)   Hartenstein, B.; Bässler, H. *Journal of Non-Crystalline Solids* **1995**, *190*, 112–116.

(31)   Arkhipov, V. I.; Heremans, P.; Emelianova, E. V.; Adriaenssens, G. J.; Bassler, H. *Journal of Physics-Condensed Matter* **2002**, *14*, 9899–9911.

(32)   Baranovskii, S. D.; Cordes, H.; Kohary, K.; Thomas, P. *Philosophical Magazine B-Physics of Condensed Matter Statistical Mechanics Electronic Optical and Magnetic Properties* **2001**, *81*, 955–964.

(33)   Cleve, B.; Hartenstein, B.; Baranovskii, S. D.; Scheidler, M.; Thomas, P.; Baessler, H.

Physical Review B **1995**, *51*, 16705.

(34)   Reed, D. A.; Ehrlich, G. *Surface Science* **1981**, *102*, 588–609.

(35)   Uebing, C.; Gomer, R. *Journal of Chemical Physics* **1991**, *95*, 7626–7635.

(36)   Myshlyavtsev, A. V.; Stepanov, A. A.; Uebing, C.; Zhdanov, V. P. *Phys. Rev. B* **1995**, *52*, 5977–5984.

(37)   Bassler, H. *Physica Status Solidi B-Basic Research* **1993**, *175*, 15–56.

(38)   Boschloo, G.; Hagfeldt, A. *Journal of Physical Chemistry B* **2005**, *109*, 12093–12098.

(39)   Vissenberg, M.C.J.M. *Physical Review B* **1998**, *57*, 12964.

(40)   Peter, L. M. *Journal of Physical Chemistry C* **2007**, *111*, 6601–6612.

(41) Petrozza, A.; Groves, C.; Snaith, H. J. *Journal of the American Chemical Society* **2008**, *130*, 12912–12920.

CHAPTER 5

Determination of the Electron Diffusion Length in Dye-sensitized Solar Cells by Random Walk Simulation

The diffusion length is a crucial parameter controlling the electron collection efficiency in dye-sensitized solar cells (DSC). In this Chapter, we carry out a direct computation of this parameter for a DSC with a short diffusion length by running a random walk numerical simulation with an exponential distribution of trap states and explicit incorporation of recombination. The diffusion length and the lifetime are estimated from the average distance travelled and the average survival time of the electrons between recombination events. The results demonstrate the well-known compensation effect between diffusion and recombination that keeps the diffusion length approximately constant on a wide range of illumination intensities or applied biases. The assumptions considered in the present model indicate that the two alternative views described in the literature to rationalize this effect (either "dynamic" or "static") are equivalent.

5. Determination of the Electron Diffusion Length in Dye-sensitized Solar Cells by Random Walk Simulation

5.1. Introduction

The good performance of DSCs[1,2] and other new generation solar cells relies on the favorable dynamic competition[3–5] between photoinduced processes and recombination pathways that cause a reduction of the collection efficiency. Among the first, the transport of photogenerated electrons through the semiconductor nanostructure is central for good performance. For a DSC device to work efficiently, photogenerated electrons travelling through the semiconductor nanostructure should be collected to a fraction close to a 100%. As the electron diffusion length L_n represents the distance that electrons travel on average before recombining with an electron acceptor, efficient cells must be characterized by L_n values that exceed the semiconductor film thickness.

As we pointed out in Chapter 2, it has been observed experimentally in common DSCs that the electron diffusion length remains approximately constant on a wide range of illumination intensities or applied biases[6–8]. This behaviour arises from the opposite dependences of D_n and τ_n with respect to the applied bias, which makes their product approximately constant. In the one hand, the diffusion coefficient increases when the illumination is augmented (or a more negative potential is applied). In contrast, the lifetime becomes shorter when the light intensity or the negative applied potential is increased. While the former is often explained by a trap-filling mechanism either in the context of the multiple-trapping model or the hopping model, the latter is somehow a more complicated effect to rationalize and two different views can be found in literature.

On the one hand, it can be assumed that if the electron transport becomes faster when the Fermi level is raised, then the probability for an electron to find an electron acceptor is larger, so that the electron lifetime is shortened. We call this interpretation the "dynamic" view and it can be found in the works of Nelson *et* al.[9], Kopidakis *et* al[10], Anta *et* al[11], Villanueva *et* al.[12,13] Also Petrozza and coworkers[14] discussed recombination in connection with this "dynamic" view. On the other hand, a careful analysis of the multiple-trapping model under the assumption that the rates for trapping and detrapping are much higher than the typical recombination rate, demonstrate that free and trapped electrons maintain a common equilibrium even if the system is perturbed by, for instance, a recombination event. This result

is due to Bisquert and Vikhrenko[15] and we call it the "static" view (in fact, this is usually referred to as the "quasi-static approximation", described in Chapter 2). From these considerations, a constant diffusion length is derived (see Eq. (2.58)). The approximation of Bisquert and Vikhrenko demonstrates that it is not necessary to resort to a dynamic, transport-limited mechanism to explain the observed behaviour of the lifetime and the diffusion length.

As discussed in Chapter 2, a later study[16] further clarified the interpretation of the electron lifetime, which was formulated in the form of Eq. (2.59), where τ_f is a free electron lifetime. This quantity is interpreted as the effective probability of survival of electrons in the conduction band. In general, τ_f depends on the specific recombination mechanism, and it will be a constant if the rate of recombination of free electrons is proportional to their density. However, the recombination mechanism may involve a combination of charge transfer channels, especially due to the contribution of a distribution of surface states[17,18]. In a first approximation the recombination rate is effectively observed to depend on a power on the free electron density[13,19,20], $U_{rec} = k_r n_c^{\beta}$, which has important implications for the variation of the diffusion length with bias illumination or potential in the solar cell[19] (for a more detailed explanation of the origin of this "non-linear" recombination we refer the reader to Chapter 6). Thus, from Eqs. (2.18) and (2.59) we obtain

$$L_n = \sqrt{D_c \tau_f} \qquad\qquad\qquad (5.1)$$

which predicts that the diffusion length should increase with the steady-state Fermi level via the Fermi level dependence of τ_f. As a matter of fact, recent reports on DSCs indicate that the electron diffusion length is not strictly constant but it increases with applied voltage[21–24]. Specifically the study by Villanueva-Cab and coworkers[25] has carefully determined the variation of L_n at different bias illumination and good agreement has been found with the β-recombination model. Hence, these recent reports suggest that equilibration (trapping) factors present in both the diffusion coefficient and the measured lifetime are essentially the same number, $\partial n_l / \partial n_c$, so that the asymmetry of these two quantities refers to the free electron lifetime, which causes a variation of the diffusion length.

The purpose of the work presented in this Chapter is twofold. On the one hand we pursue to compute the electron lifetime and electron diffusion length for a dye-sensitized solar cell, at potentiostatic conditions (fixed Fermi level) by means of the Random Walk Numerical Simulation (RWNS). On the other hand we intend to cast some light on the origin of the compensating behaviour of the electron diffusion length and to establish how the "dynamic" and the "static" views mentioned above are in fact equivalent. We will see that the RWNS

method employed here, although based on dynamic postulates (random generation of detrapping and recombination times) reaches a quasi-stationary state that reproduces the theoretical dependences predicted for the diffusion coefficient and the lifetime, hence explaining the compensation behaviour).

5.2. Results and discussion

The procedure outlined in Chapter 3 permits us to run a multi-electron calculation at fixed density or Fermi level. However, to approach conditions similar to those typical of an operational cell, a huge amount of computer time is required. To save time when computing the electron diffusion length at realistic conditions, most of the simulations presented in this Chapter are carried out using the *one-electron approximation*, also described in Chapter 3. It is demonstrated[25,26] that this procedure reproduces the electron diffusion coefficient of the full calculation with reasonable precision.

It may be argued that the one electron calculation does not correctly capture the slowing down of the lifetime by the trapping-detrapping process, that is described in the model by the factor $\partial n_l / \partial n_c$. However, it must be observed that the main limiting factor in the trapping-detrapping dynamics is detrapping from deep traps, and the fastest of such occupied traps are on average those at the Fermi level. Therefore the convenient truncation procedure still keeps the main aspect of the collective dynamics. This conclusion is further supported when the results are compared with those of the time decay of the full population by recombination, as it will be discussed below.

The RWNS procedure here devised allows for simultaneous computation of the electron diffusion coefficient, the electron lifetime and electron diffusion length at the same Fermi level position. In order to avoid excessive computational times, we have taken into account parameters reported in the literature[21,26,27] for a DSC with a solid-state hole conductor to carry out our calculations. However, in Chapter 6, simulations reproducing longer diffusion lengths than those studied in this Chapter are considered. Hence we take $t_0 = 10^{-14}$ s, $T_0 = 1100$ K and $T = 300$ K. The total trap concentration is assumed to be[28,29] $N_l = 10^{27}\,\mathrm{m^{-3}}$. In addition one recombining trap is introduced per 64000 normal traps and a further recombination probability of 0.05 is imposed. Finally a cut-off radius of 2.5 nm is introduced in the computation so that jumps to neighboured traps beyond this distance are not considered.

With these parameters the simulation predicts an electron diffusion length of 1.6 μm, which is consistent with the values reported in the literature[21,27] for this kind of solid-state solar cell.

    In Fig. (5.1) the time evolution of the derivative of the mean square displacement (related to the jump diffusion coefficient), the lifetime and the electron diffusion length is reported. It is observed that the simulation reaches rapidly a stationary situation in which the mean square displacement behaves linearly with time (constant time derivative) within the statistical uncertainty of the simulation (normal diffusion). This has been shown to correspond, in multi-electron simulations, to the situation in which the electron population reproduces Fermi-Dirac statistics[26]. On the contrary, the lifetime and the diffusion length are found to reach the stationary state at longer times. This is easy to understand if we bear in mind that the characteristic times for detrapping (as derived from Eq. (3.1) for electrons sitting at the Fermi level) are much shorter than the characteristic time for recombination (the
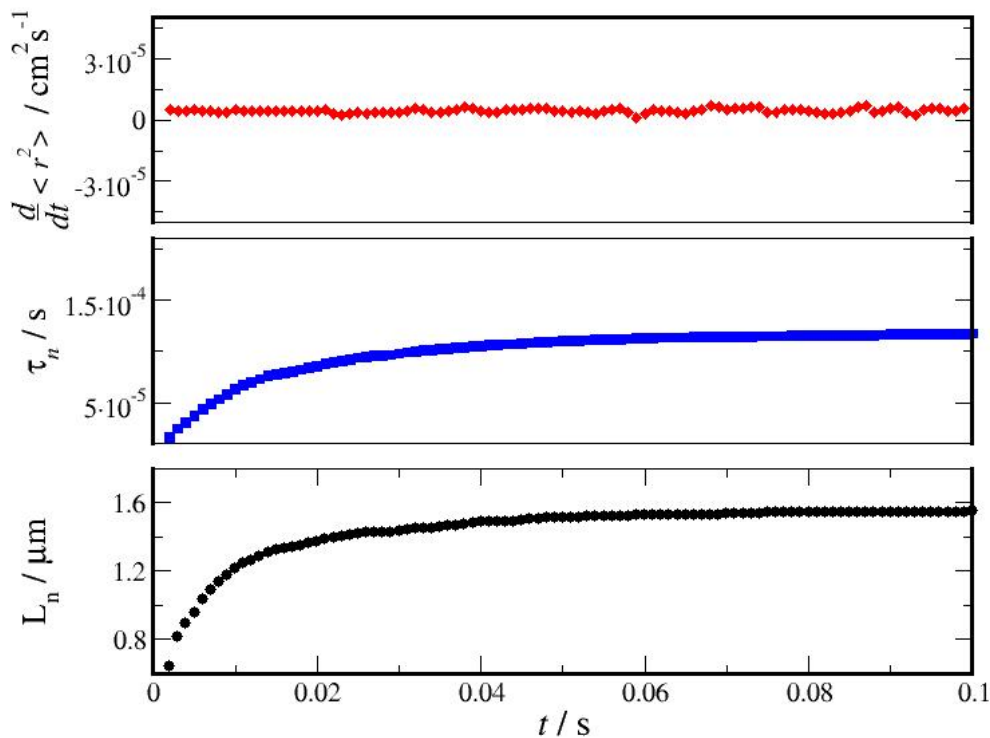
Fig. (5.1). Time evolution of the derivative of the mean square displacement (upper panel), electron lifetime (middle panel) and electron diffusion length (lower panel) in a typical RWNS calculation carried out in this work. Data shown correspond to a multi-electron calculation with 50 electrons in a simulation box of $18 \times 18 \times 18$ nm³.

lifetime). In Table (5.1) values obtained for these characteristic times are reported. The results demonstrate that the assumption on which the quasi-static approximation is based (that is, that equilibration between free and trapped electrons much faster than recombination) holds in this case. On the other hand the simulation time is long enough to sample efficiently many recombination events so that the values of the lifetime and the electron diffusion length are estimated correctly.

Table (5.1): Characteristic times for the one-electron RWNS calculations performed in this Chapter.

E_F / eV	Release time from E_F / s	Average lifetime τ_n / s	Total simulation time / s
-0.35	$7.7 \cdot 10^{-9}$	$(8.13 \pm 3.50) \cdot 10^{-5}$	0.05
-0.45	$3.7 \cdot 10^{-7}$	$(1.38 \pm 0.22) \cdot 10^{-3}$	0.5
-0.55	$1.8 \cdot 10^{-5}$	$(2.22 \pm 0.46) \cdot 10^{-2}$	1
-0.65	$8.5 \cdot 10^{-4}$	$(3.75 \pm 0.63) \cdot 10^{-1}$	50

Results for the diffusion coefficient, the lifetime and the diffusion length as a function of Fermi level can be found in Fig. (5.2). The RW simulation provides a nice demonstration of the compensation effect discussed in the Introduction. The diffusion coefficient scales exponentially with Fermi level as reported before[26,30] and shown in Chapter 4 (although for a hopping model). The slopes obtained from the simulated data were 31.86 eV[-1] and 28.09 eV[-1] for D_j and τ_n respectively. These values compare favourably with the predictions of the theoretical formula derived in the context of the multiple-trapping model (see Eq. (2.38))[30]. This equation predicts 28.15 eV[-1] for $T = 300$ K and $T_0 = 1100$ K. As a consequence of the equal but opposite behaviours of D_j and τ_n, the electron diffusion length remains constant within the statistical uncertainty of the simulation, in accordance with the predictions of the diffusion-limited model or the quasi-static approximation.

It is important to establish whether the average lifetime and average diffusion length extracted from the simulations correspond to the real quantities occurring in Eqs. (2.59) and (2.57). As mentioned above, the diffusion length appears in the solution of the 1-D diffusion equation with a first-order recombination term[31,32]. On the other hand the lifetime is the parameter controlling the exponential time decay of a first-order recombination reaction. In order to clarify this point we have computed the distribution of survival times and distances travelled by the electrons before they recombined (see Fig. (5.3)). It is found that these
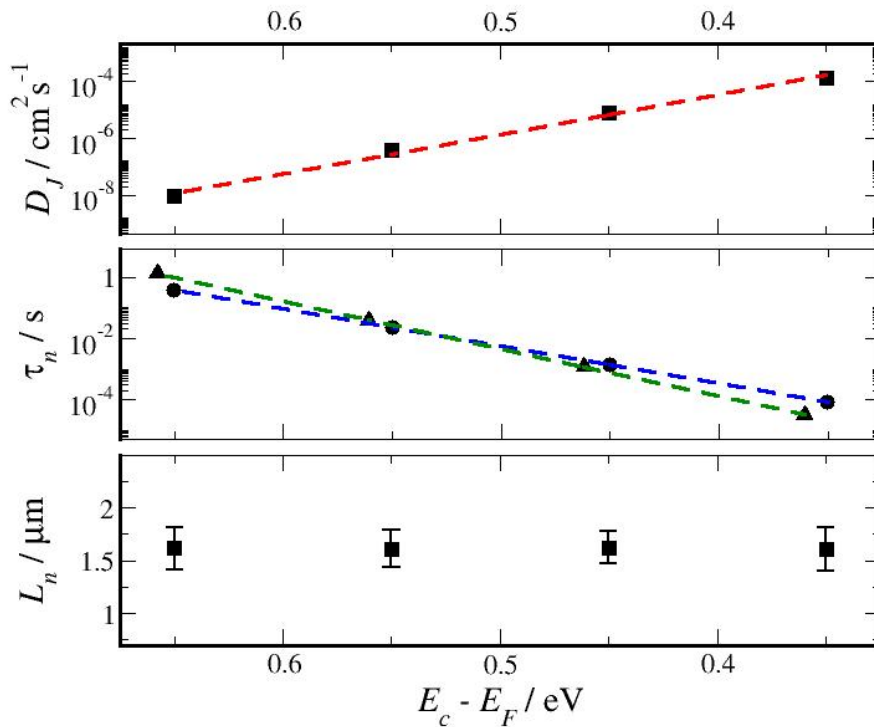
Fig. (5.2). Jump diffusion coefficient (upper panel), electron lifetime (middle panel) and electron diffusion length (lower panel) vs. Fermi level. In the middle panel two methods to compute the electron lifetime are plotted: average of survival times (circles), time decays (triangles). Note that due to the logarithmic scale, the error bars fall within the symbol size in the case of the diffusion coefficient and the lifetime.

distributions do indeed follow an exponential behaviour. However the result obtained for the distribution of distances do not fit to an exponential in the short lengths region. Ignoring this region in the fitting, we obtain reasonable agreement between the average value of the diffusion length (1.62 ± 0.15 μm) and that derived from to the fitting (1.44 μm). The agreement is more remarkable for the lifetimes: 1.38 ± 0.22 ms (average) versus 1.23 ms (fitting).

The result of this analysis indicates that the average value obtained from the simulation correspond to the real diffusion length of Eq. (2.57). A similar assumption can be established for the lifetime. However, it must be born in mind that this is normally introduced as a collective magnitude, defined from kinetic equations based on total densities. We should then distinguish between the individual magnitudes (computed by the simulation) and collective parameters in analogy with the distinction between "jump" and "chemical" diffusion
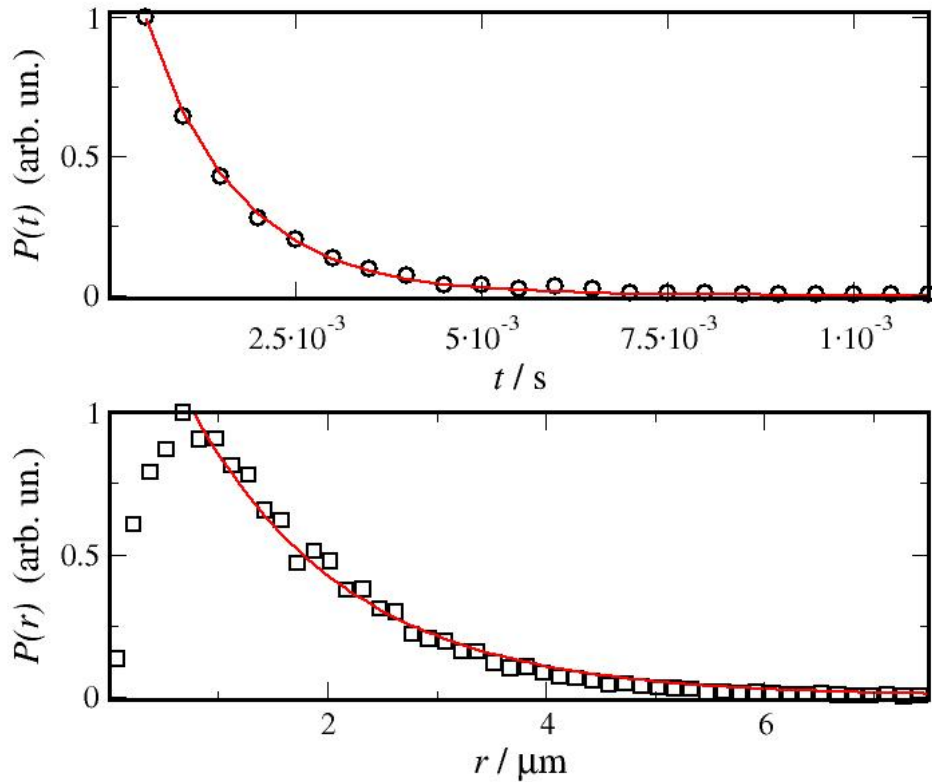
Fig. (5.3). Distribution of survival times (upper panel) and distances traveled by the electrons before recombination (lower panel) as obtained from one-electron RWNS calculations at $E_F = -0.45$ eV. The solid lines stand for fittings to an exponential function. The data are normalized with respect to the first point in the distribution.

coefficient.[33] Note in this regard that a simple relationship is found for the chemical diffusion coefficient if the trap distribution is exponential (Eqs. (2.23 and 2.37)).

$$D_n = \frac{T_0}{T} D_j \tag{5.2}$$

This relation states that the Fermi level dependence of both diffusion coefficients is the same, at least for an exponential distribution. We might think that the same relation holds for the lifetimes since an exponential behaviour with respect to Fermi level is obtained.

However, as we will show below by multi-electron calculations, this lifetime is observed to correspond to the collective lifetime τ_n. Hence we can compare directly the electron diffusion length obtained from the simulation average to that derived from Eq. (2.57). Results can be found in Table (5.2).

Table (5.2). Values of the chemical diffusion coefficient, lifetime at different Fermi levels as obtained from RW simulation. Values of L_n have been obtained from Eq. (2.57) and RW simulation respectively. Note that the diffusion coefficients shown are extracted from the simulated ones according to $D_n = (T_0/T)D_j$.

E_F / eV	D_n / $cm^2 s^{-1}$	τ_n / s	L_n / μm Eq. (2.57)	L_n / μm (RWNS)
-0.35	$(5.17 \pm 0.08)\cdot 10^{-4}$	$(8.13 \pm 3.50)\cdot 10^{-5}$	2.50 ± 0.46	1.61 ± 0.21
-0.45	$(2.80 \pm 0.42)\cdot 10^{-5}$	$(1.38 \pm 0.22)\cdot 10^{-3}$	1.97 ± 0.30	1.62 ± 0.15
-0.55	$(1.37 \pm 0.37)\cdot 10^{-6}$	$(2.22 \pm 0.46)\cdot 10^{-2}$	1.74 ± 0.42	1.61 ± 0.18
-0.65	$(3.45 \pm 1.18)\cdot 10^{-8}$	$(3.75 \pm 0.63)\cdot 10^{-1}$	1.14 ± 0.29	1.62 ± 0.20

We observe that the diffusion length obtained "indirectly" does not preserve the constancy with respect to Fermi level. This is a consequence of the fact that, due to the statistical uncertainty of the simulation, the slopes obtained for D_j and τ_n, are not exactly equal. In any case, our results show that the individual quantities maintain the same behavior that their "chemical" counterparts. Hence, the compensation behavior predicted by the theories.

The determination of the lifetime, above, has been obtained from a direct computation of the survival time of the electron population. However, experimentally the lifetime is usually obtained by monitoring the decay of the Fermi level. To provide further support to the method employed here to compute the electron lifetime, we have carried out multi-electron random walk simulations aimed to resemble a typical open-circuit voltage decay experiment[34,35]. Hence, we have run simulations with an initial number of electrons that correspond approximately to the Fermi levels studied in Table (5.2) and with no energy cut-off in the trap energy distribution. The calculation is performed with the same recombination features as in the one-electron simulations (same concentration of recombining traps and same probability of recombination). However, in this case no new electrons are introduced after recombination so that the concentration of electrons in the sample decreases with time. This a Random Walk method analogous to that used by Petrozza et al.[14] The analysis of this decay at short times shows that it is exponential, and the numerical fitting yields an approximate value of the lifetime at the corresponding value of the Fermi level. Results are shown in Fig. (5.2) (middle panel, triangles) and in Fig. (5.4). It is observed that the lifetimes reproduce quite accurately the values obtained from the "average" method. The new diffusion lengths shown in Table (5.3) also remain approximately constant, within the statistical error, upon Fermi level variation.
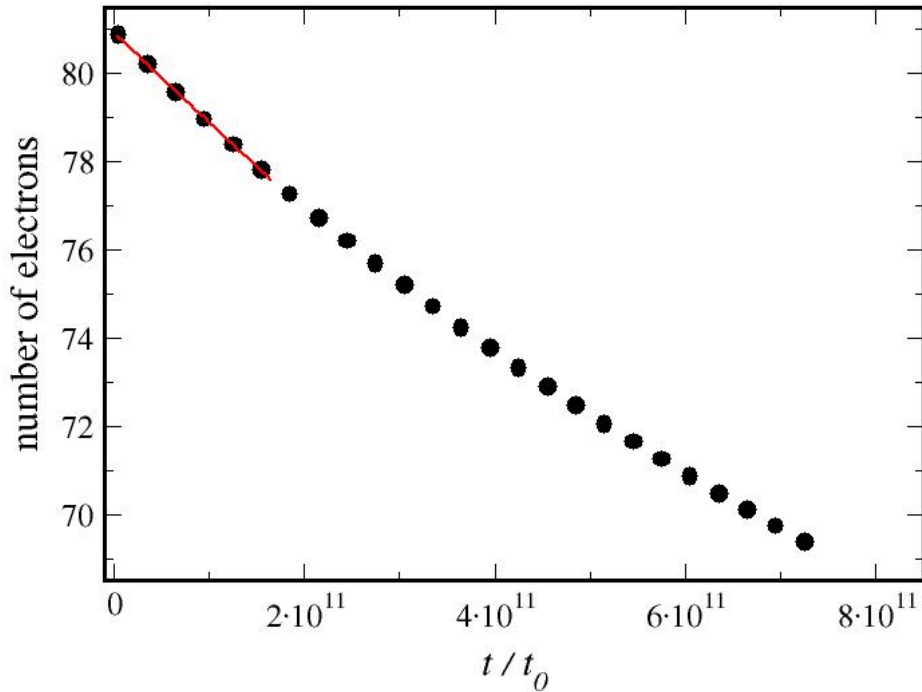
Fig. (5.4). Variation of the electron concentration with time as obtain from multi-electron random walk simulation including explicit recombination with recombining traps. The results correspond to an approximate initial Fermi level of $E_F = - 0.561$ eV. The red line represent the fit to an exponential function at short times.

Table (5.3). Values of the lifetime at different Fermi levels as obtained from multi-electron RW simulations and analysis of the decay in the population of electrons (See Fig. (5.4)). The Fermi levels were extracted from fitting the occupation probability in the multi-electron calculation. Values of L_n^{Eq} have been obtained from Eq. (2.57).

E_F / eV	τ_n / s	L_n / μm Eq. (2.57)
-0.36	$(3.15 \pm 0.04) \cdot 10^{-5}$	1.28 ± 0.02
-0.46	$(1.25 \pm 0.02) \cdot 10^{-3}$	1.87 ± 0.16
-0.56	$(3.87 \pm 0.10) \cdot 10^{-2}$	2.30 ± 0.34
-0.66	1.37 ± 0.09	2.17 ± 0.44

At this point it is important to discuss the two "views" presented at the beginning of this chapter. We must take into account that the RWNS procedure is a dynamic method in which electrons move on a random network of traps within a certain time span. If the Fermi

level is raised, the electrons move faster on average, and therefore they are more likely to encounter a recombining trap. This explains why the lifetime becomes shortened when the Fermi level is raised and supports apparently the "dynamic" view of the recombination process. However it must be taken into account that the simulation reaches at a certain time an stationary situation in which the diffusion coefficient (at earlier times) and the lifetime (at later times) remain constant for the same Fermi level. In multi-electron calculations this situation is found to correspond to a situation in which the electron population relaxes to the equilibrium Fermi distribution.[26] Hence, the results provided by the simulation arise from the fact that the system is at internal equilibrium with a trapping-detrapping rate which is much faster than the characteristic recombination time. Therefore, the "static" view in which diffusion coefficient and lifetime arise from a quasi-equilibrium with a well-defined Fermi level is in accordance with the results analyzed here.

On the basis of the preceding results we can further discuss the interpretation of transport and recombination in a DSC according to the two approaches that have been used in the literature. The transport limited recombination is a statement that recombination becomes faster (shorter lifetime) as transport becomes faster. Inherent to multiple trapping mechanisms is a displacement of electrons in the conduction band. Given a distribution of recombining traps, the only factor causing an acceleration of recombination at higher Fermi level is the progressive filling of deep traps. But this is precisely the same process causing the acceleration of the transport rate. So indeed, transport limited recombination and quasi-static model describe a unique model.

As discussed in the introduction, recombination shows additional features (i.e. a power-law dependence on free electron density) to those derived from the simple multiple-trapping description.[13,14,19,25] This means that the compensation effect that we have just demonstrated will be only partly satisfied and the electron diffusion length is not a constant. A more detailed description of this, with the reproduction of non-constant diffusion lengths will be presented in Chapter 6.

5.3. Conclusions to Chapter 5

One-electron random walk simulations within the multiple- trapping approach have been carried out. Direct computation of the diffusion length has been implemented, and values of the order of micrometers have been obtained for realistic parameters extracted from

recent literature. We find that the diffusion length maintains a constant value upon Fermi level variation. Electron lifetimes at different densities have also been computed, and we have obtained an exponential dependence with respect to the Fermi level, producing linear-log plots with slopes quite similar, although with opposite sign, also in agreement with previous experimental and theoretical studies.

The numerical method and the results obtained in this work indicate that both the "dynamic" and the "static" views to explain recombination in DSCs are indeed equivalent. Extensive multielectron calculations that take into account a more fundamental point of view that can reproduce, at a finer level, the behaviour of the diffusion lengths, are reported in Chapter 6.

References to Chapter 5

(1)   O'Regan, B.; Gratzel, M. *Nature* **1991**, *353*, 737–740.

(2)   Gratzel, M. *Nature* **2001**, *414*, 338–344.

(3)   Grätzel, M. *Journal of Photochemistry and Photobiology A: Chemistry* **2004**, *164*, 3–14.

(4)   Peter, L. M. *Journal of Physical Chemistry C* **2007**, *111*, 6601–6612.

(5)   Hamann, T. W., J., R. A. *Energy & Enviromental Science*. 2008, pp. 66–78.

(6)   Fisher, A. C.; Peter, L. M.; Ponomarev, E. A.; Walker, A. B.; Wijayantha, K. G. U. *Journal of Physical Chemistry B* **2000**, *104*, 949–958.

(7)   Peter, L. M.; Wijayantha, K. G. U. *Electrochemistry Communications* **1999**, *1*, 576–580.

(8)   Nakade, S.; Saito, Y.; Kubo, W.; Kitamura, T.; Wada, Y.; Yanagida, S. *J. Phys. Chem. B* **2003**, *107*, 8607–8611.

(9)   Nelson, J.; Haque, S. A.; Klug, D. R.; Durrant, J. R. *Physical Review B* **2001**, *63*, 6320.

(10)   Kopidakis, N.; Benkstein, K. D.; Lagemaat, J. van de; Frank, A. J. *Journal of Physical Chemistry B* **2003**, *107*, 11307–11315.

(11)   Anta, J. A.; Casanueva, F.; Oskam, G. *Journal of Physical Chemistry B* **2006**, *110*, 5372–5378.

(12)   Villanueva, J.; Anta, J. A.; Guillén, E.; Oskam, G. **2009**, *113*, 19722–19731.

(13)   Villanueva, J.; Oskam, G.; Anta, J. A. *Solar Energy Materials and Solar Cells* **2010**, *94*, 45–50.

(14)   Petrozza, A.; Groves, C.; Snaith, H. J. *Journal of the American Chemical Society* **2008**, *130*, 12912–12920.

(15)   Bisquert, J.; Vikhrenko, V. S. *Journal of Physical Chemistry B* **2004**, *108*, 2313–2322.

(16)   Bisquert, J.; Fabregat-Santiago, F.; Mora-Seró, I.; Garcia-Belmonte, G.; Giménez, S. *The Journal of Physical Chemistry C* **2009**, *113*, 17278–17290.

(17)   Bisquert, J.; Zaban, A.; Salvador, P. *Journal of Physical Chemistry B* **2002**, *106*, 8774–8782.

(18)   Salvador, P.; Hidalgo, M. G.; Zaban, A.; Bisquert, J. *Journal of Physical Chemistry B* **2005**, *109*, 15915–15926.

(19)   Bisquert, J.; Mora-Seró, I. *The Journal of Physical Chemistry Letters* **2010**, *1*, 450–456.

(20)   Wang, Q.; Ito, S.; Gratzel, M.; Fabregat-Santiago, F.; Mora-Sero, I.; Bisquert, J.; Bessho, T.; Imai, H. *Journal of Physical Chemistry B* **2006**, *110*, 25210–25221.

(21)   Fabregat-Santiago, F.; Bisquert, J.; Cevey, L.; Chen, P.; Wang, M.; Zakeeruddin, S. M.; Grätzel, M. *Journal of the American Chemical Society* **2009**, *131*, 558–562.

(22)   Wang, H.; Peter, L. M. *The Journal of Physical Chemistry C* **2009**, *113*, 18125–18133.

(23)   Barnes, P. R. F.; Anderson, A. Y.; Koops, S. E.; Durrant, J. R.; O'Regan, B. C. *The Journal of Physical Chemistry C* **2009**, *113*, 1126–1136.

(24)   Barnes, P. R. F.; Liu, L.; Li, X.; Anderson, A. Y.; Kisserwan, H.; Ghaddar, T. H.; Durrant, J. R.; O'Regan, B. C. *Nano Letters* **2009**, *9*, 3532–3538.

(25)   Villanueva-Cab, J.; Wang, H.; Oskam, G.; Peter, L. M. *The Journal of Physical Chemistry Letters* **2010**, *1*, 748–751.

(26)   Anta, J. A.; Mora-Sero, I.; Dittrich, T.; Bisquert, J. *Physical Chemistry Chemical Physics* **2008**, *10*, 4478–4485.

(27)   Wang, M.; Chen, P.; Humphry-Baker, R.; Zakeeruddin, S. M.; Grätzel, M. *ChemPhysChem* **2009**, *10*, 290–299.

(28)   Anta, J. A.; Mora-Sero, I.; Dittrich, T.; Bisquert, J. *Journal of Physical Chemistry C* **2007**, *111*, 13997–14000.

(29)   Fabregat-Santiago, F.; Mora-Sero, I.; Garcia-Belmonte, G.; Bisquert, J. *Journal of Physical Chemistry B* **2003**, *107*, 758–768.

(30)   Bisquert, J. *Physical Chemistry Chemical Physics* **2008**, *10*, 1–20.

(31)   Harrick, N. J. *Journal of Applied Physics* **1956**, *27*, 1439.

(32)   Bisquert, J. *The Journal of Physical Chemistry B* **2002**, *106*, 325–333.

(33)   Bisquert, J. *Journal of Physical Chemistry B* **2004**, *108*, 2323–2332.

(34)   Zaban, A.; Greenshtein, M.; Bisquert, J. *Chemphyschem* **2003**, *4*, 859–864.

(35)   Bisquert, J.; Zaban, A.; Greenshtein, M.; Mora-Sero, I. *Journal of the American Chemical Society* **2004**, *126*, 13550–13559.

CHAPTER 6

Origin of Non-linear Recombination in Dye-sensitized Solar Cells

In this Chapter, the transport and recombination mechanisms of photogenerated electrons in dye-sensitized solar cells are modeled by random walk numerical simulations with explicit description of the electron transfer process in terms of the Marcus-Gerischer model. The recombination rate is computed as a function of Fermi level in order to extract the electron lifetime and its influence on the electron diffusion length. The simulation method allows to relate the recombination reaction order to the trap distribution parameter, the band edge position and the reorganization energy. The results shows that a model involving electron transfer from both shallow and deep traps adequately reproduces all the experimental phenomena, including the dependence of the electron lifetime and the electron diffusion length on the open-circuit voltage when either the conduction band or the redox potential are displaced. Non linear recombination is predicted when the electron diffusion length increases with Fermi level, which is correlated with a reaction order different from one, in an open-circuit voltage decay "experiment".

6. Origin of Non-linear Recombination in Dye-sensitized Solar Cells

6.1. Introduction

In nanostructured metal oxide electrodes, recombination between photogenerated electrons in the oxide and electron acceptors in the electrolyte and at the semiconductor surface (dye cations) is a complex process in which the energetics of the semiconductor electronic structure and the distribution of relevant acceptor states play an important role. In addition, spatial disorder such as the position of the reaction centers (recombination sites, traps, etc...) and charge transport in the nanostructured oxide and in the liquid electrolyte also influence the kinetics. Charge transfer reactions across the semiconductor-electrolyte interface also include electron injection and dye regeneration[1,2]. The adequate description of these important charge transfer reactions is now becoming a primary topic in the theoretical description of nanostructured solar cells.

The fact that the recombination kinetics in the DSC exhibit non-linear features was noticed more than ten years ago in the works by Schlichtörl, van de Lagemaat, Frank, Peter and coworkers[3–6]. Later, the importance of non-linear recombination kinetics in DSC has again been stressed.[7–10] Non-linear features are detected in the non-ideal dependence of the open-circuit photovoltage on illumination intensity (with an slope larger than 59 mV/decade) and in the non-ideal behaviour of the recombination resistance with respect to applied bias (measured via impedance spectroscopy[11–13]). Moreover, non-linear effects result in the increase of the electron diffusion length as the electron density in the semiconductor is increased[8–10,14].

Non-linear recombination is normally expressed in terms of the kinetic equation

$$U_{rec} = k_r n_c^{\beta} \tag{6.1}$$

A reaction order (β) of one, indicative of simple unimolecular recombination via conduction-band states, leads to an ideal slope of 26 mV (59 mV/decade) in the *open-circuit voltage* (V_{OC}) - log(illumination intensity) plot[15] and to an electron diffusion length that is constant with respect to illumination intensity. However, reaction orders ranging between 0.6 and 0.8, indicative of *sub-linear* recombination kinetics with respect to free electron density, are generally found in dye-sensitized solar cells[10,13,16–19]. The reaction order has important implications for the photoconversion efficiency. Assuming an ideal dependence of the free

Linear and sublinear recombination

<table>
<tr>
<td>

$\beta = 1$

• Recombination rate <u>is first-order</u> with respect to free electron density
• <u>Ideal</u> slope (26 mV) of the recombination resistance with respect to free electron density
• <u>Ideal</u> slope (26 mV) of the open-circuit voltage with respect to illumination
• Diffusion coefficient and recombination constant have the same dependence with respect to total electron density: DIFFUSION LIMITED
• Diffusion length constant with respect to electron density

$$k_1(n)) = k^{ref}\left(\frac{n}{n_{ref}}\right)^{\frac{1-\alpha}{\alpha}}$$

</td>
<td>

$\beta < 1$

• Recombination rate <u>sub linear</u> with respect to free electron density
• <u>Non Ideal</u> slope (> 26 mV) of the recombination resistance with respect to free electron density
• <u>Non Ideal</u> slope (> 26 mV) of the open-circuit voltage with respect to illumination
• Diffusion coefficient and recombination constant have a different dependence with respect to total electron density: TRANSFER LIMITED
• Diffusion length increasing with electron density

$$k_1(n)) = k^{ref}\left(\frac{n}{n_{ref}}\right)^{\frac{\beta-\alpha}{\alpha}}$$

</td>
</tr>
</table>

Fig. (6.1). Comparison between linear ($\beta = 1$) and sub-linear ($\beta < 1$) recombination kinetics. k_1 is the pseudo-first order recombination constant. Taken from reference 22

electron density with respect to voltage, the described recombination rate leads to a current-voltage curve given by[8]

$$J = J_{sc} - J_0\left[\exp\left(\beta qV/k_B T - 1\right)\right] \tag{6.2}$$

which is equal to Eq. (1.1) with $\beta = 1/m$. Eq. (6.2) predicts that reaction orders significantly smaller than one lead to current-voltage curves with small fill factors, hence showing a reduced efficiency with respect to an "ideal diode" solar cell. The recombination losses can also be enhanced under illumination, as recently discussed[20,21]. Recently, non-linear recombination kinetics has been included in the numerical description of the *I-V* curve of a DSC[22].

In this Chapter we focus on the attempt to understand the effect that the energetics of the redox pair and semiconductor produce on the transport-recombination kinetics. In addition we pursue to determine the fundamental origin of a recombination order different from one. To do so, we analyze the recombination kinetics at the semiconductor oxide-electrolyte interface starting from the molecular mechanisms involved in the electron transfer reaction. As it is generally accepted that electron trapping plays a significant role in the recombination

reaction[7,23,24], we focus here on the interplay between the energetics of the electrons in the semiconductor nanostructure and the density of states of the electron acceptors. Hence, we combine the theoretical description of trap density distributions[25,26] and trap-limited transport[14,27–29] with the well-known Marcus-Gerischer (MG)[15,30] theory of charge transfer at semiconductor-electrolyte interfaces.

The MG model has been utilized[13,31] to describe the kinetics or recombination from a distribution of localized states to a distribution of acceptor states in the electrolyte. In summary, their approach is based on Eq. (2.53). This equation simply states that the recombination rate is a consequence of the interplay of three contributions: the number of states available at each value of the energy in the semiconductor (described typically by an exponential distribution for an inorganic semiconductor), the probability that this energy state is occupied (Fermi-Dirac) and the number of states available in the electrolyte, as determined by the MG formula. To obtain the net recombination rate the product of these three probabilities should be integrated to all values of the energy between the redox Fermi level (E_{redox}) and the semiconductor conduction band edge (E_c). Starting from this basic scenario, it has been derived an approximate analytical expression for the recombination rate[13,31] applying the zero temperature limit of the Fermi-Dirac distribution and assuming that the Marcus reorganization energy is much larger than the photovoltage.

According to this simplified formalism, the reaction order is given by Eq. (2.56).

$$\beta = \frac{1}{2} + \alpha \tag{6.3}$$

Hence, for characteristic temperatures or around 900-1200 K,[26,32] recombination orders of ~ 0.75-0.85 are predicted, close to the experimental values. This model is also successful to predict the correct temperature dependence of the recombination order[7], although abnormally high characteristic temperatures seem to be required to fit the experimental data. On the other hand, to assume that the reorganization energy is much larger than the photovoltage may be too strong of an approximation, since reorganization energies of the order of 0.4-1.2 eV are commonly reported for typically used redox couples[24,30,33–35]. An additional complication is that assuming that the reorganization energy is very large, excludes the possibility that the system may enter the Marcus inversion regime, a situation that has been claimed in the literature[10,30].

MG theory has recently also been applied by Ondersma and Hamann[35] to successfully predict the shape of the electron lifetime curve versus voltage in DSCs with outer-sphere

redox shuttles. The formalism of these authors is also based on the description represented by Eq. (2.53), but with explicit consideration of inner and outer reorganization energies (see Eq. (2.52)). The model devised by these authors includes electron transfer mediated by surface states, that can play a significant role in the recombination reaction. More recently Ansari-Rad et al.[36] also use Eq. (2.53) as a starting point to devise a theoretical model where the β exponent is calculated as a function of Fermi level, showing that it is always less than unity, except when the Fermi level approaches the conduction band. It has to be noted that most of these previous studies focused on the determination and analysis of the electron lifetime, a magnitude which is usually measured at open-circuit or at a position-independent Fermi level. However, a solar cell at working conditions does not operate at open circuit, but in the presence of a density gradient, which drives electrons to the external contact. Hence the interplay between transport and recombination (as manifested by the value of the diffusion length) is decisive for good electron collection at real operating conditions.

In the previous Chapter, we applied the random-walk numerical simulation method (RWNS)[27–29] to evaluate the lifetime (τ_n) and the diffusion length (L_n) for electrons moving in an exponential distribution of trap energies. This procedure requires to incorporate recombination kinetics in the algorithm, which was assumed to occur according to a constant probability. This way, only trapping/detrapping events and the population of the electronic states (traps) contribute to the Fermi level dependence of τ_n and L_n. Using this simplified method, the compensation effect predicted by various authors[37–40] can be nicely reproduced from a microscopic mechanism of transport/recombination. In this Chapter we extend this method by introducing a non-constant recombination probability, which depends on the energy of the donor and the acceptor state according to the MG model[15,41]. As stated in Eq. (2.53), the probability of recombination and the recombination rate should depend on the population of electronic states in the semiconductor (controlled by the Fermi level position) and the reorganization energy of the redox couple in the electrolyte. It is expected that all these microscopic parameters produce complex kinetics that cannot be described by a reaction order of one.

6.2. Methodology

The aim is two-fold: on the one hand we intend to analyse the problem posed by the kinetic equation and Eq (2.53) from first principles, using RWNS, a versatile tool to study, simultaneously, transport and recombination. On the other hand we intend to extend previous theoretical work by establishing unambiguously the effect of the reorganization energy and

the relative positions of redox energy and conduction band on both the diffusion length and the lifetime.

To do so, we have introduced an energy-dependent recombination mechanism in the RWNS algorithm, which is described by the MG model. The MG model has been introduced previously by a number of authors[7,15,30,31,35] to describe recombination in DSCs. To our knowledge, this work represents the first time that MG theory is incorporated in a RWNS calculation. Basically, this is done by giving a *recombining character* to the network of traps in such a way that its energy distribution serves as the medium from which a direct charge-transfer from traps is applied. However, in order to achieve a complete recombination model two alternative stochastic procedures based on the MG description have been implemented. It has to be noted that these two models represent different recombination mechanisms, in which transport plays a distinct role.

The first recombination procedure brings about the computation of a probability of recombination P_R each time an electron reaches a trap of energy E. This is obtained via the following expression

$$P_R(E) = k_{r0} \sqrt{\frac{k_B T}{4\pi\lambda}} \exp\left[-\frac{(E - E_{ox})^2}{4\lambda k_B T} \right] \tag{6.4}$$

with $k_{r0} = 2k_0 c$, where k_0 is a time constant for tunnelling and c is the concentration of oxidized species in the electrolyte in accordance to Eq. (2.50). This description, which we will call **Model 1**, can be seen as an extension of the calculations of Chapter 5 in which a constant recombination probability is replaced by a more realistic energy-dependent probability[14]. By this procedure we can simulate the interplay between the random walk of the electrons and the charge transfer to the electrolyte.

The second recombination procedure involves a formulation based on times instead of probabilities. Thus, the waiting times numerical algorithm is modified in such a way that each electron is assigned a recombination time along with its detrapping time. These recombination times are computed according to the inverse of Eq. (6.4)

$$t_i^{rec} = -\ln(R) t_{r0} \sqrt{\frac{4\pi\lambda}{k_B T}} \exp\left[\frac{(E_i - E_{ox})^2}{4\lambda k_B T} \right] \tag{6.5}$$

where R is a random number uniformly distributed between 0 and 1 and t_{r0} is a adjustable

prefactor that controls the time scale of recombination. The implementation of this algorithm (that we will call **Model 2**) is as follows: once charge carriers have been injected, detrapping and recombination times are computed for all of them via Eqs. (3.1) and (6.5) respectively. Both types of times are stored in the same list of *waiting* times in such a way that if the minimum time corresponds to detrapping, that carrier is selected to move into its target site. On the contrary, if the minimum time corresponds to recombination, the carrier is removed from the sample. Once executed either the move or the recombination, both detrapping and recombination times of the rest of the carriers are reduced by t_{min}.

A mechanism based on times rather than on rates or probabilities leads, in principle, to the same results because according to Eqs. (6.4) and (6.5) a low recombination time is equivalent to a high recombination rate (and vice versa). However, there is an important difference between both models, which is based on the sequence in which the simulation moves are executed. In **Model 1** the MG formula is applied *after* each detrapping event. Hence, transport will influence recombination to some extent. On the contrary, in **Model 2**, the application of the MG formula runs in *parallel*. Hence transport and recombination are separated and uncorrelated. Furthermore, in **Model 2** *direct transfer* between trapped electrons and electrolyte acceptors is possible, whereas in **Model 1**, only electrons that have been previously detrapped (i.e. *quasi free* electrons), are allowed to recombine. In both models, however, recombination can take place starting from any trap state (either via a previous detrapping or by direct transfer) and not only from the conduction band.[38] This is a reasonable assumption if we consider that the great majority of electrons will be trapped (approximately 90% as recently estimated)[24] and that electrons spend a much longer time in trapped states than in the conduction band.

It must be noted that in the RWNS formalism utilized in this thesis there is strictly *no conduction band* level. E_c is just the parameter that determines the transport activation energy in the multiple-trapping description of Eq. (3.1) and the origin of energies in the exponential distribution of Eq. (2.2). Furthermore, simulation times are always normalized with respect to t_0 in Eq. (3.1), which represents the average residence time of electrons in the conduction band. Hence, electrons do no effectively *stay* in the conduction band and they cannot undergo direct recombination from the conduction band, *within* this particular formalism. However, as the mechanism of recombination based on Eq. (6.4) (**Model 1**) involves that electrons should get detrapped before they have the possibility to undergo a recombination process, it can be seen as an alternative view to a "conduction band recombination probability" under certain conditions. In fact, if we bear in mind that detrapping times from shallow traps are much shorter than from deep traps and that most of the sites have energies close to the "conduction band" (for an exponential distribution) one expects that **Model 1** samples preferentially recombination from shallow traps whereas **Model 2** samples recombination from deep traps.[42]
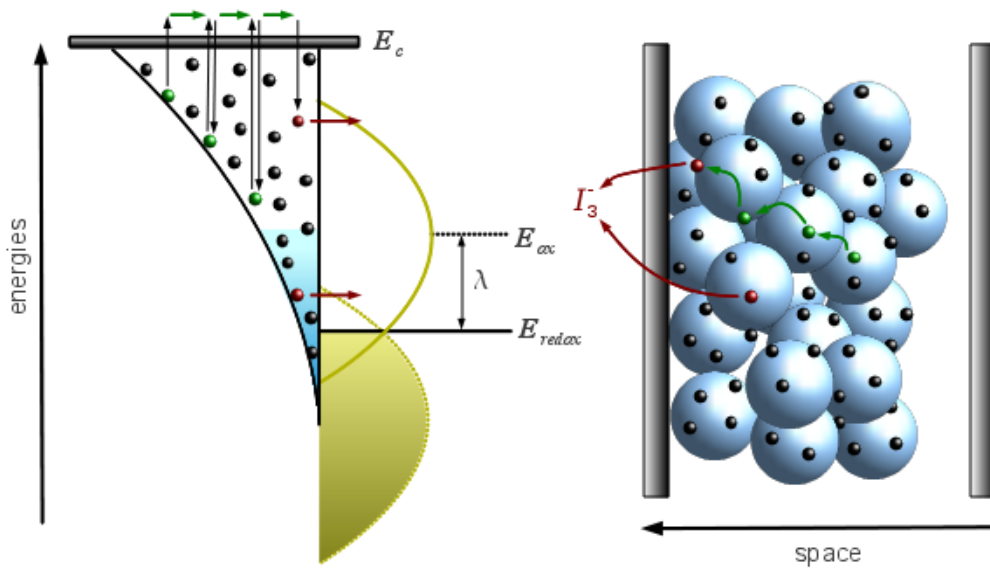
Fig. (6.2). Illustration of the transport and recombination processes studied in this Chapter. The meaning of the reorganization energy, λ, and the Fermi level position (showed as a shaded region) is explicitly indicated in the figure.

In this Chapter we study the Fermi level dependence of the electron diffusion length for both kinds of recombination mechanisms. In addition, we present the results for a hybrid model, which is a combination of both. In all cases, the recombination rate of specific electrons will depend on their energies and this will introduce a number of *recombination events* in the simulation for a given set of input parameters. Hence, the objective of the simulation procedure is to store the time and the distance that electrons survive/travel before they recombine. As we will see below, only the hybrid model is capable of adequately reproducing the behaviour of the system with respect to Fermi level and conduction band position. In Fig. (6.2), a schematic representation of the numerical procedure and the physical processes involved is shown. Using the different models, we perform random walk simulations of two experiments that are generally used to characterize recombination kinetics: (i) determination of kinetic parameters under constant illumination intensity and under open circuit voltage conditions; an (ii) open circuit voltage decay measurements upon switching off the light source.

In a first kind of simulations (steady-state RWNS), as the solar cell is simulated at open-circuit conditions and under constant illumination intensity (fixed Fermi level), a constant electron density should be maintained in the sample. This is achieved by imposing the restriction that when an electron has just recombined, another electron is immediately injected into the system in another place at random. For this *fresh* electron, both time and

distance are reset such that the average time and distance between recombination events can be computed, stored and represented versus total simulation time. Finally, these magnitudes are renormalized by the total number of electrons and the total number of recombination events so that the result is effectively an average time and distance for one single electron. We have demonstrated in Chapter 5 that this procedure yields *true* electron lifetimes and diffusion lengths[14].

In a second kind of simulations (transient RWNS), the restriction of re-introducing electrons is removed. This procedure makes it possible to simulate a typical open-circuit voltage decay experiment[41]. As no new electrons are introduced after recombination, the concentration of electrons in the sample decreases with time according to certain kinetics. It has been found that this decay can be described by a power law, such that the reaction order β with respect to free electron density can be extracted by means of a fitting procedure to the integrated version of Eq. (6.1).

In Chapter 1 we saw that the electron lifetime is defined by Eq. (1.10). The lifetime is hence defined as the variation of the recombination rate for small variations of the total density, and it is the lifetime extracted from small-perturbation techniques such as impedance spectroscopy. Alternatively a pseudo-first order lifetime can be defined[20,22,36,43] In the same way, the electron lifetime with respect to the Fermi level can be monitored from the decay according to[7,44]

$$\tau_1 = -\frac{n}{dn/dt} \tag{6.6}$$

As shown in Ref. 36, both lifetimes are not equal. In Ref. 22 it has been shown that the two life times are proportional to each other and related by a constant (equal to α/β).

In this Chapter we use Eq. (6.6) to extract the lifetime from the transient RWNS calculations. It is shown that this procedure reproduces the values of lifetimes obtained from the "average" method described above, for the same Fermi level, quite accurately. This is consistent with results contained in Chapter 5, where it was found that the distribution of survival times for electrons was exponential in a simulation performed at constant Fermi level, corresponding to first-order recombination kinetics. The time constant of this distribution coincided with the lifetime obtained by averaging the survival times of the electrons.

In order to keep the number of adjustable parameters as small as possible, we have employed values reported in the literature for most of the parameters used in the

simulations[14,30]. Hence, we use $T_0 = 700\text{-}1100$ K, $T = 300$ K, $N_l = 10^{27}$ m^{-3} (meaning an average trap-trap distance of 1 nm) and $t_0 = 10^{-14}$ s. A cut-off radius of 1.5 nm is introduced in the simulation so that jumps to neighboured traps beyond this distance are not considered. To study the effect of a shift of the band edges, we have used two different values for the position of the conduction band extracted from the work of Jennings and Wang[30]: $E_c = 0.95$ eV for the case of no additives and $E_c = 0.7$ eV in the presence of 2M Li$^+$ in the electrolyte solution. The only adjustable parameters are those controlling recombination (k_{r0} or t_{r0} (or both) and λ). Independent adjustment of k_{r0} and t_{r0} gives us freedom to favour one model over another. Both parameters depend on the distance between electron and acceptors and can vary with the composition of the electrolyte. For instance, addition of adsorptive species such us TBP or Li$^+$ can increase the distance between electrons in the semiconductor and the redox-active ions, as suggested by Nakade et al.[34] Furthermore, different tunnelling factors are expected for traps of different energy. However, for simplicity, we have considered both k_{r0} and t_{r0} factors independent of energy.

As can be seen in Appendix A, the adjustment of k_{r0} and t_{r0} for each model (and the ratio of them in the case of a combination of both) does not modify the Fermi level dependence of the lifetime and the diffusion length so we are able to represent the results normalized by the maximum value of the measured magnitudes in each case. Moreover, to avoid excessive computational times, systems with relatively small diffusion lengths have been simulated with the restriction that it must always be ensured that the time scale for trapping/detrapping is much shorter than the time scale of recombination, as shown in our previous work[14]. Finally, a sufficient number of independent simulations (defined for different random number sequences) have been carried out in order to ensure good statistics in the final results.

6.3. Results and discussion

Results of steady-state RWNS simulations using **Model 1** for two different values of the reorganization energy are presented in Fig. (6.3) (upper panel). Electron diffusion length calculations are shown as a function of the energy difference $E_F - E_{redox}$, which corresponds to the open-circuit voltage (V_{oc}) produced by the solar cell at steady-state. In the dark, $E_F - E_{redox} = 0$, and the system remains in thermodynamic equilibrium.

It is observed that the diffusion length increases with V_{oc} with an energy-dependent recombination probability provided that the reorganization energy is sufficiently low (i.e. $\lambda = 0.2$ eV). In contrast, for a higher reorganization energy ($\lambda = 0.6$ eV) the electron diffusion
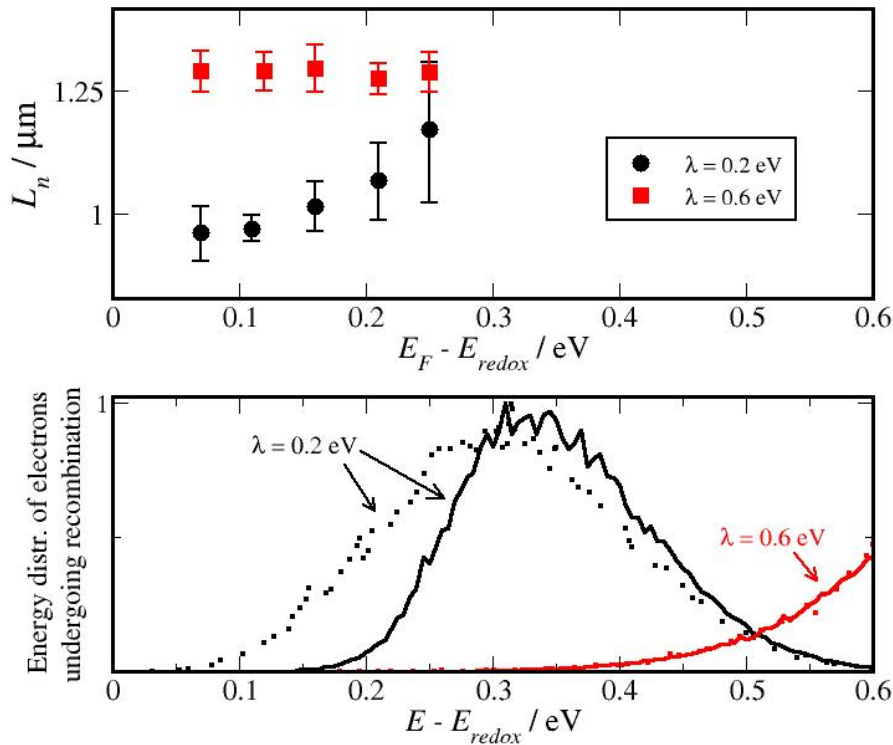
Fig. (6.3). **Top:** Electron diffusion length calculated by steady-state RWNS calculations using **Model 1** for two values of the reorganization energy. **Bottom:** Distribution of energies for electrons undergoing recombination. The same two values of the Fermi level are shown for both reorganization energies: $E_F - E_{redox} = 0.25$ eV (solid line) and $E_F - E_{redox} = 0.07$ eV (dashed line). The characteristic temperature of the trap energy distribution utilized in the simulation was $T_0 = 1100$ K and a band offset of $E_c - E_{redox} = 0.7$ eV was considered.

remains constant. The predictions of **Model 1** presented in Fig. (6.3) can be explained as follows. For an exponentially increasing trap density distribution, the detrapping probability of electrons increases upon shifting the Fermi level to higher energies. As a consequence, the time spent in the nanostructured film is shorter, making recombination less likely. However, the probability of recombination also depends on the number of acceptor states, as described by Eq. (6.4). At this point, two scenarios can be observed: (1) *Linear regime*: for a redox couple with a reorganization energy larger than V_{oc}, the recombination probability is increased due to the increase of the available acceptor states upon raising the Fermi energy. As a result, there is a compensation effect that keeps the diffusion length approximately constant. (2) *Non-linear regime*: for redox couples with a small reorganization energy, the recombination probability decreases with increasing V_{oc}, when the system enters the Marcus inverted region. In this case, the diffusion length is expected to increase with increasing (open-circuit) voltage, since the recombination kinetics become slower due to the lower probability of electron

transfer to the solution.

The origin of the dissimilar behaviour of the diffusion length can also be understood by inspecting the lower panel of Fig. (6.3), where the distribution of trap energies from which the electrons undergo a recombination event is shown. For the case in which the diffusion length does not increase with voltage, this distribution is exponential, indicating that most electrons recombine from states close to the conduction band. On the other hand, when the diffusion length increases with voltage, the distribution exhibits a maximum at intermediate energies. The appearance of this maximum is a consequence of the interplay between two opposite effects: the increase of the density of donor states characteristic of an exponential function, and the decrease of the density of acceptor states as the energy of the electron is raised. More importantly, the two regimes differ in another feature. For the linear case the distribution of states from which recombination occurs does not change when the Fermi energy, i.e. the electron density, is varied. Hence, the diffusion length remains constant. On the contrary, for the non-linear case the distribution maximum gets displaced towards lower energies. This change in the recombination probabilities explains why the diffusion length tends to increase as more electrons are accumulated in the semiconductor for the non-linear case.

The previous result shows that a non-constant behaviour of the diffusion length with respect to V_{oc} (*non-linear regime*) can be reproduced with an energy-dependent recombination probability using **Model 1**. However, it must be recognized that this regime is only accessible if the open-circuit voltage is above the most probable oxidation energy in the electrolyte (E_{ox}), i.e. in the Marcus inverted regime. This last requirement implies that for typical values of the open circuit voltage of standard DSC of 0.6-0.8 V, very small values of the reorganization energy are needed. However, values below $\lambda = 0.4$ eV are rather unrealistic[35]. On the other hand, the models of Bisquert et al.[7,15] and Villanueva-Cab et al.[45] show consistent formalisms according to which an increasing electron diffusion length with respect to V_{oc} can be achieved assuming much higher values of the reorganization energy. Hence, it is concluded that **Model 1** does not achieve an adequate description of non-linear recombination in DSCs, implying that other charge-transfer mechanisms must be taking place.

As described in the previous section, the alternative **Model 2** assumes that direct transfer between trapped electrons and electron acceptors can take place. This is implemented by computing recombination times via Eq. (6.5) and allowing for removal of electrons when these times are shorter than the transport times, in accordance with the usual RWNS
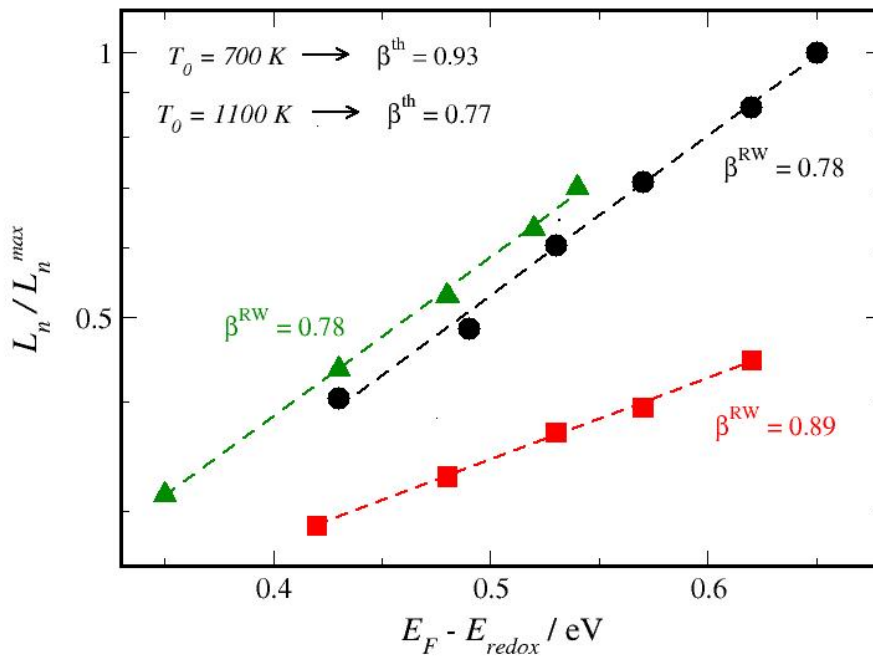
Fig. (6.4). Electron diffusion length calculated by steady-state RWNS calculations using Model 2 for different values of the reorganization energy and the characteristic temperature: $T_0 = 700$ K and, $\lambda = 2$ eV (circles), $T_0 = 700$ K and $\lambda = 2$ eV (squares) and $T_0 = 1000$ K, $\lambda = 20$ eV (triangles). Results are obtained from the Marcus-Gerischer formula (Eq. (6.5)) and a density of electronic states in the semiconductor given by Eq. (2.2). A band offset of $E_c - E_{redox} = 0.95$ eV was considered. Dashed lines correspond to fits to Eq. (2.62). "Theoretical (th)" and "simulated (RW)" values of the adimensional parameter ‾ are also indicated in the graph.

algorithm. Steady-state results for the electron diffusion length obtained by **Model 2** are presented in Fig. (6.4).

First of all, it can be observed that, in contrast to Model 1, **Model 2** predicts an increasing diffusion length versus the open-circuit voltage for a high value of the reorganization energy. Moreover, the curves exhibit exponential behaviour in accordance to the theoretical models[7,45] where Eq. (2.62) is derived[7] with a theoretical value for the exponential parameter given by Eq. (6.3). However, although the simulations with **Model 2** predict an exponential behaviour, the parameter β extracted by fitting to Eq. (2.62) does not coincide with the theoretical value of Eq. (6.3). This is due to the fact that those equations were derived under the assumption that the reorganization energy is several orders of magnitude larger than the open-circuit voltage (which is indeed a strong approximation). As a matter of fact, curves in Fig. (6.4) using a reorganization energy of $\lambda = 20$ eV do offer a

possibility to test the prediction of (6.3). Such an unrealistic value of the reorganization energy (although otherwise appropriate for theoretical reasons) permits us to obtain simulated slopes closer to the theoretical values of (6.3). On the other hand, **Model 2** reproduces qualitatively the temperature dependence of the diffusion length. Thus, it is found that for $T_0 = 1000$ K the slope of the log $(L_n/L_n^{max}$ vs. $E_F - E_{redox})$ curves is higher than for $T_0 = 700$ K in accordance to the theoretical prediction of (6.3)[7]. In summary, **Model 2** seems adequate to explain many of the experimental facts as well as the occurrence of a *non-linear regime*.

However, it is essential to find a model that it is capable of reproducing *all* experimental observations in DSCs in order to clarify the charge-transfer mechanisms involved in this type of solar cells. In this context, recent reports by Jennings et al. [10,30] showed that it is possible to induce a change from the *non-linear* to the *linear* regime by addition of lithium ions to a iodide/tri-iodide electrolyte. This change has been interpreted as a consequence of the displacement of the semiconductor conduction band towards more positive potentials upon Li^{+} addition. To describe this observation we have carried out simulations for different values of the E_c parameter with respect to the electrolyte equilibrium redox level, but keeping the total number of traps constant. In this context it has to be noted that some authors[24,35,46] have pointed out that the electrochemistry of the iodide/tri-iodide system is very complicated as it involves a multi-electron process and intermediate species such as I_2^-. However, in this work we do not study the actual mechanism of electron transfer but the effect that the relative positions of conduction band and redox level, as well as the reorganization energy, have on the recombination kinetics. Even if charge transfer involves the production of I_2^- instead of I_3^- there will always be a distribution of acceptor energies given by Eq. (2.50), which would be sensitive to displacement of either the conduction band in the semiconductor or the equilibrium redox level of the electrolyte.

Results for both models, together with experimental results from Refs. [10,30] for two compositions of the electrolyte, can be found in Fig. (6.5). As indicated in the previous section, we can represent results normalized with respect to the maximum value for both experimental and simulated cases. The simulation results show that it is possible to approximately reproduce the experimental curves using **Model 1**. However, again, an unrealistic low value for the reorganization energy ($\lambda = 0.25$ eV) is required. On the other hand, it is observed that if we use **Model 2** the diffusion length slope can not be changed when the band is displaced, neither by using a large reorganization energy ($\lambda = 2$ eV) nor an intermediate one ($\lambda = 0.6$ eV).
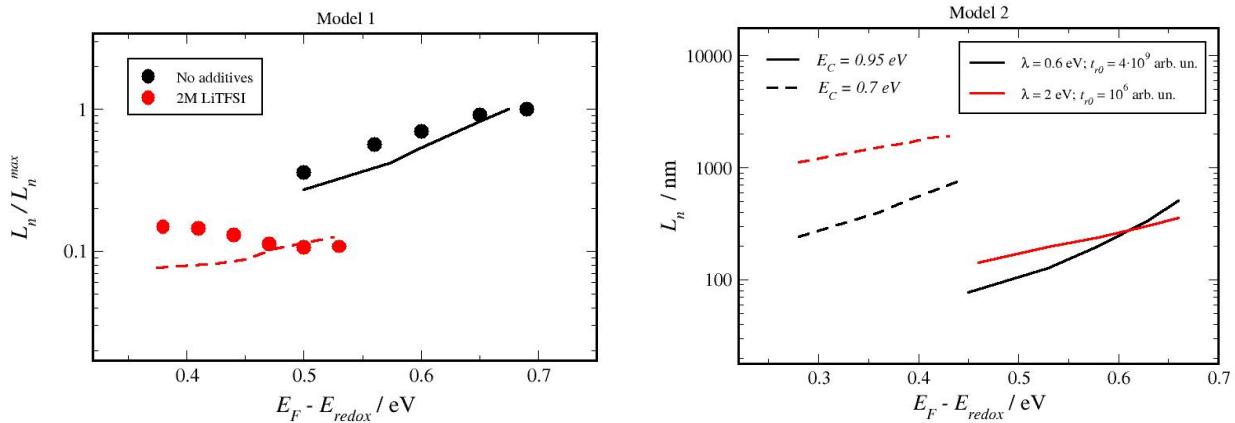
Fig. (6.5). **Left:** experimental measurements (Ref. 10) of the electron diffusion length for a DSC with Li^{+} (red circles) and without Li^{+} ions (black squares) in the electrolyte and the predictions of **Model 1** with $\lambda = 0.25$ eV, $T_0 = 700$ K and $T = 300$ K are presented. Values of $E_c - E_{redox} = 0.7$ eV (red dashed line) and 0.95 eV (black solid line) are used for a DSC with and without Li^{+} ions in the electrolyte respectively. Different values of k_{r0} (see Eq. (6.4) have been used for each case: $k_{r0} = 5 \cdot 10^{-5}$ arb. un. for $E_c - E_{redox} = 0.7$ eV and $5 \cdot 10^{-4}$ arb. un. for 0.95 eV. **Right:** Predictions of **Model 2** with the same parameters: $T_0 = 700$ K, $T = 300$ K, $E_c - E_{redox} = 0.95$ eV (solid lines) - 0.70 eV (dashed lines). Two values of the reorganization energy: $\lambda = 2$ eV (red) and $\lambda = 0.6$ eV (black) are used for each type of electrolyte.

The change of the electron diffusion length behaviour upon band displacements has been interpreted as a modification of the main recombination mechanism involved in the semiconductor/electrolyte interface, from recombination via trap states to recombination via conduction band states.[10,30] Here it is important to stress again that **Model 1** can be interpreted as an alternative view of the so-called conduction band recombination if a high enough reorganization energy is applied. Indeed, it can be seen in Fig. (6.3) that when the reorganization energy is higher than the photovoltage the energy distribution for electrons undergoing recombination is exponential meaning that most of the sites from which recombination events occur are those very close to the conduction band edge. These shallow states correspond to "nearly free" electrons, which are more likely to recombine. Hence, for an exponential distribution of trap energies, the shallow states (close to E_c) play the role of an *effective* conduction band, with faster transport and more rapid recombination if there are acceptor states available close to $E = E_c$. At the same time, **Model 2** has proven to be ideal to reproduce recombination from deep traps due to its capacity to reproduce theoretical features that take into account this specific charge-transfer mechanism. In summary, it is reasonable to assume that an adequate combination of the two models may be able to explain all the experimental phenomenology, including the effect of the change of the diffusion length slope when plotted versus V_{oc}.

In the following, RW simulation data as obtained by a combination of Model 1 and Model 2 (**Hybrid Model**) are presented. In these simulations electrons being detrapped are allowed to recombine by generating probabilities with Eq. (6.4), as defined by **Model 1**. Simultaneously, unmobile electrons are also allowed to recombine directly from traps according to waiting times obtained by Eq. (6.5), as defined by Model 2. The relative weight of each type of recombination is controlled by adjusting the parameters k_{r0} and t_{r0}, respectively.

Results obtained by this hybrid model, along with experimental data for different compositions of the electrolyte, are shown in Fig. (6.6). The calculations were carried out using $T_0 = 700$ K, $T = 300$ K, $\lambda = 0.6$ eV, $k_{r0} = 8 \cdot 10^{-5}$ arb. un., $t_{r0} = 1.25 \cdot 10^8 \ t_0$. The simulation results show that it is possible to reproduce the change of slope observed experimentally for realistic values of these microscopic parameters. It is observed, however, that a displacement of the conduction band towards lower energies (more positive electrochemical potentials),
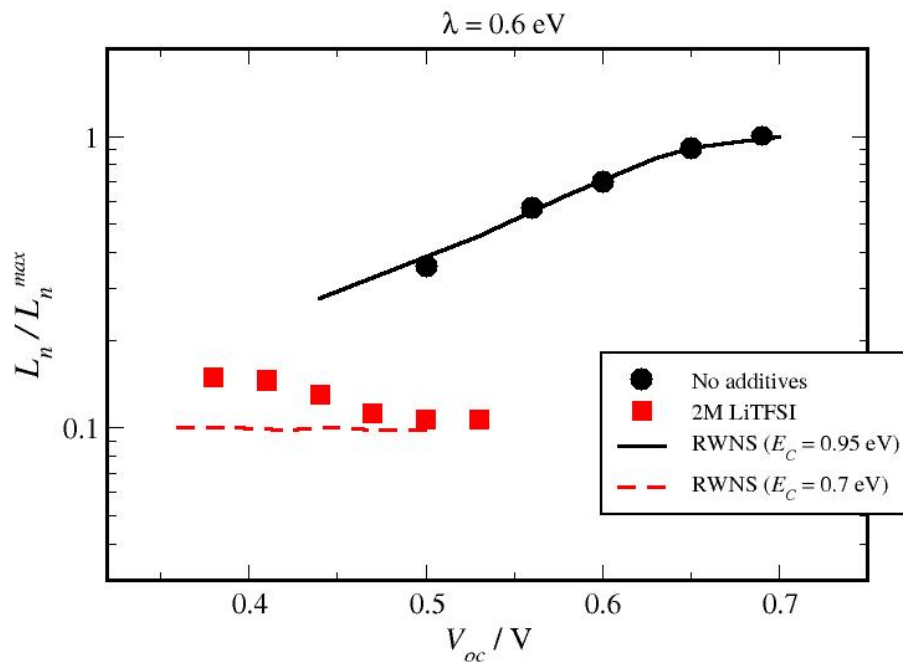
Fig (6.6). Electron diffusion length from experiments (symbols) and calculated by steady-state RWNS calculations (lines) using the combination of Model 1 (Eq. (6.4)) and Model 2 (Eq. (6.5)) (**Hybrid Model**). The simulations correspond to a system defined by $\lambda = 0.6$ eV, $T_0 = 700$ K, $T = 300$ K and $E_c - E_{redox} = 0.95$ (black) and 0.7 eV (red), using $k_{r0} = 8 \cdot 10^{-5}$ arb. un. and $t_{r0} = 1.25 \cdot 10^8 \ t_0$. Note that data are normalized with respect to the maximum value.

leads to longer diffusion lengths. Longer values of the electron diffusion length have been found experimentally when lithium ions are added in the electrolyte[30]. However it has been reported[10] that freshly fabricated DSCs with LiTFSI (simulated system) exhibited higher L_n than DSC with no additives and that after a certain time L_n decreased, although the dependence with respect to the open-circuit voltage is preserved. The lowering of the electron diffusion length maintaining the dependence at the same time has also been reproduced as can be seen in Fig. (6.6). To achieve this we have modified the prefactor k_{r0} in Eq. (6.4), specifically from $8 \cdot 10^{-5}$ to $2.5 \cdot 10^{-3}$ arb. un.

It might be argued that the chosen value of the reorganization energy is somehow arbitrary. Hence, we have tried to fit the experimental data using a large value of the reorganization energy. Results of these RW simulations are presented in Fig. (6.7) for $\lambda = 2$ eV and two different values of the recombination prefactors (k_{r0} and t_{r0}). In that case,
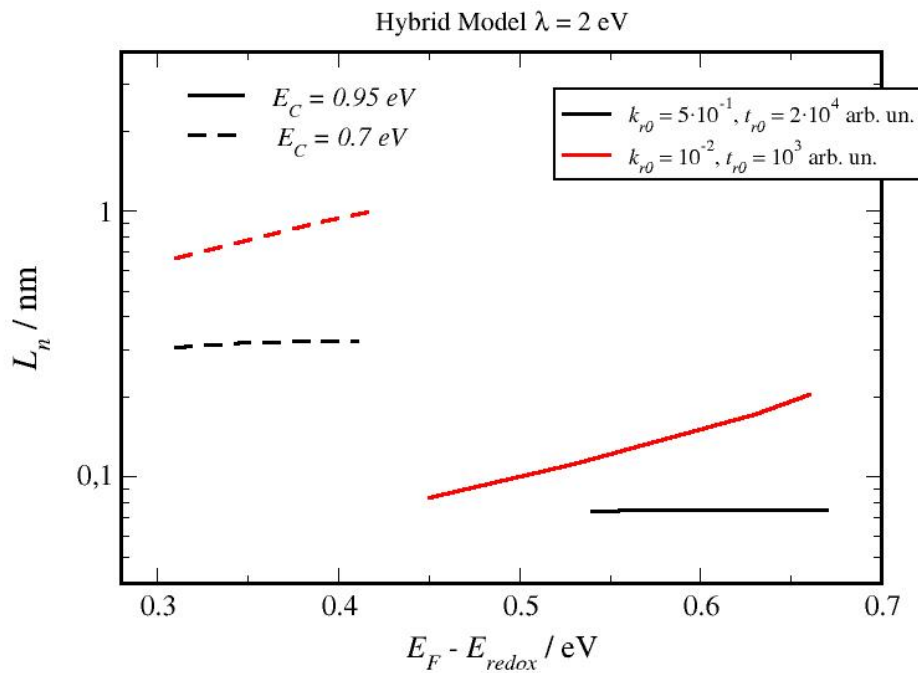
Fig. (6.7). Electron diffusion length calculated by steady-state RWNS calculations using the **hybrid model**. The simulations correspond to a system defined by $\lambda = 2$ eV, $T_0 = 700$ K, $T = 300$ K and $E_c - E_{redox} = 0.95\text{-}0.70$ eV. Results are obtained from the Marcus-Gerischer formula (Eqs. (6.4) and (6.5)) and density of electronic states in the semiconductor (Eq. (2.2), trap energy distribution).

an appreciable change of the Fermi level dependence of the diffusion length upon band shift is not observed, hence, we can conclude that only by using an intermediate value of the reorganization energy, which is lower than the two studied values of $E_c - E_{redox}$, the experimental behaviour can be reproduced. In other words, a certain contribution of the well-known Marcus inverted regime is necessary to reproduce the observed trends[30]. To further clarify this point, the energy distributions for electrons undergoing recombination corresponding to the simulations of Fig. (6.6) are shown in Fig. (6.8) for two different values of the Fermi level in each case. For $E_c = 0.95$ eV (no additives in the electrolyte), it is observed that the most probable donor energy is located in the vicinity of the Fermi level energy and is, therefore, different for each simulated open-circuit voltage. On the other hand,
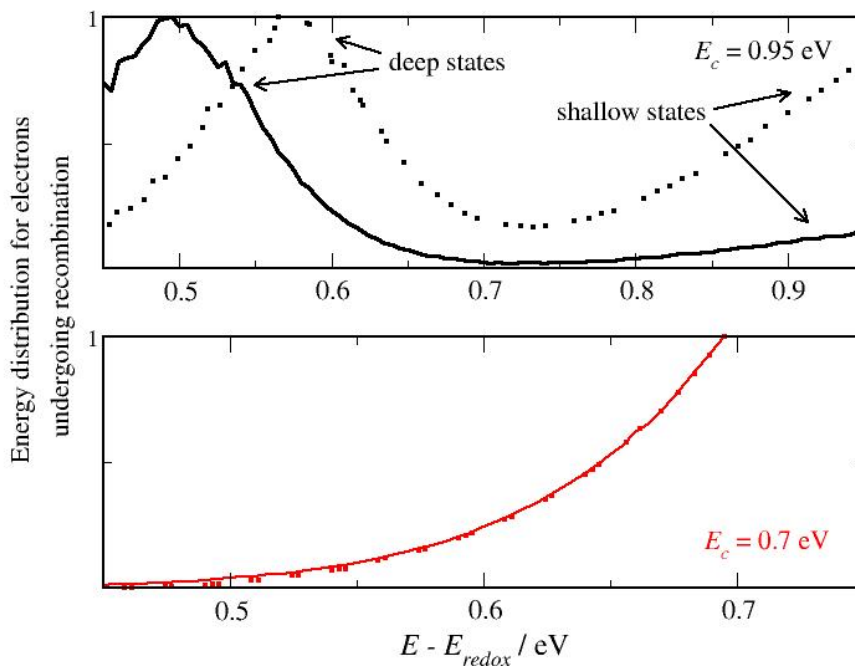
Fig. (6.8). Distribution of energies for electrons undergoing recombination for the two values of the conduction band energy studied in Fig. (6.6) as predicted by the Hybrid model. Two Fermi levels are represented for each conduction band position: For $E_c - E_{redox} = 0.95$ eV (top) the cases $E_F - E_{redox} = 0.45$ eV (solid line) and $E_F - E_{redox} = 0.58$ eV (dashed line) are represented. Likewise, for $E_c - E_{redox} = 0.7$ eV (bottom) the cases $E_F - E_{redox} = 0.39$ eV (solid line) and $E_F - E_{redox} = 0.5$ eV (dashed line) are represented. Calculations were carried out using $k_{r0} = 10^{-3}$ arb. un. and $t_{r0} = 10^7 t_0$.

for $E_c = 0.7$ eV (with 2M Li$^+$ in the electrolyte), the most probable donor energy is situated in the vicinity of the conduction band position for both cases and does not change with respect to V_{oc}. Therefore, a correspondence is actually observed between the electron diffusion length behaviour and the energy distribution function of recombination sites. This observation can be related to the Marcus inverted regime described in Fig. (6.3), where an increasing electron diffusion length is expected when the recombination site is at a higher energy than E_{ox} (the most probable energy of the electron acceptor in solution). In conclusion, the interplay of the Marcus inverted regime and the displacement of the conduction band can correctly explain the change from a V_{oc} - independent to a V_{oc} - dependent diffusion length as a change of the main charge transfer mechanism, from recombination controlled by shallow traps to recombination controlled by deep traps.

To establish the "degree of non-linearity" we should estimate the reaction order β with respect to free electron density. As indicated in the previous section and in Chapter 5, the RWNS method can be utilized to simulate an open-circuit photovoltage decay experiment. The kinetics of the recombination reaction can be numerically extracted by fitting to the expression for the *total* electron density:

$$-\frac{dn}{dt} = kn^\gamma \quad ; \quad \gamma \neq 1 \tag{6.7}$$

which can be integrated to give:

$$-\int_{n_0}^{n} \frac{dn}{n^\gamma} = k \int_{0}^{t} dt \quad \Rightarrow \quad n = (At + B)^{\frac{1}{1-\gamma}} \tag{6.8}$$

where A and B are constants. In Eqs. (6.7) and (6.8), the exponent γ is the reaction order with respect to the total electron density. Under quasi-static conditions (internal equilibrium between free and trapped electrons), the total and free electron densities are related to each other. The following relationship can be derived[4]

$$\left(\frac{n}{n_0}\right) = \left(\frac{n_c}{n_{c,0}}\right)^\alpha \tag{6.9}$$

where n_0 is the total density in the dark and $n_{c,0}$ the density of free electrons in the dark.

Introducing Eq. (6.9) in Eq. (6.7), and taking into account Eq. (6.1) we find

$$\gamma = \frac{\beta}{\alpha} \qquad\qquad (6.10)$$

Note that the reaction order with respect to the total electron density (γ) can be larger than one, even when (as it will be discussed below) the recombination rate is sub-linear with respect to free electron density ($\beta < 1$).

The result of the fits to the electron density decays between specific Fermi levels in Fig. (6.9) show that a larger slope of the electron diffusion length with respect to V_{oc} is correlated to a larger degree of non-linearity of the recombination kinetics. Hence, for the case of $E_c - E_{redox} = 0.7$ eV, where the diffusion length is independent of V_{oc} as shown in Fig. (6.6), a reaction order of $\beta \sim 0.99$ is obtained. In contrast, for the case of
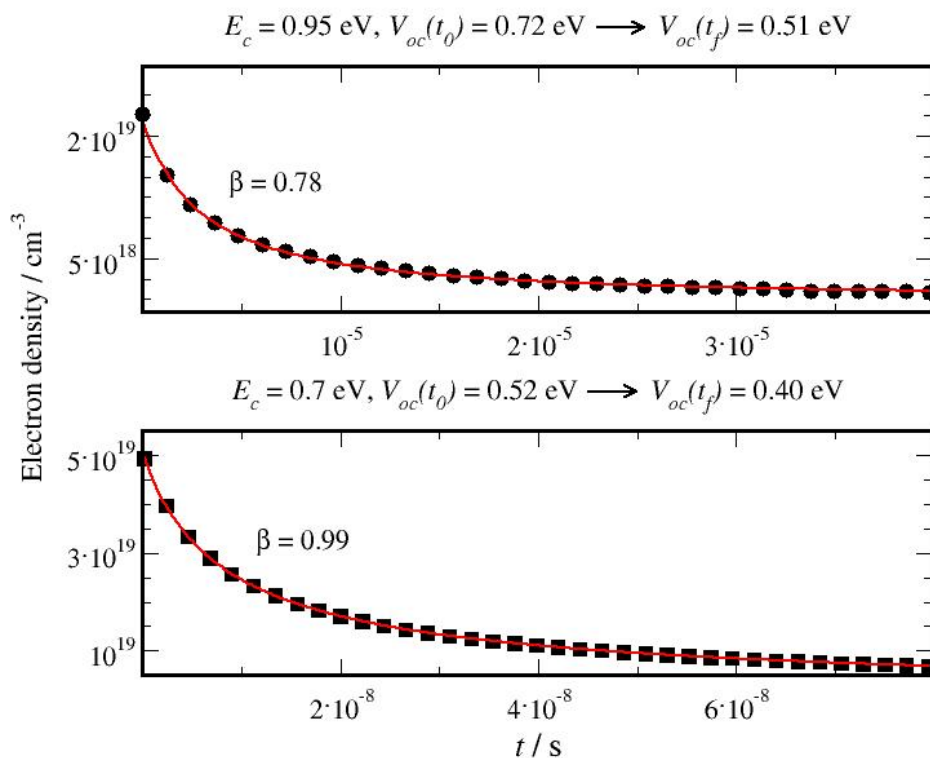
Fig. (6.9). Evolution of the total electron population in a transient RWNS calculation using the Hybrid model of recombination for the same cases as those studied in Fig. (6.6). The solid line represents the result of the fitting to Eq. (6.8). Note that results shown correspond to rapid recombination kinetics (short-diffusion length).

$E_c - E_{redox} = 0.95$ eV, where the diffusion length is dependent on V_{oc} (Fig. (6.6)), a value of β ~ 0.78 is obtained. The results were obtained for a fast recombining system (short diffusion length). However, as shown in Appendix A, modifying the value of the prefactors in Eqs. (6.4) and (6.5) does change the absolute value of L_n, but not its variation with respect to Fermi level. Hence, we can conclude that the observed correlation between non-linear recombination and diffusion length behaviour is therefore in agreement with the results of Bisquert and Mora-Seró[8] and Villanueva-Cab et al.[9]

By means of Eq. (6.6) the electron lifetime can be extracted from the electron density decays. The results are compared with the electron lifetimes obtained from the steady-state simulations using the averaging procedure in Fig. (6.10). It is found that both methods provide the same results, hence confirming that the behaviour of the diffusion length is actually connected to the kinetics of the recombination reaction. It is interesting to note that the behaviour of the lifetime is the same as observed in experiments.[10,47] Indeed, the electron
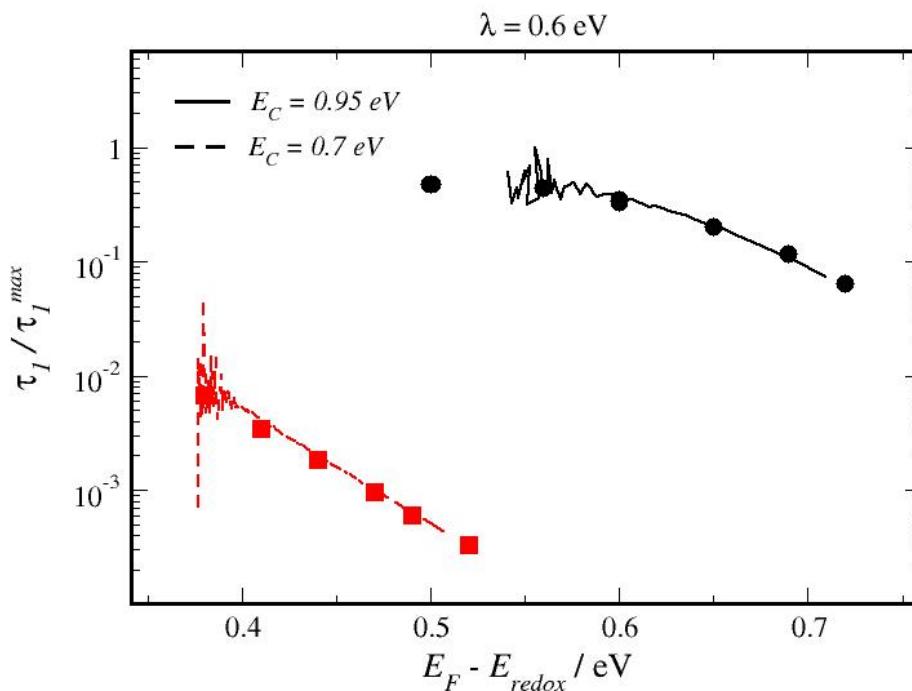
Fig. (6.10). Electron lifetimes for a system defined by $\lambda = 0.6$ eV, $T_0 = 700$ K, $T = 300$ K and $E_c - E_{redox} = 0.95$ (black) and 0.70 eV (red). Symbols stand for results of the steady-state RWNS calculations and lines refer to lifetimes extracted from transient RWNS calculations and Eq. (6.6). Calculations were carried out using the Hybrid Model with $k_{r0} = 10^{-3}$ arb. un. and $t_{r0} = 10^7 t_0$.

lifetime is reduced upon shifting the conduction band to lower energies meaning that the recombination rate is enhanced. This is an expected characteristic, since when the conduction band is lowered, it gets closer to a fixed Fermi level, which is similar to raising the Fermi level ($E_F - E_{redox}$) towards a fixed conduction band energy. As the recombination rate is increased upon addition of Li$^+$, the open-circuit voltage of the solar cell at the same illumination intensity is reduced. This suggests that it is kinetics rather than thermodynamics that determine the variation of V_{oc} in a DSC when the semiconductor conduction band is displaced. A similar effect is produced when a redox pair with a different equilibrium potential is used, as is the case for novel redox shuttles, including those based on cobalt complexes.[48–52] On the other hand, Fig. (6.10) shows that the electron lifetime slope for the case of $E_c - E_{redox}$ = 0.7 eV is higher (defined positive) than for the case of $E_c - E_{redox}$ = 0.95 eV. This is consistent with the fact that a compensation effect that maintains the diffusion length constant is accomplished in the first case but not in the second.

6.4 Conclusions to Chapter 6

Electron transport and recombination processes in dye-sensitized solar cells are described by means of a random-walk numerical simulation procedure based on the multiple-trapping model, and where recombination is explicitly considered using Marcus-Gerischer theory. This model permits to relate the non-linear features of the recombination rate usually found in the experiments with the molecular mechanisms of transport and electron transfer that take place in the nanostructured semiconductor and at the semiconductor/electrolyte interface. Only a hybrid model that takes recombination from shallow traps and from deep traps into account at the same time reproduces all the experimental observations correctly. This work helps to understand how a *non-linear regime* can arise from the relative positions of the Fermi level and the equilibrium redox potential of the electrolyte.

We have observed that non-linear recombination kinetics can be detected for high values of the reorganization energy. However, only if we consider a driving-force for recombination in the Marcus inversion regime, corresponding to a value of the oxidation energy lower than the conduction band position (small or moderate reorganization energy), it is possible to reproduce the experimental observation that a positive band-edge displacement leads to a change in the diffusion length behaviour, from being dependent on V_{oc} to becoming independent of V_{oc}. We explain the experimental observation as a consequence of a change in the main recombination mechanism involved in the system, from a shallow traps controlled charge transfer mechanism (constant diffusion length) to a deep traps controlled charge transfer mechanism (diffusion length dependent on V_{oc}). We believe that the results are very relevant to understand the performance of new *redox-shuttles* in dye-sensitized solar cells.

References to Chapter 6

(1)   Cai, J.; Satoh, N.; Han, L. *The Journal of Physical Chemistry C* **2011**, *115*, 6033–6039.

(2)   Jennings, J. R.; Liu, Y.; Wang, Q. *The Journal of Physical Chemistry C* **2011**, *115*, 15109–15120.

(3)   Schlichthorl, G.; Park, N. G.; Frank, A. J. *Journal of Physical Chemistry B* **1999**, *103*, 782–791.

(4)   Lagemaat, J. van de; Frank, A. J. *Journal of Physical Chemistry B* **2000**, *104*, 4292–4294.

(5)   Frank, A. J.; Kopidakis, N.; Lagemaat, J. van de *Coordination Chemistry Reviews* **2004**, *248*, 1165–1179.

(6)   Fisher, A. C.; Peter, L. M.; Ponomarev, E. A.; Walker, A. B.; Wijayantha, K. G. U. *Journal of Physical Chemistry B* **2000**, *104*, 949–958.

(7)   Bisquert, J.; Fabregat-Santiago, F.; Mora-Seró, I.; Garcia-Belmonte, G.; Giménez, S. *The Journal of Physical Chemistry C* **2009**, *113*, 17278–17290.

(8)   Bisquert, J.; Mora-Seró, I. *The Journal of Physical Chemistry Letters* **2010**, *1*, 450–456.

(9)   Villanueva-Cab, J.; Wang, H.; Oskam, G.; Peter, L. M. *The Journal of Physical Chemistry Letters* **2010**, *1*, 748–751.

(10)   Jennings, J. R.; Li, F.; Wang, Q. *The Journal of Physical Chemistry C* **2010**, *114*, 14665–14674.

(11)   Bisquert, J. *The Journal of Physical Chemistry B* **2002**, *106*, 325–333.

(12)   Fabregat-Santiagoa, F.; Bisquert, J.; Palomares, E.; Haque, S. A.; Durrant, J. R. *Journal of Applied Physics* **2006**, *100*.

(13)   Wang, Q.; Ito, S.; Gratzel, M.; Fabregat-Santiago, F.; Mora-Sero, I.; Bisquert, J.; Bessho, T.; Imai, H. *Journal of Physical Chemistry B* **2006**, *110*, 25210–25221.

(14)   Gonzalez-Vazquez, J. P.; Anta, J. A.; Bisquert, J. *The Journal of Physical Chemistry C* **2010**, *114*, 8552–8558.

(15)   Salvador, P.; Hidalgo, M. G.; Zaban, A.; Bisquert, J. *Journal of Physical Chemistry B* **2005**, *109*, 15915–15926.

(16)   Fabregat-Santiago, F.; Bisquert, J.; Palomares, E.; Otero, L.; Kuang, D. B.; Zakeeruddin, S. M.; Gratzel, M. *Journal of Physical Chemistry C* **2007**, *111*, 6550–6560.

(17)   Guillén, E.; Fernández-Lorenzo, C.; Alcántara, R.; Martín-Calleja, J.; Anta, J. A. *Solar Energy Materials and Solar Cells* **2009**, *93*, 1846–1852.

(18)   Guillén, E.; Azaceta, E.; Peter, L. M.; Zukal, A.; Tena-Zaera, R.; Anta, J. A. *Energy Environ. Sci.* **2011**, *4*, 3400–3407.

(19)   Guillén, E.; Idígoras, J.; Berger, T.; Anta, J. A.; Fernández-Lorenzo, C.; Alcántara, R.;

Navas, J.; Martín-Calleja, J. *Physical Chemistry Chemical Physics* **2011**, *13*, 207.

(20)   Barnes, P. R. F.; Anderson, A. Y.; Juozapavicius, M.; Liu, L.; Li, X.; Palomares, E.; Forneli, A.; O'Regan, B. C. *Phys. Chem. Chem. Phys.* **2011**, *13*, 3547–3558.

(21)   Zhu, K.; Jang, S.-R.; Frank, A. J. *The Journal of Physical Chemistry Letters* **2011**, *2*, 1070–1076.

(22)   Anta, J. A.; Idígoras, J.; Guillén, E.; Villanueva-Cab, J.; Mandujano-Ramirez, H. J.; Oskam, G.; Pelleja, L.; Palomares, E. J. *Physical Chemistry Chemical Physics* **2012**.DOI: 10.1039/c2cp40719a

(23)   Peter, L. M. *Journal of Physical Chemistry C* **2007**, *111*, 6601–6612.

(24)   Hagfeldt, A.; Boschloo, G.; Sun, L.; Kloo, L.; Pettersson, H. *Chemical Reviews* **2010**, *110*, 6595–6663.

(25)   Fabregat-Santiago, F.; Randriamahazaka, H.; Zaban, A.; Garcia-Canadas, J.; Garcia-Belmonte, G.; Bisquert, J. *Physical Chemistry Chemical Physics* **2006**, *8*, 1827–1833.

(26)   Bisquert, J.; Fabregat-Santiago, F.; Mora-Sero, I.; Garcia-Belmonte, G.; Barea, E. M.; Palomares, E. *Inorganica Chimica Acta* **2008**, *361*, 684–698.

(27)   Nelson, J. *Physical Review B* **1999**, *59*, 15374–15380.

(28)   Kopidakis, N.; Schiff, E. A.; Park, N.-G.; van de Lagemaat, J.; Frank, A. J. *The Journal of Physical Chemistry B* **2000**, *104*, 3930–3936.

(29)   Anta, J. A. *Energy and Enviromental Science* **2009**.

(30)   Jennings, J. R.; Wang, Q. *The Journal of Physical Chemistry C* **2010**, *114*, 1715–1724.

(31)   Bisquert, J.; Zaban, A.; Salvador, P. *Journal of Physical Chemistry B* **2002**, *106*, 8774–8782.

(32)   Anta, J. A.; Mora-Sero, I.; Dittrich, T.; Bisquert, J. *Journal of Physical Chemistry C* **2007**, *111*, 13997–14000.

(33)   Kuciauskas, D.; Freund, M. S.; Gray, H. B.; Winkler, J. R.; Lewis, N. S. *The Journal of Physical Chemistry B* **2001**, *105*, 392–403.

(34)   Nakade, S.; Kanzaki, T.; Kubo, W.; Kitamura, T.; Wada, Y.; Yanagida, S. *Journal of Physical Chemistry B* **2005**, *109*, 3480–3487.

(35)   Ondersma, J. W.; Hamann, T. W. *Journal of the American Chemical Society* **2011**, *133*, 8264–8271.

(36)   Ansari-Rad, M.; Abdi, Y.; Arzi, E. *J. Phys. Chem. C* **2012**, *116*, 10867–10872.

(37)   Anta, J. A.; Casanueva, F.; Oskam, G. *Journal of Physical Chemistry B* **2006**, *110*, 5372–5378.

(38)   Bisquert, J.; Vikhrenko, V. S. *Journal of Physical Chemistry B* **2004**, *108*, 2313–2322.

(39)   Nelson, J.; Haque, S. A.; Klug, D. R.; Durrant, J. R. *Physical Review B* **2001**, *63*, 6320.

(40)   Kopidakis, N.; Benkstein, K. D.; Lagemaat, J. van de; Frank, A. J. *Journal of Physical Chemistry B* **2003**, *107*, 11307–11315.

(41)   Bisquert, J.; Zaban, A.; Greenshtein, M.; Mora-Sero, I. *Journal of the American Chemical Society* **2004**, *126*, 13550–13559.

(42)   note: *The reason for that is that after a jump event the recombination of the electron is recalculated to account for the new energy of the target site. Thus, most of the electrons that may undergo recombination will be those immobile during a time that is long enough to get the shortest recombination time within the list of waiting times.*

(43)   Barnes, P. R. F.; Anderson, A. Y.; Durrant, J. R.; O'Regan, B. C. *Physical Chemistry Chemical Physics* **2011**, *13*, 5798.

(44)   Hsiao, P.-T.; Teng, H.-S. *Journal of the Taiwan Institute of Chemical Engineers* **2010**, *41*, 676–681.

(45)   Villanueva, J.; Oskam, G.; Anta, J. A. *Solar Energy Materials and Solar Cells* **2010**, *94*, 45–50.

(46)   Ardo, S.; Meyer, G. J. *Chemical Society Reviews* **2009**, *38*, 115.

(47)   Haque, S. A.; Palomares, E.; Cho, B. M.; Green, A. N. M.; Hirata, N.; Klug, D. R.; Durrant, J. R. *Journal of the American Chemical Society* **2005**, *127*, 3456–3462.

(48)   Ondersma, J. W.; Hamann, T. W. *Journal of Physical Chemistry C* **2010**, *114*, 638–645.

(49)   Nelson, J. J.; Amick, T. J.; Elliott, C. M. *J. Phys. Chem. C* **2008**, *112*, 18255–18263.

(50)   DeVries, M. J.; Pellin, M. J.; Hupp, J. T. *Langmuir* **2010**, *26*, 9082 – 9087.

(51)   Bergeron, B. V.; Marton, A.; Oskam, G.; Meyer, G. J. *J Phys Chem B* **2005**, *109*, 937–943.

(52)   Oskam; Bergeron, B. V.; Meyer, G. J.; Searson, P. C. *Journal of Physical Chemistry B* **2001**, *105*, 6867–6873.

CHAPTER 7

Charge Collection Efficiency in Nanostructured Solar Cells

The collection efficiency of carriers in solar cells based on nanostructured electrodes is determined for different degrees of morphological one-dimensional order. The transport process is modelled by RWNS in a mesoporous electrode that resembles the morphology of nanostructured TiO2 electrodes typically used in DSCs and related systems. It is found that the partially ordered electrode can almost double the collection efficiency with respect to the disordered electrode. However, this improvement depends strongly on the probability of recombination. The collection efficiency is found to reach very rapidly a saturation value, meaning that, in the region of interest, a slight degree of ordering might be sufficient to induce a large improvement in collection efficiency. A theoretical study of the influence of shape of the charge generation profile on the collection efficiency of a nanostructured solar cell is also presented. The numerical results show that if the charge generation profile is gaussian, the collection efficiency is found to increase exponentially as the centre of the gaussian approaches the collecting electrode. Furthermore, the collection efficiency is roughly independent of the gaussian width for devices where there is no bias field. Simulations where a gaussian absorption is superposed on top of an exponential profile showed that the corresponding improvement in efficiency is very much dependent on the diffusion length.

7. Charge Collection Efficiency in Nanostructured Solar Cells

7.1. Introduction

One of the reasons why new generation solar cells are attracting so much interest between scientists and technologists is the fact that they use materials in a disordered phase (although nanocrystalline in certain cases). Disordered media make unnecessary the highly expensive purification and crystallization process characteristic of high performance solar cells. Furthermore, they allow for transparency, multi-angle light harvesting, flexibility, etc. [1–5] However, there is recently a renewed interest in improving the efficiency of these devices by working with 1-dimensional (1D) ordered nanostructures such as nanowires, nanotubes, etc. [6–10] The idea is to improve the collection of charges using a photoanode where there is a more direct path towards the external circuit. This way faster transport and slower recombination is theoretically achieved, so that charge and energy losses are minimized. Nevertheless, these structures are commonly difficult to prepare with the quality required for making efficient devices. Hence, the use of 1D nanostructures leads to the following paradox: the advantages of using a disordered material is sacrificed for the sake of improving the efficiency of the device. This paradox rises the question of how important is the benefit of using 1D nanostructures.

In a report by Tirosh et al. [11], the issue of the influence of the ordering of an anatase nanocrystalline structure on electron diffusion was studied. These authors found a substantial increase in the electron diffusion coefficient when a *partial* ordering is induced in the nanocrystalline electrode by means of an electric field that is applied during the deposition procedure. This enhancement was interpreted in terms of percolation effects. The influence of the percolation path in TiO_2 nanocomposites (considered via a variable porosity) has also been studied by Dittrich et al. [12] and Ofir et al. [13] These effects have also been described successfully by numerical modelling (random walk techniques) [14–17]. The effect of morphology on charge transport has also been studied for many other systems [18–20] However, the effect of the ordering with both the consideration of transport and recombination, which is crucial to understand the performance of nanostructured solar cells, remains to be comprehensively studied. In this regard, it has been pointed out recently [21] that the alleged benefit of using 1-D nanostructures should be taken with reserve, especially for DSC architectures where charge collection already approaches a 100%.

In this Chapter we address this issue by exploring the relationship between degree of order and charge collection efficiency. The main objective is to find a semiquantitative functional relation between the increase in efficiency and an appropriate order parameter. This functional relation will help to assess the improvement produced by a hypothetical ordering of a disordered nanostructure substrate typically used in dye-sensitized solar cells[22]. This problem is addressed from the theoretical point of view, using numerical methods[23,24]. The advantage of using numerical simulation is that degree of order and the charge collection efficiency can be more easily and unambiguously measured, isolating the effect of the order from other effects such as specific surface or the recombination rate. For instance, very recently[25] *ab initio* simulation has been proven very useful to describe non-adiabatic charge transfer from quantum dots to the TiO_2 surface. Here we study the effect of order on charge transfer, including transport and recombination, but on a larger spatial scale, not accessible to *ab initio* methods. The aim is to clarify and help guiding future research, which should be focused on obtaining better functioning devices by addressing the key issues that limit efficiency[21].

7.2. Methodology: computation of the collection efficiency for realistic nanostructures

The charge collection efficiency in photoelectrochemical cells is defined as the ratio between the number of charge carriers (electrons or holes) collected in the external circuit and the number of photogenerated carriers. This can be expressed as[26]

$$\eta_{col} = \frac{\tau_{rec}}{\tau_{rec} + \tau_{tr}} \tag{7.1}$$

where τ_{rec} and τ_{tr} are the lifetime and the transport time of charge carriers, respectively (measured at coincident positions of the Fermi level). The collection efficiency has typically been discussed in the current literature in terms of the diffusion length[27–30]. As discussed in detail in Ref. 28 even if recombination is not linear, Eq. (2.57) is used to define a "small perturbation" diffusion length, which is still useful to diagnose the collection efficiency of the device. Hence, the longer is L_n, the larger is the probability of collecting charges in the external contact. Both Eqs. (7.1) and (2.57) show that good collection efficiency arises from a balance of fast transport and slow recombination. The effect expected from the use of 1D nanostructures is either to accelerate transport or to minimize recombination (or both).
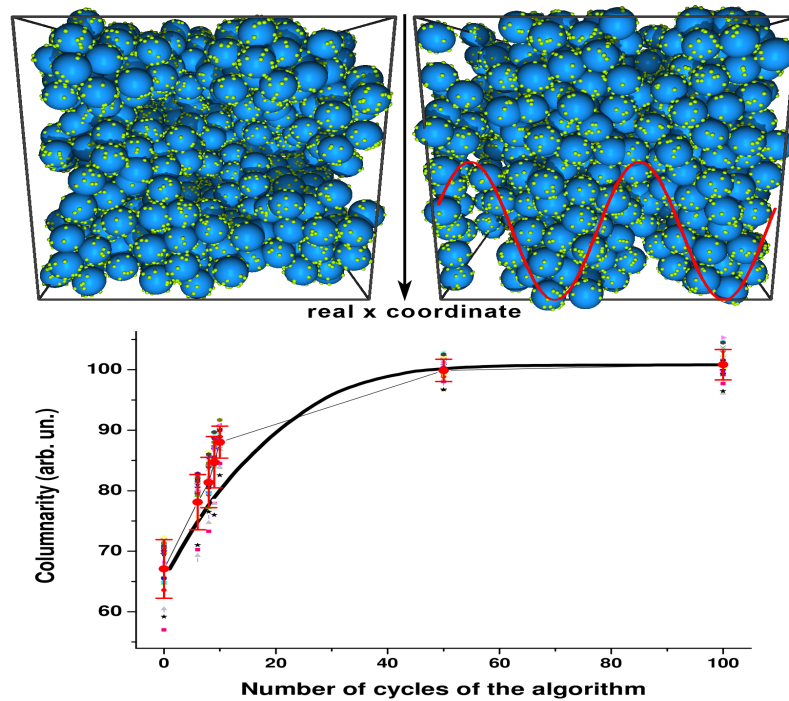
Fig. (7.1). Top left: Simulation box (size ~ 400 nm) with a random-packing of nanospheres with electron traps located on the surface (R^2 model). Top right: same as left but with a partial order induced along x-direction by Monte Carlo energy minimization. The external periodic potential is plotted with a red solid line. Bottom: "columnarity" of the array of nanospheres (symbols) for various replicas and energy difference with respect to the minimum (solid line) versus the number of cycles executed in the minimization procedure. Energy variation is normalized with respect to the starting situation, $1-(E-E_{min})/(E_{max}-E_{min})$ and scaled for comparison purposes.

With the aim of studying the effect of working with a 1D nanostructure, we introduce order in a random packing of nanospheres (see Fig. (7.1)) that simulates realistic disordered porous TiO_2 nanostructures. To do so we start from a random hierarchical packing generated by means of the cluster model[24]. In this calculation, a nanosphere radius of 20 nm has been considered and a low overlapping (about 10 %) between neighbouring nanospheres has been imposed, which was kept constant along all the simulated structures. Given the statistical uncertainty implicit to the construction algorithm, we have worked with five different replicas statistically independent, and averages were extracted. All of them comply with the following morphological parameters: specific surface area, $S = 27.0 \pm 0.8$ m²/g, porosity, $P = 56 \pm 3$ % and density, $\rho = 1.7 \pm 0.1$ g/cm³. To induce an ordering effect, these random structures are then exposed to an external 2D sinusoidal potential parallel to the collecting substrate with to complete cycles inside the simulation box (see Fig. (7.1)). By minimizing the potential energyof the system using the Monte Carlo (MC) technique[31], 1D order is progressively

induced in the system. On each iteration, all the spheres (typically ~700 spheres) were allowed to decrease its potential energy, changing the morphology of the system. As interactions are being computed, the system changes progressively its morphology from typical random-packing of particles arranged in hierarchical clusters, to 1D-ordered structures of columnar morphologies, with a preferred packing direction along the x-axis. The algorithm runs keeping the specific surface area, the porosity and density of the structure within the intervals indicated above. This way, the influence of the 1D order alone can be probed, without being affected by other structural properties. The maximum order was achieved once the algorithm was unable to find any new position for any sphere of the system that reduces the energy of the system. This typically occurred for 100 Monte Carlo cycles. This way, different particulate realistic nanostructures are built without changing no other structural parameter appart from 1D-order. Finally, following previous work,[17,32,33] we place "electron" traps on the surface of the nanospheres (R^2 model). For each of the five replicas, 25 different set of traps were placed and considered for the RW simulations described below.

The spatial location of the electron traps make it possible to measure the 1D order of the system with respect to the direction perpendicular to the collecting substrate (x-axis). To do so we choose as "order parameter" the standard deviation of the projected position of traps on the yz-plane (perpendicular plane to the preferred columnar direction) with respect to a grid of 10 x 10 cells. Hence, a larger columnar order implies a wider distribution, with a larger standard deviation, as traps tend to accumulate at specific positions in the grid. The standard deviation of the spatial location was called "columnarity", in allusion to the measurement of the quality of being "columnar" of the system. In Fig. (7.2), 2D projections on the yz-plane of the completely disordered (left) and the columnar system (right) are shown. It has to be remarked that, despite a maximum order is achieved with respect to the energy minimization in the sinusoidal potential, this numerical procedure does not produce a crystalline arrangement of particles, but a disordered arrangement where a preferential direction is imposed in the system. As can be seen in Fig. (7.2), the distribution of traps in the yz-plane is rougly homogeneous for the disordered system (left panel) whereas is completely inhomogeneous for the columnar system (right panel). The standard deviation of the number of traps that fall on each cell of the grid is used to measure the columnarity of the systems. The typical standard deviation of 10 x 10 values is close to 67±5 for the disordered system and 101±3 for the columnar system. In Fig. (7.1), the correspondence between ordering cycles and columnarity values is shown.
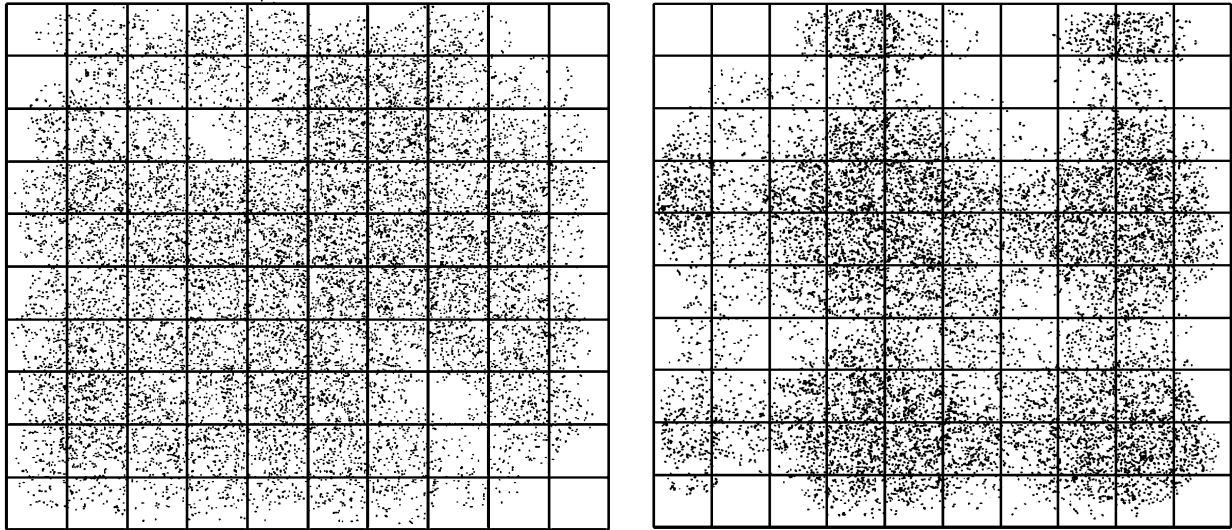
Fig. (7.2). Grid and 2D projections of the trap positions on the perpendicular plane (yz). Left: disordered system and right: columnar system. The standard deviation of set of numbers of points that falls on each cell of the grid is used to measure the order degree as a "columnarity" parameter.

Fig. (7.1) shows how the columnarity and the total energy vary with respect to the number of iterations or cycles employed in the Monte Carlo energy minimization procedure. To estimate the statistical uncertainty of the packing algorithm, results for the five replicas of the packing of nanospheres are presented. (For each replica the ordering process of energy minimization is applied). Note again that full minimization (meaning and equilibrated situation) does not imply that perfect crystalline order is achieved. It is observed that there is a direct correspondence between relative columnarity parameter and the relaxation energy. The main conclusion is that the extent of the minimization procedure (i. e. the number of MC cycles) can be used to *tune* the degree of order in the system, hence allowing for a systematic investigation of the effect on charge collection efficiency in the presence of a preferential direction in the nanostructured electrode.

The placement of "electron" traps on the surface of the nanospheres, and the ordering procedure described above provide a three-dimensional network of sites as input for a RWNS calculation[17,23,28,30,34]. Considering that the problem addressed in this Chapter is a matter of percolation, we chose the hopping model to carry out the simulation. Hence we use Miller-Abrahams hopping rates[35]. This means that hopping times for carriers moving between neighbouring traps are computed via Eq. (3.2). In addition, an exponential energy distribution of localized states given by (2.2) is used in the calculations[36]. By means of Eqs. (3.2) and (2.2), spatial and energy disorder is adequately taken into account in the transport

process. In this calculations we used[36] $T_0 = 1100$ K, $T = 300$ K, and $t_0 = 10^{-12}$ s. A surface trap density of 0.004 nm^2 (with respect to the nanosphere surface) has been considered[17]. This corresponds to a volumetric trap density of 2.3 10^{-4} nm^{-3} (meaning that traps are located at an average distance of 16 nm in the film). In connection to this, three localization radius of $\alpha_l = 2.5$, 10 and 20 nm have been studied. It is important to note that, since the traps are located on the surface of the nanospheres, and these are in contact, the actual distance between a particular trap and its neighbours is shorter, hence allowing for percolation of carriers throughout the network.

In addition to transport, also recombination should be considered to study charge collection efficiency. As in Chapter 5, we introduced a constant probability (independent of trap energy) for carrier removal. As shown there, this probability leads to an exponential distribution of survival times for carriers, which defines a carrier lifetime. This lifetime defines in turn the characteristic diffusion length of the system. This probability was adjusted to give diffusion lengths of the order of microns, leading to the general result that in typical DSCs the time scale for recombination is much longer that the time scale for transport. In this Chapter we run also calculations analogous to that of Chapter 5 to determine the characteristic diffusion lengths of the practical cases for which the charge collection efficiency is calculated. Recombination probabilities ranged between $P_R = 10^{-10}$ and 10^{-2} in arbitrary units. As described below, this is translated to a range of values for the diffusion length: the smaller is P_R the longer is the diffusion length.

As discussed in Chapter 3, the description of the solar cell at real working conditions implies to use a considerable number of carriers and trap states, which leads to very high numerical demands. To reduce the computational time, the one-electron approximation[23,37], that makes it possible to simulate transport at a given position of the Fermi level with the movement of a single carrier, has been used. On the other hand, periodic boundary conditions are considered in the three directions of space[31]. Hence, the simulation box in Fig. (7.1) is periodically replicated in such a way that if a carrier crosses one of the box boundaries, it is automatically re-injected through the opposite boundary. Nevertheless, we aim to calculate charge collection efficiency in realistic systems and this requires to consider charge generation in accordance to optical absorption lengths of the order of microns, typical of the dyes used in dye-sensitized solar cells and related devices (for instance, the extinction coefficient of typical ruthenium dyes[38] is 1.4 10^4 M^{-1}cm^{-1} at $\lambda \sim 520$ nm. For common dye loadings of 2-3 10^{-7} mol/cm^2 one obtains absorption lengths of 2-4 μm). However, the use of a simulation box of the order of microns is not computationally feasible for the trap densities used here. To

deal with this situation the procedure explained in Chapter 3 is implemented so that real coordinates can be utilized when both charge generation and collection (an illustration of this strategy is presented in Fig. (3.2).

7.3. Results and discussion

The adequate implementation of the procedure explained in Chapter 3 regarding the simulation of a macroscopic system is tested in Fig. (7.3). In the simulation, carriers are injected along the x-axis according to a probability given by the Lambert-Beer law: $\exp(-x/L_{ab})$, where L_{ab} is the characteristic optical absorption length. This depends on the
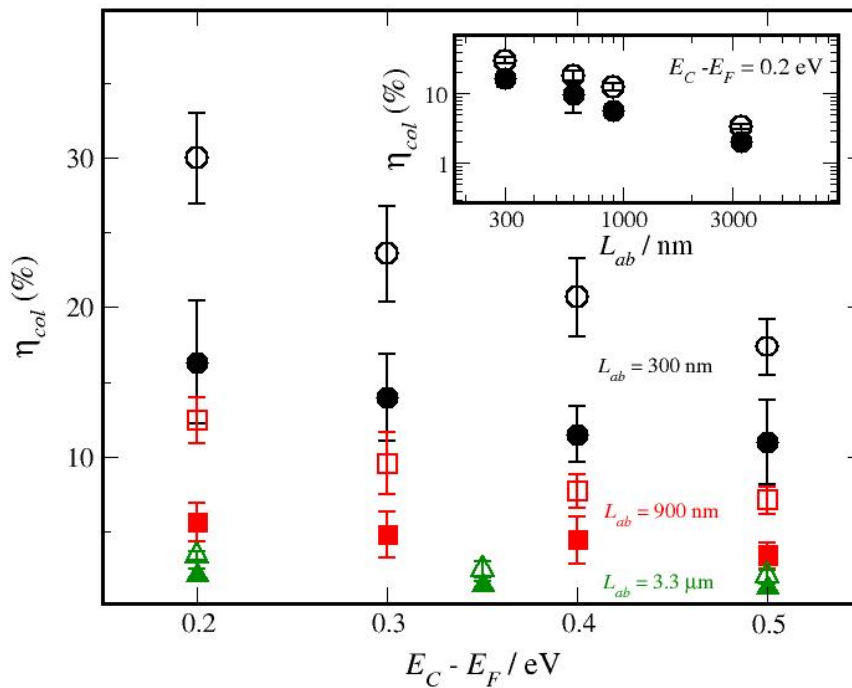
Fig. (7.3). Charge collection efficiency as a function of Fermi level position for a random packing of nanospheres (solid symbols, see top left panel in Fig. (7.1), and a fully relaxed ordered structure (open symbols, see top right panel in Fig. (7.1)) at different values of the absorption length L_{ab}. In the inset the collection efficiency is plotted versus L_{ab} for $E_c - E_F = 0.2$ eV in a double logarithmic scale. Error bars are derived from results of statistically independent morphological replicas. Simulations were carried out for the following parameters: $T_0 = 1100$ K, $T = 300$ K, $t_0 = 10^{-12}$ s, nanosphere radius = 20 nm, surface trap density=0.004 nm^{-2}, $\alpha_l = 2.5$ nm,. $P_R = 10^{-6}$ (arb. un.).

optical features of the solar cell (concentration and absorption coefficient of the absorbing material). Four cases have been considered for this parameter, ranging between $L_{ab} = 300$ and 3300 nm. In Fig. (7.3) the charge collection efficiency is plotted versus L_{ab} and the Fermi level position. The simulation results demonstrate that collection increases when the absorption length is shorter. Therefore, as expected, collection is more efficient for highly absorbing materials, because carriers are generated, on average, closer to the collecting electrode. The collection efficiency is found to depend on L_{ab} according to a power-law. This behaviour is found to be also predicted by the numerical solution of the continuity equation for electrons in the photoanode[39–41]. The RW simulations give power law exponents of 0.7-0.8, whereas the numerical solution yields 0.65 for the equivalent case (see Appendix B for more details).

On the other hand, the collection efficiency decreases as the Fermi level gets deeper into the conduction band. This behaviour is only clearly observed for short absorption lengths. For longer absorption lengths the effect of the Fermi level is marginal. This observation can be interpreted in terms of the Fermi-level dependence of the diffusion coefficient[38,42]. If E_F is raised, carriers diffuse more rapidly and the collection efficiency is increased. However, for long optical lengths, carriers are generated at further distances and the probability of recombining before being collected becomes more important. Therefore, the effect of a more rapid transport in minimized.

The influence of morphological (1D) order on charge collection efficiency is reported in Fig. (7.4) for different positions of the Fermi level and different recombination probabilities. In Fig. (7.4) the collection efficiency for the structure with the maximum degree of ordering (100 cycles in Fig. (7.1)) is compared to that of the disordered structure using the ratio η_{100}/η. The results of the simulations demonstrate that the collection efficiency can be improved by a factor close to two when a preferential direction is introduced in the system. This improvement is found to be roughly independent of Fermi level (Fig. (7.4), upper panel), suggesting that either illumination intensity or applied voltage would not modify this morphological effect.

As it could be expected, the enhancement in collection efficiency is found to depend strongly on the kinetics of carrier recombination, i.e., on carrier lifetime. In the lower panel of Fig. (7.4) the improvement factor is plotted against the recombination probability P_R. For very slow recombination, corresponding to very long diffusion lengths, the effect of the ordering is absent, since the collection efficiency approaches a 100% in both cases. This means that there is no benefit in providing a more direct percolation path to the external contact if the lifetime of electrons is long enough. The opposite situation corresponds to very rapid recombination,

137
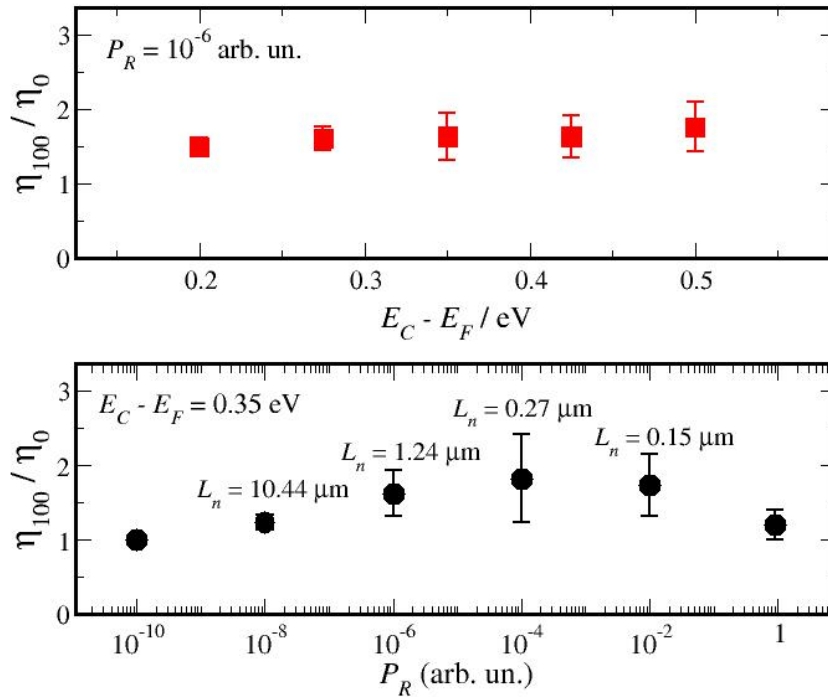
Fig. (7.4). Charge collection efficiency improvement ratio for ordered structures (100 cycles, see Fig. (7.1)) with respect to a random packing of nanospheres. Top panel: Improvement ratio versus Fermi level at constant recombination probability. Bottom panel: Improvement ratio versus recombination probability at fixed Fermi level. The results for the diffusion length from simulations on an infinite fully disordered system[29] are indicated. Error bars are derived from results of statistically independent morphological replicas. Simulations were carried out for the following parameters: $T_0 = 1100$ K, $T = 300$ K, $t_0 = 10^{-12}$ s, surface trap density = 0.004 nm^{-2}, $\alpha_l = 10$ nm, nanosphere radius = 20 nm and $L_{ab} = 3.3$ μm.

with short diffusion lengths. In that case, no benefit is observed either, because the average distance travelled by the carriers is much smaller than the characteristic length scale of the columnar order imposed in the system. As a rule of thumb, it could be stated that the "ordering" effect is only observed when the diffusion length L_n is approximately of the same order of magnitude as the optical absorption length L_{ab} and the characteristic length scale in which the order is induced. As it can be seen in the lower panel of Fig. (7.4), maximum efficiencies are obtained for recombination probabilities of $P_R = 10^{-5}$ - 10^{-3} (arb. un.). Simulations in an infinite system for a random-packing give an average[29] of $L_n \sim 1.0$ - 0.2 μm for these probabilities, whereas the value used for the absorption length was $L_{ab} = 3.3$ μm.

The possibility of tuning the degree of 1D order by a partial run of the energy minimization algorithm, permits us to investigate whether an approximate functional

relationship can be found between collection efficiency and the order parameter (columnarity). Results for this are presented in Fig. (7.5), where we have chosen an intermediate value of the recombination probability to better see the effect of the ordering. In this figure, the collection efficiency extracted from the RWNS calculations is plotted against the columnarity. The RWNS results confirm the progressive enhancement in collection efficiency when the order of the structure is increased. However, it is noteworthy that this enhancement does not occur linearly. The numerical data show that the improvement is significant even for a weak ordering of the system, with a sudden increase at intermediate values of the columnarity (~ 86, 9-10 cycles). Thus, the collection efficiency reaches rapidly a saturation value, resembling a sigmoidal function. It must be recalled that even for the
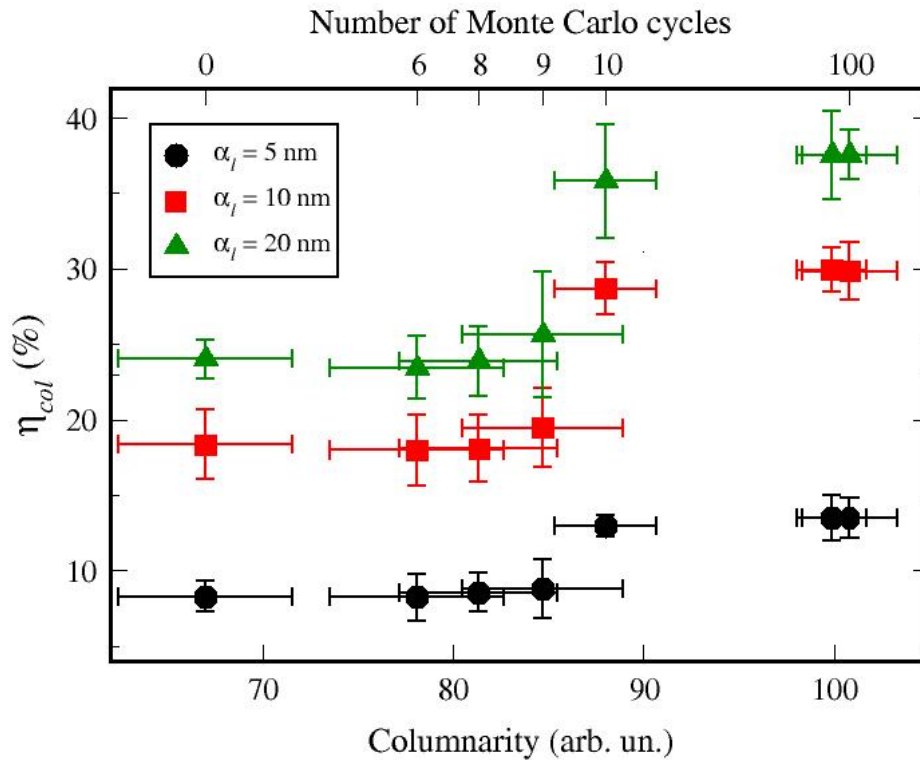
Fig. (7.5). Carrier collection efficiency as a function of the columnarity as extracted from RWNS calculations for different localization radius for an intermediate value of the recombination probability $P_R = 10^{-6}$ (arb. un.), corresponding to $L_n = 1.24$ μm. Error bars are derived from results of statistically independent morphological replicas. Simulations were carried out for the following parameters: $T_0 = 1100$ K, $T = 300$ K, $t_0 = 10^{-12}$ s, surface trap density = 0.004 nm^{-2}, nanosphere radius = 20 nm. Note that longer localization radius lead to better efficiencies, as carriers travel longer distances between recombination events.

situation with maximum columnarity (full energy minimization, 100 cycles), the system does not have perfect crystalline order. In fact it is basically a disordered structure but with a preferential alignment along the x-direction induced by the external potential. The present results suggest that the introduction of a very slight degree of order in the nanostructure can lead to a huge and abrupt increase in collection efficiency.

The reason of the abrupt jump in the collection efficiency at intermediate order seems to be related to the existence of a percolation "threshold" in the plane perpendicular to the columnar direction. The relevance of the connectivity of the transport sites in the adequate direction has been stressed out by several authors[15,19,43]. In this case we have an effect of improved connectivity, but only in one direction. This acts in the following manner: when a columnar order is induced, gaps with very low trap density are created between the columns. This hinders the perpendicular jumping of the carriers and favours their harvesting in the collecting substrate. This hypothesis can be inferred from the "softening" of the jump when longer localization radius (meaning longer diffusion lengths) are utilized in the simulation. Hence, when electrons travel shorter distances, they find more difficult to percolate in directions parallel to the collecting surface when the systems are "more columnar". However, further work is required to elucidate the precise origin of this behaviour, and the actual relationship between morphological order and transport properties in disordered semiconductors.

Effect of the shape of the absorption profile on the collection efficiency

How the charge charge collection efficiency is affected by the generation profile in nanostructured solar cells is investigated in this section. As a first approximation, this can be assumed to be exponential, as predicted by the Lambert-Beer law. This is the generation profile used so far. However, alternative charge generation profiles can be envisioned in solar cells as a consequence of inhomogeneities in the distribution of the absorbing material (arising, for instance, from a non-uniform adsorption of dye molecules in dye-sensitized solar cells) or the presence of agents that enhance light absorption at certain points like plasmonic nanoparticles[44] or scattering layers[45].

We have modelled the effect of inhomegeneities on the absorption by considering a Gaussian shape for the charge generation profile within the active conducting layer. Two parameters are here relevant to establish the effect on the efficiency, namely the mean position, or "centre" of the Gaussian (x_{centre}), and the dispersion (width) of the Gaussian (σ). The influence of these two parameters is studied in Fig. (7.6)
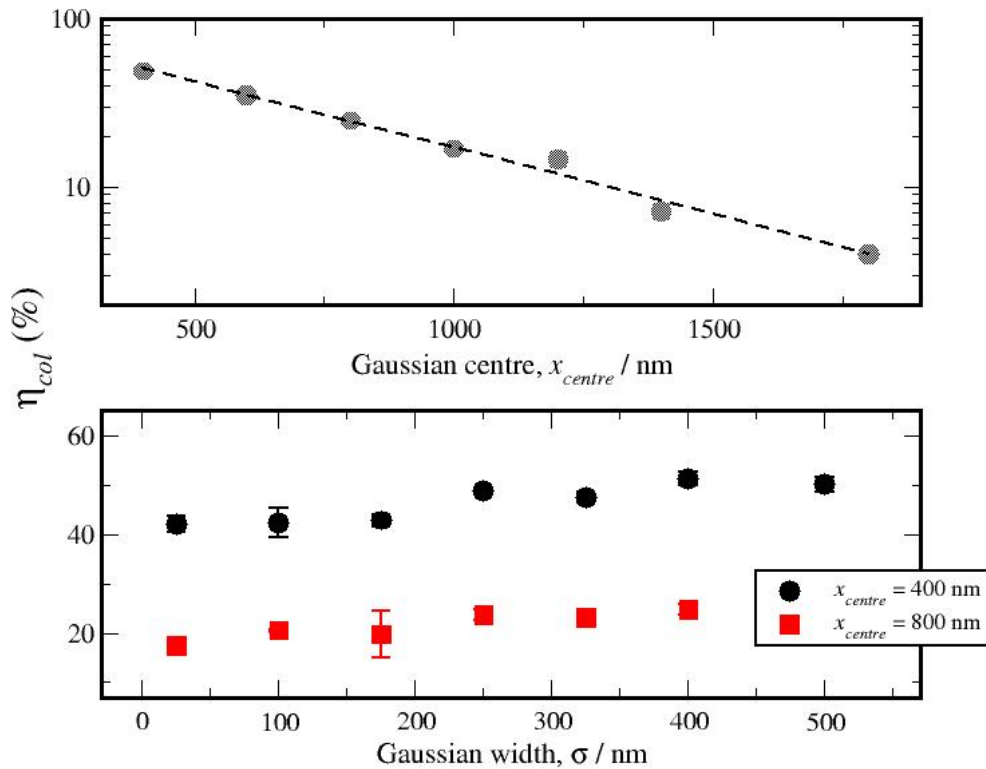
Fig. (7.6) Top panel: Charge collection efficiency results for a Gaussian generation profile (σ = 250 nm) as obtained by RWNS calculations for a fully disorder electrode (left panel of Fig. (7.1)). The efficiency is plotted as a function of the centre of the Gaussian with respect to the carrier collection boundary. Bottom panel: Same as top panel but for the efficiency plotted as a function of the width of the Gaussian generation profile and two different positions of the centre. Simulations were carried out for the following parameters: T_0 = 1100 K, T = 300 K, t_0 =10^{-12} s, surface trap density = 0.004 nm^{-2}, α_l = 10 nm, P_R = 10^{-6} arb. un.

In the upper panel of Fig. (7.6) the position of x_{centre} in the Gaussian absorption profile is moved with respect to the collecting electrode. As expected, smaller distances to the collecting electrode correlate to larger charge collection efficiencies. Interestingly, an exponential law is found between the charge collection efficiency and the distance to the collecting electrode, so that small displacements lead to large increases of the efficiency. These results indicate that it is very important to produce local enhancements of the absorption of light close to the collecting electrode. In the calculations presented in the lower panel of Fig. (7.6) the position of the Gaussian is fixed, but σ is varied. An interesting observation arises here, namely that the charge collection efficiency is roughly independent of the Gaussian width, at least for $\sigma < x_{centre}$. This result can be understood as a consequence of the

symmetry of the absorption profile and the absence of a bias field on the x-direction. Hence, as hopping moves are equally likely in both positive and negative directions, the collection of "forward" charge carriers gets compensated by the recombination losses of the "backward" carriers. Obviously this conclusion would not hold for solar cells where, for instance, an electric field is acting on the x-direction. In that case a dispersion of a localized absorption would produce different effect depending on whether the device is at forward of reversed bias. On the other hand, a non-linear recombination kinetics, recently discussed in the literature[28,46] and studied in Chapter 6 would also affect this simple result.

In Fig. (7.7) the effect of superposing a local absorption, modelled by a Gaussian, on top of a Lamber-Beer profile, is analysed. In these calculations, a Gaussian profile with
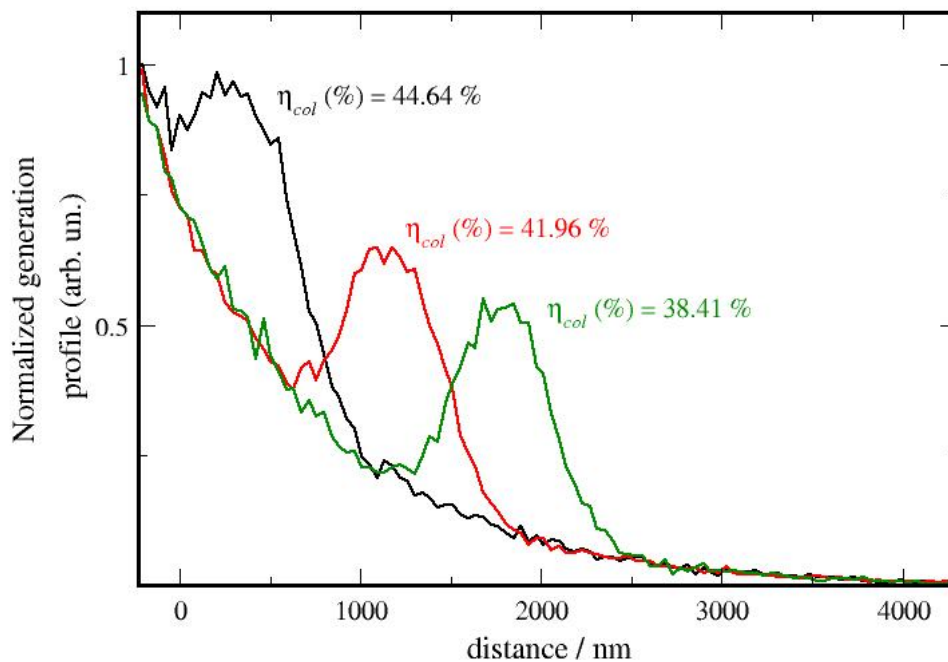
Fig. (7.7) Three different combinations of Gaussian (σ = 250 nm, x_{centre} = 1400 nm) and exponential (Lab = ~ 1000 nm) carrier generation profiles utitlized in RWNS calculations with fully disordered electrodes. Simulations were carried out for the following parameters: T_0 = 1100 K, T = 300 K, t_0 =10^{-12} s, surface trap density = 0.004 nm^{-2}, α_l = 10 nm, nanosphere radius = 20 nm and P_R = 10^{-6} arb. un. For each combination the charge collection efficiency obtained in the simulation is indicated.

$\sigma = 250$ nm, $x_{centre} = 1400$ nm is introduced. The Gaussian "bump" is added to a background exponential profile of $L_{ab} = \sim 1000$ nm. This pure exponential profile yields $\eta \sim 37\%$ for $P_R = 10^{-6}$ arb. un. and $\alpha_l = 10$ nm. This is the same case studied in Fig. (7.4) (lower panel) where a diffusion length of carriers of $L_n = 1240$ nm was obtained. These reference values are important to understand the results discussed in the following.

The introduction of the Gaussian produces, as expected, an improvement of the efficiency of the device. However this improvement is very much dependent on the position of the Gaussian. Thus, enhancing local absorption close to the collecting electrode ($x_{centre} \sim 200$ nm) increases the efficiency from 37% (pure exponential) to 44.6% (exponential plus Gaussian). In contrast, if the Gaussian is placed far from the collecting electrode ($x_{centre} \sim 1900$ nm) the charge collection efficiency is 38.4%, which means that no real improvement is produced with respect to the pure exponential. This can be easily understood bearing in mind that carriers travel in average 1240 nm before disappearing by recombination. Enhancing light absorption locally at distances larger than this value results in no net improvement of the efficiency of the solar cell. This is a very important result, because demonstrates that it is not sufficient to enhance light absorption to improve the efficiency of real devices, but this enhancement should be implemented in accordance to the charge transport properties of the conducting film.

7.4. Conclusions to Chapter 7

In this Chapter, a numerical procedure that permits to obtain the collection efficiency of photogenerated charges in nanostructured electrodes with different degrees of 1-dimensional order has been developed. The simulated system resembles a real nanostructure where charges are generated according to a Lambert-Beer with a optical length of the order of microns, and where transport and recombination are taken into account via a hopping model coupled with a constant recombination probability. The results show that collection efficiency would be almost doubled by a partial ordering of the system. The maximum efficiency enhancement only takes place if the recombination probability (which determines the characteristic diffusion length of the system) is not too rapid or too low, with a diffusion length of the same order of magnitude as the optical absorption length. Furthermore, the collection efficiency can be calculated as a function of the degree of order via a normalized order parameter. The results show that a very slight degree of 1-dimensional order can lead to a significant increase of the collection efficiency. The predictions contained in this theoretical

work might be interesting to develop strategies where a preferential direction is induced in an originally disordered structure, such as in the use of hierarchical structures studied in the recent literature. Furthermore, it is shown that the alleged benefit of using 1-D nanostructures should be taken with reserve, as only if the recombination rate has intermediate values, a clear improvement is observed.

A theoretical study of the influence of shape of the charge generation profile on the charge collection efficiency of a nanostructured solar cell has also been carried out. The numerical results show that there is a power law dependence of the collection efficiency with respect to the optical depth of the film if the charge generation profile is Lambert-Beer-like (i.e., exponential). If the profile is Gaussian, the efficiency is found to increase exponentially as the centre of the Gaussian approaches the collecting electrode. Furthermore, the collection efficiency is roughly independent of the Gaussian width for devices where there is no bias field. Simulations where a Gaussian absorption is superposed on top of an exponential profile showed that the corresponding improvement in efficiency is very much dependent on the position of the Gaussian with respect to (1) the collecting electrode and (2) the diffusion length. These results show that in practical devices it is not sufficient to enhance the absorption of light to improve the efficiency but also that this should be applied at an adequate location of the active film.

References to Chapter 7

(1)   Gratzel, M. *Nature* **2001**, *414*, 338–344.

(2)   Yoon, S.; Tak, S.; Kim, J.; Jun, Y.; Kang, K.; Park, J. *Building and Environment* **2011**, *46*, 1899–1904.

(3)   Fung, T. Y. Y.; Yang, H. *Energy and Buildings* **2008**, *40*, 341–350.

(4)   Toyoda, T.; Sano, T.; Nakajima, J.; Doi, S.; Fukumoto, S.; Ito, A.; Tohyama, T.; Yoshida, M.; Kanagawa, T.; Motohiro, T.; Shiga, T.; Higuchi, K.; Tanaka, H.; Takeda, Y.; Fukano, T.; Katoh, N.; Takeichi, A.; Takechi, K.; Shiozawa, M. *Journal of Photochemistry and Photobiology A: Chemistry* **2004**, *164*, 203–207.

(5)   Dennler, G.; Forberich, K.; Scharber, M. C.; Brabec, C. J.; Tomiš, I.; Hingerl, K.; Fromherz, T. *Journal of Applied Physics* **2007**, *102*, 054516–054516–7.

(6)   Law, M.; Greene, L. E.; Johnson, J. C.; Saykally, R.; Yang, P. *Nat Mater* **2005**, *4*, 455–459.

(7)   Galoppini, E.; Rochford, J.; Chen, H. H.; Saraf, G.; Lu, Y. C.; Hagfeldt, A.; Boschloo,

G. *Journal of Physical Chemistry B* **2006**, *110*, 16159–16161.

(8)   Gonzalez-Valls, I.; Lira-Cantu, M. *Energy Environ. Sci.* **2008**, *2*, 19–34.

(9)   Martinson, A. B. F.; McGarrah, J. E.; Parpia, M. O. K.; Hupp, J. T. *Physical Chemistry Chemical Physics* **2006**, *8*, 4655–4659.

(10)   Liu, B.; Aydil, E. S. *J. Am. Chem. Soc.* **2009**, *131*, 3985–3990.

(11)   Tirosh, S.; Dittrich, T.; Ofir, A.; Grinis, L.; Zaban, A. *Journal of Physical Chemistry B* **2006**, *110*, 16165–16168.

(12)   Dittrich, T.; Ofir, A.; Tirosh, S.; Grinis, L.; Zaban, A. *Applied Physics Letters* **2006**, *88*.

(13)   Ofir, A.; Dor, S.; Grinis, L.; Zaban, A.; Dittrich, T.; Bisquert, J. *Journal of Chemical Physics* **2008**, *128*.

(14)   Benkstein, K. D.; Kopidakis, N.; Lagemaat, J. van de; Frank, A. J. *Journal of Physical Chemistry B* **2003**, *107*, 7759–7767.

(15)   Cass, M. J.; Qiu, F. L.; Walker, A. B.; Fisher, A. C.; Peter, L. M. *Journal of Physical Chemistry B* **2003**, *107*, 113–119.

(16)   Cass, M. J.; Walker, A. B.; Martinez, D.; Peter, L. M. *Journal of Physical Chemistry B* **2005**, *109*, 5100–5107.

(17)   Anta, J. A.; Morales-Florez, V. *Journal of Physical Chemistry C* **2008**, *112*, 10287–10293.

(18)   Novak, S.; Hrach, R.; Svec, M. *Thin Solid Films* **2011**, *519*, 4012–4017.

(19)   Vehoff, T.; Baumeier, B.; Troisi, A.; Andrienko, D. *J. Am. Chem. Soc.* **2010**, *132*, 11702–11708.

(20)   Deng, H.; Zhang, R.; Bilotti, E.; Loos, J.; Peijs, T. *Journal of Applied Polymer Science* **2009**, *113*, 742–751.

(21)   Peter, L. M. *Journal of Physical Chemistry Letters* **2011**, *2*, 1861–1867.

(22)   Oskam, G. *Current Topics in Electrochemistry* **2004**, *10*, 141–162.

(23)   Anta, J. A. *Energy and Enviromental Science* **2009**.

(24)   Morales-Florez, V.; Pinero, M.; Rosa-Fox, N. D. L.; Esquivias, L.; Anta, J. A. *Journal of Non-Crystalline Solids* **2007**, *In Press*.

(25)   Long, R.; Prezhdo, O. V. *J. Am. Chem. Soc.* **2011**, *133*, 19240–19249.

(26)   Hagfeldt, A.; Boschloo, G.; Sun, L.; Kloo, L.; Pettersson, H. *Chemical Reviews* **2010**, *110*, 6595–6663.

(27)   Peter, L. M. *Journal of Physical Chemistry C* **2007**, *111*, 6601–6612.

(28)   Bisquert, J.; Mora-Seró, I. *The Journal of Physical Chemistry Letters* **2010**, *1*, 450–456.

(29)   Gonzalez-Vazquez, J. P.; Anta, J. A.; Bisquert, J. *The Journal of Physical Chemistry C* **2010**, *114*, 8552–8558.

(30)   Navas, J.; Guillén, E.; Alcántara, R.; Fernández-Lorenzo, C.; Martín-Calleja, J.; Oskam, G.; Idígoras, J.; Berger, T.; Anta, J. A. *The Journal of Physical Chemistry Letters*

2011, *2*, 1045–1050.

(31)   Bisquert, J. *Journal of Physical Chemistry C* **2007**, *111*, 17163–17168.

(32)   Frenkel, D.; Smit, B. *Academic Press* **2002**.

(33)   Kopidakis, N.; Neale, N. R.; Zhu, K.; Lagemaat, J. van de; Frank, A. J. *Applied Physics Letters* **2005**, *87*.

(34)   Hartenstein, B.; Bässler, H. *Journal of Non-Crystalline Solids* **1995**, *190*, 112–116.

(35)   Zhu, K.; Kopidakis, N.; Neale, N. R.; Lagemaat, J. van de; Frank, A. J. *Journal of Physical Chemistry B* **2006**, *110*, 25174–25180.

(36)   Miller, A.; Abrahams, E. *Physical Review* **1960**, *120*, 745–755.

(37)   Bisquert, J.; Fabregat-Santiago, F.; Mora-Sero, I.; Garcia-Belmonte, G.; Barea, E. M.; Palomares, E. *Inorganica Chimica Acta* **2008**, *361*, 684–698.

(38)   Anta, J. A.; Mora-Sero, I.; Dittrich, T.; Bisquert, J. *Physical Chemistry Chemical Physics* **2008**, *10*, 4478–4485.

(39)   Sodergren, S.; Hagfeldt, A.; Olsson, J.; Lindquist, S. E. *Journal of Physical Chemistry* **1994**, *98*, 5552–5556.

(40)   Halme, J.; Boschloo, G.; Hagfeldt, A.; Lund, P. *The Journal of Physical Chemistry C* **2008**, *112*, 5623–5637.

(41)   Villanueva, J.; Anta, J. A.; Guillén, E.; Oskam, G. **2009**, *113*, 19722–19731.

(42)   Gonzalez-Vazquez, J. P.; Anta, J. A.; Bisquert, J. *Physical Chemistry Chemical Physics* **2009**, *11*, 10359.

(43)   Chirvase, D.; Parisi, J.; Hummelen, J. C.; Dyakonov, V. *Nanotechnology* **2004**, *15*, 1317–1323.

(44)   Qi, J.; Dang, X.; Hammond, P. T.; Belcher, A. M. *ACS Nano* **2011**, *5*, 7108–7116.

(45)   Hore, S.; Vetter, C.; Kern, R.; Smit, H.; Hinsch, A. *Solar Energy Materials and Solar Cells* **2006**, *90*, 1176–1188.

(46)   Villanueva-Cab, J.; Wang, H.; Oskam, G.; Peter, L. M. *The Journal of Physical Chemistry Letters* **2010**, *1*, 748–751.

CHAPTER 8

DISORDERED SEMICONDUCTOR HETEROJUNCTIONS

A disordered semiconductor heterojunction is modelled by means of RWNS. The numerical modelling is performed by using simultaneously electrons and holes moving according to Miller-Abrahams hopping rates. In addition a tunnelling mechanism is implemented to account for electron-hole recombination. Energy disorder is taken into account via exponential distributions of trap energies for both electrons and holes and for the two semiconductors in the heterojunction. Using this numerical method, we are able to simulate charge separation through a disordered heterojunction and observe the effects on the surface photovoltage (SPV) of different parameters like the thickness of the heterostructure, the carrier concentration and the band-offset. The relationship between the simulated results and recent experimental data of ETA solar cells are thoroughly discussed. A bulk heterojunction solar cell in steady-state has been modelled by including explicitly a continuous generation of electron-hole pairs. Thus, open-circuit voltage measurements have been reproduced from splitting of Fermi levels for electrons and holes. Values of the recombination current have also been obtained by means of RWNS, in good agreement with experimental results.

8. DISORDERED SEMICONDUCTOR HETEROJUNCTIONS

8.1. Introduction

Localized states or traps in disordered materials are mostly located on the surface of grains and interfaces (as reported, for example, in amorphous silicon[1,2]). Moreover, when two disordered semiconductors with different work functions are put in contact to create an heterojunction it is known that the process of charge separation is limited by the existence of surface defects contributing to an enhancement of recombination[3]. On the other hand, as described in Chapter 1, it is known that photovoltaic effect of both ETA and BHJ solar cells are extremely dependent on an efficient separation process of photogenerated carriers. Hence, characterization of disordered semiconductor interfaces is required in order to achieve better performing devices.

Charge separation in disordered heterojunctions can be studied experimentally by surface photovoltage transients (SPV)[4–7]. The main advantage of this experimental technique is that allows to observe both diffusion and recombination mechanisms[4,5,8–10] as well as spatial charge separation processes[11] in very short distances (of the order of nm's). The SPV signal depends on the amount of charge separated in space, on the distance of center of negative and positive charges and on the dielectric constant of the semiconductor ($\epsilon\epsilon_0$, where ϵ is the relative dielectric constant and $\epsilon_0 = 8.85 \cdot 10^{-14}$ F/cm)[6]. In the general case in which there is spatial distribution of both positive and negative charge carriers in the bulk, it can be shown that SPV adopts the following form[11]

$$SPV(t) = \frac{q}{\epsilon\epsilon_0} N(t) \left(<x_p>(t) - <x_n>(t) \right) \tag{8.1}$$

where $N(t)$ is the total amount of electron-hole pairs per unit area at time t and $<x_{p(n)}>(t)$ is the mean position of holes (electrons), i.e. their "gravity" centre of charge.

However, direct interpretation of the time evolution of SPV in terms of the electronic processes taking place in thin-film heterostructures is not straightforward. In this sense, RWNS can serve as an appropriate model as it allows to establish relationships between SPV measurements and microscopic parameters of specific electronic mechanisms[12,13]. Thus, we present in this Chapter an improved RW method that can describe adequately the main

features involved in general disordered semiconductor thin-film heterostructures. Thanks to its flexibility and potentiality, this model permits interpretation of charge separation processes occurring at interfaces of many types of ETA solar cells, such as In_2S_3-In_2S_3:Cu films or TiO_2/CdS layers as well as BHJ (organic) solar cells.

Indeed, it has recently been put into question the actual mechanism of charge separation and charge transport taking place in BHJs. Specifically, it has been claimed that it is kinetics and diffusion, instead of a built-in electric field, what provides the photocurrent and the photovoltage in this type of systems[14]. To check the validity of these assumptions the present model has been adapted to simulate a typical bulk heterojunction solar cell. As no electric fields are taken into account, this model can help to clarify this controversy. In Fig. (8.1) an scheme of the system is shown. We assume that the open-circuit voltage can be calculated from splitting of Fermi levels for electrons and holes in accordance with the following expression
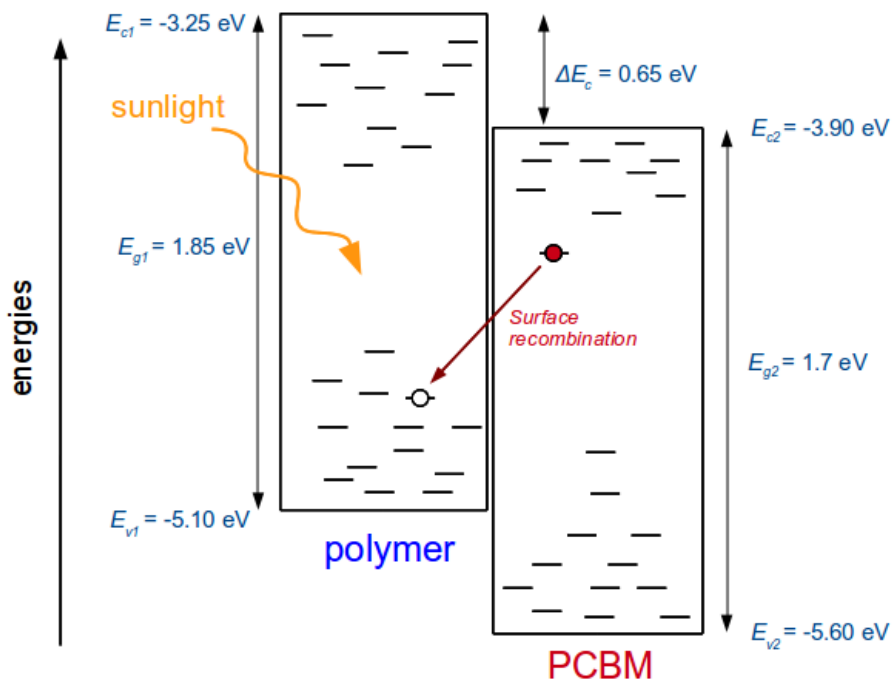
Fig. (8.1). Illustration of typical polymer-fullerene bulk heterojunction solar cell.

$$V_{oc} = \frac{1}{q} \left(E_{F_n}^{acc} - E_{F_p}^{don} \right) \tag{8.2}$$

where $E_{F_n}^{acc}$ and $E_{F_p}^{don}$ are the electron Fermi level in the acceptor semiconductor and the hole Fermi level in the donor semiconductor respectively. As a matter of fact, the experimental V_{oc} is found to depend linearly on the band offset between the acceptor and the donor, although it is always smaller[15]. In fact, and empirical shift of 0.3 eV is normally found. Hence, it is very interesting to ascertain if our hopping and recombination models, without using electric fields, are capable of reproducing this experimental phenomenology.

The configuration of the system is implemented by means of an adequate combination of spatial disorder and energy disorder. As regards the former, we run the random walk simulation on a network of traps distributed randomly in space. As for the latter, we assume again that localized states are distributed according to an exponential distribution[16,17]. In this Chapter, holes and electrons are considered simultaneously as charge carriers. Hence, we will use as trap energy distributions

$$g_n(E) = \frac{N_l}{k_B T_{0n}} \exp \left[(E - E_c)/k_B T_{0n} \right]$$

$$\tag{8.3}$$

$$g_p(E) = \frac{N_l}{k_B T_{0p}} \exp \left[(E_v - E)/k_B T_{0p} \right]$$

where N_l is the total trap density, $k_B T_{0n(p)}$ is the width of the distribution[18], E is the trap energy (negative), E_c is the electron mobility edge and E_v is the hole mobility edge. We have assumed for simplicity that the width of the distribution is the same for both electrons and holes. However, this numerical model allows also to use different distributions for both types of carriers. This possibility might be required for certain systems.

8.2. Methodology

The construction of the heterojunction is accomplished by introducing two simulation boxes, each of them acting as a different semiconductor with its specific electron and hole trap energy distributions. Thus, four different energy trap distributions are used in the system, each

of them with its own value of the band (mobility) edge. With these considerations, it is clear that an specific band-offset can arbitrarily be prescribed by choosing different conduction and valence band edges on both sides of the heterojunction. On the other hand, the thickness of both semiconductors can also be varied arbitrarily.

Periodic boundary conditions along *y-z* direction are applied. Thus, a carrier crossing a *y-z* boundary is automatically reinjected through the opposite side of the box. In addition, to simulate an ultra-thin film, we impose reflecting boundary conditions in the x-dimension so that carriers arriving an x boundary are bounced back and continue moving across the network of sites. An scheme of the simulation procedure is presented in Fig. (8.2).

The numerical procedure runs as follows. Firstly, electrons are initially placed at random on the network of traps for the second semiconductor (acting as an absorber) with holes introduced in neighbouring traps. However, in the case of the BHJ calculations, holes are generated directly in the polymer and electrons in the fullerene. This way the stationary state is more rapidly reached and the statistics is improved.
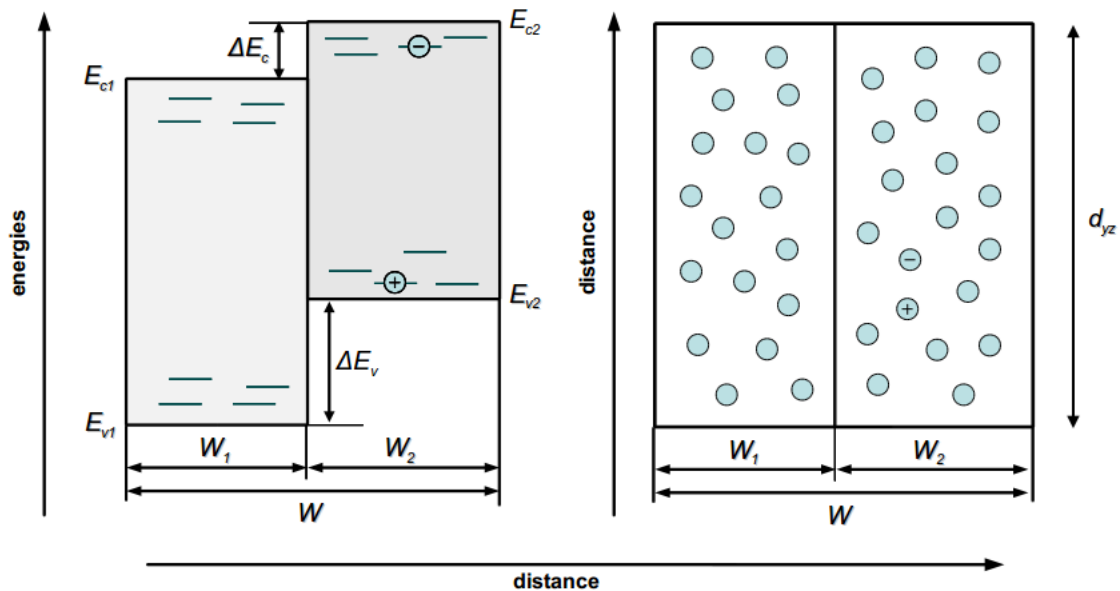
Fig. (8.2). Illustration of the system studied. A disordered heterojunction is modelled by means of band-offset of energy distributions of localized states for both electrons and holes. Hopping transport model is used for detrapping times (or rates). See text for more details.

Each carrier is then given a certain detrapping time that determines the jumping rate or probability for a carrier to jump to another site. If we assume a hopping mechanism[16,19,20] of transport, the detrapping or release time for a carrier jumping from a trap i to a trap j is derived according to Eq. (3.2).

In the same way, to account for electron-hole annihilation, a distance dependent recombination probability is introduced in the computation.[12] Here we assume that there is a tunneling mechanism in such a way that charge carriers sitting in different traps are allowed to recombine with each other due an overlap of the wave functions of separated electrons and holes[21]. Hence, we use the inverse of Eq. (2.40) to account for recombination times:

$$t_r = -\ln(R)t_{r0} \exp\left(\frac{2R_{np}}{\alpha_l}\right) \tag{8.4}$$

where t_{r0} is the inverse of a recombination frequency, α_l is the localization radius and R_{np} is the distance between electrons and holes. Note that there is no energy-dependent factor in Eq. (8.4). We have assumed that the recombination process is analogous to the hopping process and electron-hole recombination is always a process where energy is emitted (either radiatively or non-radiatively). However, energy factors might also be taken into account, especially for non-radiative recombination.

Once charge carriers have been injected, hopping and recombination times are computed for both electrons and holes via Eqs. (3.2) and (8.4) respectively. Both types of times are then stored in the same list of waiting times in such a way that if the minimum is a detrapping time then the corresponding carrier is moved into its target site, whereas if it is a recombination time the corresponding electron-hole pair is removed from the sample. This is an analogous procedure to that used in Chapter 6 for "Model 2". Once performed the move or the recombination event, the hopping and recombination times of the rest of the carriers are reduced by t_{min}. Finally, the same procedure is repeated in each simulation step so that the jump or electron-hole recombination event with the minimum waiting time can be executed.

A second section of this chapter will focus on steady-state properties of disordered semiconductor heterojunctions instead of transient dynamics. For this reason, a second type of simulations have been carried out where a continuous injection of electron-hole pairs is explicitly considered in the system, in accordance with the photon absorption frequency of solar radiation in a solar cell. In these simulations an steady-state situation is reached,

consequence of a balance between recombination and injection. This can be verified by the fact that the occupation probability fits to a Fermi-Dirac function (see Chapter 4) and that the the number of "alive" electron-hole pair is kept constant. Thus, well defined Fermi levels for holes and electrons in both semiconductors (E_{Fn}^{2} and E_{Fp}^{1}) are obtained in equilibrium.

8.3. Results and discussion

SPV measurements. Application to ETA solar cells

Using the mean positions of electrons and holes, a SPV histogram can be computed from the RW calculations (see Eq. (8.1)). To use realistic values of SPV in experiments, the following parameters have been used:[13,22] $T = 300$ K, $t_{0n} = t_{0p} = 10^{-12}$ s, $\alpha_{l} = 1$ nm, $a_{L} = 1$ nm and $\epsilon_{r} = 10$. Having fixed these, we will focus on the role that recombination mechanism (by means of t_{r0}), absorber thickness (W_{2}) and initial densities (ρ_{0n}, ρ_{0p}) play in the charge separation process taking place in the heterojunction upon photoexcitation.
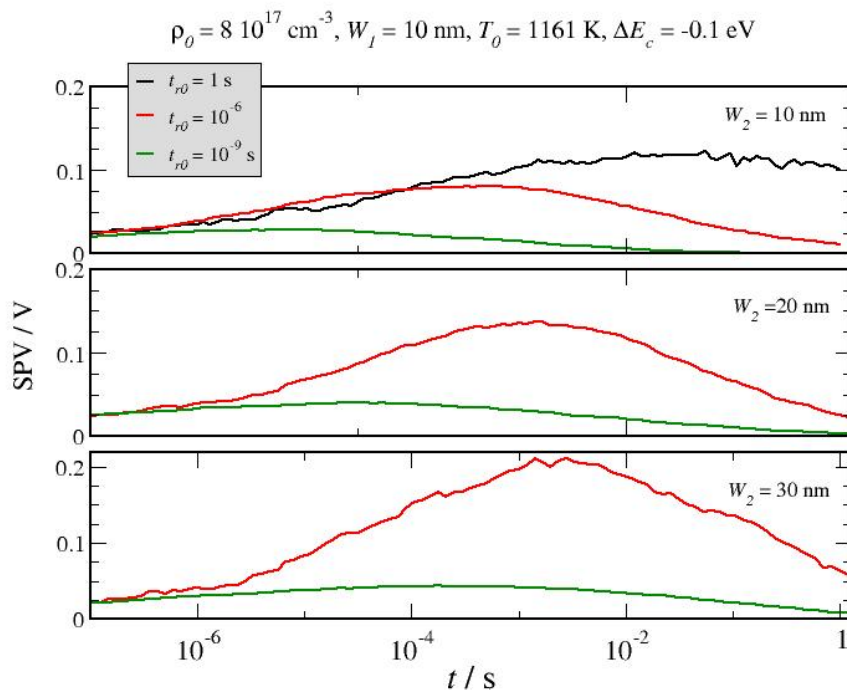
Fig. (8.3). SPV transients from RWNS calculations for different values of the thickness of the absorber and the recombination frequency ($1/t_{r0}$). Parameters used in the simulations are indicated in the Figure.

SPV transients obtained from RW calculations for different values of t_{r0} and W_2 are shown in Fig. (8.3). It can be observed that, for fixed absorber thickness, the higher the recombination time prefactor in Eq. (8.4) is, the later appears the decay. This is explained by the fact that as t_{r0} increases, the probability of recombination decreases with respect to transport, so that fewer recombination events will occur. For $t_{r0} = 1$ s, very few carriers are recombined and the SPV signal is mainly controlled by diffusion and charge separation. Thus, in this case a saturation effect related to the total thickness of the heterostructure seems to appear after charge separation process has been taken place. We can also see that variation of recombination frequencies affects the SPV maxima, making it higher as it decreases. On the other hand, comparison of the three panels indicates that for a given value of the recombination frequency the SPV maxima appears at longer times as the absorber thickness (W_2) is augmented. This is a consequence of the fact that for thicker absorbers the process of diffusion with respect to electron-hole recombination is favoured.
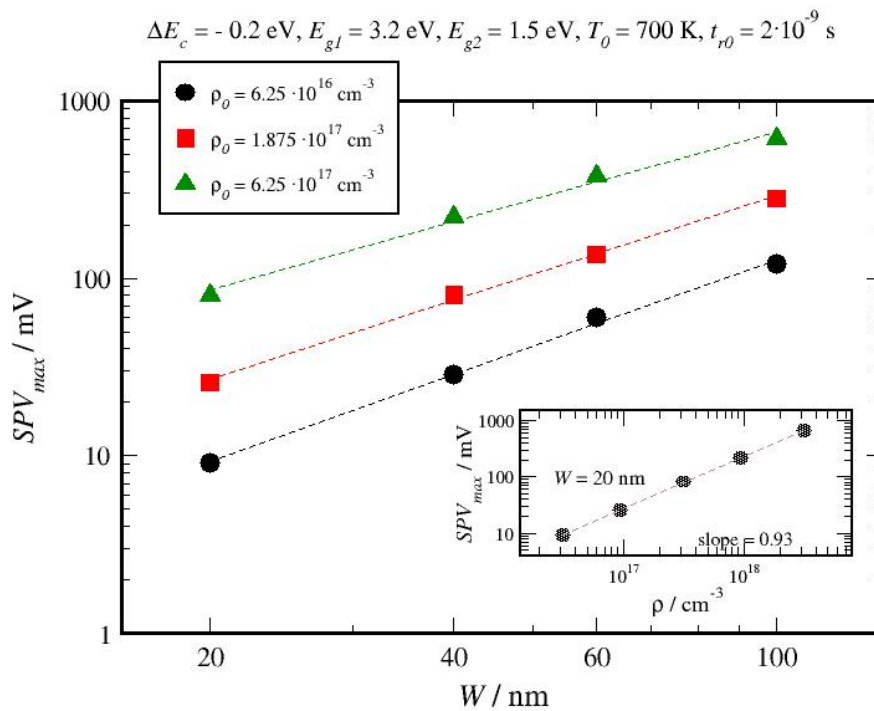
Fig. (8.4). Maximum surface photovoltage of the transient versus total width of the film for several values of the carrier concentration as obtained from RW calculations with Miller-Abrahams hopping rates and a tunnelling recombination mechanism. The dashed lines stand for linear fittings of the simulation data. The inset includes the electron density dependence.

Results of SPV maxima versus semiconductor thicknesses for various initial electron-hole densities are presented in Fig. (8.4). As it can be observed, the maximum value of the SPV transients increases with respect to the width of the heterostructure according to a power law. It is interesting to note that the exponents also increase slightly with the illumination, from a slope of *1.2,* for the minimum density ($\rho_0 = 6.25 \cdot 10^{16} \, cm^{-3}$) to a value of 1.6 for the case of $\rho_0 = 1.875 \cdot 10^{18} \, cm^{-3}$. Likewise, it is shown that the maximum value of the SPV transients increases linearly with respect to the charge density for a given value of the total thickness in the log-log scale. The exponent is close to the unity in all cases, in accordance to experimental observations[6,9]. However, a saturation effect cannot be reproduced for larger values of illumination intensities (or initial charge densities), an observation also reported in experiments. This may be a consequence of the fact that for high charge densities the recombination mechanism changes and energy factors have to be taken into account.

The charge concentration dependence of the halftime (defined as the time required for the SPV to reach half of its maximum value) is shown in Fig. (8.5). As reported in recent

$\Delta E_c = - \, 0.2 \, eV, \, E_{g1} = 3.2 \, eV, \, E_{g2} = 1.5 \, eV, \, T_0 = 700 \, K, \, t_{r0} = 2 \cdot 10^{-9} \, s$
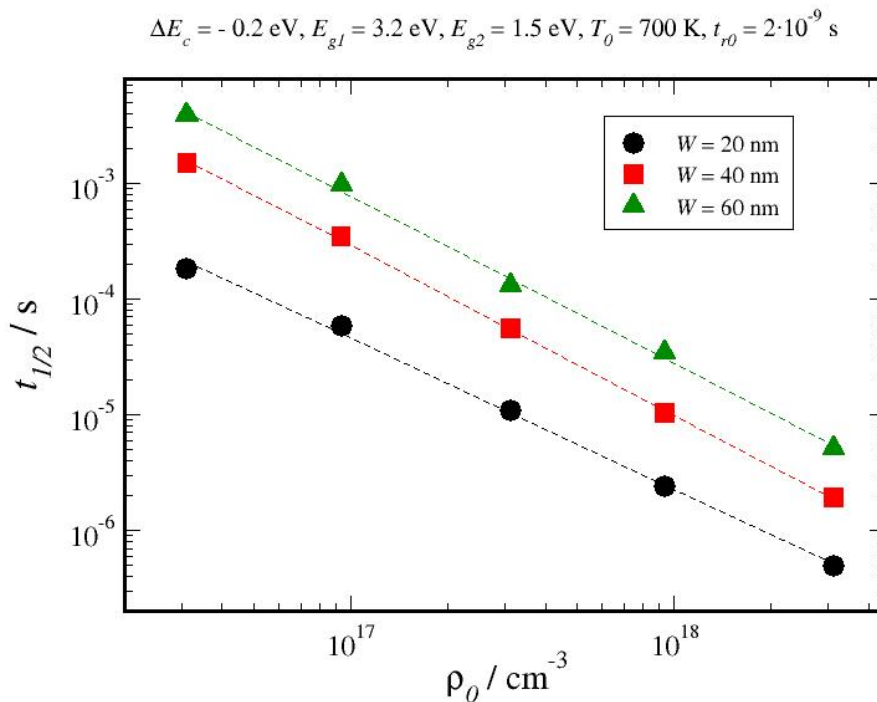
Fig. (8.5). Halftime of the transient versus carrier concentration for several values of the total width of the film as obtained from RW calculations with Miller-Abrahams hopping rates and a tunnelling recombination mechanism. The solid lines stand for linear fitting of the simulation data.

$$\rho_0 = 2.4\ 10^{18}\ \text{cm}^{-3},\ W = 20\ \text{nm},\ W_1 = 10\ \text{nm},\ T = 300\ \text{K}$$

$$T_0 = 1161\ \text{K},\ E_{g1} = 3.2\ \text{eV},\ E_{g2} = 1.5\ \text{eV}$$
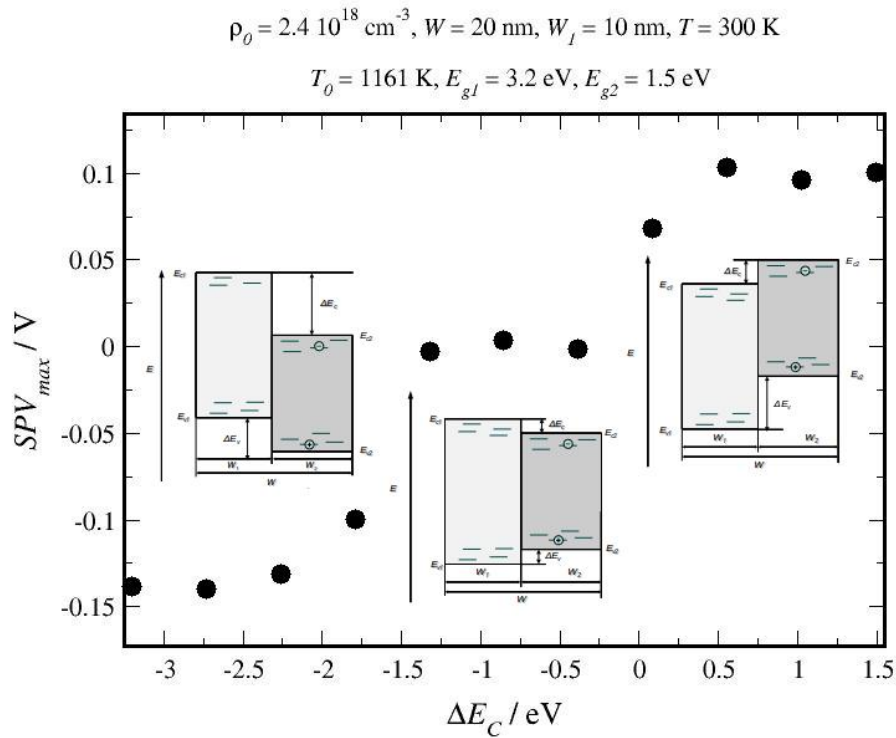
Fig. (8.6). Maximum surface photovoltage of the transients versus band-offset in a disordered heterojunction as obtained from RW calculations with Miller-Abrahams hopping rates and Tunnelling recombination mechanism.

works[6,23], a decrease of the halftime with respect to the illumination intensity is observed. This behaviour is attributed to trap-filling effects[22,24,25] and can be understood in the following way: a higher trap-density induces an increase of the Fermi level and the occupancy of the deep traps. According to Eq. (3.2) carriers move more rapidly on average between shallow traps, hence favouring a more rapid dynamics and a faster decay. Note the analogy with the transport-limited recombination model (dynamic view) of Chapter 5. The density dependence is found to follow a power law as shown in Fig. (8.5), with power exponents 1.30, 1.46 and 1.44 for $W = 20$, 40 and 60 nm, respectively. This power exponent can be related to the trap average energy[26].

SPV maxima with respect to the band-offset are presented in Fig. (8.6). The simulation shows that the SPV peak starts to be negative and becomes larger as the band-offset is augmented. Negative values of SPV are expected if we take into account that these cases correspond to values of ΔE_c and ΔE_v that permit holes to move to the first semiconductor while force electrons to stay in the absorber. When SPV > 0 the charge separation goes on the

inverse direction (see Fig. (8.2)) while no significant charge separation takes place when ΔE_c and ΔE_v are similar. In summary, in the two first cases we have a *Type-II heterojunction* while intermediate values of ΔE_c in Fig. (8.6) correspond to a *Type-I heterojunction*. Schemes of the corresponding band-offsets are presented in the inset of Fig. (8.6). The fact that the SPV maxima increase for larger band-offsets is a common experimental observation reported several times in the literature[27]. A saturation effect appears at a certain value of the band relative positions. This is an interesting result since this effect can be related to a maximum value of the open-circuit voltage (V_{oc}) that can be achieved in a solar cell based on a particular disordered heterojunction.

Steady-state RWNS. Application to BHJ solar cells.

The following parameters have been used in the computations: $T = 300$ K, $\alpha_l = 2$ nm and $a_L = 2$ nm. Likewise, we have used values for both the trap density and the average trap energy that are commonly reported in literature in order to reproduce realistic open-circuit
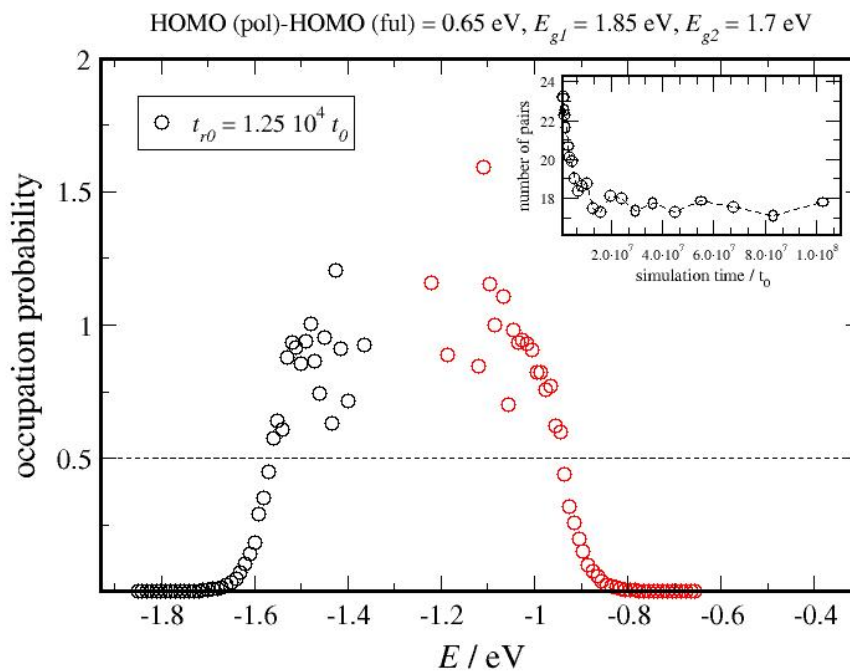
Fig. (8.7). Occupation probability of energy levels. It is observed that when an stationary state is reached then electron and hole occupancies are given by Fermi-Dirac statistics. The open-circuit photovoltage is obtained from splitting of the Fermi levels ($V_{oc} \sim 0.55$ eV).

photovoltages and photocurrents[14,15,28–30]. First of all, energy histograms of electron and hole occupancies in the fullerene and the polymer respectively are shown in Fig. (8.7). It was observed that when an stationary state is reached, signalled by constant electron and hole densities (see inset of Fig. (8.7), carrier occupancies are given by Fermi-Dirac statistics. In this way, from these energy histograms it is possible to estimate the Fermi levels and therefore the open-circuit photovoltage from Eq. (8.2). The recombination frequency prefactor t_{r0} was adjusted to reproduce the experimental V_{oc} at 1-sun illumination. Proceeding this way, $t_{r0} = 8 \cdot 10^6 \, t_0$ has been found for the case presented in Fig. (8.7).

The open-circuit voltage V_{oc} for different degrees of illumination was also calculated. Results can be seen in the upper panel of Fig. (8.8). First of all, it is found that values of the open-circuit voltage are always smaller than $E_{LUMO}(Ful) - E_{HOMO}(Pol)$, what is a common
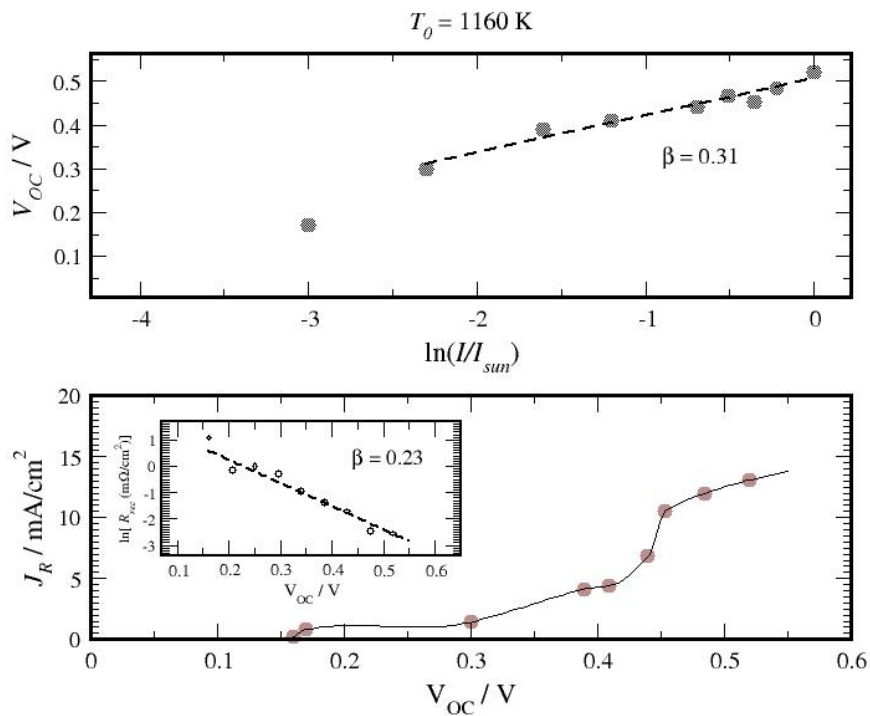
Fig. (8.8). Upper panel. Open-circuit voltage as a function of the illumination intensity from electron Fermi level in the fullerene and hole Fermi level in the polymer as obtained by RW simulations (circles). The dashed line was obtained by fitting to Eq. (8.6). Lower panel. Recombination current as a function of the open-circuit voltage. The inset includes the dependence of the recombination resistance R_{rec}, defined by Eq. (8.10), with respect to the open-circuit voltage as obtained by RWNS.

experimental observation[14]. On the other hand, an exponential dependence of V_{oc} with respect to the light intensity I is observed, as described in the following equation.

$$V_{oc} \propto \frac{k_B T}{\beta q} \ln I \tag{8.5}$$

Hence, from Eq. (8.5) we obtain $\beta = 0.31$ for a characteristic temperature of $T_0 = 1160$ K. On the other hand, the recombination current J_R as obtained by RW simulation is shown in the lower panel of Fig. (8.8) as a function of the open-circuit voltage. Realistic values of J_R were obtained as well as the same dependence than that observed experimentally[30]. The inset of the lower panel shows the dependence of the recombination resistance R_{rec} with the open-circuit voltage. The same behaviour than described by Eq. (2.48) is observed, with $\beta = 0.23$.

However, commonly reported values of β are of the order of 0.7-0.8[14]. Therefore, new calculations were carried out with the average energy width of the distributions varied down to $T_0 = 500$ K[30]. Results of this new simulations can be seen in the upper panel of Fig. (8.9). It can be observed that in this case the slope of the curve becomes more realistic ($\beta = 0.62$), what indicate that β depends "empirically" on the trap parameter $k_B T_0$.

It is interesting to note that, according to Eq. (8.2) and applying the zero-temperature limit of the Fermi-Dirac distribution for both electrons and holes, the following expression can be derived for the open-circuit photovoltage

$$V_{oc} = \frac{1}{q} \left[E_{LUMO}^{ful} - E_{HOMO}^{pol} - 2 k_B T_0 \ln \left(\frac{n_{pair}}{N_l} \right) \right] \tag{8.6}$$

where n_{pair} is the steady-state electron-hole density. Hence, it is possible to obtain V_{oc} from the steady-state electron-hole densities, once equilibrium has been reached. The result of this calculation is also observed in the upper panel of Fig. (8.9), where the same dependence than Eq. (8.5) is observed even more accurately than from direct measurements of the Fermi levels.

The recombination current, J_R, has also been measured as a function of light intensity for $T_0 = 500$ K. The results can be observed in the lower panel of Fig. (8.9). An exponential
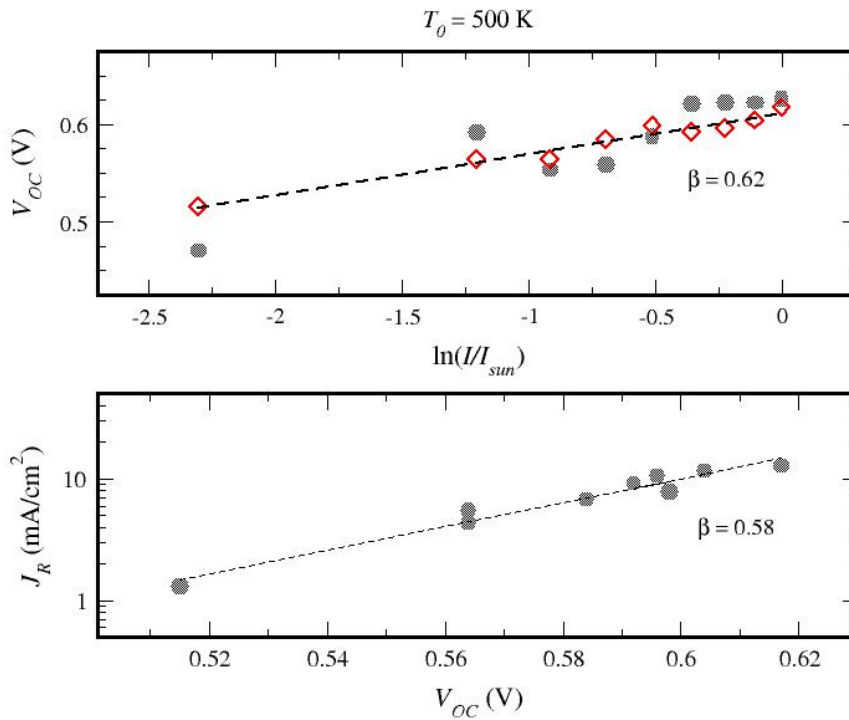
Fig. (8.9). Upper panel. Open-circuit voltage as a function of the illumination intensity from electron Fermi level in the fullerene and hole Fermi level in the polymer as obtained by RW simulations (circles) and from the steady-state electron-hole density as obtained by RW calculations (diamonds). The dashed line was obtained by fitting to Eq. (8.6). Lower panel. Recombination current as a function of the open-circuit voltage. Fitting procedure was made by adjusting Eq. (8.7).

dependence of the recombination current with respect to the open-circuit voltage was observed, according to the following equation (see Eq. (6.2))

$$J_{rec}(V) = J_0 \exp\left(\frac{\beta q V}{k_B T}\right) \tag{8.7}$$

with $\beta = 0.58$, a value close to that obtained from Eq. (8.5).

8.4. Conclusions to Chapter 8

In summary, a numerical method based on random walk simulation is devised to model charge separation in disordered heterojunctions. Charge transport is described via the

Miller-Abrahams hopping model whereas electron-hole recombination is taken into account via a tunnelling mechanism. On the one hand, we have obtained theoretical results for surface photovoltage transients in a disordered semiconductor heterojunction that adequately reproduce the experimental behaviour well known in this type of systems. We have analysed the dependence of the SPV signal on the band-offset, the width of the heterostructure and the carrier concentration. We find that the surface photovoltage increases with respect to the band-offset until a saturation effect appears at a certain value of the band positions.

On the other hand, a typical bulk heterojunction solar cell has been modelled under the assumption that charge separation is achieved by a chemical potential field, consequence of different affinities and work functions, instead of a built-in electric field. The open-circuit voltage has been determined as a function of the light intensity and the resulting dependence coincide with that obtained from experimental observations. Likewise, the recombination current has been studied at different open-circuit voltages and it has been observed that it increases exponentially with increasing voltages. The results demonstrate that the random walk method is an useful tool to study disordered heterojunctions starting from basic assumptions about electronic mechanisms in the nanoscale. Further work is however required to clarify the effects of the different parameters (for instance, the band-offset) on the open-circuit voltage and the recombination current of practical devices.

References for chapter 8

(1)   STUTZMANN, M.; JACKSON, W.; TSAI, C. *PHYSICAL REVIEW B* **1985**, *32*, 23–47.

(2)   Schulze, T.; Beushausen, H.; Leendertz, C.; Dobrich, A.; Rech, B.; Korte, L. *APPLIED PHYSICS LETTERS* **2010**, *96*.

(3)   SHOCKLEY, W.; READ, W. *PHYSICAL REVIEW* **1952**, *87*, 835–842.

(4)   Kronik, L.; Shapira, Y. *Surface Science reports* **1999**, *37*, 1–206.

(5)   Dittrich, T.; Duzhko, V.; Koch, F.; Kytin, V.; Rappich, J. *Phys. Rev. B* **2002**, *65*.

(6)   Dittrich, T.; Bönisch, S.; Zabel, P.; Dube, S. *Review of Scientific Instruments* **2008**, *79*, 113903.

(7)   Mahrov, B.; Boschloo, G.; Hagfeldt, A.; Dloczik, L.; Dittrich, T. *Appl. Phys. Lett.* **2004**, *84*, 5455.

(8)   Duzhko, V.; Koch, F.; Dittrich, T. *J. Appl. Phys.* **2002**, *91*, 9432.

(9)   Timoshenko, V. Y.; Duzhko, V.; Dittrich, T. *Physica Status Solidi a-Applied Research*

2000, *182*, 227–232.

(10)   Dittrich, T.; Mora-Sero, I.; Garcia-Belmonte, G.; Bisquert, J. *Physical Review B* **2006**, *73*.

(11)   Mora-Seró, I.; Dittrich, T.; Garcia-Belmonte, G.; Bisquert, J. *J. Appl. Phys.* **2006**, *100*, 103705.

(12)   Mora-Sero, I.; Anta, J. A.; Dittrich, T.; Garcia-Belmonte, G.; Bisquert, J. *Journal of Photochemistry and Photobiology a-Chemistry* **2006**, *182*, 280–287.

(13)   Anta, J. A.; Mora-Sero, I.; Dittrich, T.; Bisquert, J. *Journal of Physical Chemistry C* **2007**, *111*, 13997–14000.

(14)   Bisquert, J.; Garcia-Belmonte, G. *The Journal of Physical Chemistry Letters* **2011**, *2*, 1950–1964.

(15)   He, F.; Yu, L. *J. Phys. Chem. Lett.* **2011**, *2*, 3102–3113.

(16)   Monroe, D. *Physical Review Letters* **1985**, *54*, 146–149.

(17)   Bisquert, J.; Fabregat-Santiago, F.; Mora-Sero, I.; Garcia-Belmonte, G.; Barea, E. M.; Palomares, E. *Inorganica Chimica Acta* **2008**, *361*, 684–698.

(18)   Orenstein, J.; Kastner, M. *Physical Review Letters* **1981**, *46*, 1421.

(19)   *Charge Transport in Disordered Solids with Applications to Electronics*; Baranovskii, S. D., Ed.; Wiley: Weinheim, 2006.

(20)   Kopidakis, N.; Benkstein, K. D.; Lagemaat, J. van de; Frank, A. J.; Yuan, Q.; Schiff, E. A. *Physical Review B* **2006**, *73*.

(21)   Kytin, V.; Timoshenko, V. Y.; Rappich, J.; Dittrich, T. *Physica Status Solidi a-Applied Research* **2001**, *185*, R1–R3.

(22)   Anta, J. A.; Mora-Sero, I.; Dittrich, T.; Bisquert, J. *Physical Chemistry Chemical Physics* **2008**, *10*, 4478–4485.

(23)   Dittrich, T.; Duzhko, V. *PHYSICA STATUS SOLIDI A-APPLIED RESEARCH* **2003**, *197*, 107–112.

(24)   Anta, J. A.; Nelson, J.; Quirke, N. *Physical Review B* **2002**, *65*.

(25)   Anta, J. A. *Energy and Enviromental Science* **2009**.

(26)   Scher, H.; Montroll, E. W. *Physical Review B* **1975**, *12*, 2455–2477.

(27)   Mora-Seró, I.; Gross, D.; Mittereder, T.; Lutich, A. A.; Susha, A. S.; Dittrich, T.; Belaidi, A.; Caballero, R.; Langa, F.; Bisquert, J.; Rogach, A. L. *Small* **2010**, *6*, 221–225.

(28)   Hoppea, H, S., N.S. *Journal of Materials Research* **2004**, *19*, 1924–1945.

(29)   Kirchartz, T.; Pieters, B.; Kirkpatrick, J.; Rau, U.; Nelson, J. *Physical Review B* **2011**, *83*.

(30)   MacKenzie, R. C. I.; Kirchartz, T.; Dibb, G. F. A.; Nelson, J. *The Journal of Physical Chemistry C* **2011**, *115*, 9806–9813.

CONCLUSIONS

The decisive role that randomly distributed localized states dispersed in energies play for the understanding of the electron dynamics in disordered semiconductors has been analysed in this thesis. For this purpose, RWNS provides an easy-to-use tool with encouraging results. It permits to describe charge transfer processes in terms of microscopic mechanisms without the requirement of high computational times characteristic of ab initio calculations. Thus, specific transport and recombination processes that take place with the involvement of localized states can be modelled and related to macroscopic properties of the materials.

First of all, the RWNS method with Miller-Abrahams hopping rates and exponential distribution of energies on a random network of traps has been utilized to describe transport properties in random media and to obtain the jump diffusion coefficient versus Fermi level and temperature. An approximate exponential dependence is found for the former and Arrhenius behaviour for the latter. The simulation helps to distinguish between the energy of the most probable jump and an estimation of the effective transport energy that determines the transport properties of the system. Comparison of the present results with the conditions of interest in the functioning of photovoltaic devices based on nanocrystalline TiO_2 reveal that in this case the effective transport energy is approximately independent of the Fermi level. Hence the observed behaviour is similar to that found with the multiple-trapping model, making both models "indistinguishable" from the experimental point of view.

On the other hand, in order to check the influence of the exponential distribution of localized states in the processes of recombination that take place in a DSC, RW calculations have been carried out including direct computation of the electron diffusion length and the electron lifetime. On the one hand, using an energy-independent recombination rate, we have been able to reproduce experimental observations on account with trap-filling effects, such as the voltage dependence of the electron lifetime, as well as open-circuit voltage decay experiments. On the other hand, a more sophisticated charge transfer mechanism, including an energy-dependent recombination rate, has been studied. The behaviour of the electron diffusion length with respect to the Fermi level has been explained in terms of the interplay between the energy distribution of the traps in the oxide and the acceptor states in the electrolyte.

The role of different spatial configurations and morphologies in disordered materials has also been analysed. The results lead to the conclusion that a relevant collection efficiency enhancement is only achieved at intermediate values of the recombination probability. On the other hand, the results show that when this condition is accomplished just a slight partial ordering of the system is sufficient to a meaningful increase of the collection efficiency.

Finally, a disordered semiconductor heterojunction has been studied by means of RWNS. Both transient and steady-state simulations have been carried out, with applications in Extremelly Thin Absorber solar cells and Bulk Heterojunction solar cells. It has been found that charge separation and transport can be achieved without the presence of a built-in electric field. In contrast, the appearance of a built-in chemical potential explains that one type of charge can pass across the interface while the other remains in the absorber. On account of recombination, a tunnelling recombination mechanism has been implemented. From this model, the open-circuit voltage has been obtained as a function of the illumination intensity and results in agreement with experimental observations have been achieved. The surface photovoltage, another measure of charge separation, has also been obtained, and their dependence on film thickness and band offset extracted.

In summary, it has been demonstrated that these calculations can be applied to a wide variety of new generation solar cells, such as dye sensitized solar cells, extremely thin absorber solar cells or bulk heterojunction solar cells. Hence, the current intense research on photovoltaic devices based on disordered materials provides a promising field in which to apply the Random Walk Numerical Simulation method.

CONCLUSIONES

En esta tesis se ha hecho un estudio teórico de la dinámica electrónica en semiconductores desordenados mediante el método de simulación numérica de marcha electrónica (RWNS). Para ello se ha tenido en cuenta explícitamente el decisivo papel que presenta la existencia de una distribución energética cuasi-continua de estados localizados en la banda prohibida de estos materiales. Se concluye que el método RWNS proporciona una eficiente herramienta de estudio, ya que permite describir procesos de transferencia de carga en base a mecanismos microscópicos sin el requerimiento de largos tiempos de computación, característicos de cálculos ab initio. De esta manera, se puede llevar a cabo un proceso de modelización de mecanismos específicos de transporte y recombinación en presencia de una distribución dada de estados localizados que permitan relacionarlos luego con propiedades macroscópicas.

En primer lugar, se ha hecho uso del método RWNS para un análisis de la difusión electrónica en medios desordenados teniendo en cuenta una red aleatoria de trampas con una distribución en energías exponencial y una probabilidad de salto entre estados localizados dada por la fórmula de Miller-Abrahams. Se han obtenido resultados del coeficiente de difusión electrónico en función del nivel de Fermi, obteniéndose una dependencia exponencial. Asimismo, se ha observado un comportamiento tipo Arrhenius del coeficiente de difusión con respecto a la temperatura. Este tipo de cálculos ayuda a distinguir entre la energía de salto más probable y la energía de transporte efectiva, que determina las propiedades dinámicas del sistema. Por último se ha hecho llevado a cabo un análisis de los resultados en el contexto de una celda DSC basada en TiO_2. Se concluye que en condiciones de funcionamiento de este tipo de celdas la energía de transporte efectiva es aproximadamente independiente del nivel de Fermi. De esta manera, el comportamiento observado es similar al modelo multiple-trapping, dando lugar a que ambos modelos sean indistinguibles desde un punto de vista experimental.

Por otro lado, se han llevado a cabo cálculos RWNS con el objetivo de estudiar la influencia de una distribución exponencial de estados localizados en el proceso de recombinación que tiene lugar en una celda DSC. Se han realizado cálculos directos tanto de la longitud de difusión como de la vida media electrónicas. Usando una probabilidad de recombinación independiente de la energía se han podido reproducir observaciones experimentales, tales como la dependencia de la vida media electrónica con respecto al nivel de Fermi o el decaimiento del voltaje a circuito abierto, en términos de un efecto de llenado de trampas. También se ha estudiado un mecanismo de transferencia de carga más sofisticado, incluyendo una probabilidad de recombinación dependiente de la energía. Mediante este procedimiento se ha podido describir el comportamiento de la longitud de difusión con respecto al nivel de Fermi mediante la interrelación entre una distribución quasi-continua de

estados localizados en el óxido y una distribución de estados aceptores en el electrolito dada por el modelo de Marcus-Gerischer.

El papel que desempeñan diferentes configuraciones espaciales de trampas en la dinámica electrónica se ha analizado también como parte de esta tesis. Los resultados muestran que un aumento relevante de la eficiencia de recolección con el grado de orden sólo puede alcanzarse para valores intermedios de la probabilidad de recombinación. Por otro lado, cuando se cumple esta condición, un leve aumento del grado de orden es suficiente para conseguir un incremento significativo en la eficiencia de recolección de la celda.

Finalmente, se ha desarrollado un modelo para heterouniones de semiconductores desordenados. Se han realizado simulaciones de fenómenos tanto transitorios como en estado estacionario, con aplicaciones a celdas solares de absorbedor ultrafino y celdas solares orgánicas tipo "bulk heterojunction". Así, se ha observado que los procesos de separación y transporte de carga se pueden explicar en términos solamente de alineamiento entre bandas, sin necesidad de tener en cuenta un campo eléctrico interno. En cuanto a la recombinación, se ha tenido en cuenta un mecanismo de efecto túnel. Mediante el presente modelo se han obtenido voltajes a circuito abierto en función del grado de iluminación análogos a los medidos experimentalmente así como potenciales superficiales en función del alineamiento de banda y el grosor del semiconductor.

En resumen, esta tesis demuestra que el método RWNS se puede aplicar a una gran variedad de celdas solares de nueva generación, tales como DSC, ETA o BHJ, con muy buenos resultados. Por esto mismo, la intensa actividad investigadora que se está llevando a cabo actualmente en el campo de la fotovoltaica proporciona un campo muy prometedor en el que llevar a cabo cálculos de marcha aleatoria.

List of Symbols

α	ratio of absolute temperature T to the characteristic temperature T_0
α_{ab}	absorption coefficient
α_l	localization radius
a_L	size of the simulation box
β	reaction order of the recombination rate with respect to the conduction band electron density
D_n	electron diffusion coefficient
D_p	hole diffusion coefficient
D_c	conduction band electron diffusion coefficient
D_j	jump diffusion coefficient
D^*	tracer diffusion coefficient
ϵ	relative dielectric constant
ϵ_0	vacuum permittivity or dielectric constant
η	conversion efficiency
η_{col}	charge collection efficiency
E	energy
E_c	electron mobility edge
E_v	hole mobility edge
E_g	band gap of a material
E_F	Fermi level
E_{Fn}	electron Fermi level
E_{Fp}	hole Fermi level
E_{redox}	redox potential
E_0	standard reduction potential
$E_{d,n}$	electron demarcation level
$E_{d,p}$	hole demarcation level
E_{tr}	transport energy
E_{max}	maximum of the energy histograms
E'_{max}	maximum of the corrected energy histograms
$f(E - E_F)$	Fermi-Dirac occupation function for state at energy E
FF	fill factor
γ	reaction order of the recombination rate with respect to the total electron density
$g(E)$	density of localized states per unit energy per unit crystal volume
I	incident light power density
J	total current density
J_n	electron current density
J_p	hole current density
J_c	conduction band current density
J_0	saturation current
J_{sc}	short-circuit current density
k_B	Boltzmann constant
λ	reorganization energy
L	thickness of the film
L_{ab}	absorption length
L_n	electron diffusion length

μ	chemical potential
μ_n	electron mobility
μ_p	hole mobility
m	ideality factor
ν_{ij}	jump rate between localized states i and j
ν_0	attemp-to-jump frequency
ν_{rec}	recombination rate
ν_{r0}	tunnelling recombination frequency
n	photogenerated electron density
n_i	intrinsic carrier density
n_0	equilibrium electron density (chapter 1)
n_c	conduction band electron density
n_l	electron density in localized states
N_c	effective conduction band density of states
N_l	density of localized states
$N(t)$	total amount of electron-hole pairs per unit area at time t
$N(E)$	number of carriers occupying an energy between E and $E+dE$
p	photogenerated hole density
p_0	equilibrium hole density
P	porosity
P_R	probability of recombination
q	elementary charge
ρ	electron-hole pairs density
r_{cut}	cut-off radius
$< r(t)^2 >$	mean-squared displacement
R	random number
R_{np}	electron-hole pair separation
R_{rec}	recombination resistance
R_0	recombination resistance in the absence of illumination
R_s	series resistance
R_{sh}	parallel or shunt resistance
σ	width of a gaussian absorption profile
S	specific surface area
τ_c	conduction band electron lifetime in the absence of traps
τ_f	effective conduction band electron lifetime
τ_n	electron lifetime
τ_{rec}	lifetime of charge carriers
τ_{tr}	transport time of charge carriers
t	time
t_0	attempt-to-jump time
t_{r0}	tunnelling recombination time
T	absolute temperature
T_0	characteristic temperature
U_{rad}	radiative recombination rate
U_{Aug}	Auger recombination rate
U_{SRH}	Shockley-Read-Hall recombination rate
U_{rec}	recombination rate
V	voltage
V_{oc}	open-circuit voltage
W	thickness of the film

χ_n	thermodynamic factor
$<x_{p(n)}>(t)$	mean position of holes (electrons)
x_{mean}	centre of a gaussian absorption profile

Acronyms

AM	air mass
BHJ	bulk heterojunction solar cell
CdTe	cadmium telluride
CIS	copper indium selenide
CIGS	copper indium gallium diselenide
CuSCN	copper thiocyanate
CTRW	continuous time random walk
DSC	dye-sensitized solar cell
DOLS	distribution of localized states
ETA	extremely thin absorber solar cell
GaAs	gallium arsenide
HOMO	highest occupied molecular orbital
In_2S_3	Indium sulfide
LUMO	lowest unoccupied molecular orbital
MG	Marcus-Gerischer
MC	Monte Carlo
OSC	organic solar cell
RW	random walk
RWNS	random walk numerical simulation
SRH	Shockley-Read-Hall
SPV	surface photovoltage
TCO	transparent conductive oxide electrode
TiO_2	titanium dioxide
ZnO	zinc oxide

Appendix A: Invariance of the electron diffusion length behaviour with respect to recombination prefactor
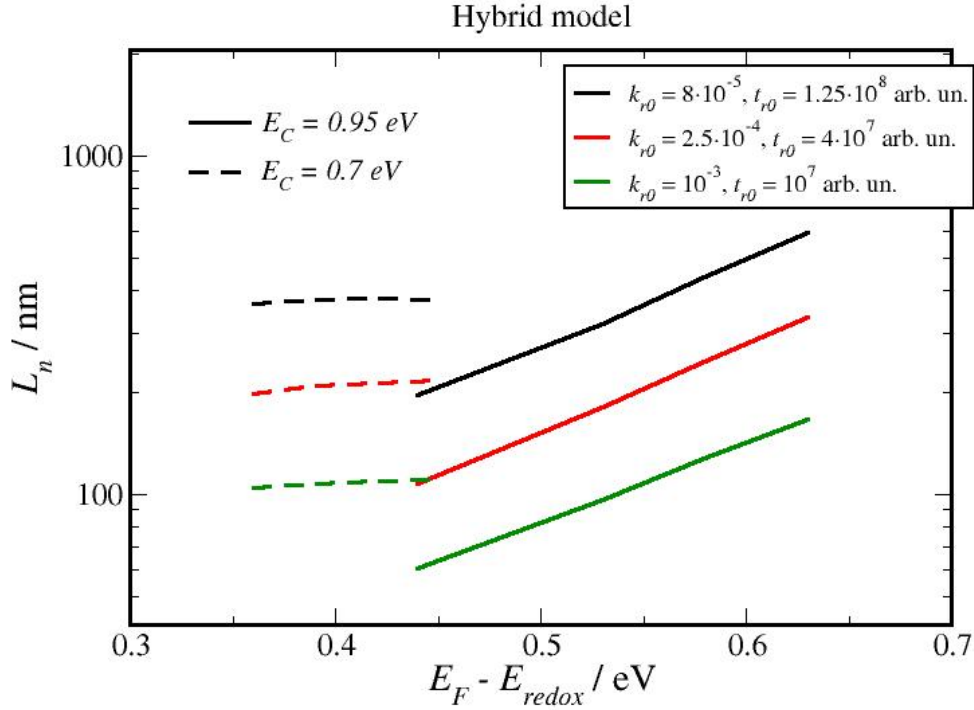
Fig. (A1). Electron diffusion length calculated by steady-state RWNS calculations using the **hybrid model** for different values of the recombination prefactors (Eqs. (6.4) and (6.5)). The simulations correspond to systems defined by $\lambda = 0.6$ eV, $T_0 = 700$ K and $T = 300$ K. Two values of the conduction-band position are considered: $E_c - E_{redox} = 0.95$ eV (solid lines) and $E_c - E_{redox} = 0.70$ eV (dashed lines). Results are obtained from the Marcus-Gerischer formula (Eqs. (6.4) and (6.5)) and a density of electronic states in the semiconductor given by Eq. (2.2).
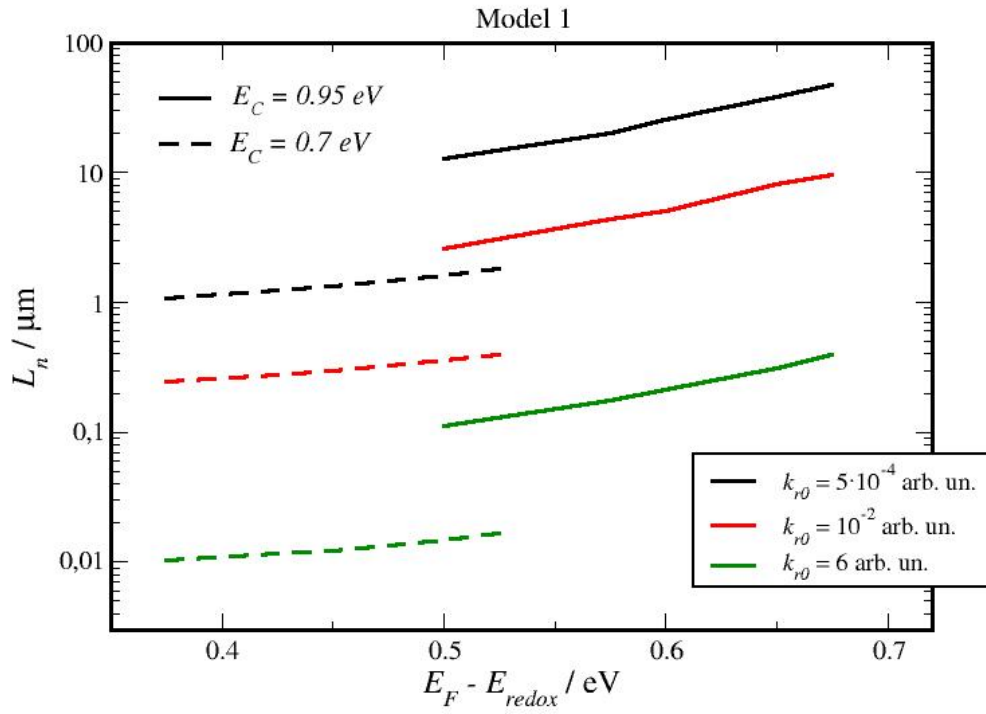
Fig. (A2). Electron diffusion length calculated by steady-state RWNS calculations using **Model 1** for different values of the recombination prefactor (Eq. (6.4)). The simulations correspond to a system defined by $\lambda = 0.25$ eV, $T_0 = 700$ K, $T = 300$ K. Two values of the conduction-band position are considered: $E_c - E_{redox} = 0.95$ eV (solid lines) and $E_c - E_{redox} = 0.70$ eV (dashed lines). Results are obtained from the Marcus-Gerischer formula (Eq. (6.4)) and density of electronic states in the semiconductor (Eq. (2.2), trap energy distribution).
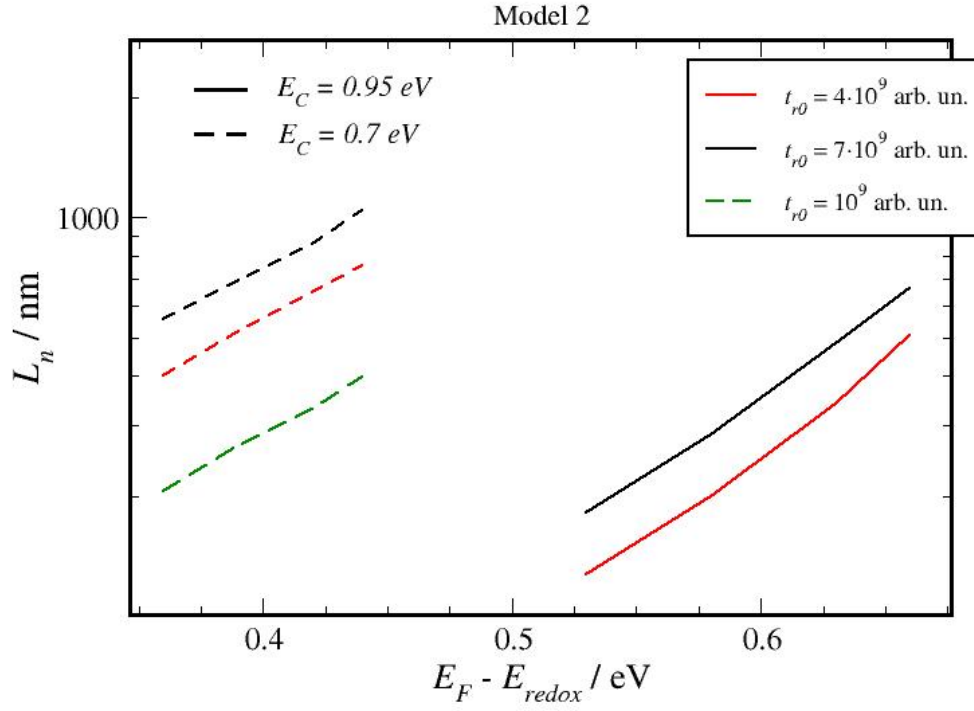
Fig. (A3). Electron diffusion length calculated by steady-state RWNS calculations using **Model 2** for different values of the recombination prefactor (Eq. (6.5)). The simulations correspond to systems defined by $\lambda = 2.0$ eV, $T_0 = 700$ K, $T = 300$ K. Two values of the conduction-band position are considered: $E_c - E_{redox} = 0.95$ eV (solid lines) and $E_c - E_{redox} = 0.70$ eV (dashed lines). Results are obtained from the based on times Marcus-Gerischer formula (Eq. (6.5)) and density of electronic states in the semiconductor (Eq. (2.2), trap energy distribution).

Appendix B: Theoretical dependence of collection efficiency on absorption length

The collection efficiency of DSC at short-circuit conditions was obtained by solving numerically the continuity equation for the total density of electrons $n(x,t)$ in the photoanode:

$$\frac{\partial n(x,t)}{\partial t} = \frac{\partial}{\partial x}\left[D_n(n(x,t))\frac{\partial n(x)}{\partial x}\right] + G(x) - k_n(n(x,t))\left[n(x,t) - n_0\right] \qquad (B1)$$

where k_n is a pseudo-first order kinetic recombination constant which can be related to the inverse of an electron lifetime:[4] $k_n = 1/\tau_n$. Note that the complex density dependence of the kinetics constants (D_n and k_n) is implicitly indicated, meaning that these magnitudes can vary with space and time. Details on this computation can be found in Refs. [5,7]

In the numerical solution of Eq. (S1), the generation term G(x) is derived from Lambert-Beer law:

$$G(x) = \int_{\lambda_{min}}^{\lambda_{max}} \phi_{inj} I_0(\lambda)\epsilon_{cell}(\lambda)\left(1 - \exp\left[-\epsilon_{cell}(\lambda)d\right]\right)\exp\left[-\epsilon_{cell}(\lambda)x\right]d\lambda \qquad (B2)$$

where ϕ_{inj} is the quantum injection yield, $I_0(\lambda)$ is the solar spectrum (here taken from the standard AM1.5G) and $\epsilon_{cell}(\lambda)$ is the wave-length dependent absorption coefficient of the dye in the solar cell.

The collection efficiency of the DSC is calculated from the ratio between the short-circuit photocurrent and the total number of electrons generated in the film. The short-circuit photocurrent is in turn estimated from the gradient of the density at contact $x = 0$

$$J_{sc} = \frac{\partial n(x,t)}{\partial x}\Big|_{x=0} \qquad (B3)$$

In Figure S2 the collection efficiency is calculated for different concentrations of the dye in the photoanode, meaning different values of the absorption length L_{abs} (obtained by fitting the generation term S2 to a single exponential function). The results reproduce a power law with a similar exponent to that found in the RW simulations shown in the main text.
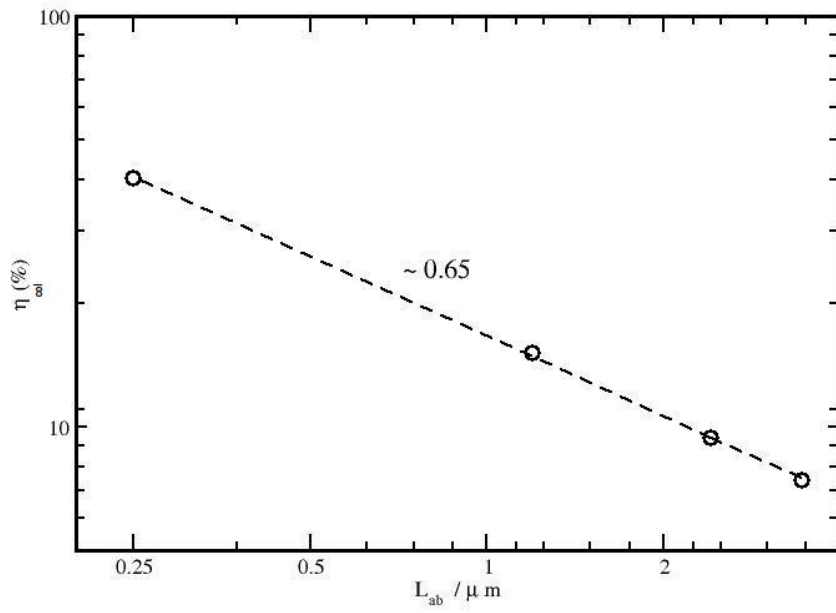
Fig. (B1). Charge collection efficiency as a function of absorption length as obtained from the numerical solution of the continuity equation with diffusion, recombination and generation terms. The recombination rate is adjusted to fit the collection efficiency obtained in the RW simulations shown in Fig. (7.3). The dashed line stands for a power-law fitting of the data, with an exponent of ~ 0.65 as shown.

```fortran
Program hjunc
!
!       ------------------------------------------------------------
!       --->  Random Walk in a heterojunction of disordered semiconductors <----
!       ------------------------------------------------------------
!
!       This is an...
!
!               ACTIVATED HOPPING CONTINUOUS TIME RANDOM WALK method
!                   AIM: SURFACE PHOTOVOLTAGES (2010)
!
!                       Original N Quirke september 1998
!                       Modified by J.A. Anta, May-August 1999
!                       Modified by J.A. Anta, September 2006 (diff coef.)
!                       Modified by J.A. Anta, November 2006 (spatial disorder)
!                       Modified by J.A. Anta, May 2007 (spatial disorder: improved)
!               Modified by J.P. Gonzalez, November 2008 (hopping model)
!               Modified by J.P. Gonzalez, September 2009 (second charge carrier)
!                       Modified by J.P. Gonzalez, May 2010 (disordered semiconductor heterojunction)
!
  IMPLICIT NONE
!
! fixed parameters:
!
  REAL*8, PARAMETER :: echarge = 1.60217733d-19 ! elementary charge
  REAL*8, PARAMETER :: melec = 9.1093897d-31 ! electron mass
  REAL*8, PARAMETER :: m2nm = 1d9 ! nanometers to meter
  REAL*8, PARAMETER :: temp2kt = 8.613278d-05 ! kelvins to eV (kT)
  REAL*8, PARAMETER :: ebin = 0.005 ! energy grid in nofe and gofe histograms
  REAL*8, PARAMETER :: epsilon0 = 8.8547d-12 ! in C/(V.nm)
!
! trap attempt frequency and time unit
!
  REAL*8 :: nu0 ! = h/(8*melec*aa**2) or 1/tunit
!
! input parameters (file="hjunc.in")
!
  INTEGER :: np           ! number of particles
  INTEGER :: nh           ! number of holes
  REAL*8 :: d,dyz         ! size length of simulation box in nm (d --> x-coordinate)
  REAL*8 :: d1            ! size length of sem.1
  REAL*8 :: rcut          ! cut-off for hopping between neighbouring traps
  REAL*8 :: nsample       ! number of samples
  REAL*8 :: temp          ! temperature in K
  REAL*8 :: maxmoves      ! maximum number of moves
  REAL*8 :: maxtime       ! maximum time of simulation in units of tunit or tunith
  REAL*8 :: tbin          ! bin size for time histograms in units of tunit
  REAL*8 :: tunit         ! time unit for electrons(t0)
  REAL*8 :: tunith        ! time unit for holes (t0h)
  REAL*8 :: ec1           ! energy of conduction band edge (0 by default) for sem.1 (eV)
  REAL*8 :: ec2           ! energy of conduction band edge (0 by default) for sem.2 (eV)
  REAL*8 :: ev1           ! energy of valence band edge (0 by default) for sem.1 (eV)
  REAL*8 :: ev2           ! energy of valence band edge (0 by default) for sem.2 (eV)
  REAL*8 :: ecut1         ! energy cutoff for exponential DOS used for electrons (eV)
  REAL*8 :: ecut2         ! energy cutoff for exponential DOS used for electrons (eV)
  REAL*8 :: ecuth1        ! energy cutoff for exponential DOS used for holes (eV)
  REAL*8 :: ecuth2        ! energy cutoff for exponential DOS used for holes (eV)
  REAL*8 :: temp01        ! characteristic temperature in K for exponential DOS used for electrons in sem.1
  REAL*8 :: temp02        ! characteristic temperature in K for exponential DOS used for electrons in sem.2
  REAL*8 :: temp0h1       ! characteristic temperature in K for exponential DOS used for holes in sem.1
  REAL*8 :: temp0h2       ! characteristic temperature in K for exponential DOS used for holes in sem.2
  REAL*8 :: alfa          ! electron localization radius (nm)
  REAL*8 :: alfah         ! hole localization radius (nm)
  REAL*8 :: alat          ! average distance between traps
  REAL*8 :: effmfac       ! rate between effective masses
  REAL*8 :: r0            ! electron Bohrs radius in angstroms (for tunneling recombination)
  REAL*8 :: tt0           ! recombination life time in units of tunit
  REAL*8 :: epsilonr      ! relative dielectric constant
  REAL*8 :: dt1           ! time length between different pulses in s
!
  INTEGER :: ndist   ! number of grid points in distribution of trap energies
  REAL*8, DIMENSION(:), ALLOCATABLE :: epiege,pcum
!
! main variables
!
  INTEGER :: ntrap   ! number of traps
  REAL*8, DIMENSION(:), ALLOCATABLE :: x,y,z        ! coordinates of electrons
  REAL*8, DIMENSION(:), ALLOCATABLE :: x0,y0,z0     ! initial coordinates of electrons
  REAL*8, DIMENSION(:), ALLOCATABLE :: xr,yr,zr     ! real coordinates of electrons
  REAL*8, DIMENSION(:), ALLOCATABLE :: xh,yh,zh     ! coordinates of holes
  REAL*8, DIMENSION(:), ALLOCATABLE :: x0h,y0h,z0h  ! initial coordinates of holes
  REAL*8, DIMENSION(:), ALLOCATABLE :: xrh,yrh,zrh  ! real coordinates of holes
  REAL*8, DIMENSION(:), ALLOCATABLE :: e            ! energy of electrons

  REAL*8, DIMENSION(:), ALLOCATABLE :: eh           ! energy of holes
  REAL*8, DIMENSION(:), ALLOCATABLE :: wte          ! hopping time of electrons
  REAL*8, DIMENSION(:), ALLOCATABLE :: wth          ! hopping time of holes
  REAL*8, DIMENSION(:,:), ALLOCATABLE :: rt         ! recombination times
  INTEGER, DIMENSION(:), ALLOCATABLE :: ijumph      ! hopping-to trap of holes
  INTEGER, DIMENSION(:), ALLOCATABLE :: itraph      ! trap number of holes
  INTEGER, DIMENSION(:), ALLOCATABLE :: ijumpe      ! hopping-to trap of electrons
  INTEGER, DIMENSION(:), ALLOCATABLE :: itrape      ! trap number of electrons
  LOGICAL, DIMENSION(:), ALLOCATABLE :: otrape      ! if .true. trap is occupied by an electron
  LOGICAL, DIMENSION(:), ALLOCATABLE :: otraph      ! if .true. trap is occupied by a hole
  LOGICAL, DIMENSION(:), ALLOCATABLE :: oexist      ! if .true. electron "exists"
  LOGICAL, DIMENSION(:), ALLOCATABLE :: oexisth     ! if .true. hole "exists"
  REAL*8, DIMENSION(:), ALLOCATABLE :: etrape       ! trap energy (for electron ditribution)
  REAL*8, DIMENSION(:), ALLOCATABLE :: etraph       ! trap energy (for hole ditribution)
  REAL*8, DIMENSION(:), ALLOCATABLE :: xtrap        ! trap x-coordinate
  REAL*8, DIMENSION(:), ALLOCATABLE :: ytrap        ! trap y-coordinate
  REAL*8, DIMENSION(:), ALLOCATABLE :: ztrap        ! trap z-coordinate
  REAL*8, DIMENSION(:), ALLOCATABLE :: svoltage     ! surface photovoltage (in Vm-2)
  INTEGER, DIMENSION(:,:), ALLOCATABLE :: ivec      ! neighbour list
  INTEGER, DIMENSION(:), ALLOCATABLE :: iv          ! number of neighbours
  REAL*8 :: tev           ! kT (temperature) in eV
  REAL*8 :: tev01         ! kT0 (characteristic temperature) in eV for electrons for sem.1
  REAL*8 :: tev02         ! kT0 (characteristic temperature) in eV for electrons for sem.2
  REAL*8 :: tev0h1        ! kT0 (characteristic temperature) in eV for holes for sem.1
  REAL*8 :: tev0h2        ! kT0 (characteristic temperature) in eV for holes for sem.2
  REAL*8 :: time          ! elapsed time
  REAL*8 :: emean         ! centre of gaussian DOS
  INTEGER :: nbins        ! number of time bins in total simulation time per sample
  REAL*8 :: ener          ! compute total energy of electrons
  REAL*8 :: dist          ! square displacement
  INTEGER, DIMENSION(:), ALLOCATABLE :: nalive
  INTEGER, DIMENSION(:), ALLOCATABLE :: halive
  INTEGER, DIMENSION(:), ALLOCATABLE :: nalive1
  INTEGER, DIMENSION(:), ALLOCATABLE :: nalive2
  INTEGER, DIMENSION(:), ALLOCATABLE :: halive1
  INTEGER, DIMENSION(:), ALLOCATABLE :: halive2
!
! output parameters
!
  INTEGER :: initbin1    ! initial point in "nofe" and "gofe" histograms
  INTEGER :: initbin2    ! initial point in "nofe" and "gofe" histograms
  INTEGER :: initbinh1   ! initial point in "nofe" and "gofe" histograms
  INTEGER :: initbinh2   ! initial point in "nofe" and "gofe" histograms
  INTEGER :: ehistbin1   ! number of points in "nofe" and "gofe" histograms
  INTEGER :: ehistbin2   ! number of points in "nofe" and "gofe" histograms
  INTEGER :: ehistbinh1  ! number of points in "nofe" and "gofe" histograms
  INTEGER :: ehistbinh2  ! number of points in "nofe" and "gofe" histograms
  REAL*8, DIMENSION(:), ALLOCATABLE :: nofe1    ! energy level population (for electrons)
  REAL*8, DIMENSION(:), ALLOCATABLE :: nofe2    ! energy level population (for electrons)
  REAL*8, DIMENSION(:), ALLOCATABLE :: nofeh1   ! energy level population (for holes)
  REAL*8, DIMENSION(:), ALLOCATABLE :: nofeh2   ! energy level population (for holes)
  REAL*8, DIMENSION(:), ALLOCATABLE :: gofe1    ! density of states (for electrons)
  REAL*8, DIMENSION(:), ALLOCATABLE :: gofe2    ! density of states (for electrons)
  REAL*8, DIMENSION(:), ALLOCATABLE :: gofeh1   ! density of states (for holes)
  REAL*8, DIMENSION(:), ALLOCATABLE :: gofeh2   ! density of states (for holes)
!
! others
!
  INTEGER :: i,j,k,isx,isy,isz,i1,i2,nn,nyz,p,l,m
  REAL*8 :: r,tr,t1,t2,rt1,re,rh,delta,ti,rdist,rdisth,xtr,it1
  INTEGER :: ixsr,isxl,isyr,isyl,iszr,iszl,idir,idir1
  INTEGER :: ik,it,is,iis,index,index0,npulse
  REAL*8 :: isample
  REAL*8 :: imoves,imovess
  REAL*8 :: ekk1,ekk2,ekkh1,ekkh2,ngofe,nnofe,sumae,sumah
  REAL*8 :: xtrapi,ytrapi,ztrapi,xtrapih,ytrapih,ztrapih
  REAL*8 :: djx,djy,djz,jump2,rcut2,rcut2x
  REAL*8 :: xmean,xmeanh,sep
  INTEGER :: ive,ike
  REAL*8 :: dxq,dyq,dzq,qdist,dxr,dyr,dzr,recd
  REAL*8 :: renorm
  INTEGER :: ap,ah,ap1,ap2,ah1,ah2
  LOGICAL :: einjected,hinjected
!
  OPEN(14,file="hjunc.in")
  OPEN(15,file="hjunc.out")
!  OPEN(20,file="recomb.dat")
!
! read input parameters
!
  READ(14,*) np
  READ(14,*) nh
```

```fortran
      READ(14,*) d,dyz
      READ(14,*) d1
      READ(14,*) rcut
      READ(14,*) maxmoves
      READ(14,*) nsample
      READ(14,*) temp
      READ(14,*) maxtime
      READ(14,*) tbin
      READ(14,*) tunit
      READ(14,*) tunith
      READ(14,*) ec1
      READ(14,*) ec2
      READ(14,*) ev1
      READ(14,*) ev2
      READ(14,*) ecut1
      READ(14,*) ecut2
      READ(14,*) ecuth1
      READ(14,*) ecuth2
      READ(14,*) temp01
      READ(14,*) temp02
      READ(14,*) temp0h1
      READ(14,*) temp0h2
      READ(14,*) alfa
      READ(14,*) alfah
      READ(14,*) alat
      READ(14,*) effmfac
      READ(14,*) r0
      READ(14,*) tt0
      READ(14,*) epsilonr
      READ(14,*) dt1
!
! convert to internal units
!
      tev = temp*temp2kt
      tev01 = -temp01*temp2kt
      tev02 = -temp02*temp2kt
      tev0h1 = -temp0h1*temp2kt
      tev0h2 = -temp0h2*temp2kt
      nbins = nint(maxtime/tbin)
      renorm =1d9*((dyz*1d-9)**2)*epsilon0*epsilonr/echarge ! for SPV in V
!
      ALLOCATE (x(400),y(400),z(400),e(400),wte(400),itrape(400),ijumpe(400),oexist(400))
      ALLOCATE (x0(400),y0(400),z0(400))
      ALLOCATE (xr(400),yr(400),zr(400))
      ALLOCATE (xh(400),yh(400),zh(400),eh(400),wth(400),itraph(400),ijumph(400),oexisth(400))
      ALLOCATE (x0h(400),y0h(400),z0h(400))
      ALLOCATE (xrh(400),yrh(400),zrh(400))
      ALLOCATE (svoltage(nbins))
      initbin1 = int(ec1/ebin)-1
      initbin2 = int(ec2/ebin)-1
      initbinh1 = int(ev1/ebin)
      initbinh2 = int(ev2/ebin)
      ehistbin1 = int((-ecut1+ec1)/ebin)
      ehistbin2 = int((-ecut2+ec2)/ebin)
      ehistbinh1 = int((ecuth1+ev1)/ebin)-1
      ehistbinh2 = int((ecuth2+ev2)/ebin)-1
      ALLOCATE (nofe1(ehistbin1:initbin1),nofe2(ehistbin2:initbin2),nofeh1(initbinh1:ehistbinh1),nofeh2(initbinh2:ehistb
inh2))
      ALLOCATE (gofe1(ehistbin1:initbin1),gofe2(ehistbin2:initbin2),gofeh1(initbinh1:ehistbinh1),gofeh2(initbinh2:ehistb
inh2))
      ALLOCATE (rt(400,400))
      ALLOCATE (nalive(nbins),nalive1(nbins),nalive2(nbins))
      ALLOCATE (halive(nbins),halive1(nbins),halive2(nbins))
!
      nu0 = 1./tunit
!
      WRITE(*,'(/10x," program HJUNC "/)')
      WRITE(*,'(" sample size (x, and yz) = ",f10.5,1x,f10.5" nm")') d,dyz
      WRITE(*,'(" semiconductor 1 size (x, and yz) = ",f10.5,1x,f10.5" nm")') d1,dyz
      WRITE(*,'(" semiconductor 2 size (x, and yz) = ",f10.5,1x,f10.5" nm")') d-d1,dyz
      WRITE(*,'(" Trap attempt frequency = ",es15.5," secs-1")') nu0
      WRITE(*,'(" Time unit = ",es15.5," secs")') tunit
      WRITE(*,'(" number of electrons = ",i4)') np
      WRITE(*,'(" number of holes = ",i4)') nh
      WRITE(*,'(" Maximum time of simulation = ",es15.5," tunit(s)")') 10**maxtime
!     WRITE(*,'(" Maximum time of simulation = ",es15.5," tunit(s)")') maxtime
      WRITE(*,'(" Temperature = ",f7.2," K")') temp
      WRITE(*,'(" Semiconductor 1 conduction band = ",f7.2," eV")') ec1
      WRITE(*,'(" Semiconductor 2 conduction band = ",f7.2," eV")') ec2
      WRITE(*,'(" Semiconductor 1 valence band = ",f7.2," eV")') ev1
      WRITE(*,'(" Semiconductor 2 valence band = ",f7.2," eV")') ev2
      WRITE(*,'(" Band gap of sem.1 = ",f7.2," eV")') abs(ev1-ec1)
      WRITE(*,'(" Band gap of sem.2 = ",f7.2," eV")') abs(ev2-ec2)
      WRITE(*,'(" Ecut1 = ",f7.2," eV")') ecut1
      WRITE(*,'(" Ecut2 = ",f7.2," eV")') ecut2
      WRITE(*,'(" Ecuth1 = ",f7.2," eV")') ecuth1
      WRITE(*,'(" Ecuth2 = ",f7.2," eV")') ecuth2
      WRITE(*,'(" Rate between effective masses = ",f7.2," eV")') effmfac
      WRITE(*,'(" alpha1 = ",f7.4)') -tev/tev01
      WRITE(*,'(" alpha2 = ",f7.4)') -tev/tev02
      WRITE(*,'(" alphah1 = ",f7.4)') -tev/tev0h1
      WRITE(*,'(" alphah2 = ",f7.4)') -tev/tev0h2
      WRITE(*,'(/2x,"( kT = ",f10.7,", E (= -dV/dx) = ",f10.7, " eV )"/)') &
           tev
      WRITE(15,'(/10x," program HJUNC "/)')
      WRITE(15,'(" sample size (x, and yz) = ",f10.5,1x,f10.5" nm")') d,dyz
      WRITE(15,'(" semiconductor 1 size (x, and yz) = ",f10.5,1x,f10.5" nm")') d1,dyz
      WRITE(15,'(" semiconductor 2 size (x, and yz) = ",f10.5,1x,f10.5" nm")') d-d1,dyz
      WRITE(15,'(" Trap attempt frequency = ",es15.5," secs-1")') nu0
      WRITE(15,'(" Time unit = ",es15.5," secs")') tunit
      WRITE(15,'(" number of electrons = ",i4)') np
      WRITE(15,'(" number of holes = ",i4)') nh
      WRITE(15,'(" Maximum time of simulation = ",es15.5," tunit(s)")') 10**maxtime
!     WRITE(15,'(" Maximum time of simulation = ",es15.5," tunit(s)")') maxtime
      WRITE(15,'(" Temperature = ",f7.2," K")') temp
      WRITE(15,'(" Semiconductor 1 conduction band = ",f7.2," eV")') ec1
      WRITE(15,'(" Semiconductor 2 conduction band = ",f7.2," eV")') ec2
      WRITE(15,'(" Semiconductor 1 valence band = ",f7.2," eV")') ev1
      WRITE(15,'(" Semiconductor 2 valence band = ",f7.2," eV")') ev2
      WRITE(15,'(" Band gap of sem.1 = ",f7.2," eV")') abs(ev1-ec1)
      WRITE(15,'(" Band gap of sem.2 = ",f7.2," eV")') abs(ev2-ec2)
      WRITE(15,'(" Ecut1 = ",f7.2," eV")') ecut1
      WRITE(15,'(" Ecut2 = ",f7.2," eV")') ecut2
      WRITE(15,'(" Ecuth1 = ",f7.2," eV")') ecuth1
      WRITE(15,'(" Ecuth2 = ",f7.2," eV")') ecuth2
      WRITE(15,'(" Rate between effective masses = ",f7.2," eV")') effmfac
      WRITE(15,'(" alpha1 = ",f7.4)') -tev/tev01
      WRITE(15,'(" alpha2 = ",f7.4)') -tev/tev02
      WRITE(15,'(" alphah1 = ",f7.4)') -tev/tev0h1
      WRITE(15,'(" alphah2 = ",f7.4)') -tev/tev0h2
      WRITE(15,'(/2x,"( kT = ",f10.7,", E (= -dV/dx) = ",f10.7, " eV )"/)') &
           tev
!
! **** Build up trap network ****************************************
!
      nn = nint(d/alat)
      nyz = nint(dyz/alat)
      ntrap = nn*nyz**2

      ALLOCATE (otrape(ntrap),otraph(ntrap),etrape(ntrap),etraph(ntrap),xtrap(ntrap),ytrap(ntrap),ztrap(ntrap))
      ALLOCATE (ivec(ntrap,700),iv(ntrap))
!
! CREATE random lattice
!
      call random_seed
      DO ik=1,ntrap
         call random_number(r)
         xtrap(ik) = r*d
         call random_number(r)
         ytrap(ik) = r*dyz
         call random_number(r)
         ztrap(ik) = r*dyz
      ENDDO
!
! computing neighbour list
!
      WRITE(*,'(" Computing neighbour list... ")')
      ivec = 0
      iv = 0
      rcut2 = rcut*rcut
      DO ik=1,ntrap
         rcut2x = rcut2
111      DO it = ik+1,ntrap
            djx = xtrap(ik)-xtrap(it)
            djy = ytrap(ik)-ytrap(it)
            djz = ztrap(ik)-ztrap(it)
!           P.B.C here: (Not for x-coordinate...)
!            djx = djx - d*nint(djx/d)
            djy = djy - dyz*nint(djy/dyz)
            djz = djz - dyz*nint(djz/dyz)
!
            jump2 = djx**2 + djy**2 + djz**2
            IF (jump2.lt.rcut2x) THEN
               iv(ik) = iv(ik) + 1
               iv(it) = iv(it) + 1
               ivec(ik,iv(ik)) = it
```

```fortran
            ivec(it,iv(it)) = ik
         ENDIF
      ENDDO
!
      IF (iv(ik).le.1) THEN
         rcut2x = rcut2x + 1
         WRITE(*,'("changing cut-off -->",f10.5," nm")') sqrt(rcut2x)
         WRITE(15,'("changing cut-off -->",f10.5," nm")') sqrt(rcut2x)
         GOTO 111
      ENDIF
      IF (mod(ik,1000).eq.0) print *, 'ik = ',ik
      WRITE(56,*) ik,iv(ik)
   ENDDO
!
! *********************************************************************
! ***** loop over different trap energy realizations ***************
! *********************************************************************
!
  nofe1 = 0
  nofe2 = 0
  nofeh1 = 0
  nofeh2 = 0
  gofe1 = 0
  gofe2 = 0
  gofeh1 = 0
  gofeh2 = 0
  svoltage = 0.0
  imoves = 0.0
  nalive = 0
  halive = 0
  nalive1 = 0
  nalive2 = 0
  halive1 = 0
  halive2 = 0
!
  DO isample=1,nsample
!
     WRITE(*,'(/" --> Simulation for sample = ",es15.4/40("*"))') isample
     WRITE(15,'(/" --> Simulation for sample = ",es15.4/40("*"))') isample
!
     x = 0
     y = 0
     z = 0
     e = 0
     xh = 0
     yh = 0
     zh = 0
     eh = 0
     otrape = .false.
     otraph = .false.
     oexist = .false.
     oexisth = .false.
     ener = 0.0
     dist = 0.0
     imovess = 0.0
     sep = 0
     index0 = 0
     index = 0
     npulse = 0
     DO j=1,np
        oexist(j) = .true.
     ENDDO
     DO j=1,nh
        oexisth(j) = .true.
     ENDDO
!
!    allocate energies to trap sites (for electron distribution)
!
     DO ik = 1,ntrap
        IF (xtrap(ik).lt.d1) THEN
           ekk1 = edist1()
           etrape(ik) = -ekk1+ec1
           gofe1(int((-ekk1+ec1)/ebin)-1) = gofe1(int((-ekk1+ec1)/ebin)-1) + 1
        ELSE
           ekk2 = edist2()
           etrape(ik) = -ekk2+ec2
           gofe2(int((-ekk2+ec2)/ebin)-1) = gofe2(int((-ekk2+ec2)/ebin)-1) + 1
        ENDIF
     ENDDO
!
!    allocate energies to trap sites (for hole distribution)
!
     DO ik = 1,ntrap
```

```fortran
        IF (xtrap(ik).lt.d1) THEN
           ekkh1 = edisth1()
           etraph(ik) = ekkh1+ev1
           gofeh1(int((ekkh1+ev1)/ebin)-1) = gofeh1(int((ekkh1+ev1)/ebin)-1) + 1
        ELSE
           ekkh2 = edisth2()
           etraph(ik) = ekkh2+ev2
           gofeh2(int((ekkh2+ev2)/ebin)-1) = gofeh2(int((ekkh2+ev2)/ebin)-1) + 1
        ENDIF
     ENDDO
!
     OPEN(31,file='enerhist1.dat',status='unknown')
     DO i=int(ec1/ebin)-1,ehistbin1,-1
        ngofe = gofe1(i)/sum(gofe1)/ebin
        IF (ngofe.ne.0) THEN
           WRITE(31,'(4(e12.5,1x))') real(i)*ebin,ngofe
        ENDIF
     ENDDO
     CLOSE(31)
!
     OPEN(33,file='enerhist2.dat',status='unknown')
     DO i=int(ec2/ebin)-1,ehistbin2,-1
        ngofe = gofe2(i)/sum(gofe2)/ebin
        IF (ngofe.ne.0) THEN
           WRITE(33,'(4(e12.5,1x))') real(i)*ebin,ngofe
        ENDIF
     ENDDO
     CLOSE(33)
!
     OPEN(35,file='enerhisth1.dat',status='unknown')
     DO i=int(ev1/ebin),ehistbinh1
        ngofe = gofeh1(i)/sum(gofeh1)/ebin
        IF (ngofe.ne.0) THEN
           WRITE(35,'(4(e12.5,1x))') real(i)*ebin,ngofe
        ENDIF
     ENDDO
     CLOSE(35)
!
     OPEN(37,file='enerhisth2.dat',status='unknown')
     DO i=int(ev2/ebin),ehistbinh2
        ngofe = gofeh2(i)/sum(gofeh2)/ebin
        IF (ngofe.ne.0) THEN
           WRITE(37,'(4(e12.5,1x))') real(i)*ebin,ngofe
        ENDIF
     ENDDO
     CLOSE(37)
!
!    Total simulation time
!
     WRITE(*,'(" Total simulation time = ",e15.5," secs")') 10**maxtime
!    WRITE(*,'(" Total simulation time = ",e15.5," secs")') maxtime
     WRITE(*,'(" Time window = ",e15.5," secs")') tbin
     WRITE(15,'(" Total simulation time = ",e15.5," secs")') 10**maxtime
!    WRITE(15,'(" Total simulation time = ",e15.5," secs")') maxtime
     WRITE(15,'(" Time window = ",e15.5," secs")') tbin
     WRITE(*,*)'total number of traps', ntrap
     WRITE(15,*)'total number of traps', ntrap
!
     WRITE(*,*) 'distribute electrons throughout sample...'
     WRITE(15,*) 'distribute electrons throughout sample...'
!
!    distribute electrons throughout sample
!
     DO j=1,np ! loop over number of particles
!
!  random distribution of electrons...
!
21      CONTINUE
        call random_number(r)
        ik=int(r*ntrap+1)
        IF (otrape(ik)) GOTO 21    ! trap already occupied
        IF (xtrap(ik).lt.d1) GOTO 21
!
        e(j) = etrape(ik)
        x(j) = xtrap(ik)
        y(j) = ytrap(ik)
        z(j) = ztrap(ik)
        itrape(j) = ik
        otrape(ik) = .true.    ! trap occupied
     ENDDO
!
     WRITE(*,*) 'compute waiting times and jumps for each electron...'
     WRITE(15,*) 'compute waiting times and jumps for each electron...'
```

```fortran
!
      DO j=1,np ! compute waiting times and jumps for each electron using hopping model
!
         call settime(j) ! this sets up wte(j) and ijumpe(j) using hopping model
!
         Note: along the simulation, every electron should have a waiting time
               and a most probable jump (specified by the trap number of the trap
               it jumps to)
!
      ENDDO
!
      WRITE(*,*) 'distribute holes throughout sample...'
      WRITE(15,*) 'distribute holes throughout sample...'
!
!     distribute holes throughout sample
!
      DO j=1,nh ! loop over number of particles
!
      ive = iv(itrape(j))
!
22       CONTINUE
         call random_number(r)
         ike = int(r*ive+1.0)
         ik = ivec(itrape(j),ike)   ! choose randomly an electron neighbour
!
         IF (otraph(ik)) GOTO 22    ! trap already occupied by a hole
         IF (xtrap(ik).lt.d1) GOTO 22
!
         eh(j) = etraph(ik)
         xh(j) = xtrap(ik)
         yh(j) = ytrap(ik)
         zh(j) = ztrap(ik)
         itraph(j) = ik
         otraph(ik) = .true.    ! trap occupied
      ENDDO
!
      WRITE(*,*) 'compute waiting times and jumps for each hole...'
      WRITE(15,*) 'compute waiting times and jumps for each hole...'
!
      DO j=1,nh ! compute waiting times and jumps for each hole
!
         call settimeh(j) ! this sets up wth(j) and ijumph(j) using hopping model
!
         Note: along the simulation, every hole should have a waiting time
               and a most probable jump (specified by the trap number of the trap
               it jumps to)
!
      ENDDO
!
      DO i=1,np ! compute recombination times
!
         call recombt(i)
!
      ENDDO
!
!     initial positions
!
      x0 = x
      y0 = y
      z0 = z
      xr = x
      yr = y
      zr = z
      x0h = xh
      y0h = yh
      z0h = zh
      xrh = xh
      yrh = yh
      zrh = zh
!
!     ----------------------------------------------------
!     begin simulation run
!     ----------------------------------------------------
!
      einjected = 0
      hinjected = 0
      time = 0
      it1 = 0
!
      WRITE(*,*) 'begin simulation run...'
      WRITE(15,*) 'begin simulation run...'
!      WRITE(20,*) 'begin simulation run...'
!
      DO WHILE(.true.)
!
      IF (imoves.ge.maxmoves) THEN
           WRITE(*,*) 'maximum number of moves about to be exceed', maxmoves
           WRITE(15,*) 'maximum number of moves about to be exceed', maxmoves
           STOP
      ENDIF
!
!     Electron injection after an arbitrary amount of time...
!
      IF (int(time/dt1).gt.npulse) THEN
         npulse = npulse + 1
         einjected = .false.
         hinjected = .false.
!         WRITE (*,*) 'new injection of an electron hole pair'
23       CONTINUE
         call random_number(r)
         l = int(r*ntrap)+1
         IF (otrape(l)) GOTO 23
         IF (xtrap(l).lt.d1) GOTO 23
         DO j = 1,np
            IF (l.eq.ijumpe(j)) GOTO 23
         ENDDO
         otrape(l) = .true.
!
24       CONTINUE
         call random_number(r)
         m = int(r*ntrap)+1
         IF (otraph(m)) GOTO 24
         IF (xtrap(m).lt.d1) GOTO 24
         DO j = 1,nh
            IF (m.eq.ijumph(j)) GOTO 24
         ENDDO
         otraph(m) = .true.
!
         DO j=1,np
            IF (.NOT.oexist(j)) THEN
               oexist(j)=.true.
               itrape(j) = l
               e(j) = etrape(l)
               x(j) = xtrap(l)
               y(j) = ytrap(l)
               z(j) = ztrap(l)
               call settime(j) ! this sets up wte and ijumpe
               call recombt(j)
               einjected = .true.
!               WRITE(*,*) 'an old electron reborns',j
               EXIT
            ENDIF
         ENDDO
         IF (.NOT.einjected) THEN
            np = np + 1
            oexist(np)=.true.
            itrape(np) = l
            e(np) = etrape(l)
            x(np) = xtrap(l)
            y(np) = ytrap(l)
            z(np) = ztrap(l)
            call settime(np) ! this sets up wte and ijumpe
            call recombt(np)
!            WRITE(*,*) 'a new electron is injected',j
            einjected = .true.
         ENDIF
         DO j=1,nh
            IF (.NOT.oexisth(j)) THEN
               oexisth(j)=.true.
               itraph(j) = m
               eh(j) = etraph(m)
               xh(j) = xtrap(m)
               yh(j) = ytrap(m)
               zh(j) = ztrap(m)
               call settimeh(j) ! this sets up wth and ijumph
               call recombth(j)
               hinjected = .true.
!               WRITE(*,*) 'an old hole reborns',j
               EXIT
            ENDIF
         ENDDO
         IF (.NOT.hinjected) THEN
            nh = nh + 1
            oexisth(nh)=.true.
            itraph(nh) = m
            eh(nh) = etraph(m)
```

```fortran
              xh(nh) = xtrap(m)
              yh(nh) = ytrap(m)
              zh(nh) = ztrap(m)
              call settimeh(nh) ! this sets up wth and ijumph
              call recombth(nh)
!             WRITE(*,*) 'a new hole is injected',j
              hinjected = .true.

            ENDIF

          ENDIF
!
!       search for minimum electron hopping time (t1)
!
        t1 = 1d80
        DO i=1,np
          IF (wte(i).lt.t1) THEN
            IF (oexist(i)) THEN
              IF (.not.otrape(ijumpe(i))) THEN ! ... to a non-occupied trap
                t1 = wte(i)
                i1 = i
              ENDIF
            ENDIF
          ENDIF
        ENDDO
!
!       search for minimum hole hopping time (t2)
!
        t2 = 1d80
        DO i=1,nh
          IF (wth(i).lt.t2) THEN
            IF (oexisth(i)) THEN
              IF (.not.otraph(ijumph(i))) THEN ! ... to a non-occupied trap
                t2 = wth(i)
                i2 = i
              ENDIF
            ENDIF
          ENDIF
        ENDDO
!
!       minimum recombination time is selected
!
        rt1 = 1d80
        DO i=1,np
          IF (.not.oexist(i)) CYCLE
          DO j=1,nh
            IF (.not.oexisth(j)) CYCLE
            IF (rt(i,j).lt.rt1) THEN
              rt1 = rt(i,j)
              re = i
              rh = j
            ENDIF
          ENDDO
        ENDDO
!
!       move particle with the minimum time or tunneling recombination event occurs
!
        IF ((rt1.lt.t1).AND.(rt1.lt.t2)) THEN

          oexist(re)=.false.    ! remove electron
          otrape(itrape(re)) = .false.
          oexisth(rh)=.false.   ! remove hole
          otraph(itraph(rh)) = .false.
!
          dxr = xtrap(itrape(re))-xtrap(itraph(rh))
          dyr = ytrap(itrape(re))-ytrap(itraph(rh))
          dzr = ztrap(itrape(re))-ztrap(itraph(rh))
!
!          dxr = dxr - d*nint(dxr/d)
          dyr = dyr - dyz*nint(dyr/dyz)
          dzr = dzr - dyz*nint(dzr/dyz)

          recd = sqrt((dxr**2) + (dyr**2) + (dzr**2))

          WRITE(20,*) recd
          IF (xtrap(itrape(re)).ge.d1) THEN
            IF (xtrap(itraph(rh)).gt.d1) THEN
              WRITE(*,*) 'recombination event occurs at the absorber...'
              WRITE(20,*) 'recombination event occurs at the absorber...'
            ELSE IF (xtrap(itraph(rh)).le.d1) THEN
              WRITE(*,*) 'recombination event occurs at the interface...'
              WRITE(20,*) 'recombination event occurs at the interface...'
            ENDIF
          ELSE
```

```fortran
            IF (xtrap(itraph(rh)).le.d1) THEN
              WRITE(*,*) 'recombination event occurs at the first semiconductor...'
              WRITE(20,*) 'recombination event occurs at the fist semiconductor...'
            ELSE IF (xtrap(itraph(rh)).gt.d1) THEN
              WRITE(*,*) 'recombination event occurs at the interface...'
              WRITE(20,*) 'recombination event occurs at the interface...'
            ENDIF
          ENDIF
!
        ELSE

          IF (t1.le.t2) THEN
            IF (oexist(i1)) call move(i1)      ! move an electron
          ELSE
            IF (oexisth(i2)) call moveh(i2)    ! move a hole
          ENDIF

        ENDIF
!
!       set new hopping time
!
        IF ((rt1.gt.t1).OR.(rt1.gt.t2)) THEN

          IF (t1.le.t2)  THEN
            IF (oexist(i1)) call settime(i1) ! this sets up wte(i1) and ijumpe(i1) using hopping model
            IF (oexist(i1)) call recombt(i1) ! new recombination times
          ELSE
            IF (oexisth(i2)) call settimeh(i2) ! this sets up wth(i2) and ijumph(i2) using hopping model
            IF (oexisth(i2)) call recombth(i2) ! new recombination times
          ENDIF

        ENDIF
!
!       record move
!
        imoves = imoves + 1
        imovess = imovess + 1
!
!       reduce hopping times by "t1", "rt" or "t2" and advance time
!
        IF ((rt1.lt.t1).AND.(rt1.lt.t2)) THEN

          DO i=1,np
            IF (.not.oexist(i)) CYCLE
            wte(i) = wte(i) - rt1
          ENDDO

          DO i=1,nh
            IF (.not.oexisth(i)) CYCLE
            wth(i) = wth(i) - rt1
          ENDDO

          time = time + rt1    ! advance time

        ELSE

          IF (t1.le.t2) THEN

            DO i=1,np
              IF (.not.oexist(i)) CYCLE
              IF (i.ne.i1) wte(i) = wte(i) - t1
            ENDDO

            DO i=1,nh
              IF (.not.oexisth(i)) CYCLE
              wth(i) = wth(i) - t1
            ENDDO

            DO i=1,np
              IF (.not.oexist(i)) CYCLE
              DO j=1,nh
                IF (.not.oexisth(j)) CYCLE
                rt(i,j) = rt(i,j) - t1
              ENDDO
            ENDDO

            time = time + t1   ! advance time

          ELSE

            DO i=1,np
              IF (.not.oexist(i)) CYCLE
              wte(i) = wte(i) - t2
```

```fortran
          ENDDO

          DO i=1,nh
              IF (.not.oexisth(i)) CYCLE
              IF (i.ne.i2) wth(i) = wth(i) - t2
          ENDDO

          DO i=1,np
              IF (.not.oexist(i)) CYCLE
              DO j=1,nh
                  IF (.not.oexisth(j)) CYCLE
                  rt(i,j) = rt(i,j) - t2
              ENDDO
          ENDDO

          time = time + t2    ! advance time

        ENDIF

      ENDIF
!
!     If maximum time exceeded finish calculation
!
      IF (log10(time).gt.maxtime) THEN  ! Maximum time about to be exceed: Finish simulation
          svoltage(index0+1:nbins) = svoltage(index0+1:nbins) + sep
          WRITE(*,*) 'finish simulation---> maxtime about to be exceed = ', log10(time),maxtime
          WRITE(15,*) 'finish simulation---> maxtime about to be exceed = ', log10(time),maxtime
!          WRITE(20,*) 'finish simulation---> maxtime about to be exceed = ', log10(time),maxtime
          EXIT
      ENDIF
!
!     If electrons run out finish calculation
!
      IF (count(oexist).eq.0) THEN
          index = int(log10(time)/tbin)+1
          svoltage(index0+1:index) = svoltage(index0+1:index) + sep
          WRITE(*,*) 'finish simulation---> number of "alive" electrons = ',count(oexist)
          WRITE(15,*) 'finish simulation---> number of "alive" electrons = ',count(oexist)
!          WRITE(20,*) 'finish simulation---> number of "alive" electrons = ',count(oexist)
          EXIT
      ENDIF
!
!     compute mean position of electrons and holes
!
      xmean = 0
      xmeanh = 0
      DO j=1,np
          IF (oexist(j)) xmean = xmean + x(j)
          IF (oexisth(j)) xmeanh = xmeanh + xh(j)
      ENDDO
      xmean = xmean/count(oexist)
      xmeanh = xmeanh/count(oexisth)
!
!     compute mean separation between surviving electrons and holes
!
      sep = (xmeanh-xmean)*count(oexist)/renorm
      IF (int(log10(time)/tbin)+1.gt.index0) THEN
          WRITE(*,*) 'isample = ',isample,index,time !,x,y,z
          WRITE(15,*) 'isample = ',isample,index,time !,x,y,z
      ENDIF
!
!  compute surface photovoltage (logarithmic computation)
!
      IF (int(log10(time)/tbin)+1.gt.0) THEN
          index = int(log10(time)/tbin)+1
          svoltage(index0+1:index) = svoltage(index0+1:index) + sep
!
          ap=0
          ah=0
          ap1=0
          ap2=0
          ah1=0
          ah2=0
          DO j=1,np
              IF (oexist(j)) THEN
                  ap = ap + 1
                  IF (x(np).lt.d1) THEN
                      ap1 = ap1 + 1
                  ELSE
                      ap2 = ap2 + 1
                  ENDIF
              ENDIF
          ENDDO
                  DO j=1,nh
                      IF (oexisth(j)) THEN
                          ah = ah + 1
                          IF (xh(nh).lt.d1) THEN
                              ah1 = ah1 + 1
                          ELSE
                              ah2 = ah2 + 1
                          ENDIF
                      ENDIF
                  ENDDO
              nalive(index0+1:index) = nalive(index0+1:index) + ap
              halive(index0+1:index) = halive(index0+1:index) + ah
              nalive1(index0+1:index) = nalive1(index0+1:index) + ap1
              nalive2(index0+1:index) = nalive2(index0+1:index) + ap2
              halive1(index0+1:index) = halive1(index0+1:index) + ah1
              halive2(index0+1:index) = halive2(index0+1:index) + ah2
!
              index0 = index
          ENDIF
!
!     compute occupancy histograms
!
      DO i=1,np
          IF (oexist(i)) THEN
              IF (xtrap(itrape(i)).lt.d1) THEN
                  nofe1(int(e(i)/ebin)-1) = nofe1(int(e(i)/ebin)-1) + 1
              ELSE
                  nofe2(int(e(i)/ebin)-1) = nofe2(int(e(i)/ebin)-1) + 1
              ENDIF
          ENDIF
      ENDDO
!
      DO i=1,nh
          IF (oexisth(i)) THEN
              IF (xtrap(itraph(i)).lt.d1) THEN
                  nofeh1(int(eh(i)/ebin)-1) = nofeh1(int(eh(i)/ebin)-1) + 1
              ELSE
                  nofeh2(int(eh(i)/ebin)-1) = nofeh2(int(eh(i)/ebin)-1) + 1
              ENDIF
          ENDIF
      ENDDO
!
      ENDDO
!
! -------------------------------------------------
!  simulation ends
! -------------------------------------------------
!
      WRITE(15,'(5x," number of moves = ",es15.5)') imovess
      WRITE(*,'(5x," number of moves = ",es15.5)') imovess
      WRITE(15,'(5x," total number of moves = ",es15.5)') imoves
      WRITE(*,'(5x," total number of moves = ",es15.5)') imoves
!
!  Compute number of samples to average
!
      OPEN(17,file="isamples.dat")
      WRITE(17,*) isample
      CLOSE(17)
!
!  Compute surface photovoltage
!
      OPEN(27,file='spv.dat',status='unknown')
      OPEN(29,file='spv2.dat',status='unknown')
      DO i=1,nbins
          WRITE(27,*) real(i)*tbin,svoltage(i)/real(isample)
!  WRITE(27,*) (real(i)*tbin)+log10(tunit),svoltage(i)/real(isample)
          WRITE(29,*) (10**(i*tbin))*tunit,svoltage(i)/real(isample)
      ENDDO
      CLOSE(27)
      CLOSE(29)
!
      OPEN(47,file='nalive.dat',status='unknown')
      OPEN(49,file='halive.dat',status='unknown')
      DO i=1,nbins
          WRITE(47,*) real(i)*tbin,nalive(i)/real(isample),nalive1(i)/real(isample),nalive2(i)/real(isample)
          WRITE(49,*) real(i)*tbin,halive(i)/real(isample),halive1(i)/real(isample),halive2(i)/real(isample)
      ENDDO
      CLOSE(47)
      CLOSE(49)
!
!  compute energy distribution of particles
!
      OPEN(39,file='distr1.dat',status='unknown')
```

```fortran
         DO i=int(ec1/ebin)-1,ehistbin1,-1
            ngofe = gofe1(i)/sum(gofe1)/ebin
            nnofe = nofe1(i)/sum(nofe1)*ap1/(ntrap*(d1/d))/ebin
            IF (ngofe.ne.0) THEN
               WRITE(39,'(4(e12.5,1x))')  real(i)*ebin,nnofe/ngofe
            ENDIF
         ENDDO
         CLOSE(39)
!
         OPEN(41,file='distr2.dat',status='unknown')
         DO i=int(ec2/ebin)-1,ehistbin2,-1
            ngofe = gofe2(i)/sum(gofe2)/ebin
            nnofe = nofe2(i)/sum(nofe2)*ap2/(ntrap*((d-d1)/d))/ebin
            IF (ngofe.ne.0) THEN
               WRITE(41,'(4(e12.5,1x))')  real(i)*ebin,nnofe/ngofe
            ENDIF
         ENDDO
         CLOSE(41)
!
         OPEN(43,file='distrh1.dat',status='unknown')
         DO i=int(ev1/ebin),ehistbinh1
            ngofe = gofeh1(i)/sum(gofeh1)/ebin
            nnofe = nofeh1(i)/sum(nofeh1)*ah1/(ntrap*(d1/d))/ebin
            IF (ngofe.ne.0) THEN
               WRITE(43,'(4(e12.5,1x))')  real(i)*ebin,nnofe/ngofe
         ENDIF
         ENDDO
         CLOSE(43)
!
         OPEN(45,file='distrh2.dat',status='unknown')
         DO i=int(ev2/ebin),ehistbinh2
            ngofe = gofeh2(i)/sum(gofeh2)/ebin
            nnofe = nofeh2(i)/sum(nofeh2)*ah2/(ntrap*((d-d1)/d))/ebin
            IF (ngofe.ne.0) THEN
               WRITE(45,'(4(e12.5,1x))')  real(i)*ebin,nnofe/ngofe
            ENDIF
         ENDDO
         CLOSE(45)
!
      ENDDO
!
! ***********************************************************************
! ***** END loop over different trap energy realizations **************
! ***********************************************************************
!
      WRITE(*,'(/"End of sample"/)')
      WRITE(15,'(/"End of sample"/)')
!  WRITE(20,'(/"End of sample"/)')
      CLOSE(14)
      CLOSE(15)
!  CLOSE(20)
!
      CONTAINS
!
      SUBROUTINE settime(i)
!
!    this subroutine computes the minimum hopping time for electron "i"
!    and the neighbouring trap for which that time corresponds
!    using hopping transport model
!
      IMPLICIT NONE
      INTEGER, INTENT(IN) :: i
      INTEGER :: ik,ivh,ikh,j,k
      REAL*8 :: rdist,ti,dxe,dye,dze
      REAL*8, DIMENSION(:), ALLOCATABLE :: wti
      INTEGER, DIMENSION(:), ALLOCATABLE :: wi

      ALLOCATE (wti(700),wi(700))

      IF (.NOT.otrape(itrape(i))) STOP 'electron is not occuping its own trap!!'

      ivh = iv(itrape(i))

      DO ikh = 1,ivh

         ik = ivec(itrape(i),ikh)

         dxe = xtrap(ik)-x(i)
         dye = ytrap(ik)-y(i)
         dze = ztrap(ik)-z(i)

!          dxe = dxe - d*nint(dxe/d)
           dye = dye - dyz*nint(dye/dyz)
```

```fortran
           dze = dze - dyz*nint(dze/dyz)

           rdist = sqrt((dxe**2) + (dye**2) + (dze**2))

!    hopping times for each neighbour are calculated using hopping model

           IF  ((ik.gt.ntrap).OR.(ik.eq.itrape(i))) THEN   ! trap does not exist, trap occupied or same trap

              wti(ikh) = 1d80

           ELSE IF (otrape(ik)) THEN   ! trap already occupied by an electron

              wti(ikh) = 1d80

           ELSE

              call random_number(r)
              wti(ikh) = -log(r)*exp((2*rdist)/alfa)*exp(((etrape(ik)-e(i))+abs(etrape(ik)-e(i)))/(2*tev))

           ENDIF

           wi(ikh) = ik

      ENDDO
!
!    The minimum hopping time for electron i is calculated
!
54    ti = 1d80
      DO ikh = 1,ivh
         IF (wti(ikh).lt.ti) THEN
            wte(i) = wti(ikh)
            ti = wti(ikh)
            ijumpe(i) = wi(ikh)
            k = ikh
         ENDIF
      ENDDO

      DO j=1,np
         IF (.not.oexist(j)) CYCLE
         IF ((j.ne.i).AND.(ijumpe(i).eq.ijumpe(j))) THEN   ! same "ijump" trap; problems in future!!
            wti(k) = 1d80
            GOTO 54
         ENDIF
      ENDDO

      DEALLOCATE (wti,wi)
!
!    controls:
!
      IF (itrape(i).eq.ijumpe(i)) THEN
         print *, i,itrape(i),ivh,ikh,ik,ijumpe(i),wte(i)
         STOP 'SETTIME: jumping to the same trap!!!'
      ENDIF
      IF (otrape(ijumpe(i))) THEN
         print *, i,itrape(i),ivh,ikh,ik,ijumpe(i),wte(i)
         STOP 'SETTIME: jumping to an occupied trap!!!'
      ENDIF
!
      END SUBROUTINE settime
!
      SUBROUTINE settimeh(i)
!
!    this subroutine computes the minimum hopping time for hole "i"
!    and the neighbouring trap for which that time corresponds using hopping transport model
!
      IMPLICIT NONE
      INTEGER, INTENT(IN) :: i
      INTEGER :: ik,ivh,ikh,j,k
      REAL*8 :: rdisth,ti,dxh,dyh,dzh
      REAL*8, DIMENSION(:), ALLOCATABLE :: wti
      INTEGER, DIMENSION(:), ALLOCATABLE :: wi

      ALLOCATE (wti(700),wi(700))

      IF (.NOT.otraph(itraph(i))) STOP 'electron is not occuping its own trap!!'

      ivh = iv(itraph(i))

      DO ikh = 1,ivh

         ik = ivec(itraph(i),ikh)

!        dxh = xtrap(ik)-xh(i)
```

```fortran
          dyh = ytrap(ik)-yh(i)
          dzh = ztrap(ik)-zh(i)

          dxh = dxh - d*nint(dxh/d)
          dyh = dyh - dyz*nint(dyh/dyz)
          dzh = dzh - dyz*nint(dzh/dyz)

          rdisth = sqrt((dxh**2) + (dyh**2) + (dzh**2))

!    hopping times for each neighbour are calculated using hopping model

          IF  ((ik.gt.ntrap).OR.(ik.eq.itraph(i)))  THEN   ! trap does not exist, trap occupied or same trap

             wti(ikh) = 1d80

          ELSE IF (otraph(ik)) THEN   ! trap already occupied by a hole

             wti(ikh) = 1d80

          ELSE

             call random_number(r)
             wti(ikh) = -log(r)*effmfac*exp((2*rdisth)/alfah)*exp(((eh(i)-etraph(ik))+abs(etraph(ik)-eh(i)))/(2*te
v))

          ENDIF

          wi(ikh) = ik

       ENDDO
!
!    The minimum hopping time for hole i is calculated
!
55   ti = 1d80
       DO ikh = 1,ivh
          IF (wti(ikh).lt.ti) THEN
             wth(i) = wti(ikh)
             ti = wti(ikh)
             ijumph(i) = wi(ikh)
             k = ikh
          ENDIF
       ENDDO
!
       DO j=1,nh
          IF (.not.oexisth(j)) CYCLE
          IF ((j.ne.i).AND.(ijumph(i).eq.ijumph(j))) THEN   ! same "ijump" trap; problems in future!!
             wti(k) = 1d80
             GOTO 55
          ENDIF
       ENDDO

       DEALLOCATE (wti,wi)
!
!    controls:
!
       IF (itraph(i).eq.ijumph(i)) THEN
          print *, i,itraph(i),ivh,ikh,ik,ijumph(i),wth(i)
          STOP 'SETTIMEH: jumping to the same trap!!!'
       ENDIF
       IF (otraph(ijumph(i))) THEN
          print *, i,itraph(i),ivh,ikh,ik,ijumph(i),wth(i)
          STOP 'SETTIMEH: jumping to an occupied trap!!!'
       ENDIF
!
     END SUBROUTINE settimeh
!
     SUBROUTINE recombt(i)
!
!    this subroutine computes the recombination time between particles
!
       IMPLICIT NONE
       INTEGER, INTENT(IN) :: i
       INTEGER :: j,k
       REAL*8 :: qdist,dxq,dyq,dzq
!
!    tunneling recombination times are computed
!
       DO j=1,nh
          IF (.not.oexisth(j)) CYCLE
          dxq = x(i)-xh(j)
          dyq = y(i)-yh(j)
          dzq = z(i)-zh(j)
!
```

```fortran
!          dxq = dxq - d*nint(dxq/d)
          dyq = dyq - dyz*nint(dyq/dyz)
          dzq = dzq - dyz*nint(dzq/dyz)
!
          qdist = sqrt((dxq**2) + (dyq**2) + (dzq**2))
!
          call random_number(r)
!          rt(i,j) = -log(r)*tt0*exp(abs(qdist)/r0)*exp(abs(e(i)-eh(j))/tev)
          rt(i,j) = -log(r)*tt0*exp(2*abs(qdist)/r0)
       ENDDO
!
     END SUBROUTINE recombt
!
     SUBROUTINE recombth(j)
!
!    this subroutine computes the recombination time between particles
!
       IMPLICIT NONE
       INTEGER, INTENT(IN) :: j
       INTEGER :: i,k
       REAL*8 :: qdist,dxq,dyq,dzq
!
!    tunneling recombination times are computed
!
       DO i=1,np
          IF (.not.oexist(i)) CYCLE
          dxq = x(i)-xh(j)
          dyq = y(i)-yh(j)
          dzq = z(i)-zh(j)
!
!          dxq = dxq - d*nint(dxq/d)
          dyq = dyq - dyz*nint(dyq/dyz)
          dzq = dzq - dyz*nint(dzq/dyz)
!
          qdist = sqrt((dxq**2) + (dyq**2) + (dzq**2))
!
          call random_number(r)
!          rt(i,j) = -log(r)*tt0*exp(abs(qdist)/r0)*exp(abs(e(i)-eh(j))/tev)
          rt(i,j) = -log(r)*tt0*exp(abs(qdist)/r0)
       ENDDO
!
     END SUBROUTINE recombth
!
     SUBROUTINE move(i)
!
!    this subroutine moves electron i to trap ijump(i)
!
       IMPLICIT NONE
       INTEGER, INTENT(IN) :: i
       REAL*8 :: xtrapi,ytrapi,ztrapi,dx,dy,dz
!
!    controls:
!
       IF (itrape(i).eq.ijumpe(i)) STOP 'MOVE: electron jumping to the same trap!!!'
       IF (otrape(ijumpe(i))) STOP 'MOVE: electron jumping to an occupied trap!!!'
!
!    occupancy policy
!
          otrape(itrape(i)) = .false. ! leave old trap free
          otrape(ijumpe(i)) = .true.  ! make new trap occupied
!
          xtrapi = xtrap(ijumpe(i))
          ytrapi = ytrap(ijumpe(i))
          ztrapi = ztrap(ijumpe(i))
!
!    real coordinates
!
          dx = xtrapi-x(i)
          dy = ytrapi-y(i)
          dz = ztrapi-z(i)
!          dx = dx - d*nint(dx/d)
          dy = dy - dyz*nint(dy/dyz)
          dz = dz - dyz*nint(dz/dyz)
          xr(i) = xr(i) + dx
          yr(i) = yr(i) + dy
          zr(i) = zr(i) + dz
!
!    electron jumps to trap "ijump(i)"
!
          itrape(i) = ijumpe(i)
          e(i) = etrape(ijumpe(i))
          x(i) = xtrapi
          y(i) = ytrapi
          z(i) = ztrapi
```

```fortran
!
  END SUBROUTINE move
!
  SUBROUTINE moveh(i)
!
!   this subroutine moves hole i to trap ijump(i)
!
    IMPLICIT NONE
    INTEGER, INTENT(IN) :: i
    REAL*8 :: xtrapih,ytrapih,ztrapih,dxh,dyh,dzh

!
!   controls:
!
    IF (itraph(i).eq.ijumph(i)) STOP 'MOVEH: hole jumping to the same trap!!!'
    IF (otraph(ijumph(i))) STOP 'MOVEH: hole jumping to an occupied trap!!!'
!
!     occupancy policy
!
          otraph(itraph(i)) = .false. ! leave old trap free
          otraph(ijumph(i)) = .true.  ! make new trap occupied
!
          xtrapih = xtrap(ijumph(i))
          ytrapih = ytrap(ijumph(i))
          ztrapih = ztrap(ijumph(i))
!
!     real coordinates
!
          dxh = xtrapih-xh(i)
          dyh = ytrapih-yh(i)
          dzh = ztrapih-zh(i)
!         dxh = dxh - d*nint(dxh/d)
          dyh = dyh - dyz*nint(dyh/dyz)
          dzh = dzh - dyz*nint(dzh/dyz)
          xrh(i) = xrh(i) + dxh
          yrh(i) = yrh(i) + dyh
          zrh(i) = zrh(i) + dzh
!
!     hole jumps to trap "ijump(i)"
!
          itraph(i) = ijumph(i)
          eh(i) = etraph(ijumph(i))
          xh(i) = xtrapih
          yh(i) = ytrapih
          zh(i) = ztrapih
!
  END SUBROUTINE moveh
!
  FUNCTION edist1()
!
!  uses DOS to set the energy of a site
!
    IMPLICIT NONE
    INTEGER :: j
    REAL*8 :: edist1
    REAL*8 :: r,delta
    REAL*8 :: a1,a2,a3

! use exponential DOS :
    DO WHILE(.true.)
       call random_number(r)
       edist1 = tev01*log(1-r)
       IF (edist1.lt.0) CYCLE
       IF (edist1.lt.ecut1) EXIT
    ENDDO
!
 END FUNCTION edist1
!
  FUNCTION edist2()
!
!  uses DOS to set the energy of a site
!
    IMPLICIT NONE
    INTEGER :: j
    REAL*8 :: edist2
    REAL*8 :: r,delta
    REAL*8 :: a1,a2,a3

! use exponential DOS :
    DO WHILE(.true.)
       call random_number(r)
       edist2 = tev02*log(1-r)
       IF (edist2.lt.0) CYCLE
       IF (edist2.lt.ecut2) EXIT
    ENDDO
!
  END FUNCTION edist2
!
  FUNCTION edisth1()
!
!  uses DOS to set the energy of a site
!
    IMPLICIT NONE
    INTEGER :: j
    REAL*8 :: edisth1
    REAL*8 :: r,delta
    REAL*8 :: a1,a2,a3

! (2) use exponential DOS :
    DO WHILE(.true.)
       call random_number(r)
       edisth1 = tev0h1*log(1-r)
       IF (edisth1.lt.0) CYCLE
       IF (edisth1.lt.ecuth1) EXIT
    ENDDO
!
  END FUNCTION edisth1
!
  FUNCTION edisth2()
!
!  uses DOS to set the energy of a site
!
    IMPLICIT NONE
    INTEGER :: j
    REAL*8 :: edisth2
    REAL*8 :: r,delta
    REAL*8 :: a1,a2,a3
!
! (2) use exponential DOS :
    DO WHILE(.true.)
       call random_number(r)
       edisth2 = tev0h2*log(1-r)
       IF (edisth2.lt.0) CYCLE
       IF (edisth2.lt.ecuth2) EXIT
    ENDDO
!
  END FUNCTION edisth2

END PROGRAM hjunc
```

```fortran
Program nanowalk
!
!      --------------------------------------------------------------------------
!      ---> NANOWALK: Random Walk in media with Spacial and Energy Disorder <----
!      --------------------------------------------------------------------------
!
!    This is an...
!
!             ACTIVATED HOPPING CONTINUOUS TIME RANDOM WALK method
!                    WITH PERIODIC BOUNDARY CONDITIONS
!             AIM: CURRENT-VOLTAGE CHARACTERISTICS+MOBILITIES
!             AIM: DIFFUSSION COEFFICIENTS (2006)
!
!                  Original N Quirke september 1998
!                  Modified by J.A. Anta, May-August 1999
!                  Modified by J.A. Anta, September 2006 (diff coef.)
!                  Modified by J.A. Anta, November 2006 (spatial disorder)
!                  Modified by J.A. Anta, May 2007 (spatial disorder: improved)
!                  Modified by J.P. Gonzalez, May 2010 (recombination features)
!
   IMPLICIT NONE
!
! fixed parameters:
!
   REAL*8, PARAMETER :: pi = 3.1415926535898, half = 1./2., third = 1./3.
   REAL*8, PARAMETER :: h = 6.6260755e-34
   REAL*8, PARAMETER :: hbar = h/(2*pi)
   REAL*8, PARAMETER :: echarge = 1.60217733d-19 ! elementary charge
   !REAL*8, PARAMETER :: echarge = 1.0 ! elementary charge
   REAL*8, PARAMETER :: melec = 9.1093897d-31 ! electron mass
   REAL*8, PARAMETER :: m2nm = 1d9 ! nanometers to meter
   !REAL*8, PARAMETER :: m2nm = 1 ! angstroms to meters
   REAL*8, PARAMETER :: temp2kt = 8.617366d-05 ! kelvins to eV (kT)
   INTEGER, PARAMETER :: spr = 1 ! multiplies the number of sites on x-direc.
   REAL*8, PARAMETER :: ebin = 0.005 ! energy grid in nofe and gofe histograms
!
! trap attempt frequency and time unit
!
   REAL*8 :: nu0 ! = h/(8*melec*aa**2) or 1/tunit
   REAL*8 :: e0  ! h*nu0
   REAL*8 :: const ! = sqrt(2*melec/echarge)/hbar
!
! input parameters (file="nanowalk.in")
!
   INTEGER :: np       ! number of particles
   REAL*8  :: d,dyz    ! size length of simulation box in nm (d --> x-coordinate)
   REAL*8  :: dsurf    ! surface trap density (nm**-2)
   REAL*8  :: rcut     ! cut-off for hopping between neighbouring traps
   INTEGER :: nsample  ! number of samples
   REAL*8  :: temp     ! temperature in K
   REAL*8  :: appfield ! applied field in Vm-1
   REAL*8  :: maxmoves ! maximum number of moves
   INTEGER :: nbins    ! number of time bins in total simulation time per sample
   REAL*8  :: tbin     ! bin size for time histograms in units of tunit
   INTEGER :: iebins   ! number of initial time bins neglected on average
   REAL*8  :: tunit    ! time unit (t0)
   REAL*8  :: ec       ! energy of conduction band edge (0 by default) (eV)
   REAL*8  :: ecut     ! energy cutoff for exponential DOS (eV)
   REAL*8  :: temp0    ! characteristic temperature in K for exponential DOLS
   REAL*8  :: alfa     ! localization radius (nm)
   REAL*8  :: rprob    ! recombination probability (number between 0 and 1)
   REAL*8  :: lambda,eredox ! Marcus: reorg. energy (eV), redox pair eq. energy (eV)
   REAL*8  :: kcb,tss  ! Marcus: prefactors for probs and times
   LOGICAL*2 :: multtrap ! if .true. waiting times are computed using multiple trapping model
   LOGICAL*2 :: onelec  ! if .true. single electron aproximation is used
   REAL*8  :: ef       ! Fermi energy when using single electron aproximation
   REAL*8  :: alat     ! distance between traps
!
! input parameters (file="etraps.in","rtraps.in")
!
   INTEGER :: ndist    ! number of grid points in distribution of trap energies
   REAL*8, DIMENSION(:), ALLOCATABLE :: epiege,pcum
   INTEGER :: nspheres ! number of nanospheres in input sample
   REAL*8  :: dsphere ! diameter of nanosphere in nm
!
! main variables
!
   INTEGER :: ntrap    ! number of traps
   REAL*8, DIMENSION(:), ALLOCATABLE :: x,y,z       ! coordinates of electrons
   REAL*8, DIMENSION(:), ALLOCATABLE :: x0,y0,z0    ! initial coordinates of electrons
   REAL*8, DIMENSION(:), ALLOCATABLE :: xr,yr,zr    ! real coordinates of electrons
   REAL*8, DIMENSION(:), ALLOCATABLE :: x0e,y0e,z0e ! initial coordinates of electrons
   REAL*8, DIMENSION(:), ALLOCATABLE :: xre,yre,zre ! real coordinates of electrons

   REAL*8, DIMENSION(:), ALLOCATABLE :: e        ! energy of electrons
   REAL*8, DIMENSION(:), ALLOCATABLE :: wt       ! hopping time of electrons
   REAL*8, DIMENSION(:), ALLOCATABLE :: rt       ! recombination times
   INTEGER, DIMENSION(:), ALLOCATABLE :: ijump   ! hopping-to trap of electrons
   INTEGER, DIMENSION(:), ALLOCATABLE :: itrap   ! trap number of electrons
   INTEGER, DIMENSION(:), ALLOCATABLE :: iback   ! "previous" trap of electrons
   LOGICAL, DIMENSION(:), ALLOCATABLE :: otrap ! if .true. trap is occupied
   LOGICAL, DIMENSION(:), ALLOCATABLE :: rtrap ! if .true. recombinable trap
   REAL*8, DIMENSION(:), ALLOCATABLE :: etrap  ! trap energy
   REAL*8, DIMENSION(:), ALLOCATABLE :: xtrap  ! trap x-coordinate
   REAL*8, DIMENSION(:), ALLOCATABLE :: ytrap  ! trap y-coordinate
   REAL*8, DIMENSION(:), ALLOCATABLE :: ztrap  ! trap z-coordinate
   REAL*8, DIMENSION(:), ALLOCATABLE :: xss    ! sphere x-coordinate
   REAL*8, DIMENSION(:), ALLOCATABLE :: yss    ! sphere y-coordinate
   REAL*8, DIMENSION(:), ALLOCATABLE :: zss    ! sphere z-coordinate
   REAL*8, DIMENSION(:), ALLOCATABLE :: ibytime ! current histogram
   REAL*8, DIMENSION(:), ALLOCATABLE :: msd    ! mean square displacement
   REAL*8, DIMENSION(:), ALLOCATABLE :: aener  ! average energy of electrons
   REAL*8, DIMENSION(:), ALLOCATABLE :: nldiff ! diffusion length
   REAL*8, DIMENSION(:), ALLOCATABLE :: ntlife ! lifetime
   REAL*8, DIMENSION(:), ALLOCATABLE :: adist  ! average square displacemente
   INTEGER, DIMENSION(:,:), ALLOCATABLE :: ivec ! neighbour list
   INTEGER, DIMENSION(:), ALLOCATABLE :: iv  ! number of neighbours
   REAL*8 :: tev     ! kT (temperature) in eV
   REAL*8 :: tev0    ! kT0 (characteristic temperature) in eV
   REAL*8 :: delapp  ! force in eV/AA (potential gradient)
   REAL*8 :: time    ! elapsed time
   REAL*8 :: emean   ! centre of gaussian DOS
   REAL*8 :: facnorm ! normalization factor for intensities
   REAL*8 :: rho     ! carriers density
   REAL*8 :: maxtime ! maximum time of simulation in units of tunit
   REAL*8 :: ener    ! compute total energy of electrons
   REAL*8 :: ldiff   ! diffusion length of electrons
   REAL*8 :: tlife   ! half life of electrons
   REAL*8 :: dist    ! square displacement
   INTEGER :: nsurf  ! number of traps per nanosphere
   REAL*8 :: rsphere ! radius of nanosphere in nm
   LOGICAL*2 :: esite   ! if .true. upward jump
   LOGICAL*2 :: forward ! if .true. "forward" jump
!
! output parameters
!
   REAL*8 :: jcur    ! current density
   REAL*8 :: umob    ! mobility
   INTEGER :: ehistbin ! number of points in "nofe" and "gofe" histograms
   REAL*8, DIMENSION(:), ALLOCATABLE :: nofe  ! energy level population
   REAL*8, DIMENSION(:), ALLOCATABLE :: gofe  ! density of states
   REAL*8, DIMENSION(:), ALLOCATABLE :: tgofe
   REAL*8, DIMENSION(:), ALLOCATABLE :: sgofe ! density of surface states
   REAL*8, DIMENSION(:), ALLOCATABLE :: emov  ! target energies for upward jumps
   REAL*8, DIMENSION(:), ALLOCATABLE :: aemov ! target energies for all the jumps
   REAL*8, DIMENSION(:), ALLOCATABLE :: etrans ! "effective transport energy"
!
! others
!
   INTEGER :: i,j,k,l,isx,isy,isz,istep,i1,ir,ioutput,nn,nyz
   REAL*8 :: r,tr,t1,rt1,delta,sigma,xs,ys,zs,ti,rdist
   INTEGER :: ixsr,isxl,isyr,isyl,iszr,iszl,idir,idir1
   INTEGER :: ik,it,is,iis,nrem,ndatos,contt
   INTEGER :: isample
   REAL*8 :: nrecomb,nrecomb1,nrecomb2
   REAL*8 :: imoves,imovest
   REAL*8 :: jcurtsum,mjcurt,ekk,ngofe,nsgofe,nnofe,suma,nemov,naemov,netrans
   REAL*8 :: theta,phi
   REAL*8 :: advance,xtrapi,ytrapi,ztrapi,rtrap2
   REAL*8 :: djx,djy,djz,jump2,rcut2,rcut2x
   REAL*8, DIMENSION(:), ALLOCATABLE :: idisp
   REAL*8, DIMENSION(:), ALLOCATABLE :: te
!
   const = sqrt(2*melec*echarge)/hbar
!
   OPEN(14,file="nanowalk.in")
   OPEN(15,file="nanowalk.out")
   !OPEN(16,file="etraps.in")
   CALL system("rm -f msdata")
!
! read input parameters
!
   READ(14,*) np
   READ(14,*) d,dyz
   READ(14,*) dsurf
   READ(14,*) rcut
   READ(14,*) maxmoves
```

```fortran
      READ(14,*) nsample
      READ(14,*) temp
      READ(14,*) appfield
      READ(14,*) nbins
      READ(14,*) tbin
      READ(14,*) iebins
      READ(14,*) tunit
      READ(14,*) ec
      READ(14,*) ecut
      READ(14,*) temp0
      READ(14,*) dsphere
      READ(14,*) alfa
      READ(14,*) lambda,eredox
      READ(14,*) kcb,tss
      READ(14,*) multtrap
      READ(14,*) onelec
      READ(14,*) ef
      READ(14,*) alat
!
! convert to internal units
!
      tev = temp*temp2kt
      tev0 = -temp0*temp2kt
      delapp = appfield/m2nm
!
      ALLOCATE (x(np),y(np),z(np),e(np),wt(np),itrap(np),ijump(np),iback(np))
      ALLOCATE (x0(np),y0(np),z0(np))
      ALLOCATE (xr(np),yr(np),zr(np))
      ALLOCATE (x0e(np),y0e(np),z0e(np))
      ALLOCATE (xre(np),yre(np),zre(np))
      ALLOCATE (ibytime(nbins))
      ALLOCATE (msd(nbins),nldiff(nbins),ntlife(nbins),aener(nbins),adist(nbins))
      ehistbin = int((ecut-ec)/ebin)+1
      ALLOCATE (nofe(ehistbin),gofe(ehistbin),tgofe(ehistbin),sgofe(ehistbin),emov(ehistbin),aemov(ehistbin),etrans(ehis
tbin))
      ALLOCATE (idisp(np),te(np))
      ALLOCATE (rt(np))
!
      nu0 = 1./tunit
      maxtime = nbins*tbin
!
      WRITE(*,'(/10x," program NANOWALK HOPPING  "/)')
      WRITE(*,'(" sample size (x, and yz) = ",f10.5,1x,f10.5" nm")') d,dyz
      WRITE(*,'(" Trap attempt frequency = ",e15.5," secs-1")') nu0
      WRITE(*,'(" Time unit = ",e15.5," secs")') tunit
      WRITE(*,'(" number of electrons = ",i4)') np
      WRITE(*,'(" Maximum time of simulation = ",e15.5," tunit(s)")') maxtime
      WRITE(*,'(" Temperature = ",f7.2," K")') temp
      WRITE(*,'(" Ec = ",f7.2," eV")') ec
      WRITE(*,'(" Ecut = ",f7.2," eV")') ecut
      WRITE(*,'(" alpha = ",f7.4)') -tev/tev0
      WRITE(*,'(" Applied field = ",d9.3," Vm-1")') appfield
      WRITE(*,'(/2x,"( kT = ",f10.7,", E (= -dV/dx) = ",f10.7, " eV )"/)') &
            tev,delapp
      WRITE(15,'(/10x," program NANOWALK HOPPING "/)')
      WRITE(15,'(" sample size (x, and yz) = ",f10.5,1x,f10.5" nm")') d,dyz
      WRITE(15,'(" Trap attempt frequency = ",e15.5," secs-1")') nu0
      WRITE(15,'(" Time unit = ",e15.5," secs")') tunit
      WRITE(15,'(" number of electrons = ",i4)') np
      WRITE(15,'(" Maximum time of simulation = ",e15.5," tunit(s)")') maxtime
      WRITE(15,'(" Temperature = ",f7.2," K")') temp
      WRITE(15,'(" Ec = ",f7.2," eV")') ec
      WRITE(15,'(" Ecut = ",f7.2," eV")') ecut
      WRITE(15,'(" alpha = ",f7.2)') -tev/tev0
      WRITE(15,'(" Applied field = ",d9.3," Vm-1")') appfield
      WRITE(15,'(/2x,"( kT = ",f10.7,", E (= -dV/dx) = ",f10.7, " eV )"/)') &
            tev,delapp
!
!    nn = 18
!    alat = 1.0
      nn = nint(d/alat)
      nyz = nint(dyz/alat)
      ntrap = nn*nyz**2
!    d = alat*nn
!    dyz = alat*nn

      ALLOCATE (otrap(ntrap),rtrap(ntrap),etrap(ntrap),xtrap(ntrap),ytrap(ntrap),ztrap(ntrap))
      ALLOCATE (ivec(ntrap,700),iv(ntrap))

! JUST TO CHECK: simple cubic lattice
!
!    ik = 0
!    DO isx=1,nn
!      DO isy=1,nyz
!        DO isz=1,nyz
!          ik = ik + 1
!          xtrap(ik) = (isx-1)*alat
!          ytrap(ik) = (isy-1)*alat
!          ztrap(ik) = (isz-1)*alat
!        ENDDO
!      ENDDO
!    ENDDO
!
! CREATE random lattice
!
      call random_seed
      ik = 1
      DO ik=1,ntrap
         call random_number(r)
         xtrap(ik) = r*d
         call random_number(r)
         ytrap(ik) = r*dyz
         call random_number(r)
         ztrap(ik) = r*dyz
      ENDDO

      DO ik=1,ntrap
         WRITE (25,*) ik,xtrap(ik),ytrap(ik),ztrap(ik)
      ENDDO
!
! computing neighbour list
!
      WRITE(*,'(" Computing neighbour list... ")')
      ivec = 0
      iv = 0
      rcut2 = rcut*rcut
      DO ik=1,ntrap
         rcut2x = rcut2
111   DO it = ik+1,ntrap
!
         djx = xtrap(ik)-xtrap(it)
         djy = ytrap(ik)-ytrap(it)
         djz = ztrap(ik)-ztrap(it)
!      P.B.C here:
         djx = djx - d*nint(djx/d)
         djy = djy - dyz*nint(djy/dyz)
         djz = djz - dyz*nint(djz/dyz)
!
         jump2 = djx**2 + djy**2 + djz**2
         IF (jump2.lt.rcut2x) THEN
            iv(ik) = iv(ik) + 1
            iv(it) = iv(it) + 1
            ivec(ik,iv(ik)) = it
            ivec(it,iv(it)) = ik
         ENDIF
      ENDDO
      IF (iv(ik).le.1) THEN
         rcut2x = rcut2x + 1
         write(*,'("changing cut-off -->",f10.5," nm")') sqrt(rcut2x)
         write(15,'("changing cut-off -->",f10.5," nm")') sqrt(rcut2x)
         GOTO 111
      ENDIF
      IF (mod(ik,1000).eq.0) print *, 'ik = ',ik
      WRITE(56,*) ik,iv(ik)
      ENDDO
!
! **************************************************************
! ***** loop over different trap energy realizations **************
! **************************************************************
!
      jcurtsum = 0
      nofe = 0
      gofe = 0
      tgofe = 0
      sgofe = 0
      emov = 0
      aemov = 0
      etrans = 0
      msd = 0
      nldiff = 0.0
      ntlife = 0.0
      aener = 0.0
      adist = 0.0
      imovest = 0.0
!
      DO isample=1,nsample
!
```

```fortran
      WRITE(*,'(/" --> Simulation for sample = ",i6/40("*"))') isample
      WRITE(15,'(/" --> Simulation for sample = ",i6/40("*"))') isample
!
      x = 0
      y = 0
      z = 0
      e = 0
      ndatos = 0
      ldiff = 0.0
      tlife = 0.0
      idisp = 0
      otrap = .false.
      rtrap = .false.
      ener = 0.0
      dist = 0.0
      nrecomb = 0.0
      nrecomb1 = 0.0
      nrecomb2 = 0.0
!
!     allocate energies to trap sites
!
      DO ik = 1,ntrap
        ekk = edist()
        etrap(ik) = ekk
        IF ((onelec).AND.(ekk.ge.ef))  otrap(ik) = .true. ! if .true. one electron aprox. is used.
        IF (.NOT.otrap(ik)) THEN
           gofe(int(ekk/ebin)+1) = gofe(int(ekk/ebin)+1) + 1
        ENDIF
        tgofe(int(ekk/ebin)+1) = tgofe(int(ekk/ebin)+1) + 1
      ENDDO
!
      WRITE(*,'(" Total simulation time = ",e15.5," secs")') maxtime
      WRITE(*,'(" Time window = ",e15.5," secs")') tbin
      WRITE(15,'(" Total simulation time = ",e15.5," secs")') maxtime
      WRITE(15,'(" Time window = ",e15.5," secs")') tbin
!
      WRITE(*,*)'total number of traps', ntrap
      WRITE(15,*)'total number of traps', ntrap
!
!     distribute particles randomly throughout sample
!
      DO j=1,np ! loop over number of particles

22      CONTINUE
        call random_number(r)
        ik=int(r*ntrap+1)
        IF (otrap(ik)) GOTO 22    ! trap already occupied
        e(j) = etrap(ik)
        x(j) = xtrap(ik)
        y(j) = ytrap(ik)
        z(j) = ztrap(ik)
        itrap(j) = ik
        otrap(ik) = .true.   ! trap occupied
      iback(j) = ik

      ENDDO
!
      DO j=1,np ! compute waiting times and jumps for each electron
!
        IF (multtrap)  THEN

           call settime1(j) ! this sets up wt(j) and ijump(j)

        ELSE

           call settime2(j) ! this sets up wt(j) and ijump(j)

      ENDIF
!
      ENDDO
!
      DO i=1,np ! compute recombination times
!
         call recombt(i)
!
      ENDDO
!
!     initial positions
!
      x0 = x
      y0 = y
      z0 = z
      xr = x
```

```fortran
      yr = y
      zr = z
      x0e = x
      y0e = y
      z0e = z
      xre = x
      yre = y
      zre = z
!
!     ------------------------------------------------------
!     begin simulation run
!     ------------------------------------------------------
!
      time = 0
      te = 0
      ioutput = 0
      imoves = 0.0

      DO WHILE(.true.)
!
    IF (imovest.ge.maxmoves) THEN
          WRITE(*,*) 'maximum number of moves about to be exceed', maxmoves
          WRITE(15,*) 'maximum number of moves about to be exceed', maxmoves
          STOP
      ENDIF
!
!     security: if two electrons in the same trap or tend to jump to the same trap, stop
!
      DO i=1,np-1
         DO j=i+1,np
            IF (itrap(i).eq.itrap(j)) THEN  ! TWO ELECTRONS SHARE THE SAME BED!
               WRITE(*,*) 'TWO electrons share the same bed!',i,j,itrap(i)
               WRITE(*,*) 'INMORAL --> FORBIDDEN'
               STOP
            ENDIF
            IF (ijump(i).eq.ijump(j)) THEN  ! TWO ELECTRONS WANT THE SAME BED!
               WRITE(*,*) 'TWO electrons tend to jump to the same trap!',i,j,ijump(i)
               WRITE(*,*) 'PROBLEMS IN FUTURE --> FORBIDDEN'
               STOP
            ENDIF
         ENDDO
      ENDDO
!
      IF ((count(otrap).ne.np).AND.(.NOT.onelec)) THEN
         WRITE(*,*) &
            'occupied traps does not coincide with total number of particles'
         WRITE(*,*) 'count, np -->',count(otrap),np
      STOP
      ENDIF
!
!     search for minimum hopping time...
!
      t1 = 1d50
      DO i=1,np
        IF (wt(i).lt.t1) THEN
           IF (.not.otrap(ijump(i))) THEN ! ... to a non-occupied trap
              t1 = wt(i)
              i1 = i
           ENDIF
        ENDIF

      ENDDO
!
!     more controls
!
      IF (t1.eq.1d50) stop 'problems on minimum hopping time searching --> possible problems on settime subroutine'
      IF (itrap(i1).eq.ijump(i1)) stop 'electron is moving to its own trap!!'
      DO i=1,np
        IF (wt(i).lt.0) stop 'negative hopping times!!'
      ENDDO
!
!     minimum recombination time is selected
!
      rt1 = 1d50
      DO i=1,np
        IF (rt(i).lt.rt1) THEN
           rt1 = rt(i)
           ir = i
        ENDIF
      ENDDO
!
!     recombination or hops
!
```

```fortran
        IF (rt1.le.t1) THEN
!
!  compute diffusion length and lifetime
!
          ndatos = ndatos + 1
          ldiff = ldiff + idisp(ir)
          tlife = tlife + te(ir)
          x0e(ir) = xre(ir)
          y0e(ir) = yre(ir)
          z0e(ir) = zre(ir)
          te(ir) = 0.0
          otrap(itrap(ir)) = .false.
          nrecomb = nrecomb + 1
          nrecomb2 = nrecomb2 + 1
          sgofe(int(e(ir)/ebin)+1) = sgofe(int(e(ir)/ebin)+1) + 1  ! distribution of surface states
21        call random_number(r)
          l = int(r*ntrap)+1
          IF (otrap(l)) GOTO 21
          DO j = 1,np
             IF (j.eq.ir) CYCLE
             IF (l.eq.ijump(j)) GOTO 21
          ENDDO
          itrap(ir) = l
          otrap(itrap(ir)) = .true.
          e(ir) = etrap(l)
          x(ir) = xtrap(l)
          y(ir) = ytrap(l)
          z(ir) = ztrap(l)
!
          IF (multtrap)  THEN
             call settime1(ir) ! this sets up wt(i1) and ijump(i1)
          ELSE
             call settime2(ir) ! this sets up wt(i1) and ijump(i1)
          ENDIF
          call recombt(ir)
!
          DO i=1,np
             IF (i.ne.ir) THEN
                wt(i) = wt(i) - rt1
                rt(i) = rt(i) - rt1
             ENDIF
             te(i) = te(i) + rt1
          ENDDO
!
          time = time + rt1   ! advance time
!
        ELSE
!
!     move electron "i1" to trap ijump(i1).
!
          call move(i1)
          imoves = imoves + 1        ! record moves
          imovest = imovest + 1
!
          DO i=1,np
             IF (i.ne.i1) THEN
                wt(i) = wt(i) - t1
                rt(i) = rt(i) - t1
             ENDIF
             te(i) = te(i) + t1
          ENDDO
!
          time = time + t1   ! advance time
!
          idisp(i1) = sqrt((xre(i1)-x0e(i1))**2 + (yre(i1)-y0e(i1))**2 + (zre(i1)-z0e(i1))**2)
          call random_number(r)
          rprob = kcb*sqrt(tev/(4*pi*lambda))*exp(-(eredox-e(i1)-lambda)**2/(4*lambda*tev))
          IF (r.lt.rprob) THEN
             ndatos = ndatos + 1
             ldiff = ldiff + idisp(i1)
             tlife = tlife + te(i1)
             x0e(i1) = xre(i1)
             y0e(i1) = yre(i1)
             z0e(i1) = zre(i1)
             te(i1) = 0.0
             otrap(itrap(i1)) = .false.
             nrecomb = nrecomb + 1
             nrecomb1 = nrecomb1 + 1
             sgofe(int(e(i1)/ebin)+1) = sgofe(int(e(i1)/ebin)+1) + 1  ! surface states distribution
23           call random_number(r)
             l = int(r*ntrap)+1
             IF (otrap(l)) GOTO 23
             DO j = 1,np
                IF (j.eq.i1) CYCLE
                IF (l.eq.ijump(j)) GOTO 23
             ENDDO
             itrap(i1) = l
             otrap(itrap(i1)) = .true.
             otrap(l) = .true.
             e(i1) = etrap(l)
             x(i1) = xtrap(l)
             y(i1) = ytrap(l)
             z(i1) = ztrap(l)
          ENDIF

          IF (multtrap)  THEN
             call settime1(i1) ! this sets up wt(i1) and ijump(i1)
             call recombt(i1)  ! it sets up a new recombination time
          ELSE
             call settime2(i1) ! this sets up wt(i1) and ijump(i1)
             call recombt(i1)  ! it sets up a new recombination time
          ENDIF
!
        ENDIF
!
!     If maximum time exceeded finish calculation
!
        IF (time.gt.maxtime) EXIT
!
!  compute energy of electrons
!
        ener = ener + sum(e)
!
!     film maker...
!
!     write(33,'(e10.5,1x,f10.5,1x,f10.5,1x,f10.5)') time,x(1),y(1),z(1)
!
!     output after ~tbin
!
        IF (nint(time/tbin).gt.ioutput) THEN
           ioutput = ioutput + 1
           WRITE(*,*) 'isample = ',isample,ioutput,time !,x,y,z
           WRITE(*,*) maxval(e),minval(e),maxloc(e),minloc(e)
!
!  compute average square displacement
!
        adist(nint(time/tbin)) = adist(nint(time/tbin)) + dist/imoves
!
!  compute diffusion length and lifetime
!
        IF (nrecomb.gt.0) THEN
           nldiff(nint(time/tbin)) = nldiff(nint(time/tbin)) + ldiff/ndatos
           ntlife(nint(time/tbin)) = ntlife(nint(time/tbin)) + tlife/ndatos
        ENDIF
!
!     compute occupancy histogram
!
        DO i=1,np
           nofe(int(e(i)/ebin)+1) = nofe(int(e(i)/ebin)+1) + 1
        ENDDO
!
!  compute average energy of electrons
!
        aener(nint(time/tbin)) = aener(nint(time/tbin))+ ener/imoves/np
!
!     compute mean square displacement
!
           suma = 0.0
           DO i=1,np
              suma = suma + (xr(i)-x0(i))**2 + (yr(i)-y0(i))**2 + (zr(i)-z0(i))**2
           ENDDO
           suma = suma/real(np)
           msd(nint(time/tbin)) = msd(nint(time/tbin)) + suma
        ENDIF
!
      ENDDO
!
!  -----------------------------------------------
!  simulation ends
!  -----------------------------------------------
!
      facnorm = (dyz/m2nm)**2*tbin*tunit/echarge*imoves
!
!  multiply current density histogram by number of particles
!
      facnorm = facnorm/real(np)
!
```

```fortran
      WRITE(15,'(5x," number of recombination events for low energy traps = ",es15.5)') nrecomb1
      WRITE(*,'(5x," number of recombination events for low energy traps  = ",es15.5)') nrecomb1
      WRITE(15,'(5x," number of recombination events for deep traps = ",es15.5)') nrecomb2
      WRITE(*,'(5x," number of recombination events for deep traps  = ",es15.5)') nrecomb2
      WRITE(15,'(5x," number of total recombination events = ",es15.5)') nrecomb
      WRITE(*,'(5x," number of total recombination events = ",es15.5)') nrecomb
      WRITE(15,'(5x," number of moves = ",es15.5)') imoves
      WRITE(*,'(5x," number of moves = ",es15.5)') imoves
      WRITE(15,'(5x," total number of moves = ",es15.5)') imovest
      WRITE(*,'(5x," total number of moves = ",es15.5)') imovest
!
!     Compute number of samples to average
!
      OPEN(17,file="isamples.dat")
      WRITE(17,*) isample
      CLOSE(17)
!
      OPEN(22,file='msdata',status='unknown',access='append')
      WRITE(22,*) isample,umob,mjcurt/appfield
7     CLOSE(22)
!
      OPEN(26,file='enerhist.dat',status='unknown')
      OPEN(28,file='sdist.dat',status='unknown')
      OPEN(30,file='efermi.dat',status='unknown')
!      DO i=1,ehistbin
      DO i=int(ec/ebin)+1,ehistbin
        ngofe = gofe(i)/sum(tgofe)/ebin
!        ngofe = gofe(i)/ntrap/ebin
        nsgofe = sgofe(i)/sum(tgofe)/ebin
!        nsgofe = sgofe(i)/ntrap/ebin
        nnofe = nofe(i)/sum(nofe)*np/ntrap/ebin
    nemov = emov(i)/sum(emov)*np/ebin
    naemov = aemov(i)/sum(aemov)*np/ebin
    netrans = etrans(i)/sum(etrans)*np/ebin
!        nnofe = nnofe/tev
    IF (ngofe.ne.0) THEN
          WRITE(26,'(4(e12.5,1x))') real(i)*ebin,ngofe
          WRITE(28,'(4(e12.5,1x))') real(i)*ebin,nsgofe
          WRITE(30,'(4(e12.5,1x))') real(i)*ebin,nnofe/ngofe
      ENDIF
    ENDDO
    CLOSE(26)
    CLOSE(28)
    CLOSE(30)
!
      msd = msd/real(isample)
      OPEN(24,file='msd.dat',status='unknown')
      DO i=1,nbins
        WRITE(24,*) i*tbin*tunit,msd(i)*1d-14   ! Jump Diffusion (cm-3)
      ENDDO
      CLOSE(24)
!
      OPEN(70,status='unknown',file='difflng.dat')
      OPEN(71,status='unknown',file='lifetime.dat')
      OPEN(72,status='unknown',file='avgener.dat')
      DO i=1,nbins
    WRITE(70,*) i*tbin*tunit,nldiff(i)/real(isample)
    WRITE(71,*) i*tbin*tunit,ntlife(i)*tunit/real(isample)
    WRITE(72,*) i*tbin*tunit,aener(i)/real(isample),adist(i)/real(isample)
      ENDDO
      CLOSE(70)
      CLOSE(71)
      CLOSE(72)
!
   ENDDO
!
! ***********************************************************************
! ***** END loop over different trap energy realizations **************
! ***********************************************************************
!
   facnorm = (dyz/m2nm)**2*tbin*tunit/echarge*imoves
!
   WRITE(*,'(/"Final results:"/)')
   WRITE(15,'(/"Final results:"/)')
!
   CLOSE(14)
   CLOSE(15)
!  CLOSE(16)
!
   CONTAINS
! subroutines and functions are the same as those of the previous code


END PROGRAM nanowalk
```